Rotary Solid Desiccant Dehumidifiers

Analysis of Models and Experimental Investigation

by

Kenneth John Schultz

A thesis submitted in partial fulfillment of the requirements for the degree of

Doctor of Philosophy

(Mechanical Engineering)

at the

University of Wisconsin - Madison

1987

A dissertation entitled

Rotary Solid Desiccant Dehumidifiers

Analysis of Models and Experimental Investigation

submitted to the Graduate School of the

University of Wisconsin-Madison in partial fulfillment of

the requirements for the degree of Doctor of Philosophy

by

Kenneth J. Schultz

Degree to be awarded: December 19_____ May 19_____ August 19 87

Approved by Dissertation Readers:

John W Mitchell
Major Professor

06/25/87
Date of Examination

S. A. Klein

Michael Corradini

Dean, Graduate School

Abstract

The development and design of rotary desiccant dehumidifiers for use in air conditioning systems depends in part on models which describe the heat and mass transfer processes in the dehumidifier. Two particular models which have been used extensively in the past are described. One is a finite difference solution of a set of governing partial differential equations. The other uses a heuristic approach in which discretized sections of the dehumidifier are modeled as simple steady-state counterflow heat and mass exchangers.

Errors in the system of equations comprising the heuristic model are exposed by deriving a similar set of equations directly from the partial differential equations. The significance of these errors and the overall accuracy of the heuristic model are tested by comparison with the finite difference model.

A facility for testing the performance of rotary desiccant dehumidifiers is described. The facility includes all necessary controls and instrumentation and is operated with the aid of a microcomputer-based data acquisition and control system. Three spirally wound parallel passage rotary desiccant dehumidifiers are also described.

The accuracy of the finite difference model is tested by comparison with experimental data. Pressure drop results are used to estimate the distributions of the nonuniformly sized passages. Procedures are presented for determining the active amount of desiccant in the dehumidifier and for estimating the effective overall heat and mass transfer coefficients. The model is adjusted to account for nonuniformly sized passages and nonhomogeneous distributions of matrix properties which significantly affect the performance of dehumidifiers.

Acknowledgements

My tenure here at the Solar Energy Laboratory has been very challenging, rewarding, and most of all, enjoyable. This is a special place made possible by a group of special people. To Jack Duffie, thanks for picking me out of your Solar class and offering me this opportunity. Your personal interest in Debbie and I has been comforting. To Bill Beckman and Sandy Klein, I know it was mostly grading homework, but the chance to help you with your classes meant a lot to me. The teacher I hope someday to be is guided by the example you set. To John Mitchell, your interest, encouragements, and special patience in directing me through this project have been greatly appreciated. Thank you also for showing me some of the things that are really important in this world.

It has been a pleasure to work with the students and staff here. I have met many wonderful people and will always remember these times with fondness. Thanks to Shirley for her helpfulness. To Eric, thanks for sharing your knowledge and insights with me. It has been a privilege to work with you.

The opportunity to work at the Solar Energy Research Institute contributed much to my personal and professional growth. Thanks to Terry Penney for shielding me from much of the bureaucracy that is DOE. Your support and guidance during this project is appreciated. Thanks to Ahmad, Dennis, Federica, and Bharathan for your help and friendship. Thanks also to Ian Maclaine-cross for sharing your experience and enthusiasm for desiccant cooling with me.

Finally, to Debbie. I am lost for words to fully express my appreciation for all of your patience and understanding. *I love you!* (I won't risk asking if you would still have married me if you knew it was going to take this long.) To my parents, thanks for your confidence and love. Your "forever in college" son is finally done.

Financial assistance for this work was provided by the Solar Heating and Cooling Research and Development Branch, Office of Conservation and Solar Applications, U.S. Department of Energy.

Table of Contents

Abstract ii

Acknowledgements iii

List of Figures ix

List of Tables xiv

Nomenclature xvi

Chapter 1 Introduction 1

1.1 Solid desiccant cooling research 2

1.1.1 Desiccant materials 3

1.1.2 Components 3

1.1.3 Desiccant cooling systems 4

1.2 Analysis tools for desiccant dehumidifiers 4

1.2.1 Detailed models 5

1.2.2 Equilibrium models 7

1.2.3 Simplified models 8

1.3 Thesis objectives 8

1.3.1 Comparison of models 9

1.3.2 Comparison of models with experimental data 10

1.3.3 Supporting work 11

Chapter 2 Models of Rotary Heat and Mass Exchangers 12

2.1 Mathematical description of rotary heat and mass exchangers 13

2.1.1 Nomenclature, coordinate system, and assumptions 13

2.1.2 Humidity ratio as mass transfer potential 15

2.1.3 Mass fraction as mass transfer potential 17

2.2 Maclaine-cross' finite difference model - MOSHMX 18

2.2.1 Finite difference equations 19

2.2.2 Solution procedure 21

2.2.3 Comparison of MOSHMX using humidity ratio and mass fraction potentials 25

2.3 Barlow's "pseudo-steady-state" model - DESSIM 25

2.3.1 Description of PSS concept 27

2.3.2 Modifications of PSS model 31

2.3.3 Alternate set of finite difference equations 32

2.3.4 Comparison of the PSS equations with the finite difference equations 36

2.3.5 Comparison of the PSS and finite difference solutions 37

2.3.6 Modeling of a direct solar-regenerated collector/ dehumidifier 43

2.4 Conclusions 46

Chapter 3 Description of Experimental Facility and Data Analysis Procedures 48

3.1 General layout of the experimental facility 48

3.2 Instrumentation 52

3.3 Equipment and controls 55

3.4 Data acquisition and control system (DACS) 56

3.5 Data analysis procedure 59

3.5.1 Seal leakage corrections 59

3.5.2 Mass and energy balance closure 61

3.5.3 Pressure drop corrections 63

3.5.4 Summary 64

Chapter 4 Description of Test Dehumidifiers 65

4.1 Dehumidifier matrix geometries 65

4.2 Construction of the test dehumidifiers 67

4.3 Dimensional statistics of the test dehumidifiers 70

Chapter 5 Analysis of the Experimental Data and Comparison with Models .. 78

5.1 Pressure drop analysis 78

5.1.1 General formulation 79

5.1.2 Experimental pressure drop results 80

5.1.3 Model for distribution of passage sizes 82

5.1.4 Comparison of experiments and model 84

5.2 Low rotation speed analysis 90

5.2.1 Mass of silica gel in the wheels 91

5.2.2 Specific heat of the matrix 95

5.3 High rotation speed analysis 98

5.3.1 High rotation speed model 98

5.3.2 Correction of experimental effectivenesses to "infinite" rotation speed 100

5.3.3 Experimental overall heat and mass transfer coefficients 105

5.3.4 Effect of distribution of passage sizes on effective transfer coefficients 112

5.4 Comparison of MOSHMX predictions with experimental results 119

5.4.1 Uniformly spaced passages and homogeneous matrix properties 122

5.4.2 Uniform passage spacings and *non*homogeneous matrix properties 124

5.4.3 Modeling of a distribution of passage sizes explicitly with MOSHMX 139

5.5 Summary 143

Chapter 6 Conclusions and Recommendations 145

6.1 Models of desiccant dehumidifiers 145

6.2 Experimental facility and test dehumidifiers 146

6.2.1 Experimental facility 147

6.2.2 Test dehumidifiers 147

6.3 Validation of model against experiments 148

6.3.1 Pressure drop analysis 148

6.3.2 Desiccant properties 149

6.3.3 Effective overall transfer coefficients 149

6.3.4 Nonhomogeneous matrix properties 150

Appendix A Description of Ventilation Cycle Desiccant Air Conditioning System 151

A.1 Cycle description 151

A.2 Current state of the art 153

A.3 Ventilation cycle performance map 156

Appendix B Air, Water, and Desiccant Properties 158

B.1 Water and water vapor 158

B.2 Moist air 159

B.3 Silica gel properties 161

B.3.1 "IDES = A" equilibrium properties 161

B.3.2 "IDES = B" equilibrium properties 162

B.3.3 Matrix enthalpy 163

B.4 Miscellaneous properties 165

Appendix C The Analogy Method 166

C.1 Transformation of the equations 166

C.2 Analogy solution 168

C.3 Wave analysis 170

Appendix D Uncertainty Analysis 175

D.1 Primary measurements 175

D.1.1 Temperature 175

D.1.2 Pressure 176

D.1.3 Flow rates 176

D.1.4 Humidity ratio 177

D.1.5 Wheel rotation speed 178

D.2 Corrected measurements 178

D.2.1 Corrections for seal leakage rates 178

D.2.2 Mass and energy balance closure 179

D.3 Uncertainties in the wheel parameters 179

D.4 Nondimensional groups 179

D.4.1 Reynolds number 179

D.4.2 Apparent friction factor - Reynolds number 180

D.4.3 Effective Nusselt and Sherwood numbers and overall Lewis number 180

D.5 Uncertainties in MOSHMX predictions 181

Appendix E Tabulation of Experimental Data 182

References 204

List of Figures

Figure — Page

Chapter 1

Chapter 2

2.1. Nomenclature and coordinate system for a rotary desiccant dehumidifier. 14

2.2 MOSHMX finite difference element. 20

2.3 Representative element for "pseudo-steady-state model in DESSIM. 28

2.4 Comparison of the DES-FD and DES-MX models. 35

2.5 Comparison of DES-FD and DES-PSS "effectiveness" relations. 38

2.6 Differences in process stream outlet states predicted by the DES-PSS, DES-PSSe, and DES-MXy models for $Ntu_{y,j} = 10$. The DES-MXy results extrapolated to zero grid size are used as a basis. The dehumidifier and conditions are described in Table 2.2. 41

2.7 Differences in process stream outlet states predicted by the DES-PSS, DES-PSSe, and DES-MXy models for $Ntu_{y,j} = 20$. The DES-MXy results extrapolated to zero grid size are used as a basis. The dehumidifier and conditions are described in Table 2.2. 42

2.8 Process stram outlet state profiles predicted by DES-PSSe and DES-MXy. 44

Chapter 3

3.1 Schematic diagram of the desiccant cooling test facility at the Solar Energy Research Institute. 49

3.2. Photograph of the test facility. 50

3.3. Photograph of the instrument rack for the test facility. 51

3.4 Schematic diagram of measurement sensor locations. 53

List of Figures (cont.)

Figure		Page
3.5	Array of thermocouples and sampling tubes at outlet face of the dehumidifier wheel.	54
3.6	Flow chart of data acquisition/control program structure.	58
3.7	Air leakage paths through the circumferential and radial seals of the dehumidifier.	60
Chapter 4		
4.1	Photograph of the original dehumidifier wheel tested at SERI.	68
4.2	Schematic representation of dehumidifier wheel and housing.	69
4.3	Picture of the rewound wheel.	71
4.4	Picture of the microbead wheel.	72
4.5	Sketch of representative passage channel.	75
Chapter 5		
5.1	Experimental pressure drop results for the three wheels tested. estimated uncertainties are shown by the crossed lines (see Appendix D).	81
5.2	Effective fully developed friction factor - Reynolds number for the lognormal distribution.	85
5.3	Effective slope of the dimensionless pressure drop versus entrance length relation for the lognormal distribution with channel entrance coefficient as a parameter.	86
5.4	a) Lognormal distributions of passage sizes for the three test dehumidifiers estimated from pressure drop results. b) Individual channel mass flow rates. c) Bin fraction weighted flow rate distributions. $ReD_{hu}/4L = 0.40$.	89
5.5	Schematic representation of transfer zone breakthrough at low rotation speeds.	92
5.6	Experimentally determined silica gel masses in the three wheels.	94

List of Figures (cont.)

Figure		Page
5.7	Matrix specific heats determined from experimental data at low rotation speeds.	97
5.8	Humidity ratio and temperature effectivenesses predicted by MOSHMX at high rotation speeds.	101
5.9	Correlation of rotary heat exchanger effectiveness correction to "infinite" rotation speed.	103
5.10	Humidity ratio and temperature effectivenesses predicted by MOSHMX corrected to "infinite" rotation speed.	104
5.11	Effective Nusselt numbers determined from high rotation speed experimental data.	106
5.12	Effective Sherwood numbers determined from high rotation speed experimental data.	108
5.13	Overall Lewis numbers determined from high rotation speed experimental data.	109
5.14	Comparison of MOSHMX predictions with the high rotation speed experimental data. a) rewound wheel. b) microbead wheel.	111
5.15	Representation of a wheel with a distribution of passage sizes as a set of parallel exchangers.	113
5.16	Effective Nusselt number for a lognormal distribution.	115
5.17	Simple mass transfer resistance model considering the desiccant to be a sheet lining the wall of a parallel plate passage.	118
5.18	Overall Lewis number for a lognormal distribution as a function of the ratio of the solid- to air-side mass transfer resistances.	120
5.19	Overall Lewis number as a function of the width of the lognormal distribution.	121
5.20	Comparison of of the process outlet states predicted by MOSHMX (uniform and homogeneous model) with experimental data from original wheel.	123
5.21	Representation of a wheel with nonhomogeneous matrix properties as two parallel exchangers.	125

List of Figures (cont.)

Figure		Page
5.22	Comparison of homogeneous and nonhomogeneous models corresponding to point "9" in Fig. 5.20 (original wheel).	127
5.23	Comparison of the process outlet states predicted by MOSHMX (uniform and *non*homogeneous model) with experimental data from the original wheel.	128
5.24	Comparison of process outlet states pridicted by MOSHMX with experimental data from the original wheel for a range of regeneration inlet states.	131
5.25	Comparison of process outlet states predicted by MOSHMX with experimental data from the original wheel for a range of process inlet states.	132
5.26	Comparison of process outlet states predicted by MOSHMX with experimental data from the rewound wheel for a range of inlet humidity ratios.	133
5.27	Comparison of prcess outlet states predicted by MOSHMX with experimental data from the rewound wheel for a range of flow rates.	134
5.28	Comparison of process outlet states predicted by MOSHMX with experimental data from the microbead wheel for a range of inlet humidity ratios.	136
5.29	Comparison of process outlet states predicted by MOSHMX with experimental data from the microbead wheel for a range of flow rates.	137
5.30	Profiles of outlet states as a function of rotation angle for experiment 05-06-86 2A (original wheel, also point "11" in Fig. 5.23).	138
5.31	Comparison of explicit model for distribution of passage sizes with other models and experiment 11-18-85 2A (rewound wheel).	140
5.32	Profiles of the process stream outlet states predicted by MOSHMX for several bins representing a distribution of passage sizes.	142

Appendix A

A.1	Ventilation cycle desiccant air conditioning system.	152

List of Figures (cont.)

Figure Page

A.2 Performance of the ventilation cycle as a function of the dehumidifier outlet state for the conditions in Table A.2. a) cooling capacity. b) thermal *COP*. 157

Appendix B

B.1 Van den Bulck's and Brandemuehl's isotherms for regular density silica gels. 164

Appendix C

C.1 Combined potentials for a dehumidifier matrix composed of silica gel alone. 169

C.2 Dehumidifier process stream outlet state in terms of F_i effectivenesses. 171

C.3 Time-distance mapping showing the normalized F_1 (upper) and F_2 (lower) wave fronts within a dehumidifier operating near optimum rotation speed. 173

C.4 Time-distance mapping showing temperature (upper) and humidity ratio (lower) profiles within a dehumidifier corresponding to Fig. C.3. 174

List of Tables

Table		Page
Chapter 1		
Chapter 2		
2.1	Comparison of MOSHMX predictions for rotary dehumidifier outlet states using humidity ratio (MOSHMXw) and mass fraction (MOSHMXy) as mass transfer potentials.	26
2.2	Description of dehumidifier and conditions modeled in comparison of PSS and finite difference models. (see DESSIM paper)	40
Chapter 3		
3.1	Typical seal leakage rates for the first wheel.	60
3.2	Summary of uncertainties in corrected experimental measurements.	64
Chapter 4		
4.1	Summary of the physical parameters for the test dehumidifiers.	73-74
Chapter 5		
5.1	Experimental pressure drop parameters and estimated distribution of passage spacings.	87
5.2	Linear least squares fits to experimentally determined Nu_e and Le_o.	110
Appendix A		
A.1	Summary of desiccant cooling system development.	154
A.2	Parameters for system modeled in Fig. A.2.	156

List of Tables (cont.)

Table		Page
Appendix E		
E.1	Experimental data from *original* wheel corrected for leakage rates and unbalances.	183
E.2	Experimental data from *rewound* wheel corrected for leakage rates and unbalances.	186
E.3	Experimental data from *microbead* wheel corrected for leakage rates and unbalances.	190
E.4	List of figures with corresponding table of data.	195
E.5	Low rotation speed experiments considered in section 5.2.	195
E.6	High rotation speed experiments considered in section 5.3.3 and Figs. 5.11, 5.12, and 5.13.	197
E.7	High rotation speed experiments considered in Fig. 5.14.	199
E.8	Experimental data from *original* wheel for variation in rotation speed (associated with Figs. 5.20 and 5.23).	200
E.9	Experimental data from *original* wheel for variation in regeneration inlet state (associated with Fig. 5.24).	201
E.10	Experimental data from *original* wheel for variation in process inlet state (associated with Fig. 5.25).	201
E.11	Experimental data from *rewound* wheel for variation in inlet humidity ratio (associated with Fig. 5.26).	202
E.12	Experimental data from *rewound* wheel for variation in flow rates (associated with Fig. 5.27).	202
E.13	Experimental data from *microbead* wheel for variation in inlet humidity ratio (associated with Fig. 5.28).	203
E.14	Experimental data from *microbead* wheel for variation in flow rates (associated with Fig. 5.29).	203

Nomenclature

A_c	cross-sectional flow area
A_s	exchanger transfer area
B	parameter defined in Eq. (2.12)
c	specific heat [J/kg-C]
C	local capacity rate ratio for a node
C	capacity rate [kg/s, W/C]
COP	coefficient of performance
D_h	hydraulic diameter [m]
E	counterflow effectiveness
E_w, E_h	experimental mass and energy balance errors [kg_W/s, W]
E_{wr}, E_{hr}	relative errors, defined by Eqs. (3.4) [ ]
f	Fanning friction factor [ ]
F	characteristic potentials defined in Appendix C
g	mass transfer coefficient (humidity ratio) [$kg_W/(m^2\text{-s-}kg_W/kg_{DA})$]
g^*	mass transfer coefficient (mass fraction) [$kg_W/(m^2\text{-s-}kg_W/kg_{TOT})$]
h	heat transfer coefficient [W/m^2-C]
h	air enthalpy on dry air basis [J/kg_{DA}]
h_s	differential heat of sorption [J/kg_W]
h_v	heat of vaporization of water [J/kg_W]
h_{WV}	enthalpy of water vapor [J/kg_W]
H	enthalpy of matrix on dry desiccant basis [J/kg_{DD}]
ΔH_W	integral heat of wetting [J/kg_{DD}]
IDES	desiccant ID, see Appendix B
K	finite difference "effectiveness", entrance pressure drop coefficient [ ]
L	length of flow passages [m]
Le	Lewis number for air [ ]
Le_o	overall Lewis number, defined by Eq. (27) [ ]
$\dot{m}$	mass flow rate of air [kg/s]
M_{DD}	mass of dry desiccant [kg_{DD}]
$\dot{N}$	wheel rotation speed [rev/hr]

N_m, N_f	number of space and time steps, respectively
Ntu	number of transfer units, defined by Eqs. (4) [ ]
Nu	Nusselt number, hD_h/k [ ]
R	gas constant for air, 289.6 J/kg-K
$\Re$	universal gas constant, 8314.4 J/kgmole-K
Re	Reynolds number [ ]
ΔP	pressure drop [Pa]
Pr	Prandtl number for air
Sc	Schmidt number for air
Sh	Sherwood number, $gD_h/\rho D_{aw}$ [ ]
t	air temperature [C]
T	temperature of matrix [C]
v	velocity of air [m/s]
w	air humidity ratio [kg_W/kg_{DA}]
W	water content of desiccant [kg_W/kg_{DD}]
x	nondimensional axial distance, z/L [ ]
y	mass fraction of water vapor in air [kg_W/kg_{TOT}]
z	axial distance [m]

Greek symbols

β_j	ratio of period j length to total period T [ ]
γ	property analogous to ratio of the specific heats of the matrix and of air for sensible heat exchange
Γ	ratio of desiccant "flow rate" to air flow rate, defined by Eq. (2.4) [ ]
Δ	difference
$\varepsilon, \varepsilon^\infty$	effectiveness, adjusted to "infinite" rotation speed [ ]
η	analogy effectiveness, see Appendix C [ ]
θ	nondimensional time or angular position, τ/T [ ]
Λ	local number-of-transfer-units for a node [ ]
μ	viscosity of air [kg/m-s]
ξ	fraction of flow through "high" specific heat wheel
ρ	density of air [kg/m^3]
σ	(analogous) ratio of specific heats, standard deviation [ ]

τ	time [s]
T	rotational period [s]
ϕ	rotation angle, relative humidity [ ]
χ	distribution bin fraction [ ]

Subscripts

a	air on total mass basis, air-side
A	air on dry mass basis
app	apparent
DA	dry air
DD	dry desiccant
DM	dry matrix
e	effective
E	in equilibrium with desiccant
ex	extrapolated value
h	heat transfer
i	inlet, analogy potential
j	flow stream or period reference: 1=process, 2=regeneration
3-j	"other" flow stream or period
k	channel index
m	mass transfer
M	matrix on dry desiccant basis
min	refers to period with minimum capacity rate
o	outlet, overall
s	solid-side
t	temperature
TOT	total mass basis
u	uniform
w	humidity ratio
W	water
WL	liquid water
*	intermediate state in "pseudo-steady-state" model

Chapter 1

Introduction

Open-cycle desiccant air conditioning systems have been investigated extensively over the past two decades. These systems have the potential to be economically competitive with conventional vapor compression air conditioning and provide the consumer with lower cooling costs (Booz-Allen and Hamilton, 1980, 1981; Scholten and Morehouse, 1983). Desiccant systems are driven by low-temperature thermal energy and are compatible with the use of solar energy and waste heat resources (Jurinak, et al., 1984; Mitchell, 1986). It is this aspect that has spurred much of the past research and development of desiccant systems.

Interest in solar-powered air conditioning has dwindled with the demise of renewable energy tax credits and the falling price of oil. However, increasing prices for electricity have opened opportunities for gas-fired cooling technologies including desiccant systems (Kosar, 1986). In addition, many electrical utilities are facing future shortfalls of generating capacity. Large scale penetration of desiccant systems into the cooling market may allow construction of expensive new electrical generating capacity to be delayed (Chinery, 1986).

A variety of air conditioning systems which use desiccant dehumidifiers have been proposed for applications in residential and commercial buildings. The performance of these systems is steadily improving. ASK Corp. (formerly American Solar King) is marketing a ventilation cycle[1] residential desiccant air

---

[1]The ventilation cycle desiccant air conditioning system and the ASK Corp. machine are described in Appendix A.

conditioning system (Venhuizen, 1984; Coellner, 1986). Cargocaire Engineering Corp. is developing a desiccant dehumidifier/vapor compression hybrid system (Bowlen, 1986). In these combined systems, the dehumidifier efficiently removes moisture from the air stream to be conditioned leaving only the sensible cooling load for the vapor compression system. Initial testing has occurred in supermarket applications (Cohen, et al., 1984, 1986). Meckler (1987) has integrated central dehumidification using desiccants into institutional building HVAC systems. However, further development is needed if desiccant cooling is to successfully compete with conventional systems in a wider range of applications and markets.

Desiccant systems employ both liquid and solid desiccants. The work presented here considers only dehumidifiers which use solid desiccants and are operated adiabatically. Liquid desiccant and cross-cooled solid desiccant systems have been reviewed by Schlepp and Schultz (1984).

1.1 Solid desiccant cooling research

Jurinak (1982) has compiled a history of solid desiccant cooling research and development through the early 1980's. Penney and Maclaine-cross (1986) and Chinery and Penney (1987) have summarized current desiccant cooling activities. The major areas of research confronting desiccant cooling concern desiccant materials, component performance and design, and system configuration and optimization. While representing a convenient grouping, these catagories are by no means independent of one another.

1.1.1 Desiccant materials

The sorption properties of the desiccant greatly affect the performance of the dehumidifier and of the complete system. The choice of desiccant and matrix thermal properties depends on the system configuration, operating conditions, and dehumidifier design constraints. Accurate characterization of desiccant properties and an understanding of how the sorption properties affect the heat and mass transfer processes are necessary to the design of high performance dehumidifiers. A variety of models have been used to study the effects of the desiccant and matrix thermal properties on the performance of dehumidifiers (for example: Barlow and Collier, 1981; Jurinak and Mitchell, 1984b; Grolmes and Epstein, 1985; and Collier, et al., 1986).

1.1.2 Components

The performance of each individual component affects the overall performance of the system. Research on desiccant cooling system components is directed at establishing an understanding of the fundamental processes occurring in each and the design and development of practical high performance components.

Desiccant dehumidifiers are the most difficult of the components to characterize and the least developed. The design of matrix geometries with high heat and mass transfer and low pressure drop characteristics which can be cost-effectively manufactured is crucial to the success of desiccant cooling systems. Models can be used to aid the design and development of high performance dehumidifiers. However, accurate models require a complete understanding of

the heat and mass transfer processes occurring in the dehumidifier and should be subjected to experimental verification.

1.1.3 Desiccant cooling systems

A variety of desiccant cooling system configurations have been considered. Much of the past work has focused on the development of residential-sized systems based on the ventilation cycle. Several advanced cycles have been proposed (Maclaine-cross, 1985a) and have been shown to potentially have substantially higher performance (Crum, et al., 1987). In addition to the Cargocaire hybrid system under development, a variety of other hybrid systems have been studied (for example: Howe, et al., 1983; Sheridan and Mitchell, 1985; Burns, et al., 1985a,b; Worek and Moon, 1986).

Estimates of the overall performance of a system must be made to determine its competitiveness with conventional systems. Design point analyses are informative but not generally sufficient. Simulations of system performance require accurate, computationally simple models. Tests of actual systems are needed to prove design concepts and ensure that component interactions are properly accounted for. Development of control strategies which optimize system performance and analyses of the effects of transient operating conditions are also called for.

1.2 Analysis tools for desiccant dehumidifiers

A complete experimental investigation of desiccant systems would require considerable time and money. Theory, supported by experiment, provides a basic understanding of the processes occurring in a component or system. Models,

based on theory, then become tools for the efficient investigation of desiccant cooling topics. Indeed, much of the work mentioned above has been done using models.

1.2.1 Detailed models

The detailed modeling of adiabatic desiccant dehumidifiers is a difficult task. The mathematical formulation is described by partial differential equations for the conservation of mass and energy, for the rate of heat and mass transfer between the air and the desiccant, and for the rate of transfer within the desiccant. The equations are coupled by generally nonlinear equilibrium properties. Rotating wheels and switched beds require periodic boundary conditions. In addition, the equations contain transfer coefficients and other parameters that are difficult to quantify.

Ruthven (1984) discusses many of the models used in the analysis of batch-type adsorption processes. Analytical and numerical solutions have been developed for isothermal and adiabatic operation with various assumptions about transfer resistances, equilibrium relations, and initial conditions.

The diffusional resistance to the transfer of moisture in desiccant particles (the "solid-side" resistance) is an important factor in the performance of dehumidifiers. In many of the past dehumidifiers, this resistance was significant and was a major reason for the low performance of the systems of which they were a part. Pesaran (1983) has surveyed diffusion mechanisms and Pesaran and Mills (1984) have solved the diffusion equation within the desiccant particle in modeling the behavior of silica gel packed-beds. Majumdar, et al., (1985) have

taken a similar approach in modeling the moisture transfer resistance in the voids of a desiccant felt.

By constructing a dehumidifier from parallel plates coated with small silica gel particles, Biswas, et al., (1984) were able to reduce the effect of solid-side resistance. Kim, et al., (1985) successfully predicted single-blow experimental results with an overall air-side resistance model. The use of parallel channel, laminar flow dehumidifiers with small solid-side resistances has lead to improved performance of desiccant cooling systems. This also simplifies the modeling of high performance dehumdifiers.

Finite difference solutions of a set of partial differential equations assuming overall air-side transfer coefficients have proven to be versatile tools in the analysis of desiccant dehumidifiers. Bullock and Threlkeld (1966) used such a model to successfully predict the performance of a "thick" batch-type dehumidifier. Pla-Barby, et al., (1978) and Barker and Kettleborough (1980a) have extended this model to investigate the periodic steady-state performance of rotary packed-bed silica gel wheels. Holmberg (1979) has also derived a similar model and has included longitudinal heat conduction in the matrix.

The finite difference model developed by Maclaine-cross (1974) has been used extensively to investigate the steady-state performance of desiccant dehumidifiers and cooling systems (for example: Jurinak, 1983; Jurinak and Mitchell, 1984a,b). The model is similar to Lambertson's (1958) model for rotary heat exchangers. Comparison of the model with experimental data (van Leersum and Close, 1982) from a rotary packed-bed silica gel wheel was not successful because of the large solid-side resistance present. Brandemuehl (1982) has also

used this model to investigate the effects of nonuniform inlet states and transient operation.

Barlow (1982) has proposed a "pseudo-steady-state" model which considers discrete sections of the dehumidifier to act as simple steady-state heat and mass exchangers. The heat and mass transfer calculations are uncoupled at each time step to simplify the procedure. Fair agreement with limited experimental data from a single-blow parallel passage matrix coated with silica gel has been obtained (Schlepp and Barlow, 1984).

In spite of its heuristic nature, studies using Barlow's model have been influential in desiccant cooling research. The computer code is well documented and easy to follow. The program has been used to estimate the performance of desiccant cooling systems (Schlepp and Barlow, 1984), study the effects of desiccant properties (Barlow and Collier, 1981; Collier, et al., 1986), and has been modified to model a direct solar regenerated collector/dehumidifier (Schultz, et al., 1987). The availability and ease of use of the program have made the model an attractive research tool.

1.2.2 Equilibrium models

Several models have been developed which assume that equilibrium exists between the air stream and the desiccant, for example, Epstein, et al., (1985), Grolmes and Epstein (1985), and Van den Bulck, et al., (1985a). These models have been used only for qualitative investigation of the effects of sorption properties and ideal dehumidifier behavior.

1.2.3 Simplified models

A variety of simplied models have been used for system design point calculations and long term simulations. Maclaine-cross and Banks (1972) have transformed the dehumidifier equations into two uncoupled sets of equations which are analogous to those for heat transfer alone. The dehumidifier is then modeled as the superposition of two independent exchangers using the known heat exchanger solutions (Kays and London, 1984). Simplifications of this analogy method have been used extensively in system simulations (for example, Howe, et al., 1983; Jurinak, et al., 1984; Turner, et al., 1987). Jurinak and Banks (1982) and Banks (1985) have numerically evaluated the analogy method against Maclaine-cross' finite difference model and found it to be satisfactory for simulation purposes.

Van den Bulck, et al., (1985b) have generated an effectiveness - number-of-transfer-units (ε-Ntu) model for a silica gel dehumidifier based on their equilibrium model and Maclaine-cross' finite difference model. Van den Bulck, et al., (1986) and Crum, et al., (1987) have used this model in systems studies.

Another technique used has been to simply correlate the results of more detailed models (for example: Barker and Kettleborough, 1980b; Majumdar, et al., 1982). These sorts of models can only be as good as the more detailed models on which they are based.

1.3 Thesis objectives

The detailed models described above are mathematical representations of the heat and mass transfer processes in the dehumidifier. In general, it is not the

technique for solving the equations that is in question regarding the accuracy with which the behavior of real components can be predicted. Rather, it is the assumptions and approximations that were made in arriving at the original set of equations that must be tested.

A major assumption made in the models is the use of overall air-side transfer coefficients, especially for mass transfer. These coefficients should be obtainable from established heat and mass transfer theory for the models to be useful. In addition, the flow channels are generally assumed to be uniformly sized and the matrix and desiccant materials to be homogeneously distributed. This may not be the case for real dehumidifiers.

Accurate predictions of actual dehumidifier and system performance are needed to improve current desiccant cooling systems and to judge the benefits of future advances. Many dehumidifier models have been developed to aid the investigation of desiccant cooling systems. However, few experimental results on high performance rotary dehumidifiers and desiccant cooling systems have been reported and so the accuracy with which many of the models describe real dehumidifiers has not been fully determined.

1.3.1 Comparison of models

The detailed models for rotary desiccant dehumidifiers discussed above have been derived from essentially the same set of governing equations. The models should therefore generate nearly identical results if carefully implemented, even though the differencing techniques may not have been the same. Barlow's model, however, is less rigorous due to its uncoupling of the heat and mass transfer calculations.

The objective of Chapter 2 is to verify the accuracy of Barlow's model and the results that have been obtained from its use. A comparison of the "pseudo-steady-state" equations is made with a set of finite difference equations derived from a conventional set of partial differential conservation and rate equations. The results of Barlow's model are then compared with those from Maclaine-cross' finite difference model to assess its accuracy and efficiency.

1.3.2 Comparison of models with experimental data

None of the rotary dehumidifier models have been compared satisfactorily with experimental data from high performance rotary dehumidifiers. Chapter 3 describes the test facility established at the Solar Energy Research Institute for this purpose. The author spent two years at SERI participating in the design, construction, and operation of the facility. The data acquisition, reduction, and correction procedures developed by the author are also given. The parallel passage silica gel dehumidifiers used in the experiments are described in Chapter 4.

The objective of Chapter 5 is to verify the accuracy of Maclaine-cross' finite difference model (that is, the assumptions upon which it is based) by comparing it with the experimental data. The experimental data are used to deduce the pressure drop characteristics and the overall air-side transfer coefficients for the model and these are related to established theory. The effects of nonuniformly-sized flow channels and a nonhomogeneous distribution of matrix properties is taken into account. The accuracy of the model is assessed by direct comparison with the experimental data over a wide range of operating conditions.

1.3.3 Supporting work

The conclusions drawn from this work and recommendations for continuing work are presented in Chapter 6.

In addition, several appendices are attached. Appendix A presents a description of the ventilation cycle desiccant cooling system and a summary of its development. Appendix B contains the air, water, and desiccant property relations used in this work. A brief outline of the analogy theory of Maclaine-cross and Banks is presented in Appendix C to support its use in Maclaine-cross' finite difference model and the analysis of the experimental heat and mass transfer results. A discussion of the analysis of the uncertainties in the experimental measurements and parameters is presented in Appendix D. A summary of the experimental data is tabulated in Appendix E.

Chapter 2

Models of Rotary Heat and Mass Exchangers

Of the models developed to investigate rotary desiccant dehumidifiers, the three most used have been those based on the analogy theory of Maclaine-cross and Banks (1972; Jurinak, 1982), the finite difference model of Maclaine-cross (1974; Jurinak, 1982), and the "pseudo-steady-state" model of Barlow (1982). The analogy solutions have been compared with Maclaine-cross' finite difference model (Jurinak, 1982; Jurinak and Banks, 1982; Banks, 1985). Since the finite difference solutions of Pla-Barby, et al., (1978) and Holmberg (1979) were derived from essentially the same set of partial differential equations, they should produce very similar results to Maclaine-cross' model.

Barlow's (1982) "pseudo-steady-state" model is not as rigorous as the finite difference models. The model results in a straightforward computational procedure based on dimensional engineering quantities and is set in a modular program that is well documented and easy to follow. Up to ten flow streams, each with different inlet conditions, flow rates and directions, and period lengths, can be handled. The properties of the desiccant and matrix can be varied along the flow length.

The model has been used to study the effects of desiccant properties (Barlow and Collier, 1981; Collier, et al., 1986), estimate desiccant cooling system performance (Schlepp and Barlow, 1984), and has been modified to model the performance of a direct solar-regenerated collector/dehumidifier (Schultz, et al., 1987). Validation of the model is limited to fair agreement with single-blow experimental data (Barlow, 1982; Schlepp and Barlow, 1984).

The purpose of the work in this chapter is to test the validity of the "pseudo-steady-state" model. The basis for the concept is established by comparing the equations used with a set of finite difference equations derived from a conventional set of governing partial differential equations. The predictions of the model for the performance of a rotary dehumidifier are then compared with those from Maclaine-cross' finite difference model.

2.1 Mathematical description of rotary heat and mass exchangers

2.1.1 Nomenclature, coordinate system, and assumptions

Fig. 2.1 illustrates the nomenclature and coordinate system for a counterflow rotary exchanger. The coordinate system is fixed with respect to the wheel. Also shown is a small element of the exchanger idealized as a parallel passage channel. The following assumptions are made:

1. There is no carryover or leakage of fluid from one air stream to the other.
2. The air and matrix states within the wheel are radially uniform as are the inlet air states.
3. The thermal and moisture storage capacities of the air in the matrix are small compared to the matrix capacities.
4. The axial and circumferential diffusion of heat and moisture in both the matrix and the air streams is small.
5. The heat and mass transfer processes between the matrix and the air stream can be described by composite or overall transfer coefficients which include both the air-side and solid-side transfer resistances.
6. The coupling of heat and mass transfer occurs only through the interdependence of the tranfer potentials. Thermal diffusion and Dufor effects are negligible.
7. The pressure is constant throughout the wheel.

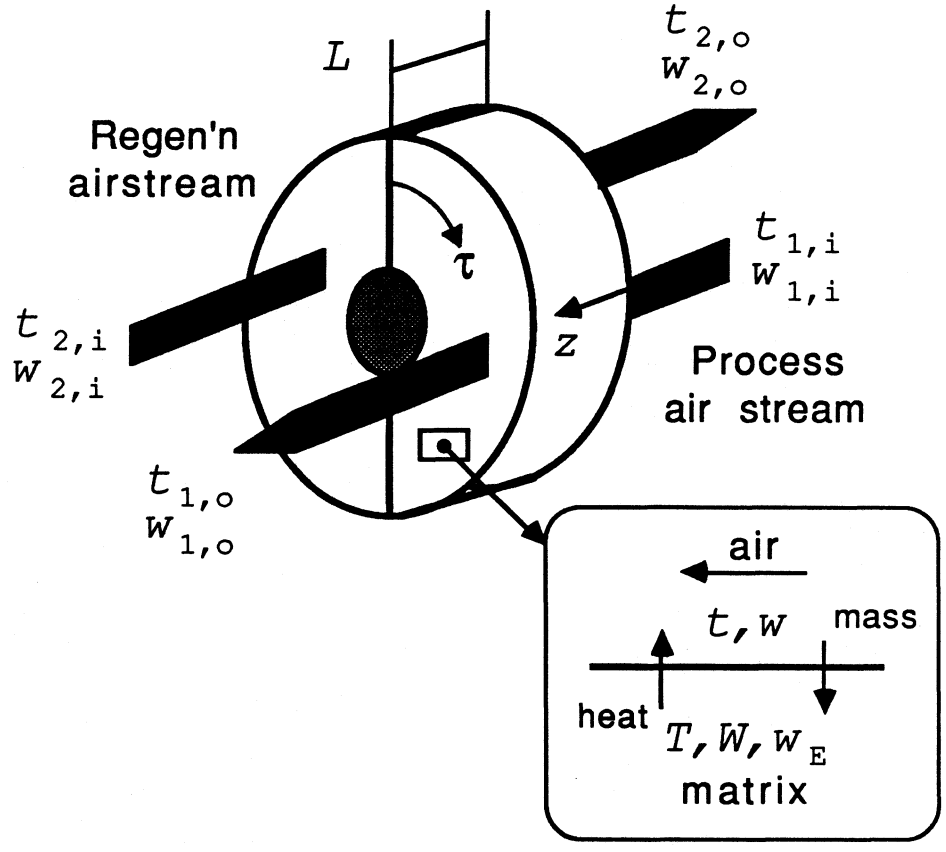

Fig. 2.1 Nomenclature and coordinate system for a rotary dessicant dehumidifer.

Molar concentration, mass fraction, and humidity ratio have all been used as driving potentials for mass transfer in the analyses of desiccant dehumidifiers. For the small concentrations of water vapor in air encountered in desiccant cooling systems, the differences between the various potentials are negligible. Since Maclaine-cross' model uses humidity ratio and Barlow's model uses mass fraction as the mass transfer potential, both formulations will be presented below.

2.1.2 Humidity ratio as mass transfer potential

For simplicity, the humidity ratio is commonly used as the driving potential for mass transfer and the following transfer rate and conservation equations for water and energy can be formulated (Bullock and Threlkeld, 1966; Maclaine-cross and Banks, 1972; Holmberg, 1979; Van den Bulck, et al., 1986):

(2.1)

water transfer rate

$$\frac{\partial w}{\partial x} = Ntu_{w,j}(w_E - w) \qquad \text{(a)}$$

conservation of water

$$\frac{\partial w}{\partial x} + \beta_j \Gamma_j \frac{\partial W}{\partial \theta} = 0 \qquad \text{(b)}$$

energy transfer rate

$$\frac{\partial h}{\partial x} = Ntu_{t,j} c_A (T - t) + Ntu_{w,j} h_{WV} (w_E - w) \qquad \text{(c)}$$

conservation of energy

$$\frac{\partial h}{\partial x} + \beta_j \Gamma_j \frac{\partial H}{\partial \theta} = 0 \qquad \text{(d)}$$

The independent variables of axial distance and time have been nondimensionalized with

$$x = z/L \qquad \theta = \tau/T \qquad (2.2)$$

Time and rotation angle are related by

$$\frac{\tau}{T} = \frac{\phi}{2\pi} \qquad \beta_j = \frac{T_j}{T} = \frac{\Phi_j}{2\pi} \qquad (2.3)$$

The period fractions, β_j, may not sum to unity if portions of the frontal area of the wheel are blocked by seals or other obstructions separating the two flow streams.

The parameter Γ_j is the mass capacity rate ratio (the ratio of the mass "flow rate" of the matrix to that of the dry air) and is given by

$$\Gamma_j = \frac{M_{DD}/T}{\dot{m}_{DA,j}} \qquad (2.4)$$

The number-of-transfer-units for mass and heat transfer are given by

$$Ntu_{w,j} = \frac{gA_{s,j}}{\dot{m}_{DA,j}} \qquad Ntu_{t,j} = \frac{hA_{s,j}}{\dot{m}_{DA,j}c_A} \qquad (2.5)$$

where the overall transfer coefficients, g and h, account for resistances in both the

air and the solid. An overall Lewis number is defined as the ratio of the heat and mass tranfer Ntu's,

$$Le_o = \frac{Ntu_t}{Ntu_w} = \frac{h}{gc_A} \tag{2.6}$$

The above equations are nonlinear and coupled through the equilibrium relations

$$W = W(T, w_E) \qquad H = H(T, W) \qquad h = h(t, w) \tag{2.7}$$

The property relations for moist air and the desiccants used in this work are presented in Appendix B.

2.1.3 Mass fraction as mass transfer potential

Other authors (for example, Barlow, 1982; Pesaran and Mills, 1984) have used water vapor mass fraction as the driving potential for mass transfer. The conservation equations are the same as above in this formulation, however, the transfer rate equations become

(2.8)

$$\frac{\partial y}{\partial x} = Ntu_{y,j}(1-y)\,(y_E - y) \tag{a}$$

$$\frac{\partial h}{\partial x} = Ntu_{t,j}c_A(T - t) + Ntu_{y,j}\frac{h_{WV}}{(1-y)}(y_E - y) \tag{c}$$

The mass tranfer Ntu's in this case are defined as

$$Ntu_{y,j} = \frac{g^* A_{s,j}}{\dot{m}_{a,j}} \tag{2.9}$$

where m_a is the total mass flow of moist air (air and water vapor). Using an analogy to heat transfer, the coefficients g and g^* will generally be evaluated from identical relationships and the resulting Ntu_y will be smaller than Ntu_w by the ratio of the total to dry air flow rate ($\approx 1+w$, about 1-2%). Because of this and the small differences in the mass transfer potentials, the two formulations will produce slightly different results. These differences are quantified in the next section.

2.2 Maclaine-cross' finite difference model - MOSHMX

Maclaine-cross has developed a FORTRAN program called MOSHMX[2] which represents a finite difference solution of Eqs. (2.1). The version of MOSHMX used here models the periodic steady-state operation of a rotary heat and mass exchanger with two counterflow air streams. Jurinak and Mitchell (1984a) have modeled additional purge streams. In addition, the inlet air states are assumed to be uniform and constant. Brandemuehl (1982) has considered nonuniform and transient inlet conditions with MOSHMX. Also, the heat and mass transfer Ntu's are assumed to be constant throughout each period. This is expected to be reasonable for parallel channel laminar flow matrices and simplifies the analysis.

---

[2]**MOSHMX** stands for **M**ethod **O**f **S**olving **H**eat and **M**ass **X**(trans)fer.

A summary of the method and equations are presented here. The complete development is contained in Maclaine-cross (1974).

2.2.1 Finite difference equations

By using Eqs. (2.7), Maclaine-cross replaced enthalpies with temperatures as dependent variables. He also combined Eqs. (2.1a) and (2.1c) to arrive at the following set of partial differential equations (Maclaine-cross, 1974; Jurinak, 1982),

(2.10)

$$\frac{\partial w}{\partial x} = Ntu_{w,j}(w_E - w) \qquad \text{(a)}$$

$$\frac{\partial w}{\partial x} + \beta_j \Gamma_j \frac{\partial W}{\partial \theta} = 0 \qquad \text{(b)}$$

$$\frac{\partial t}{\partial x} = Ntu_{t,j} c_A (T - t) \qquad \text{(c)}$$

$$\frac{\partial h}{\partial t}\frac{\partial t}{\partial x} + \frac{\partial h}{\partial w}\frac{\partial w}{\partial x} + \beta_j \Gamma_j \frac{\partial H}{\partial T}\frac{\partial T}{\partial \theta} + \beta_j \Gamma_j \frac{\partial H}{\partial W}\frac{\partial W}{\partial \theta} = 0 \qquad \text{(d)}$$

To obtain the difference equations, the "inlet" and "outlet" states of a discrete element, shown schematically in Fig. 2.2, are expressed as a Taylor's series about the "center" of the element, for example,

$$t_i = t - \frac{\partial t}{\partial x}\frac{\Delta x}{2} + \frac{k^2 t}{\partial x^2}\frac{\Delta x^2}{8} - \frac{\partial^3 t}{\partial x^3}\frac{\Delta x^3}{48} + \ldots \qquad (2.11)$$

Subtraction of Eq. (2.11) from a similar equation for t_o gives a second order accurate estimate of the derivative at the "center" of the node. A second order

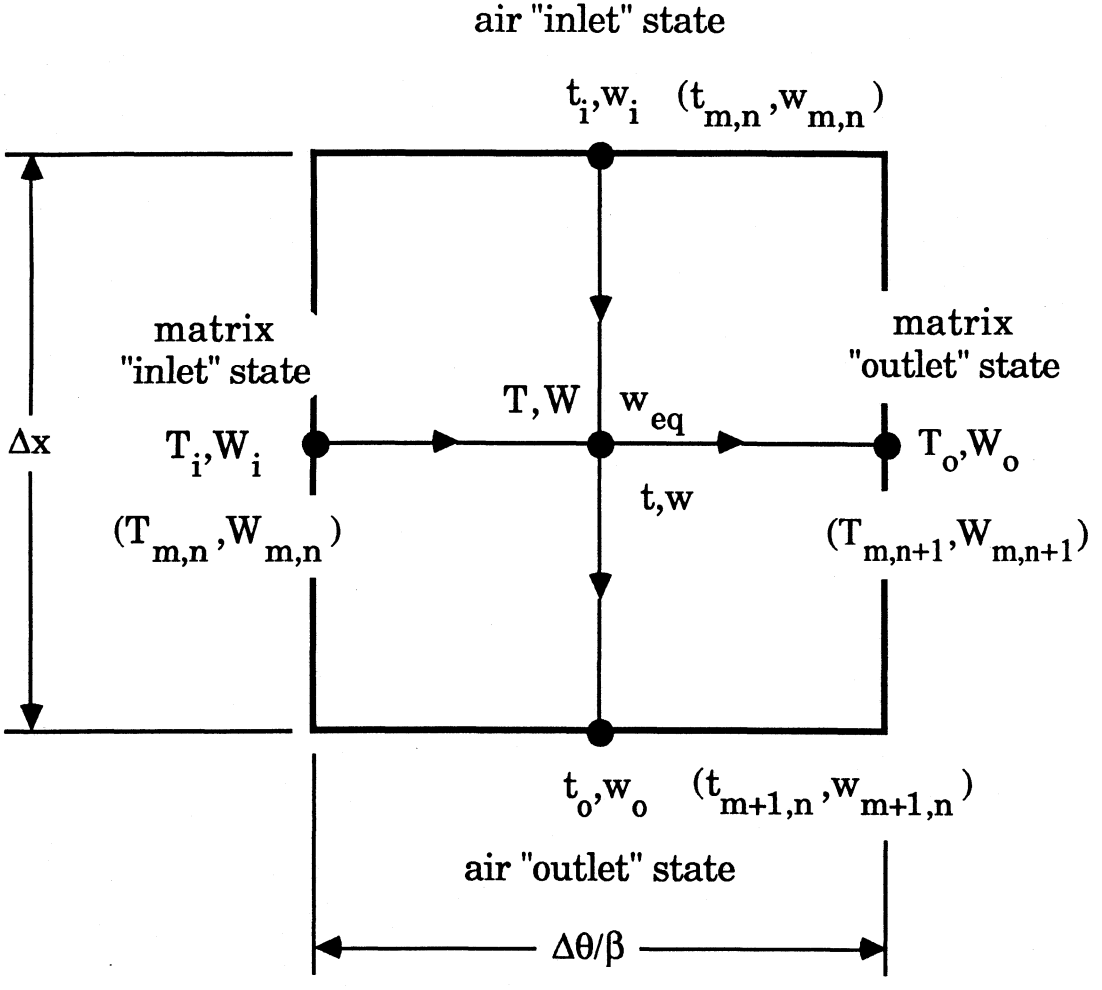

Fig. 2.2 MOSHMX finite difference element.

accurate estimate of the state at the "center" of the node is obtained by adding these same equations. Substitution of these and similar relations for the other dependent variables into the partial differential equations results in a set of difference equations which can be written in matrix form as shown in Eqs. (2.12) on the following page. The parameter B has been introduced to allow both formulations of the mass transfer potentials to be included. The formulation is second order accurate and implicit. It is similar to that used by Lambertson (1958) in his study of rotary heat exchangers.

2.2.2 Solution procedure

Through various row operations, Eqs. (2.12) can be placed in upper triangular form and solved by back substitution without need for iteration. Two passes are used however. In the first pass, properties are evaluated at the "inlet" states and estimates of the "outlet" states are calculated. In the second pass, properties are evaluated at the average of the "inlet" and estimated "outlet" states and the "outlet" states are recalculated. This procedure is analogous to a second order Runge-Kutta method and maintains the second order accuracy of the difference scheme (Maclaine-cross, 1974).

The calculational procedure essentially follows an angular slice of the wheel as it rotates from one air stream to the other. To begin, the temperature and water content of the matrix as it rotates into the process stream are estimated. Together with the specified process air inlet state, Eqs. (2.12) are solved for the first element's "outlet" air state (which becomes the "inlet" air state to the next element) and the "outlet" matrix state (which becomes the "inlet" matrix state at the next time step). The procedure then marches down the length

$$\begin{bmatrix} \frac{Le_o}{2} + \frac{1}{Ntu_m \Delta x} & 0 & -\frac{Le_o}{2} & 0 \\ 0 & \frac{1}{\Delta x} & 0 & \frac{\beta\Gamma}{\Delta\theta} \\ 0 & 1 + \frac{2B}{Ntu_m \Delta x} & -\left(\frac{\partial w_E}{\partial T}\right)_W & -\left(\frac{\partial w_E}{\partial W}\right)_T \\ \frac{1}{\Delta x}\left(\frac{\partial h}{\partial t}\right)_w & \frac{1}{\Delta x}\left(\frac{\partial h}{\partial w}\right)_t & \frac{\beta\Gamma}{\Delta\theta}\left(\frac{\partial H}{\partial T}\right)_W & \frac{\beta\Gamma}{\Delta\theta}\left(\frac{\partial H}{\partial W}\right)_T \end{bmatrix} \begin{bmatrix} t_o - t_i \\ w_o - w_i \\ T_o - T_i \\ W_o - W_i \end{bmatrix} = \begin{bmatrix} Le_o(t_i - T_i) \\ 0 \\ 2(w_i - w_{Ei}) \\ 0 \end{bmatrix} \qquad \text{Eq. (2.12)}$$

For MOSHMXw: $Ntu_m = Ntu_w$ $B = 1$

For MOSHMXy: $Ntu_m = Ntu_y$ $B = (1+w_E)$

of the wheel and then rotates to the next time step. The average air outlet states are the time-step-weighted-averages of the "outlet" states from the last element as the slice of the wheel rotates through each period.

The periodic steady-state operation of a dehumidifier is obtained by two methods. In one, the slice of the wheel is followed until the change in outlet states from one rotation to the next and the overall mass balance closure are within a small tolerance, for example,

$$E_{wr} = \frac{\Sigma \dot{m}_j (w_{j,i} - w_{j,o})}{(\Sigma \dot{m}_j | w_{j,i} - w_{j,o} |)/2} < 2 \cdot 10^{-6} \qquad (2.13)$$

This procedure essentially follows the transient response of the wheel from the initial assumed matrix profile to that at periodic steady-state. In addition, a matrix method (essentially a Newton-Raphson technique) is used to enhance the rate of convergence when the transient method is slow (Maclaine-cross, 1974; Jurinak, 1982). Because the water conservation equation, Eq. (2.10a), is linear with constant coefficients, the finite difference scheme explicitly conserves water (except for roundoff errors). Although the coefficients in the energy equation, Eq. (2.10c), are nonlinear, an energy balance analogous to Eq. (2.13) generally closes to within $2 \cdot 10^{-4}$.

MOSHMX contains algorithms for choosing appropriate space and time step sizes. The number of space steps was determined mainly through numerical experimentation (Maclaine-cross, 1974),

$$N_m = Int[0.85 (Max (Ntu_{m,j}))^{1/2} + 1.6] \qquad (2.14)$$

The time step is then chosen with the aid of the analogy theory which is briefly

described in Appendix C. In the analogy theory (Banks, 1972; Maclaine-cross and Banks, 1972), the partial differential equations are transformed into two sets of approximately uncoupled equations which have the same form as those for heat transfer alone. They describe two transfer zones that move through the wheel at speeds inversely proportional to the quantity $\gamma_{ij}\Gamma_j$ where γ_i is analogous to the ratio of the specific heat of the matrix to that of the air in sensible heat exchangers. To follow the i^{th} wave front, the space and time steps should be related to the wave speed by

$$\frac{\Delta x}{\Delta(\theta_i/\beta_j)} = \frac{N_{f,ij}}{N_m} \approx \frac{1}{\gamma_{ij}\Gamma_j} \tag{2.15}$$

where $N_{f,ij}$ is the number of time steps for the i^{th} transfer wave in period j. Ideally, only N_m of the $N_{f,1j}$ small time steps of size $\Delta\theta_1$ are needed to follow the faster first wave through period j of the wheel. However, to account for the spreading of the wave front due to nonconstant properties and finite transfer coefficients, more are used; $2N_m$ time steps have been found adequate for silica gel and halide salt wheels (Maclaine-cross, 1974; Jurinak, 1982). The rest of the period is covered by larger time steps of size $\Delta\theta_2$ determined from Eq. (2.15). The number actually used is $N_{f,2j}$ times the fraction of the time remaining in the period. The version of MOSHMX used here also allows the user to input explicit values for the number of space and time steps.

By using the second order accuracy of the difference equations, an estimate of the solution at zero grid size can be obtained by quadratically extrapolating the results from three progressively smaller grid sizes in which the ratio of $\Delta x/\Delta\theta$ is kept constant (Maclaine-cross, 1974, Carnahan, et al., 1969). For $\Delta x_1/\Delta x_2 = 2$ and $\Delta x_1/\Delta x_3 = 3$, the extrapolation is given by

$$s_{ex} = (27s_3 - 16s_2 + s_1)/12 \tag{2.16}$$

where s represents temperature and humidity ratio.

2.2.3 Comparison of MOSHMX using humidity ratio and mass fraction potentials

From the finite difference equations, Eqs. (2.12), it can be seen that the only difference between the humidity ratio formulation (referred to as "MOSHMXw") and mass fraction formulation ("MOSHMXy") is a small difference in the effective mass transfer Ntu's, Ntu_m/B. If the mass transfer coefficients are identical in the two formulations, the effective mass transfer Ntu for MOSHMXy will be smaller than that for MOSHMX$_w$ by a factor of approximately $1/(1+w)^2$, or about 2-4% smaller for nominal air conditions. The overall Lewis number for MOSHMXy should be $(1+w)$ times larger so that the heat transfer Ntu's remain the same.

Numerical experimentation has shown that the largest differences in predicted outlet states of the two formulations occur near minimum dehumidification. Table 2.1 shows a such a comparison. The differences are larger at lower Ntu's as the effectiveness of an exchanger is more sensitive to Ntu there. However, the differences are small and negligible from a practical standpoint.

2.3 Barlow's "pseudo-steady-state" model - DESSIM

Barlow (1982) developed the program DESSIM[3], based on his "pseudo-steady-state" (PSS) model, as a simple tool for modeling the periodic steady-state

---

[3]DESSIM stands for **DES**iccant **SIM**ulation program.

Table 2.1 Comparison of MOSHMX predictions for rotary dehumidifier outlet states using humidity ratio (MOSHMXw) and mass fraction (MOSHMXy) as mass transfer potentials.

Operating conditions:

$t_{1,i}$ = 30.0 C
$t_{2,i}$ = 80.0 C
c_{DM} = 1500 J/kg$_{DD}$-C
$\Gamma_1 = \Gamma_2$ = 0.20
$w_{1,i}$ = 14.0 g/kg
$w_{2,i}$ = 12.5 g/kg
P_{tot} = 101325 Pa
$Ntu_1 = Ntu_2$

Silica gel dehumidifier (IDES=A)[1]

Ntu_m	$t_{1,o}$ C	$w_{1,o}$ g/kg	$h_{1,o}$ kJ/kg	[2]$\Delta t_{1,o}$ C	$\Delta w_{1,o}$ g/kg	$\Delta h_{1,o}$ kJ/kg
MOSHMXw - humidity ratio as potential, $Le_{o,1} = Le_{o,2} = 1.0$						
5.00	57.048	6.865	75.349			
10.00	60.927	5.603	76.011			
20.00	63.134	4.930	76.497			
MOSHMXy - mass fraction as potential, $Le_{o,1} = Le_{o,2} = 1.0136$						
4.93	57.010	6.886	75.365	-0.038	0.021	0.016
9.87	60.902	5.616	76.019	-0.025	0.013	0.008
19.73	63.124	4.936	76.502	-0.010	0.006	0.004
MOSHMXy - mass fraction as potential, $Le_{o,1} = Le_{o,2} = 1.0$						
5.00	57.031	6.874	75.356	-0.017	0.009	0.007
10.00	60.916	5.609	76.014	-0.011	0.006	0.003
20.00	63.130	4.932	76.499	-0.004	0.002	0.002

[1]See Appendix B.

[2]$\Delta \equiv$ (humidity ratio model) - (mass fraction model)

operation of rotary dehumidifiers. The model is of a heuristic nature based on the assumption that the dehumidifier can be described as a set of uncoupled steady-state heat and mass exchangers. A summary of the PSS concept is presented here in nondimensional form. To simplify the comparison of DESSIM and MOSHMX, the heat and mass transfer Ntu's are assumed to be constant throughout each period. Barlow (1982) and Schultz, et al., (1987) give a more detailed description in the original dimensional terms.

2.3.1 Description of PSS concept

As in MOSHMX, DESSIM follows a differential angular slice of the wheel, discretized along its length, as it rotates from one air stream to the next. However, rather than applying a true finite differencing procedure to the governing partial differential equations, each element is considered as a simple steady-state counterflow heat and mass exchanger. A representative element is shown in Fig. 2.3 and is essentially identical to the MOSHMX element in Fig. 2.2.

In the PSS concept, each element is first considered to be an isothermal counterflow mass exchanger. This effectively uncouples the heat and mass transfer for the time interval. The "outlet" air mass fraction from the element is given by

$$y_o = y_i - E_m(y_i - y_{Ei}) \tag{2.17}$$

where E is the counterflow effectiveness,

$$E = \frac{1 - e^{-\Lambda(1-C)}}{1 - Ce^{-\Lambda(1-C)}} \tag{2.18}$$

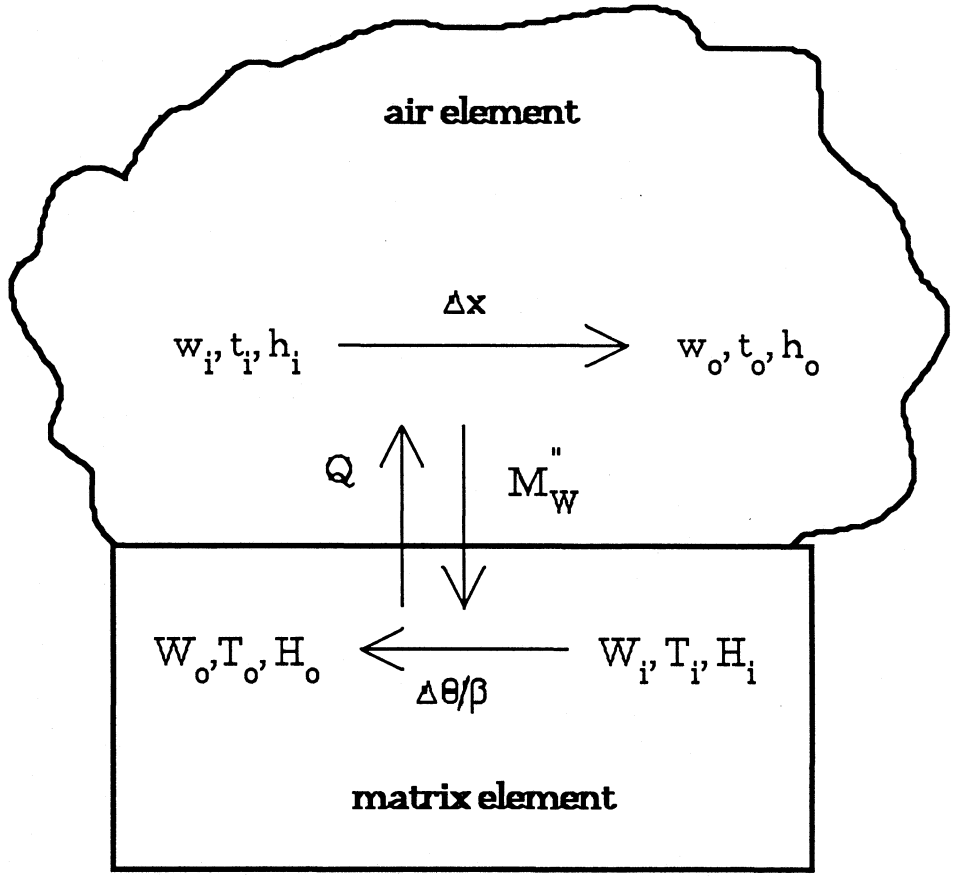

Fig. 2.3 Representative element for "pseudo-steady-state" model in DESSIM.

and the local number-of-transfer-units, Λ, and capacity rate ratio, C, for mass transfer for the element are given by

$$\Lambda_m = Nt u_y \Delta x \qquad C_m = \frac{1}{\sigma_m \beta \Gamma} \frac{\Delta\theta}{\Delta x}$$

$$\sigma_m = \frac{1+w_E}{1+w} \frac{1+w_E}{1+W} \frac{\partial W}{\partial w_E}\Bigg)_T \tag{2.19}$$

The subscript j denoting the period under consideration has been dropped for convenience. The derivatives of matrix properties will be written on a dry mass basis as the property relations, Eqs. (2.7), are generally of this form and have already been worked out for use in MOSHMX. σ_m is analogous to the ratio of specific heats for heat transfer. The derivative term replaces the inverse of the Henry number used in gas/liquid mass exchangers (Edwards, et al., 1973). The water adsorbed by (or desorbed from) the matrix element is then determined from a simple mass balance,

$$W_o = W_i - \frac{1}{\beta\Gamma} \frac{\Delta\theta}{\Delta x} (w_o - w_i) \tag{2.20}$$

Second, an energy balance is performed on the matrix alone (no heat transfer to the air) to account for the thermal energy released by the adsorbed water. The resulting intermediate matrix temperature is given by

$$T_\star = T_i + (h_s / c_M)(W_o - W_i)$$

$$c_M = c_{DM} + W_o c_{WL} \tag{2.21}$$

In Barlow's development, the heat of sorption is approximately accounted for by a separate term in the intermediate energy balance rather than through the integral heat of wetting term in the matrix enthalpy function (Eq. B.??). As a result, the specific heat of the matrix incorrectly neglects the temperature dependence of the integral heat of wetting (compare Eq. (2.21) with Eq. (2.33)), although the error is only about 3% for a silica gel matrix.[4]

Third, the heat transfer from the matrix to the air stream is calculated considering the element to be a counterflow heat exchanger. The "outlet" air temperature is given by

$$t_o = t_i - E_h(t_i - T_*) \tag{2.22}$$

where Eq. (2.18) is used for the effectiveness with the following parameters,

$$\Lambda_h = Le_o Ntu_y \Delta x \qquad C_h = \frac{1}{\sigma_h \beta \Gamma} \frac{\Delta\theta}{\Delta x}$$
$$\sigma_h = c_M / c_A \tag{2.23}$$

A final energy balance then determines the "outlet" matrix temperature at the end of the time step,

$$T_o = T_* + \frac{1}{\sigma_h \beta \Gamma} \frac{\Delta\theta}{\Delta x}(t_i - t_o) \tag{2.24}$$

The "outlet" states of an element are calculated by one pass through the

---

[4]This is for the Brandemuehl isotherm (IDES=B) in Appendix B, which is similar in formulation to that used by Barlow in his original development of DESSIM. For Van den Bulck's isotherm (IDES=A), the integral heat of wetting is independent of temperature.

above set of equations resulting in a potentially efficient numerical procedure. Property evaluations are made at the "initial" conditions that exist when the calculations are performed. Two time step sizes are used. The size is changed when the outlet humidity ratio from the wheel passes through its minimum (maximum) value during the process (regeneration) period. Choice of space and time step size is at the discretion of the user; optimum values must be determined through numerical experimentation and past experience.

To determine the periodic steady-state solution of a dehumidifier, a transient procedure identical to that in MOSHMX is used. The periodic steady-state condition is reached when the average air outlet state from one revolution is within a small tolerance of the state from the previous revolution as measured by the amount of water adsorbed during the process period.

2.3.2 Modifications to PSS model

Eqs. (2.21) and (2.24) do not explicitly conserve energy due to the nonlinear nature of the coefficients with respect to the dependent variables.[5] This situation is easily corrected by replacing these equations with

$$\begin{aligned} H_{\star} &= H(T_i, W_i) - (1/\beta\Gamma)\,[h(t_i, w_o) - h(t_i, w_i)] \\ T_{\star} &= T(H_{\star}, W_o) \\ H_o &= H_{\star} - (1/\beta\Gamma)\,[h(t_o, w_o) - h(t_i, w_o)] \\ T_o &= T(H_o, W_o) \end{aligned} \tag{2.25}$$

[5]Energy balances were not checked in Barlow's original program. This author has inserted a calculation of the energy balance closure into the version of the program used here.

respectively, where enthalpy is used as an intermediate dependent variable and the corresponding temperatures are found from the property relations. When modeling a dehumidifier at periodic steady-state, this formulation significantly improves the energy balance closure to the same order of magnitude as for MOSHMX.

Coupling between the heat and mass transfer can be introduced by replacing Eq. (2.17) with

$$Y_o = Y_i - E_m(Y_i - Y_E(T, W_i))$$

where the equilibrium mass fraction is evaluated at the average matrix temperature for the time step. This can also be written as

$$Y_o = Y_i - E_m(Y_i - Y_{Ei}) + E_m \frac{1}{2} \frac{1}{(1+w_E)^2} \frac{\partial w_E}{\partial T}\Bigg)_W (T_o - T_i) \qquad (2.26)$$

where Y_E has been expanded in a Taylor's series about T. An iterative procedure is now required to solve the complete set of equations which destroys the simplicity of the "pseudo-steady-state" concept.

2.3.3 Alternate set of finite difference equations

Writing Eq. (2.8b) on a wet-mass basis and combining with Eq. (2.8a) results in the following transfer rate equation,

$$\frac{\partial Y}{\partial \theta} = \left(\frac{1-Y}{1-y}\right)^2 \frac{Ntu_y}{\beta\Gamma} (1-y)\,(Y_E - y) \qquad (2.27)$$

which can be written as

$$\frac{\partial y_E}{\partial \theta} - \frac{1}{(1+w_E)^2}\frac{\partial w_E}{\partial T}\Bigg)_W \frac{\partial T}{\partial \theta} = \frac{1}{\beta\Gamma\dfrac{(1+w_E)^2}{1+w}\dfrac{\partial W}{\partial w_E}\Bigg)_T} Ntu_y (y_E - y) \tag{2.28}$$

by expressing the time derivative of $Y(T, y_E)$ in terms of T and y_E.

Using a differencing scheme identical to that used in MOSHMX (see Eq. (2.11)), the following set of equations is obtained,

(2.29)

$$y_o = y_i - K_m(y_i - y_{Ei}) + K_m \frac{1}{2}\frac{1}{(1+w_E)^2}\frac{\partial w_E}{\partial T}\Bigg)_W (T_o - T_i) \quad \text{(a)}$$

$$W_o = W_i - \frac{1}{\beta\Gamma}\frac{\Delta\theta}{\Delta x}(w_o - w_i) \quad \text{(b)}$$

$$t_o = t_i - K_h(t_i - T_o) + K_h \frac{1}{2}\frac{h_s}{c_M}(W_o - W_i) \quad \text{(c)}$$

$$T_o = T_i + \frac{h_s}{c_M}(W_o - W_i) - \frac{1}{\sigma_h\beta\Gamma}\frac{\Delta\theta}{\Delta x}(t_o - t_i) \quad \text{(d)}$$

The "effectiveness" parameters, K_m and K_h, are given by

$$K = \frac{\Lambda}{1 + (\Lambda/2)(1+C)} \tag{2.30}$$

This equation is identical in form to that obtained by Lambertson (1958) in his finite difference analysis of rotary sensible heat exchangers. The appropriate parameters for mass and heat transfer are

$$\Lambda_m = \frac{Ntu_y}{1+w}\Delta x \qquad C_m = \frac{1}{\sigma_m\beta\Gamma}\frac{\Delta\theta}{\Delta x} \qquad \sigma_m = \left(\frac{1+w_E}{1+w}\right)^2 \frac{\partial W}{\partial w_E}\Bigg)_T \tag{2.31}$$

$$\Lambda_h = Le_o Ntu_y \Delta x \qquad C_h = \frac{1}{\sigma_h \beta \Gamma} \frac{\Delta\theta}{\Delta x} \qquad \sigma_h = \frac{c_M}{c_A} \tag{2.32}$$

$$c_M = \left.\frac{\partial H}{\partial T}\right)_W = c_{DM} + W c_{WL} + \left.\frac{\partial \Delta H_w}{\partial T}\right)_W \tag{2.33}$$

Note that the temperature dependence of the integral heat of wetting has been correctly accounted for. As for MOSHMX, this difference scheme is also second order accurate. Stability of the numerical solution is maintained by choosing Δx and $\Delta\theta$ such that K is less than unity.

Because of the modular nature of the DESSIM program, it is very easy to insert the various sets of equations into the overall calculational procedure. This has been done by the author for Eqs. (2.29) (referred to as "DES-FD") and for Eqs (2.12) ("DES-MXy"[6]). Again, the nonlinearities in the energy conservation equation prevent Eqs. (2.29) from exactly conserving energy. This problem can be corrected by using enthalpies as intermediate variables ("DES-FDe") as discussed in section 2.3.3. As expected, the two formulations predict nearly identical dehumidifier outlet states as shown in Fig. 2.4. The differences between the DES-FD and DES-FDe results are mainly due to errors in energy closure which are approximately 2 orders of magnitude larger for the DES-FD model. The figure also shows that the discretization errors quickly become negligibly small as the grid size is reduced.

Since Eq. (2.29a) depends on the temperature calculated in Eq. (2.29d),

---

[6]DES-MXy and MOSHMXy predict identical outlet states through 3 decimal places when identical discretizations are used. This verifies that the overall DESSIM structure is equivalent to MOSHMX.

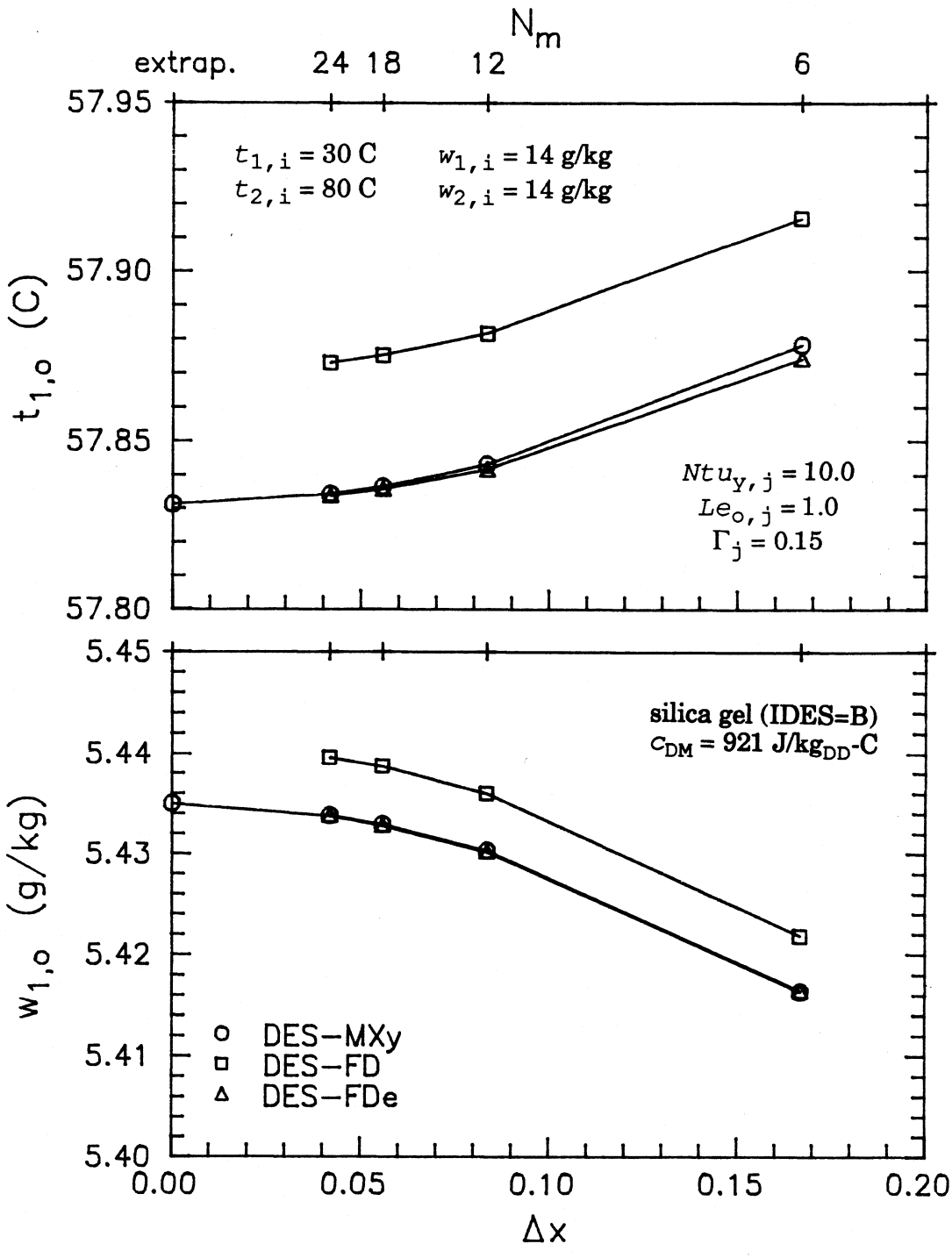

Fig. 2.4 Comparison of the DES-FD and DES-MX models.

an iterative procedure is required. Convergence of various schemes was found to be slow. Because of this, DES-FD requires approximately 5 times the computation time of DES-MXy to determine the steady-state performance of a rotary dehumidifier. However, Eqs. (2.29) have been shown to be equivalent to the MOSHMX equations and are in a form that are easily compared to the PSS equations.

2.3.4 Comparison of the PSS equations with the finite difference equations

For comparison with the finite difference equations, Eqs. (2.29), the PSS equations are rewritten below in which Eq. (2.21) for the intermediate matrix temperature has been substituted into Eqs. (2.22) and (2.24),

(2.34)

$$y_o = y_i - E_m(y_i - y_{Ei}) \qquad \text{(a)}$$

$$W_o = W_i - \frac{1}{\beta\Gamma}\frac{\Delta\theta}{\Delta x}(w_o - w_i) \qquad \text{(b)}$$

$$t_o = t_i - E_h(t_i - T_i) + E_h\frac{h_s}{c_M}(W_o - W_i) \qquad \text{(c)}$$

$$T_o = T_i - \frac{h_s}{c_M}(W_o - W_i) - \frac{1}{\sigma_h\beta\Gamma}\frac{\Delta\theta}{\Delta x}(t_o - t_i) \qquad \text{(d)}$$

Comparison of Eqs. (2.34b,d) and Eqs. (2.29b,d) show that the water and energy conservation equations are identical. The major difference occurs in the PSS mass transfer equation, Eq. (2.34a), which lacks the temperature term that couples the heat transfer to the mass transfer in Eq. (2.29a). Note that the modification to the PSS model through Eq. (2.26) results in the correct coupling.

Other major differences occur in the "effectiveness" relations, Eqs. (2.18) and (2.30), and the absence of a factor of $^1/_2$ in the third term of PSS Eq. (2.34c) compared with Eq. (2.29c). The definitions of the "effectiveness" parameters, Λ and C (Eqs. (2.19,23) and (2.31-33)), and the states used to evaluate properties represent minor differences.

The finite difference "effectiveness", K, and the PSS counterflow effectiveness, E, are compared in Fig. 2.5. The equations are identical for $C = 1$. There is very little difference between the two relations at the same C for $\Lambda < 1$. Therefore, with the proper choice of sufficiently small space and time steps, the use of the counterflow effectiveness in the PSS model should not lead to large errors.

As the space step, Δx (and therefore Λ), decreases, the element "effectiveness" also decreases and so the difference between the element "outlet" and "inlet" states becomes small. In Eqs. (2.29a,c), the last term goes to zero like K^2 as Δx goes to zero, while the second term goes to zero like K. The last term becomes negligible compared with the second term at sufficiently small space steps. Eqs. (2.34a,c) then become equivalent to Eqs. (2.29a,c). Therefore, the PSS concept and the finite difference solution should converge as the discretization becomes small.

2.3.5 Comparison of the PSS and finite difference solutions

The "pseudo-steady-state" (DES-PSS and DES-PSSe, the energy-conserving version) and finite difference (DES-MXy[7]) solutions are compared

---

[7]DES-MXy was used as the finite difference solution because it is much more efficient computationally.

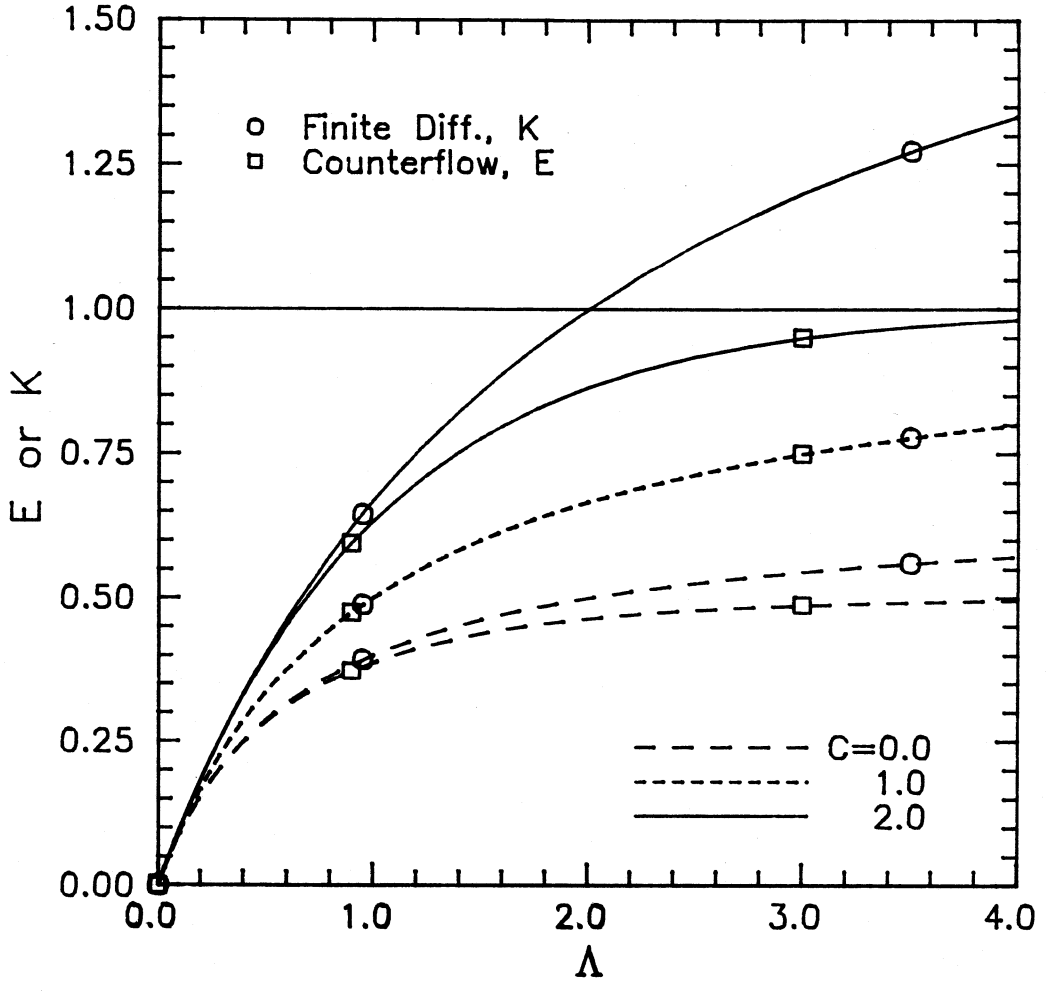

Fig. 2.5 Comparison of DES-FD and DES-PSS "effectiveness" relations.

here by modeling a silica gel dehumidifier at two levels of performance for the conditions shown in Table 2.2. The two time step sizes were chosen based on the discretization derived from the analogy method in MOSHMXy. Using the DES-MXy results extrapolated to zero grid size as a basis, Figs. 2.6 and 2.7 show the differences in the steady-state outlet temperatures and humidity ratios predicted by the models as a function of grid size.

The behavior of the DES-PSS solution as the grid size becomes small confirms that it does indeed converge to the finite difference solution as discussed in the previous section. Errors caused by the nonconservation of energy tend to be small. However, the discretization errors tend to be much larger for the PSS models than for the finite difference solution, especially when a second large time step ($\Delta\theta_2$) is used. For small Δx where the "effectivenesses" E and K are nearly equal, the absence of the temperature term in the PSS mass transfer equation, Eq. (2.34a), is responsible for much of the error. Without this term, DES-PSS tends to overpredict the amount of water adsorbed in the process period, resulting in a lower outlet humidity ratio. Because more water is transferred, more adsorption energy is released, resulting in a higher process outlet temperature from DES-PSS. For large Δx, the "effectiveness" E_y can be sufficiently less than K_y that DES-PSS underpredicts the amount of water adsorbed in the process period, resulting in a larger outlet humidity ratio. In addition, the heat transfer is also underpredicted, resulting in a lower outlet temperature. A range of other operating conditions showed similar errors.

Fig. 2.8 shows the process stream outlet temperature and humidity profiles as a function of rotation angle. DES-PSS predicts the proper outlet profiles in general. This is because errors passed from one space or time step to

Table 2.2 Description of dehumidifier and conditions modeled for comparison of PSS and finite difference models.

Dehumidifier description and operating parameters:

$t_{1,i} = 30$ C $\qquad w_{1,i} = 14$ g/kg

$t_{2,i} = 80$ C $\qquad w_{2,i} = 14$ g/kg

$Ntu_{y,j} = 10, 20 \qquad \Gamma_j = 0.2$

$Le_{o,j} = 1.0$

silica gel (IDES=B[1])

$c_{DM} = 921$ J/kd$_{DD}$-C

Model parameters:

$$\frac{\Delta\theta_1}{\Delta x \beta_1 \Gamma_1} = 0.454 \qquad \frac{\Delta\theta_2}{\Delta\theta_1} = 1, 10$$

Extrapolated DES-MXy outlet states:

$Ntu_{y,j} = 10$:	$t_{1o,ex} = 58.744$ C	$w_{1o,ex} = 5.471$ g/kg
$Ntu_{y,j} = 20$:	$t_{1o,ex} = 60.707$ C	$w_{1o,ex} = 4.823$ g/kg

[1]See Appendix B.

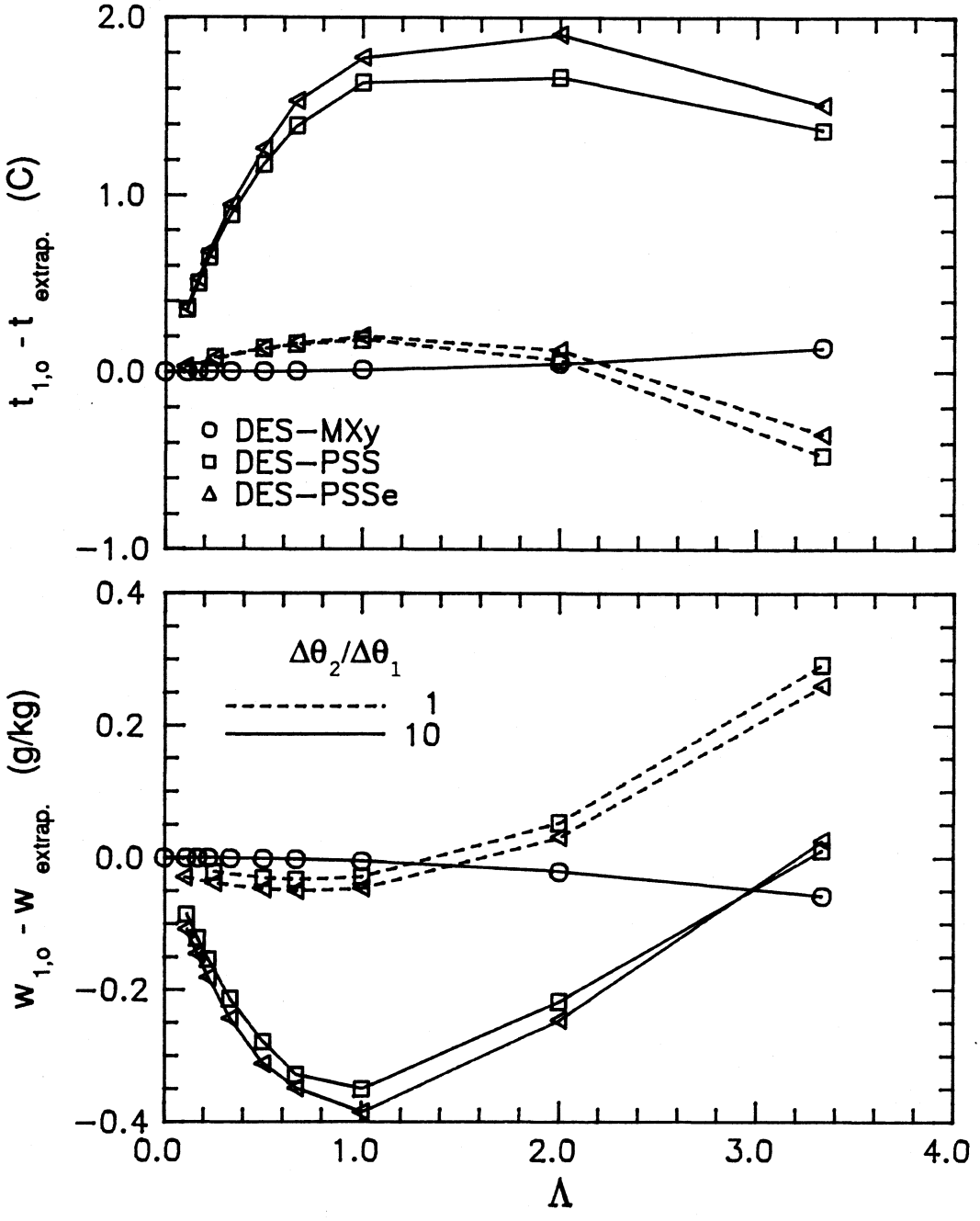

Fig. 2.6 Differences in process stream outlet states predicted by the DES-PSS, DES-PSSe, and DES-MXy models for $Ntu_{y,j} = 10$. The DES-MXy results extrapolated to zero grid size are used as a basis. The dehumidifer and conditions are described in Table 2.2.

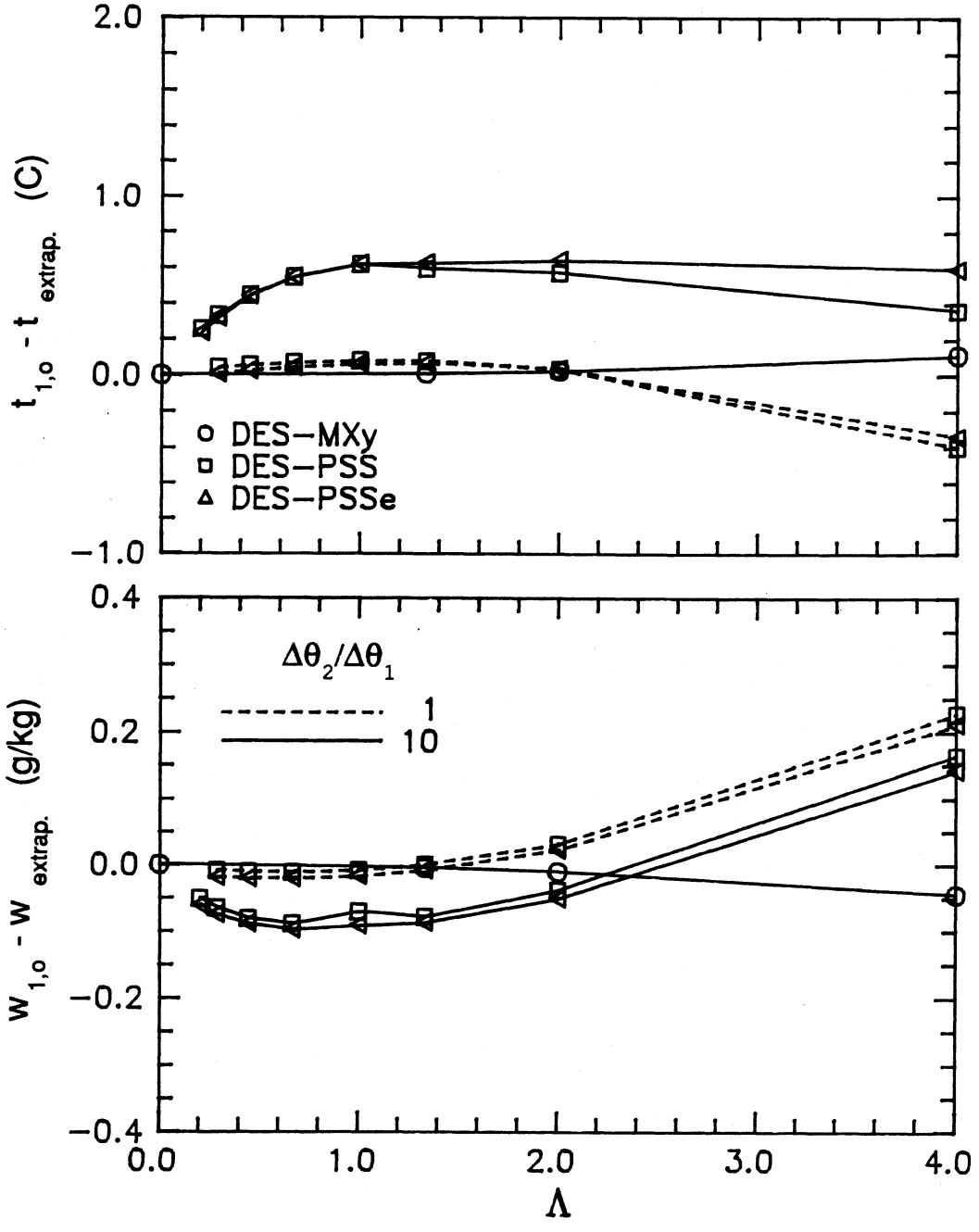

Fig. 2.7 Differences in process stream outlet states predicted by the DES-PSS, DES-PSSe, and DES-MXy models for $Ntu_{y,j} = 20$. The DES-MXy results extrapolated to zero grid size are used as a basis. The dehumidifer and conditions are described in Table 2.2.

the next tend to produce compensating errors. However, DES-PSS predicts an unrealistic initial outlet humidity ratio at $\theta=0$ that is greater than the regeneration inlet state. For large grid sizes, this initial overprediction is significant and adversely affects the profile for the rest of the period. For large time step sizes, the DES-PSS procedure begins to show some apparent instabilities to which the finite difference scheme is not subject. These instabilities are created by the errors, which increase as the time step increases, introduced by the local decoupling of the mass transfer from the heat transfer. In addition, a comparison of the profiles inside the wheel reveals that the DES-PSS errors are even greater there.

Experimentally, the process stream outlet temperature and humidity ratio can be measured practically to within ± 0.5 C and ± 0.2 g/kg, respectively. Therefore, the differences between the PSS solution when carefully done (that is, using small space steps and only one small time step size) and the finite difference solution appear not to be significant. Under these conditions, however, the DES-PSS model requires about 80% more computation time than does the DES-MXy model to achieve the same level of accuracy.

2.3.6 Modeling of a direct solar-regenerated collector/dehumidifier

Several researchers (Ohigashi, et al., 1983; Saito, 1987) have proposed regenerating the desiccant by direct exposure to solar radiation rather than relying on convection heat transfer from a (solar) heated air stream. In addition, the collector and dehumidifier are combined into one component. Finite difference models were used in these studies to investigate the performance of the devices.

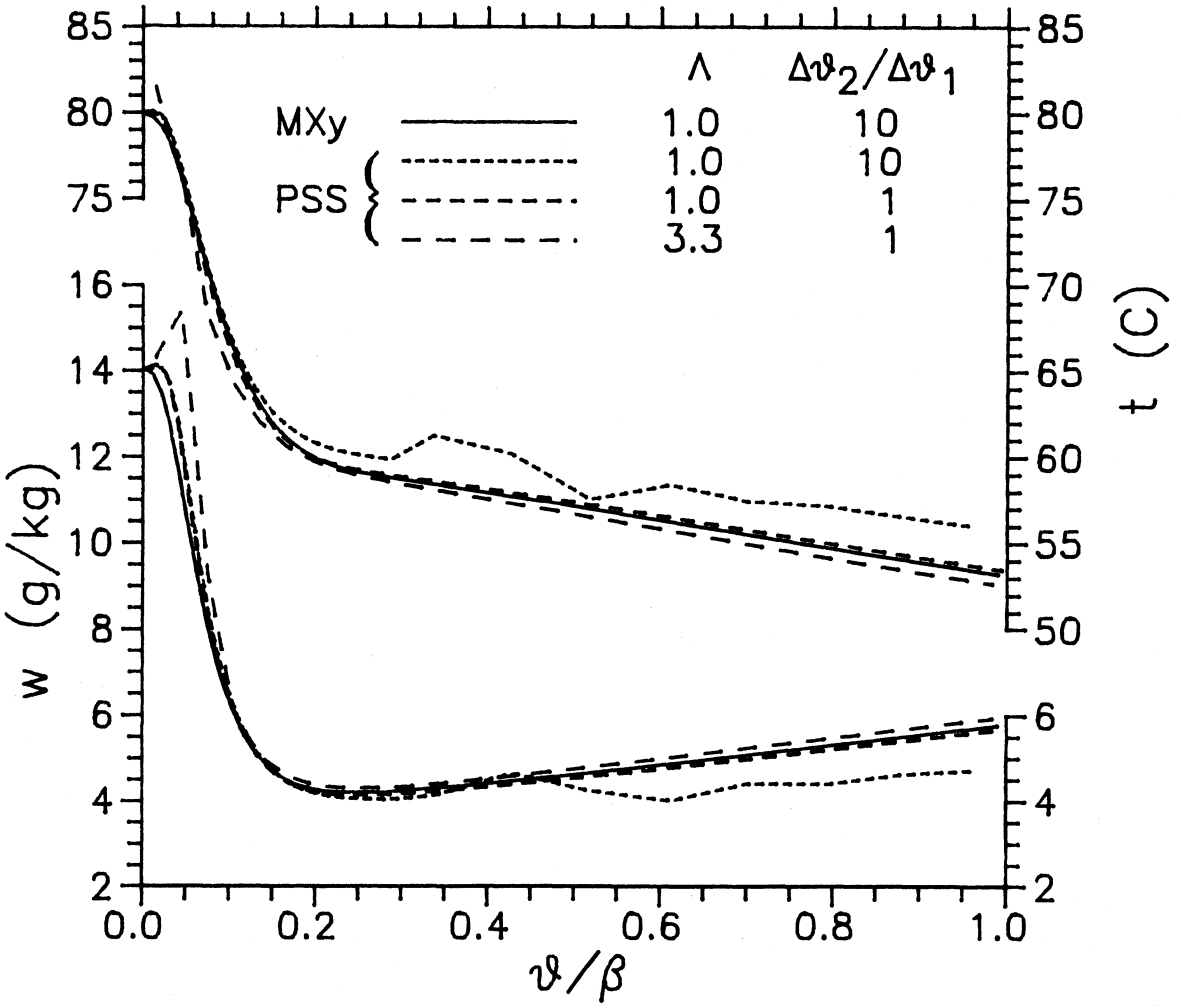

Fig. 2.8 Process stream outlet state profiles predicted by DES-PSSe and DES-MXy.

In the direct solar-regenerated collector/dehumidifier studied by Schultz, et al., (1987) a desiccant-coated "belt" rotates through a solar collector where the regeneration energy is supplied by direct absorption of solar radiation. To model this device, the PSS model was modified to account for the solar radiation gain by including an additional term in the intermediate energy balance, Eq. (2.21),

$$T_* = T_i + [h_s (W_o - W_i) + Q_s] / c_M \tag{2.35}$$

where

$$Q_s = [F_R (\tau\alpha) I_s - F_R U_L (T_i - t_\infty)] \Delta\theta T / (M_{DD}/A_s) \tag{2.36}$$

is the net solar energy gained by the node during the time step and has been modeled following Duffie and Beckman (1980). This approach can also be inserted into the finite difference solutions. The solar gain is easily incorporated into the DES-FD and DES-PSS equations by

$$\text{changing} \quad h_s (W_o - W_i) \quad \text{to} \quad h_s (W_o - W_i) + Q_s$$

in Eqs. (2.29c,d) and Eqs. (2.34c,d), respectively.

During the regeneration period, the energy gain from the solar radiation can be 2-5 times the magnitude of the energy removed as water is desorbed from the matrix. This results in changes in the matrix temperature for the time step that are 1-4 times that of the adiabatic case and in the opposite direction. The errors introduced in the PSS model by locally uncoupling the mass transfer from the heat transfer will then be larger than in the adiabatic case. However, these errors produce compensating effects at the next step, so the overall qualitative description provided by the model should be satisfactory.

The study indicates that a ventilation system employing such a collector/dehumidifier has a very low thermal coefficient of performance ($COP \approx 0.2$) compared with a system with a "conventional" dehumidifier. In addition, extensive collector area is needed to provide sufficient capacity for cooling a typical residence. This and the other studies suggest that these devices can operate effectively at low insolation levels and thus may have some advantages in some geographic regions.

2.4 Conclusions

A comparison of the system of equations used in the "pseudo-steady-state" (PSS) model with a set of finite difference equations has shown that the PSS model ignores the local coupling of the heat and mass transfer processes in a desiccant dehumidifier. It appears that the greatest consequence of this is on the numerical stability of the computational scheme. By careful choice of space and time steps, the PSS model can accurately predict dehumidifier performance relative to a more fundamental finite difference model. However, this requires a greater computational effort.

The heuristic nature of the PSS concept allowed the relatively simple development of a tool for dehumidifier analysis. The above comparison lends support to the results and conclusions reached with the PSS model that have been previously published. It is recommended, however, that future quantitative work be based on a more fundamental development, such as Maclaine-cross' finite difference model.

The MOSHMX finite difference equations, Eqs. (2.12), are second order accurate, stable with respect to time step, and can be solved without iteration.

Substitution of these equations into the overall DESSIM program results in a straightward, accurate, and efficient tool for the investigation of desiccant dehumidifiers. The MOSHMX program contains further enhancements such as improved convergence rate, logical "automatic" choices for step sizes, and extrapolation to zero grid size. However, the difference equations (like most for modeling rotary dehumidifiers) are derived from a set of partial differential equations based on several assumptions, the most questionable of these is the use of an overall, lumped mass transfer coefficient. The rest of this work attempts to evaluate this assumption as well as address several other issues regarding the modeling of "real" dehumidifiers.

Chapter 3

Description of Experimental Facility and Data Analysis Procedures

As part of this work, the author had the opportunity to participate in the desiccant cooling research program at the Solar Energy Research Institute (SERI) in Golden, Colorado. The test facility established there was designed to be a flexible apparatus for characterizing the performance of desiccant cooling system components. The author contributed to the design, construction, programming, and operation of the facility. This chapter briefly describes the test facility, experimental procedure, and data reduction process. Further documentation can be found in the following SERI reports: Schlepp, et al., (1984), Schultz and Schlepp (1984), Schultz (1986), Bharathan, et al., (1986a,b).

3.1 General layout of the experimental facility

Fig. 3.1 shows the general layout of the test facility. Figs. 3.2 and 3.3 are photographs of the overall facility and the instrumentation rack. The flow loops are constructed of 0.305 m (12 in.) diameter spiral pipe and contain all equipment and controls necessary to supply two air streams of a given flow rate, temperature, and humidity ratio to the test unit. The test unit consists of the rotary dehumidifier, its housing, and the instrumentation to allow for full characterization of its performance.

Transition sections connect the round duct with the approximately 0.8 m diameter half-circle of the dehumidifier wheel. These sections were meant to expand the air smoothly and provide a uniform velocity field at the inlet face of the dehumidifier. They did not work as planned because of the jet of air leaving

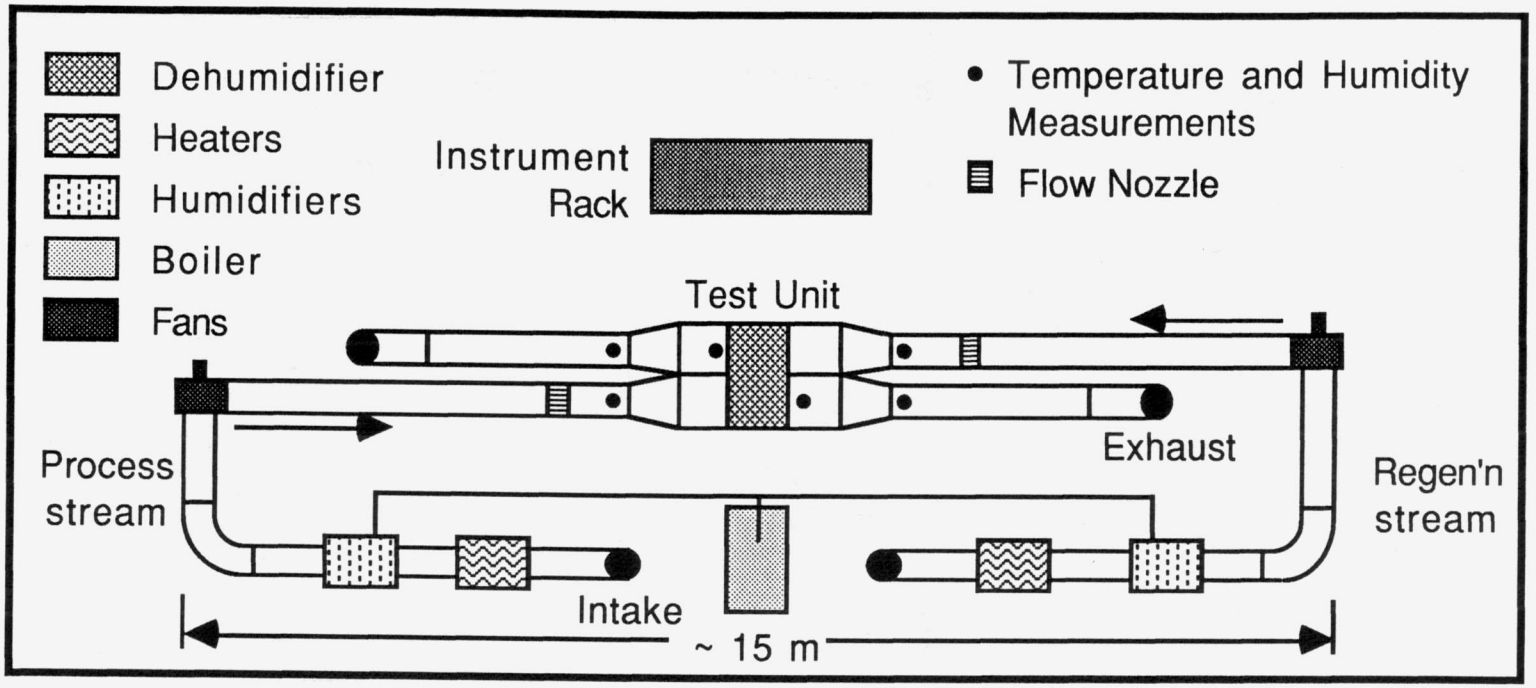

Fig. 3.1 Schematic diagram of the dessicant cooling test facility at the Solar Energy Research Institute.

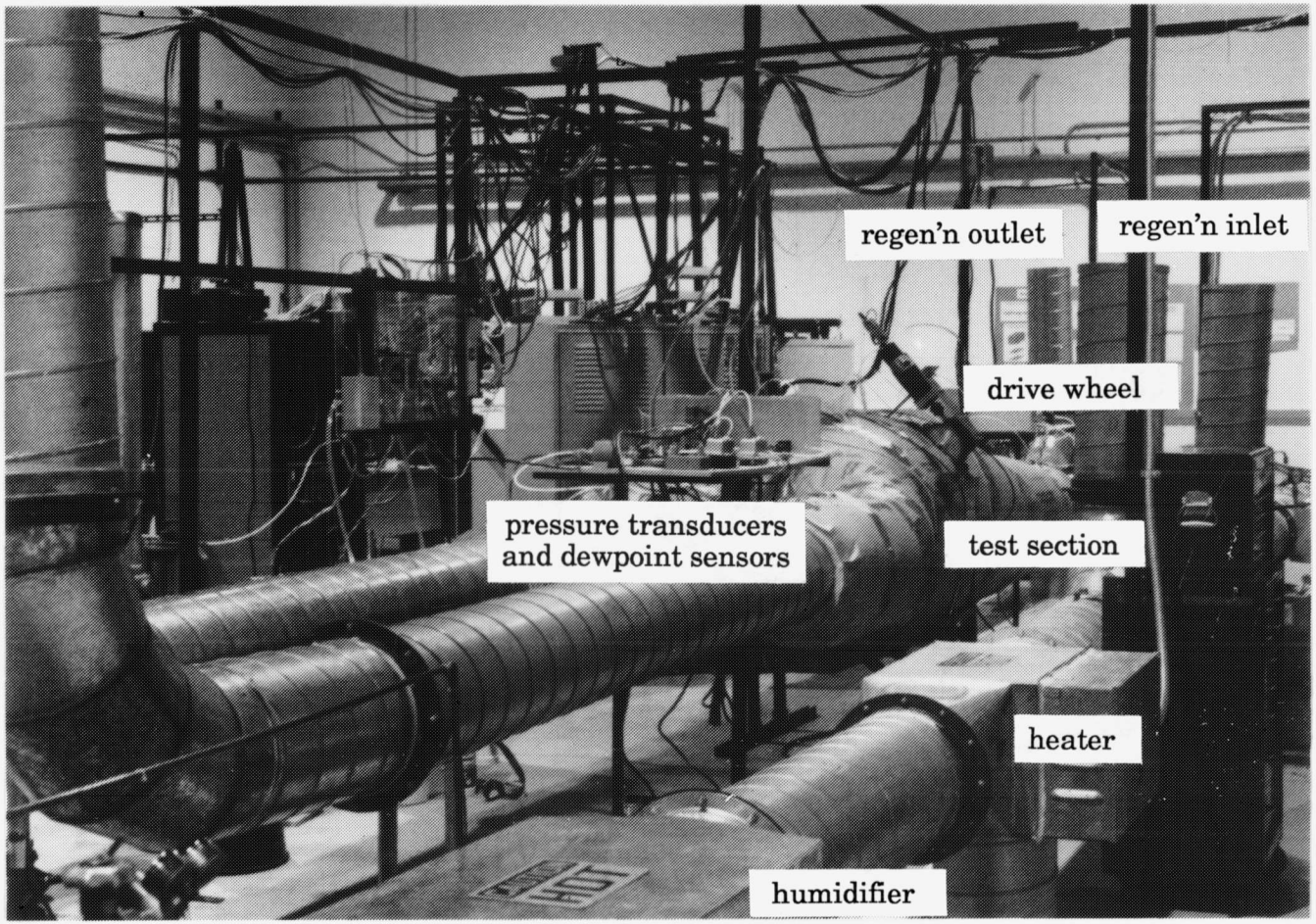

Fig. 3.2 Photograph of the test facility.

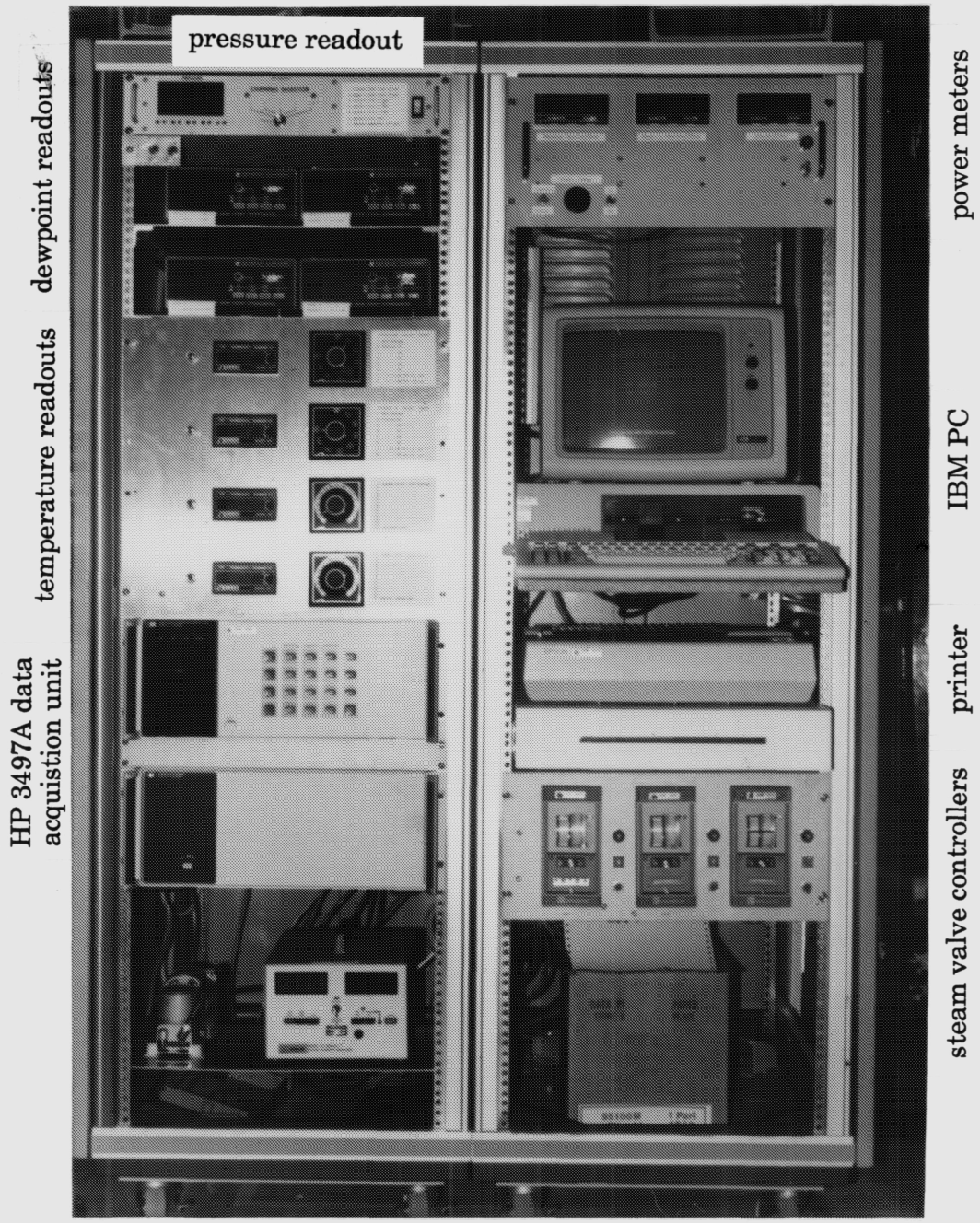

Fig. 3.3 Photograph of the instrument rack for the test facility.

the flow nozzles just upstream of the entrance to the sections. However, measurements of the velocity profiles at the outlet of the dehumidifier indicate a relatively uniform flow through the wheel. The sections of ductwork between the inlet and outlet thermocouple locations are insulated with fiber glass bats to reduce heat losses.

3.2 Instrumentation

Choices of instrumentation and installation were the responsibility of the author. Fig. 3.4 shows schematically the location of the various sensors for the measurements. The measurement uncertainties are discussed in Appendix D and summarized at the end of this chapter.

Temperature measurements are made with copper/constantan (type T) thermocouples. Arrays of four thermocouples in parallel placed just upstream and downstream of the transition sections measure the bulk inlet and outlet temperatures. In these locations, the sensors are exposed to uniform, well-mixed flows. The profiles at the outlet face of the wheel are made with a grid of thermocouples shown in Fig. 3.5.

Humidity measurements are made by pulling a small stream of air through tubes to optical-sensing dew point hygrometers. Four instruments are used; two to monitor the bulk inlet conditions and two for the outlet conditions. During transient operation, the bulk outlet conditions are measured. Once steady-state operation has been reached, the outlet profiles are measured by sampling an array of tubes shown in Fig. 3.5 using switching valves. Standard ASHRAE (1977) relations are used to convert the dew point measurements to humidity ratios.

Pressure measurements are required for several purposes: 1) pressure

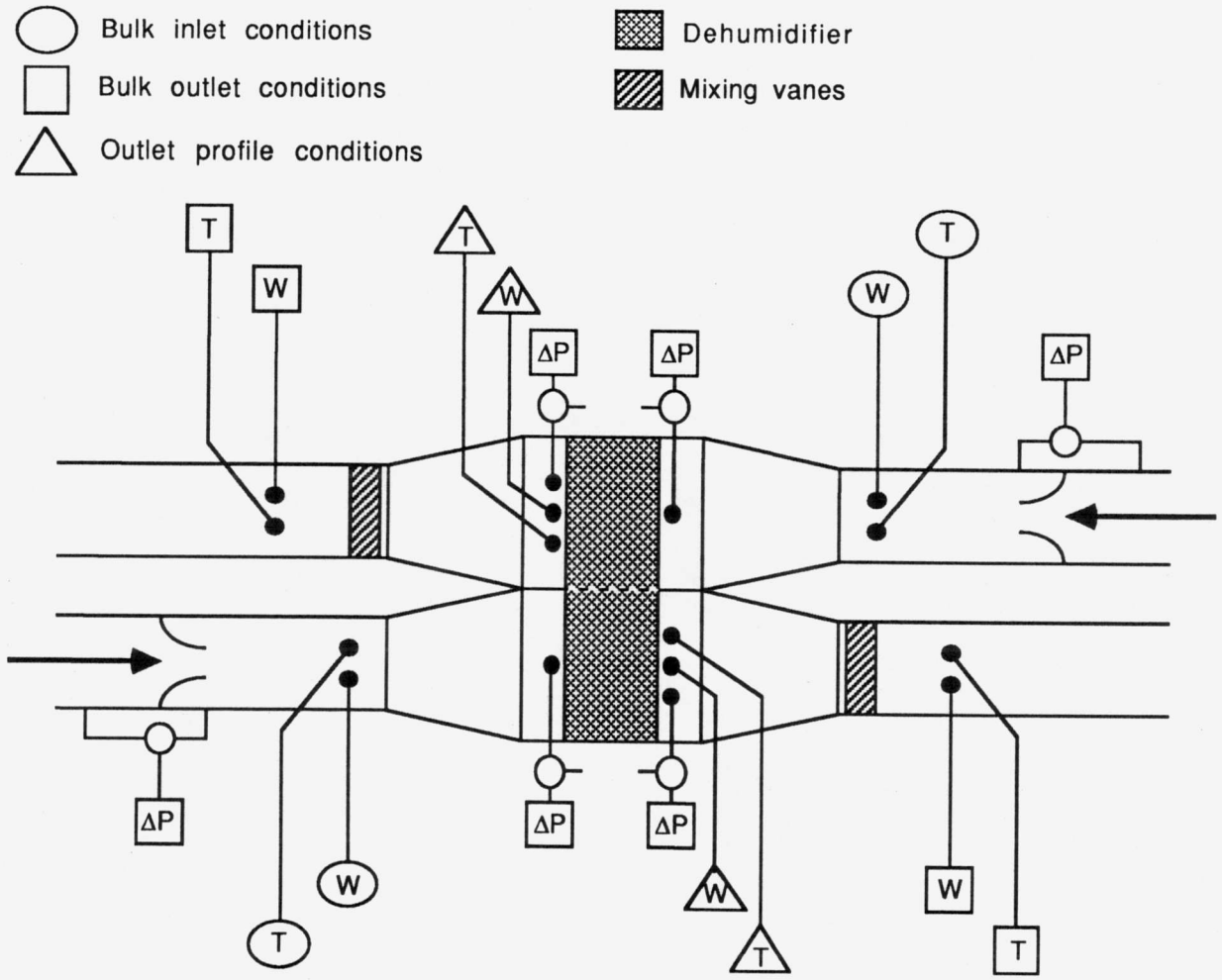

Fig. 3.4 Schematic diagram of measurement sensor locations.

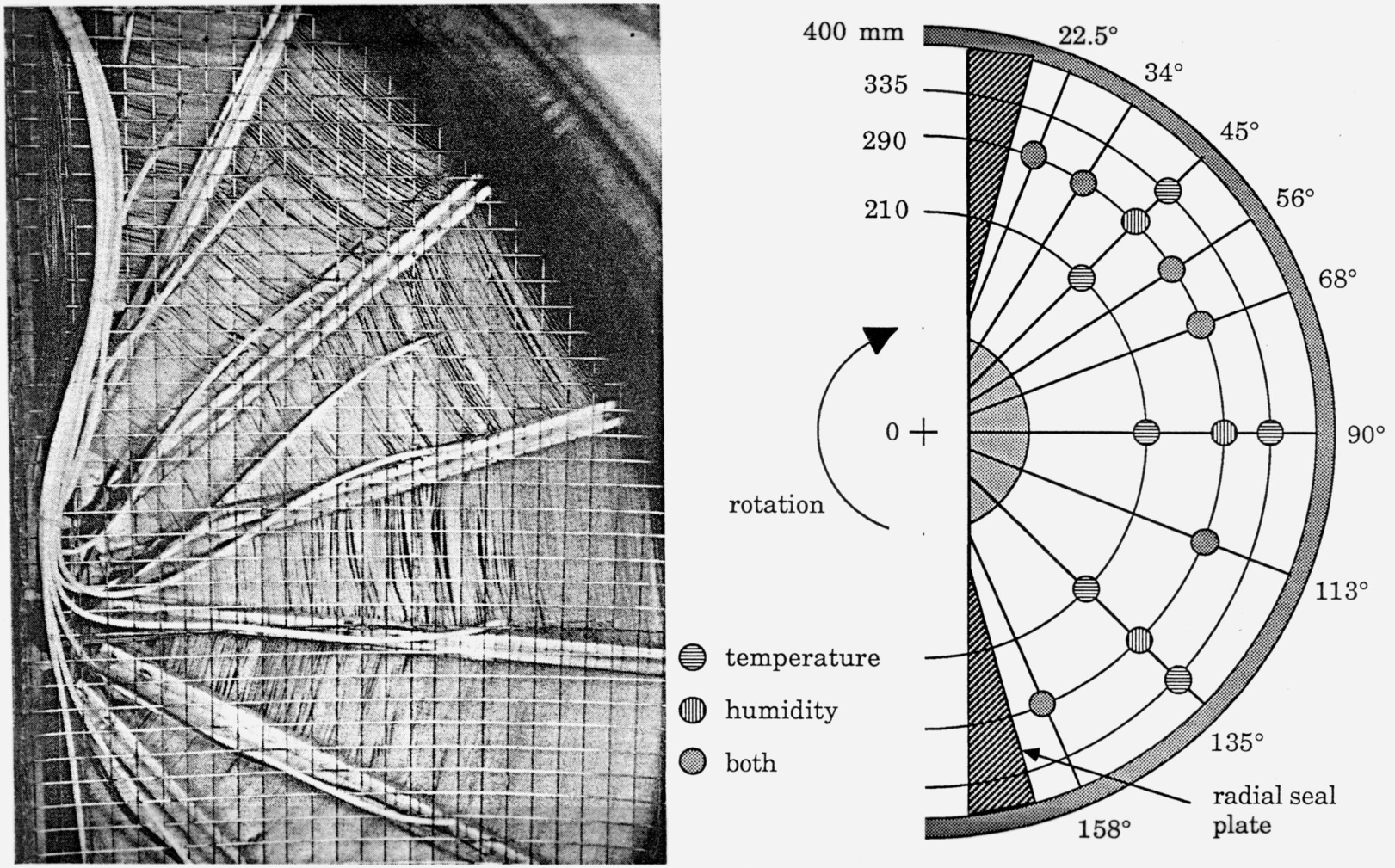

Fig. 3.5 Array of thermocouples and sampling tubes at outlet face of the dehumidifier wheel.

drop characteristics of the wheel, 2) pressure differences that cause leakage across the seals which separate the air streams, 3) pressure differences across the flow nozzles, and 4) absolute pressures for air density and humidity ratio calculations. Capacitance-type sensors are employed. Two differential sensors monitor the flow rates and four measure the pressure difference between each face of the dehumidifier and the ambient. The absolute pressure in the laboratory is measured by another capacitance-type sensor. All required absolute and differential pressures can be calculated from this arrangement.

Air flow rates are obtained by measuring the pressure difference across ASME standard long-radius nozzles of diameter 101.6 mm (4.000 in.). Ten diameters of duct and flow straighteners are present upstream of the nozzles. The discharge coefficient and air mass flow rate are determined from relations in Bean (1971).

The rotation rate of the dehumidifier wheel is measured by monitoring the output of the feedback tachometer on the wheel drive motor. This signal was calibrated by manually timing the dehumidifier rotation speed.

3.3 Equipment and Controls

Air flow rates are controlled by blowers with variable speed motors. The speed of the motor is controlled by a current signal from the data acquisition/control system (DACS). Differential/proportional control through the data acquistion/control program developed by the author is used to update the signal based on the deviation of the measured flow rate from the setpoint. Air mass flow rate can be brought to the setpoint in 20-30 seconds and typically held within ±0.5% of the setpoint.

Temperature of the air streams is controlled by electric resistance heaters.

Energy input is regulated by silicon controlled rectifiers which receive current signals from the DACS. Again, differential/proportional control through the data acquisition/control program is used. The response time of the heaters is rather slow so large "step" changes in temperature can take 5-10 minutes. This needs to be improved for investigations of transient behavior. Once the setpoints have been reached, temperatures can be held within ±0.2 C.

Inlet humidity conditions are maintained by injecting steam produced by an electric boiler into the air streams. Control of steam flow proved to be a difficult task due to boiler pressure flucuations and the highly nonlinear characteristics of the control valves. As the final solution, the process stream humidity is controlled by a hardware differential/integral controller which receives a signal from a relative humidity sensor and sends a signal to a pneumatic control valve. The regeneration humidity is controlled by manually setting the signal to the control valve (which requires constant "tweeking"). The process stream humidity ratio can be maintained to within ±0.3 g/kg of the setpoint. Variations in regeneration stream humidity ratio of ±0.7 g/kg are typical.

The dehumidifier wheel is driven by a DC servomotor turning a rubber-rimmed wheel in contact with the circumference of the dehumidifier. The servomotor is powered by an amplifier which receives a setpoint control signal from the DACS. Tachometer feedback from the motor to the amplifier ensures a constant rotation speed to within ±0.03 rev/hr.

3.4 Data acquistion and control system (DACS)

Data acquistion and system control are coordinated through a Hewlett Packard HP 3497A Data Acquisition/Control Unit. This unit contains a digital

voltmeter with 5-$^1/_2$ digit resolution and 1 μV sensitivity. It also contains cards for receiving data signals and sending control signals.

Sampling, conversion, and storage of data and system control are performed by an IBM PC. Communication between the IBM PC and the HP 3497A occurs over an RS-232 serial interface. Programming is done using IBM BASICA, both interpreted and compiled versions. Data is stored directly to diskettes and also ouput to a line printer.

A flow chart of the structure of the data acquisition/control program developed by the author is shown in Fig. 3.6. In the set-up section, the setpoints for up to 5 experiments can be entered. After an experiment is begun, the computer instructs the data acquisition unit to take the required voltage measurements. Pressure measurements are made by averaging 5 readings taken over a short interval to reduce the effect of turbulence in the flows. A single reading is used for all other measurements. The voltage data is then transmitted to the computer and converted to engineering units. These measurements are compared with the setpoints and the control signals are updated. Finally, the data for the time step is displayed on screen and stored on diskette. This portion of the program takes approximately 6 seconds when running the compiled version. Typically, a 10 second data taking interval is used.

The above sequence occurs in both the transient and steady-state modes. During the steady-state mode, running averages of all the measurements since the steady-state mode was entered are updated after each sequence. Entering and exiting the steady-state mode are operator determined. Typically, steady-state conditions are averaged over 10-20 minutes of operation.

After the steady-state mode has been completed, measurements of the outlet temperature and humidity profiles can be taken. Additional temperature

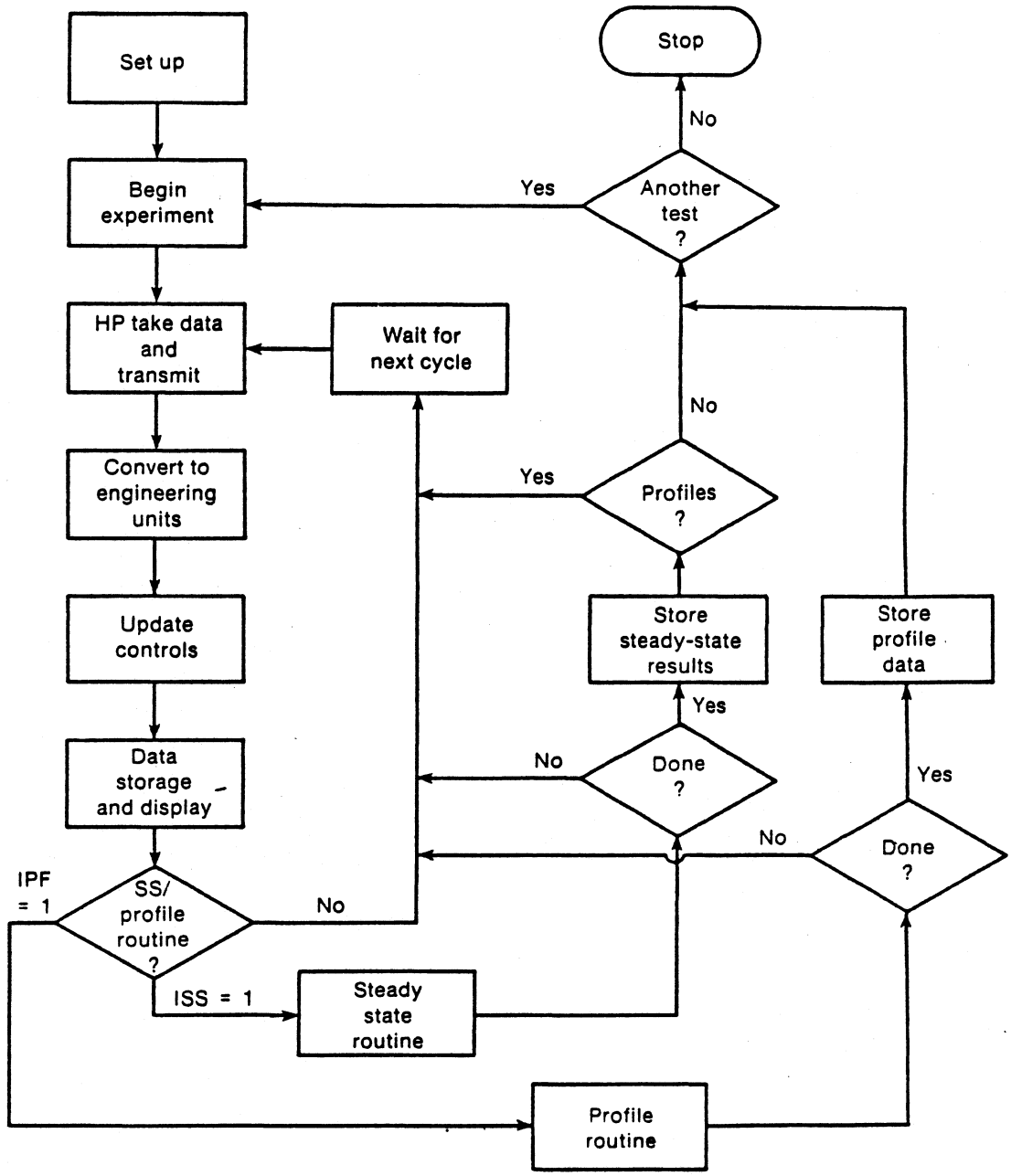

Fig. 3.6 Flow chart of data acquisition/control program structure.

measurements are made and averaged over the duration of the profile measurements. Humidity measurements are made one port at a time per face as selected by a switching valve and averaged over 2-5 minutes (depending on rotation speed) allowing 1 minute for the sensors to equilibrate with each new sample.

3.5 Data analysis procedures

Two corrections are made to the raw data collected in the experiments. First, the effects of air leakage through seals around the dehumidifier and separating the two flow streams is included in the outlet state measurements because of the sensor locations. Since the performance of the dehumidifier matrix alone without regard for the unit packaging is desired, these leakage rates were measured and correlated and the measured outlet states were corrected to the case of no leakage. Second, these corrected outlet states were adjusted by imposing mass and energy balances on the wheel. In addition, the measured pressure drops are corrected for the entrance contraction and exit expansion losses.

3.5.1 Seal leakage corrections

Fig. 3.7 depicts the various paths by which air can leak around the dehumidifier. For the wheel tested by the author (see Chapter 4), a series of tests were run from which each of these leakages could be determined and correlated as a function of the appropriate pressure difference; typical values are shown in Table 3.1. The leakage out of the system occurs through the circumferential seals and then out through the slot in the housing for the drive wheel. The tests showed that some of the air that leaks past the front circumferential seal leaks

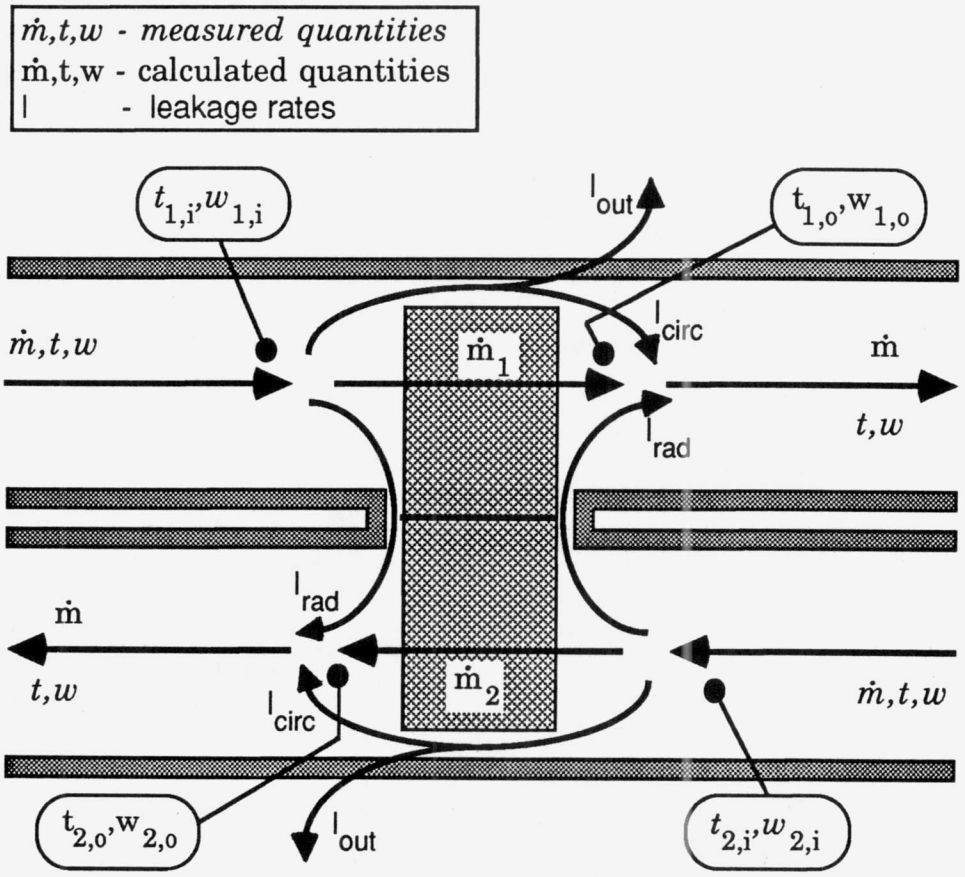

Fig. 3.7 Air leakage paths through the circumferential and radial seals of the dehumidifer.

Table 3.1. Typical seal leakage rates for first wheel.

location	percentage of inlet flow	
	process stream	regeneration stream
out	3.0 - 3.5	1.0 - 1.5
circumferential	2.0 - 2.5	2.0 - 2.5
radial	3.8 - 4.3	3.8 - 4.3

back into the ducting through the back circumferential seal as shown in the figure. The gap between the wheel and the housing is sufficiently narrow to provide the pressure drop necessary for this to occur.

For the two wheels tested by SERI, similar tests were done (Bharathan, et al., 1986a,b). However, the circumferential leakage was assumed to be across the seal from inside to outside for both the front and back seals. It may have been that the gap between the wheel and the housing was larger for these wheels, resulting in essentially ambient pressure in the gap. However, this can not be verified and seems unlikely from the dimensions reported for these wheels (Bharanthan, et al., 1986a,b).

Because of the leakage rates, the mass flow rate through the wheel is less than the measured value and the outlet states measured downstream of the wheel contain the effects of mixing of the leakage flows with that from the wheel (see Fig. 3.7). To obtain the performance of the dehumidifier wheel alone (the outlet states shown in boxes in Fig. 3.7), the measured data from the experiments were corrected for these leakage rates using simple mass and energy balances applied to the mixing processes. For the first wheel tested, the temperature corrections were generally less than 0.1 C and those for humidity ratio ranged from 0.1-0.4 g/kg.

3.5.2 Mass and energy balance closure

Errors in the mass and energy balance closures (using the data corrected for leakages) are given by

$$E_w = \sum_j \dot{m}_{DA,j} (w_{j,i} - w_{j,o})$$
$$E_h = \sum_j \dot{m}_{DA,j} (h_{j,i} - h_{j,o}) \qquad (3.1)$$

The measured inlet states are assumed to be accurate, in part because they are not affected by the leakage corrections. The (leakage corrected) outlet states are then adjusted by imposing mass and energy balance closure, for example

$$\begin{aligned} 0 &= \Sigma_j \dot{m}_{DA,j}(w_{j,i} - (w_{j,o}+e_j)) \\ &= \Sigma_j \dot{m}_{DA,j}(w_{j,i} - w_{j,o}) - \Sigma_j \dot{m}_{DA,j}e_j \end{aligned} \tag{3.2}$$

where

$$\Sigma_j \dot{m}_{DA,j}e_j = E_w$$

The errors, e_j, are then assumed to be equal and the outlet states become,

$$\begin{aligned} w'_{j,o} &= w_{j,o} + E_w/(\dot{m}_{DA,1}+\dot{m}_{DA,2}) \\ h'_{j,o} &= h_{j,o} + E_h/(\dot{m}_{DA,1}+\dot{m}_{DA,2}) \\ t'_{j,o} &= t(h'_{j,o}, w'_{j,o}) \end{aligned} \tag{3.3}$$

Further references to dehumidifier outlet conditions in this work will to be to these corrected values. The corrections are generally within the experimental uncertainties (see Appendix D). The mass and energy balance errors relative to the average change in state of the two air streams are calculated as

$$\begin{aligned} E_{wr} &= E_w/[(\Sigma_j \dot{m}_{DA,j}|w_{j,i} - w_{j,o}|)/2] \\ E_{hr} &= E_h/[(\Sigma_j \dot{m}_{DA,j}|h_{j,i} - h_{j,o}|)/2] \end{aligned} \tag{3.4}$$

Typical values for these errors are 0.5% - 3% for mass balances and 5% - 10% for energy balances. The mass balance errors are equally greater than and less than zero indicating that the humidity ratio measurements likely do not contain systematic errors. The energy balance errors are generally positive which indicates there are small heat losses from the system. The larger magnitude of

the relative energy unbalance is a consequence of the nearly isenthalpic nature of the adiabatic sorption process and the small change in enthalpy of each air stream.

3.5.3 Pressure drop corrections

The measured pressure drops include the losses caused by contraction of the air flow from the inlet ducting area to free flow area of the matrix and a similar exit expansion loss. To obtain just the pressure drop of the matrix core, these losses were subtracted from the measured pressure drop,

$$\Delta P_{core} = \Delta P_{meas} - \Delta P_{inlet} - \Delta P_{exit} \tag{3.5}$$

Assuming potential flow in the inlet region, the inlet pressure loss is given by Kays and London (1984) as

$$\Delta P_{inlet} = (1/2\rho)\,(\dot{m}/A_c)^2[1 - (A_c/A_d)^2] \tag{3.6}$$

where A_c is the free flow area of the matrix and A_d is the area of the inlet and exit ducting. The exit "loss" is assumed to be an unrestrained expansion from a parabolic to uniform velocity profile (Kays and London, 1984)

$$\Delta P_{exit} = (1/2\rho)\,(\dot{m}/A_c)^2[(A_c/A_d)^2 - 1 + K_{exit}] \tag{3.7}$$

$$K_{exit} = 1.0 - 2.4(A_c/A_d) + (A_c/A_d)^2 \tag{3.8}$$

The "measured" core pressure drop then includes only the core friction and pressure losses associated with the development of the parabolic velocity profile in the entrance region.

The above corrections were approximately 1% of the core pressure drop and of opposite sign. The total corrections were therefore very small.

3.5.4 Summary

The corrected experimental measurements for the steady-state performance of three dehumidifiers (described in Chapter 4) are reported in Appendix E. The uncertainties in the measurements, including those introduced by the correction procedures, are discussed in Appendix D and are summarized in Table 3.2.

Table 3.2 Summary of uncertainties in corrected experimental measurements.

temperatures	
inlet	±0.37 C
outlet	±0.50 C
air humidity ratios	
inlet	±2.3%
outlet	±2.7%
pressure differences	±1.0%
air mass flow rates	±2.6%
wheel rotation speed	±1.0%

Chapter 4

Description of Test Dehumidifiers

This chapter presents a brief discussion of the matrix geometries that have been considered for use in dehumidifiers and provides a rationale for the parallel plate design chosen for the three dehumidifiers tested at SERI. The construction of the dehumidifiers is described and the dimensional statistics for the three wheels are given.

4.1 Dehumidifier matrix geometries

Desiccant dehumidifiers for air conditioning systems must combine high heat and mass transfer performance and low pressure drop characteristics into a compact design. A variety of dehumidifier matrix geometries have been considered.

AiResearch used a packed-bed of silica gel particles in a drum-type design in their prototype desiccant cooling system (Rousseau, 1982). Van Leersum and Close (1982) have tested a silica gel packed-bed wheel (approx. 3 mm diameter particles). Large desiccant particles were used to allow a reasonable pressure drop. The performance of both of these devices suffered because of the solid-side mass transfer resistance in the particles.

The dehumidifier used by the Institute of Gas Technology (IGT) in its prototype cooling system consisted of a laminar flow corrugated fiber glass matrix impregnated with a molecular sieve (Jurinak, 1982; Barlow, 1983). The level of performance of the system was similar to that of the AiResearch unit (thermal COP $\approx$ 0.5, Macriss and Zawacki, 1982). While having low pressure drop and

high heat transfer performance, Barlow (1983) speculates that the relatively thick walls of the matrix present a significant resistance to the diffusion of moisture.

Researchers at UCLA (Biswas, et al., 1984; Kim, et al., 1985) constructed a dehumidifier for single-blow testing by coating Lexan® sheets with a single layer of small (0.12-0.25 mm) silica gel particles. Barlow (Schlepp and Barlow, 1984) combined this concept with that for spirally winding a polyester film into a parallel plate matrix for sensible heat exchangers developed at the Commonwealth Scientific and Industrial Research Organization (CSIRO), Australia (Dunkle, et al., 1980). A small single-blow prototype has been constructed and tested (Schlepp and Barlow, 1984). The cross-cooled bed developed at the Illinois Institute of Technology (IIT) is also based on the parallel plate design (Worek and Lavan, 1982).

The parallel plate channel has the largest ratio of Stanton number (heat transfer) to friction factor (pressure drop) of any laminar flow parallel channel geometry (Kays and London, 1984). However, difficulties exist in manufacturing such a device, some of which will be apparent in the next section. In any case, the dehumidifiers in the ASK residential desiccant cooling machine and the Cargocaire hybrid system both consist of a laminar flow thin-walled corrugated matrix which has been impregnated with lithium chloride.

The decision to use a parallel plate design for the test dehumidifiers at SERI was based on two considerations. First, the friction factor and heat and mass transfer coefficients for laminar flow between parallel plates (with constant temperature and constant flux boundary conditions) are well established (Kays and London, 1984). Second, it was desired to avoid problems with potential restrictions regarding the use of a commercially available matrix.

4.2 Construction of the test dehumidifiers

Three dehumidifier wheels have been tested at SERI. The first wheel was tested by the author, the others by SERI personnel after the author's return to the University of Wisconsin.

The matrix material for the test dehumidifiers consists simply of a doubled-sided tape (polyester film with acrylic adhesive) coated with a layer of silica gel particles. For the first wheel, approximately 400 m of tape were coated with irregularly shaped crushed-type silica gel particles and spliced into two rolls (Schultz, 1986). These were then shipped to Rotary Heat Exchangers, Pty., Ltd., Australia, for winding using the process by which they produce parallel plate rotary heat exchangers from polyester film. In the process, the tape is spirally wrapped with each winding separated by aluminum spacers held in place by a set of 16 radial spokes. Figs. 4.1 and 4.2 contain pictures of the dehumidifier; a schematic representation is also shown in Fig. 4.2. The wheel is approximately 0.8 m in diameter and 0.2 m in depth. The nominal passage gap is 1.01 mm.

Due to manufacturing difficulties, the windings in the final product were not as tight as desired and the resulting passage spacing was rather nonuniform. This problem was created by compression of the desiccant coated sheet between the spacers. The forces exerted down along the spokes by the outer windings caused the irregular shaped desiccant particles to deform the polyester film (see Fig. 4.5). This compression released the tension of the inner windings, resulting in sagging of the windings.

After testing of this dehumidifier wheel (referred to as the "original" wheel) by the author and his return to the University of Wisconsin, SERI

Fig. 4.1 Photograph of the original dehumidifier wheel tested at SERI.

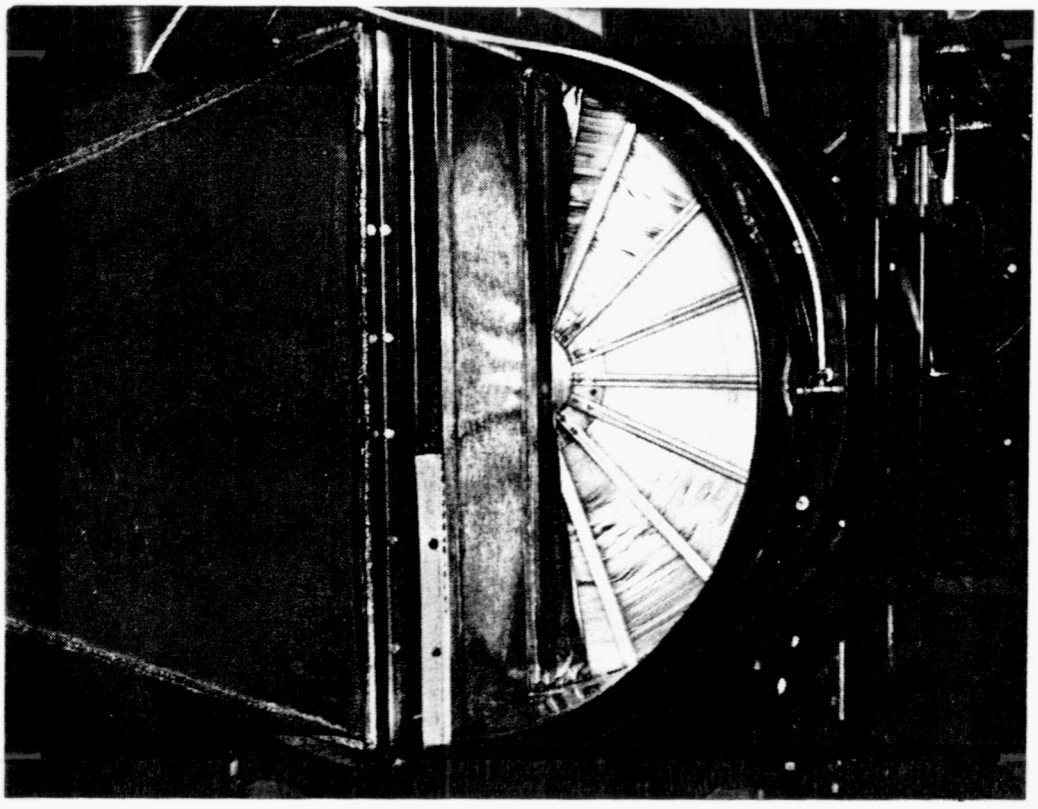

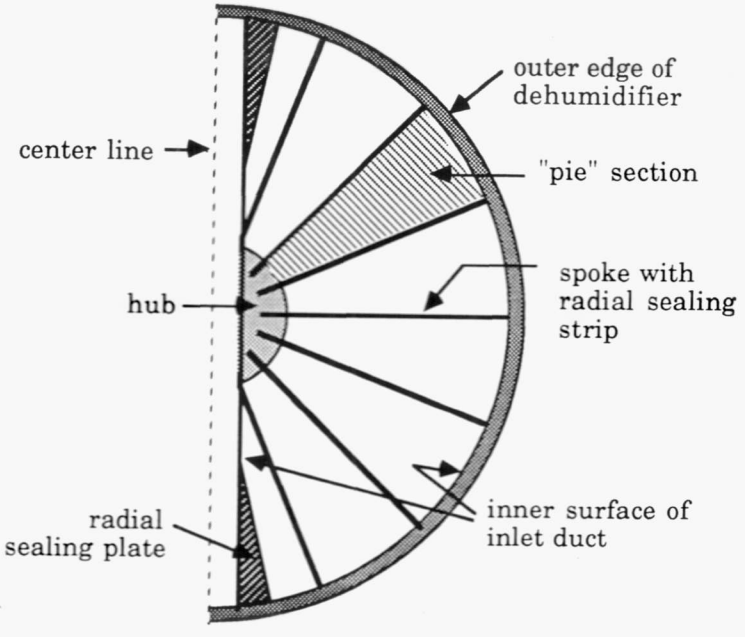

Fig. 4.2 Schematic representation of dehumidifier wheel and housing.

personnel disassembled the wheel and rewound it in an attempt to obtain a more uniformly spaced matrix. In rewinding the wheel, the spacers were epoxied to the spokes to prevent compression of the coated tape (Bharathan, et al., 1986a). Fig. 4.3 appears to indicate that a degree of success was achieved, however, the pressure drop analysis in Chapter 5 shows that a significant distribution of passage sizes remains. The nominal passage gap for this wheel, the "rewound" wheel, is 1.15 mm.

SERI constructed a third wheel using a smaller, spherical, more uniformly sized desiccant particle coated onto a proportionately thinner tape substrate (Bharathan, et al., 1986b). This reduced the compression problem and allowed a very uniformly spaced matrix to be constructed as shown in Fig. 4.4. The depth of this wheel, referred to as the "microbead" wheel, is only 0.1 m. The nominal passage gap is 0.80 mm. The spacers were made from stainless steel.

In addition to the distribution of passage sizes in these wheels, the thermal properties of the matrix are nonhomogeneous due to the localized additional heat capacity of the spokes and spacers. This creates an additional challenge in the modeling of these wheels.

4.3 Dimensional statistics of the test dehumidifiers

Table 4.1 summarizes the physical description of the test dehumidifiers. As pictured in Fig. 4.5, the silica gel particles create a very rough channel surface and make estimation of an effective passage spacing uncertain from geometry considerations alone. The pressure drop and heat and mass transfer results are quite sensitive to the values of the hydraulic diameter and so it is important that the passage gap be known precisely.

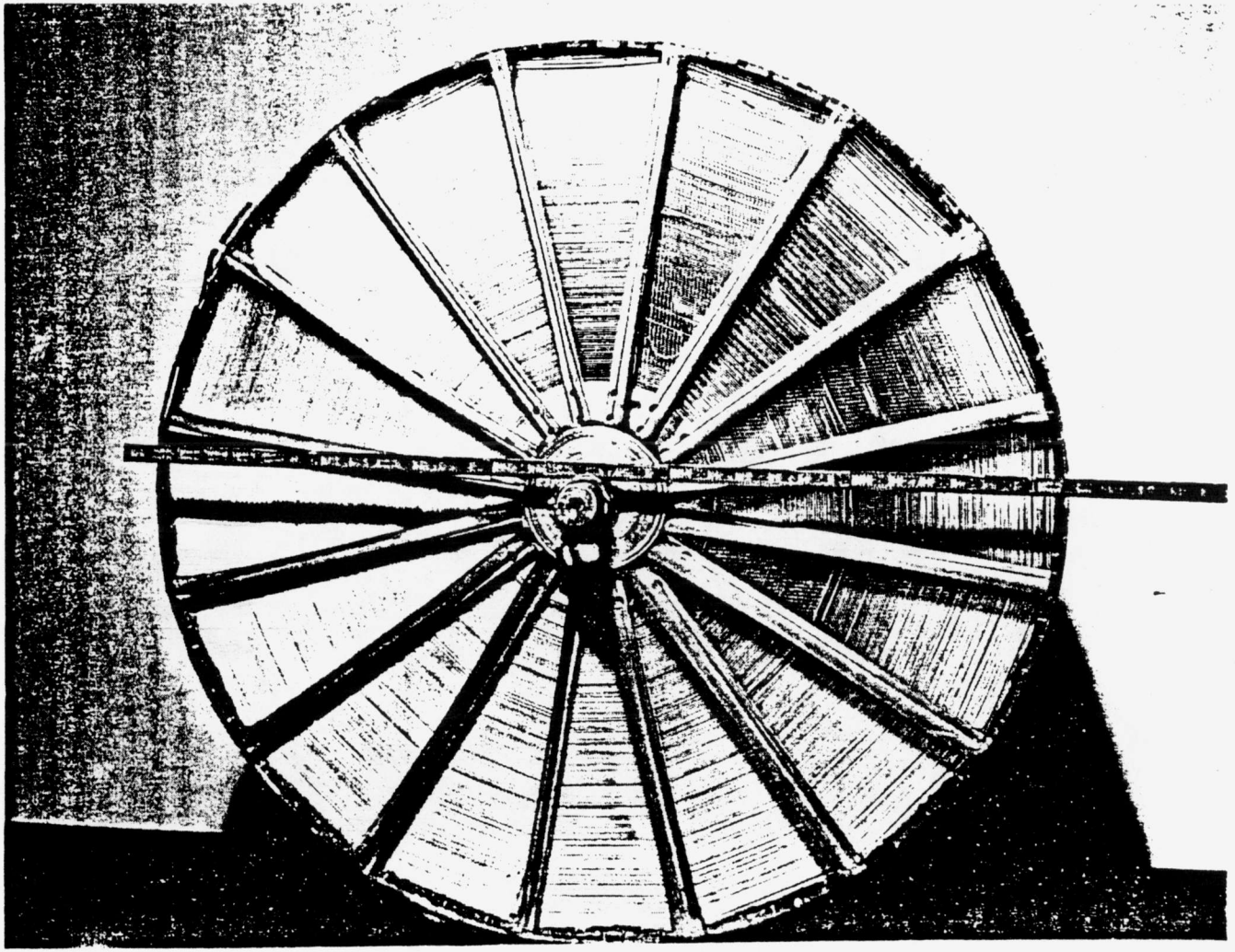

Fig. 4.3 Picture of rewound wheel.

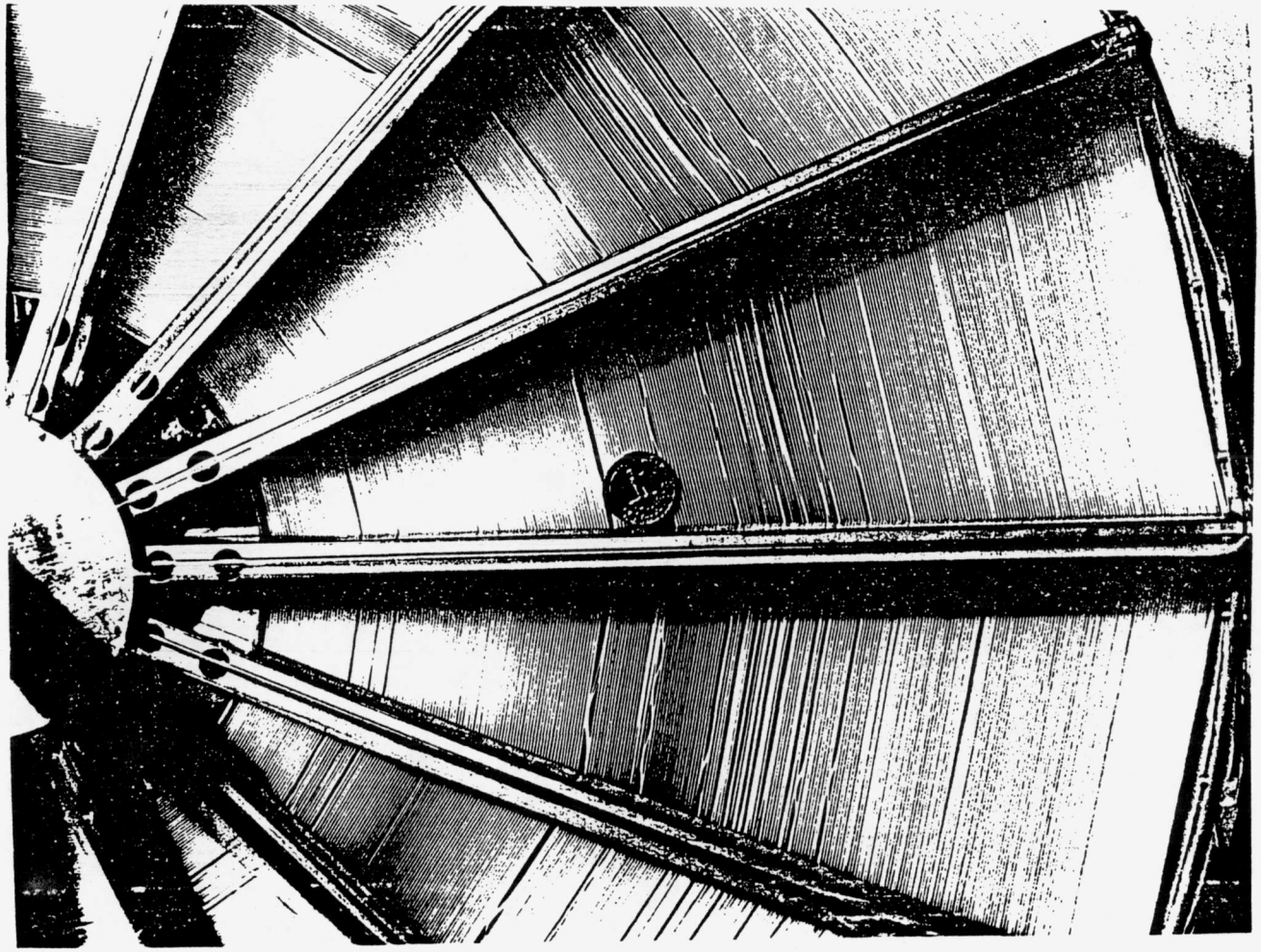

Fig. 4.4 Picture of the microbead wheel.

Table 4.1 Summary of the physical parameters for the test dehumidifiers.

Description	original	rewound	microbead	units
nominal outer diameter	800	800	800	mm
nominal hub diameter	200	200	175	mm
depth of matrix, L	203	203	100	mm
number of tape windings	181	168	302	
Davison silica gel type	grade 11 [1] crushed	grade 11 [1] crushed	grade 3A [2] Microbead™	
particle diameters, D_p				
average	0.27	0.27	0.095	mm
range	.15-.30	.15-.30	.074-.105	mm
tape thickness (polyester)	25 [3]	25 [3]	10 [4]	μm
adhesive (acrylic)	25	25	10	μm/ea.

[1]Davison Chemical Division, W.R. Grace & Co., Baltimore, MD.

[2]Fuji Davison Chemical Ltd., Japan.

[3]ARclad® 5190, Adhesives Research, Inc., Glen Rock, PA.

[4]TESAFIX™ 4973, Tesa Tapes, Inc.

Continued on next page.

Table 4.1 Continued.

Description	original		rewound		microbead		units
nominal passage spacing	1.62		1.76		1.01		mm
effective sheet thicks	0.61	±3%	0.61	±3%	0.21	±3%	mm
nominal passage size	1.01		1.15		0.80		mm
nom. hydraulic dia., D_{hu}	2.02	±2%	2.30	±2%	1.60	±1%	mm
entr. length param., $D_{hu}/4L$	.00249		.00283		.00400		
net face area	.449		.449		.441		m^2
fraction per period, β_j	.465		.465		.465		
void fraction	.623		.653		.792		
flow area per period, $A_{c,j}$	.130	±2%	.136	±2%	.162	±2%	m^2
transfer area per period, $A_{s,j}$	50.8		47.5		41.0		m^2
gel surface density	0.276		0.276		0.091		kg_{DD}/m^2
coated tape density	0.370		0.370		0.121		kg/m^2
calculated gel mass	15.1	±3%	14.1	±3%	4.01	±3%	kg_{DD}
experimental gel mass	13.7	±4%	12.8	±4%	3.63	±4%	kg_{DD}
specific heat of silica gel	921		921		921		J/kg-C
specific heat of tape	1250		1250		1250		J/kg-C
specific heat of spacers	896	(Al)	896	(Al)	460	(SS)	J/kg-C
mass of spacers	8.32		7.72		14.7		kg
calculated specific heat							
tape and gel	1420		1420		1400		J/kg_{DD}-C
with spacers	1965	±10%	1960	±10%	3260	±10%	J/kg_{DD}-C
experimental specific heat							
low rotation speed	3100	±10%	3100	±10%	3100	±10%	J/kg_{DD}-C

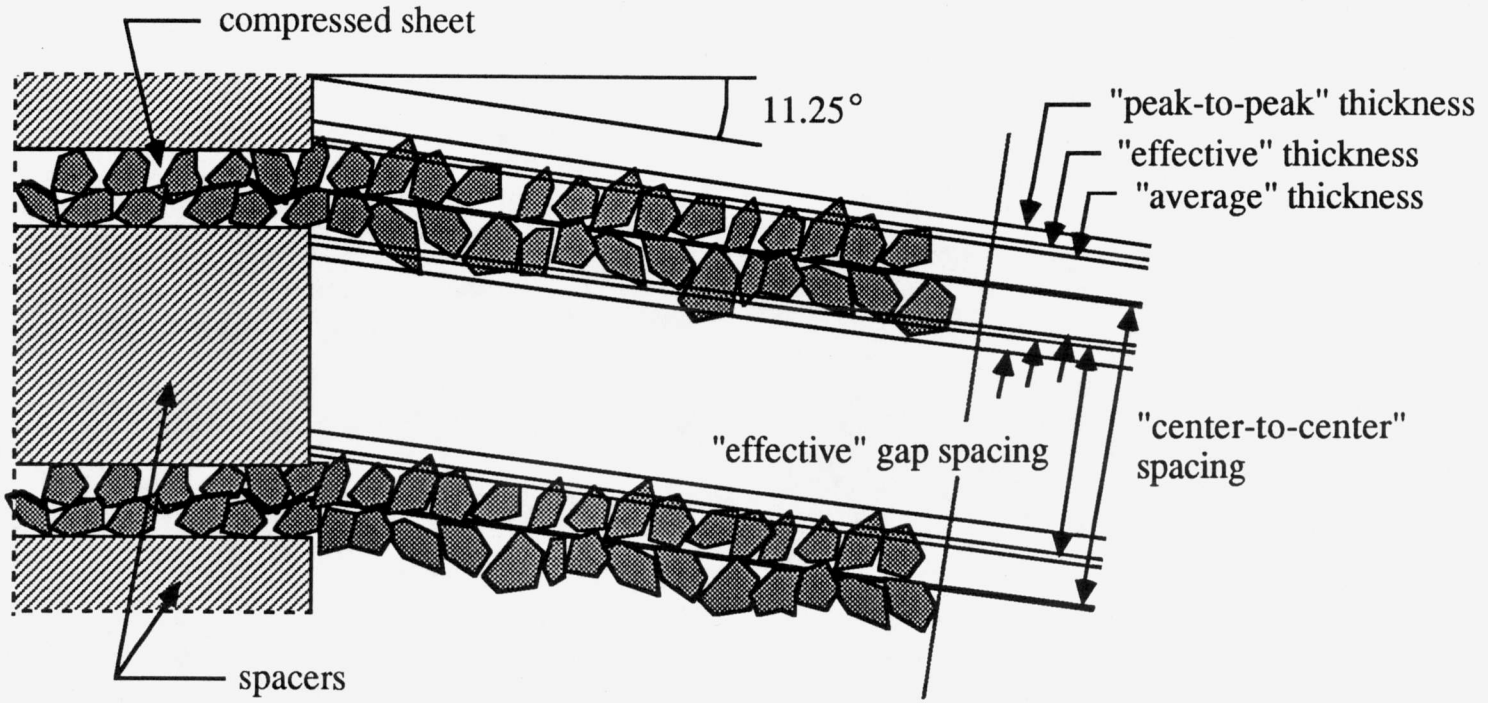

Fig. 4.5 Sketch of representative passage channel.

The "peak-to-peak" thickness of the sheet used in the original and rewound wheels was measured to be 0.70 mm. Based on the average particle diameter of 0.27 mm and a tape thickness of 0.03 mm, the "average" sheet thickness should be 0.57 mm. Van den Bulck (1987) has used this same coated tape in a single-blow matrix in which the passage spacing is very uniform and easily adjustable. From pressure drop results at two different spacings, he determined the effective thickness of the coated tape to be 0.61 mm (±3%). This represents an approximately 4% decrease in the actual hydraulic diameter from that calculated using the "average" sheet thickness. It also indicates that substantial portions of the particles are sticking into the flow stream. The effective thickness of the microbead sheet is taken to be between the "peak-to-peak" (0.24 mm) and "average" (0.20 mm) thicknesses in proportion to that found for original wheel.

The net face area of the wheel includes only the free flow area and that occupied by the desiccant sheets. The area occupied by the spacers (and the sheets between the spacers) and the center hub have been subtracted. The void fraction is calculated from the center-to-center sheet spacing and the effective tape thickness.

The radial seals consist of strips of plastic attached to each spoke. These strips make contact with a wedge-shaped plate as the wheel rotates from one air stream to the next (see Fig. 4.2). The sealing plate is one "pie" section wide and so the minimum face area for a stream is $^{7}/_{16}$ of the net face area. This occurs when one seal begins to make contact as it leaves the period and another breaks contact as it enters the period. The measured pressure drop across the wheel oscillates with an amplitude of approximately ±6% as it rotates. Since the

pressure drop is inversely proportional to the face area for laminar flow, the apparent face area changes ±6% in magnitude depending on the position of the spokes. The average fraction of the face area available to each flow stream is then

$$\beta_j = \frac{7/16}{1 - .06} = 0.465 \tag{4.1}$$

This also indicates that at times nearly half, .465·(1+.06) = .493, of the net flow area is seen by each flow stream as the wheel rotates. The fraction of the total rotation period that a section of the matrix is exposed to an air stream is taken as the average fraction of the face area available to that air stream.

The transfer area is taken simply as the length of tape (estimated from geometrical considerations) times the depth of the matrix multipied by the two sides. The fact that the inside and outside windings have only one surface exposed is accounted for. In Van den Bulck's (1987) analysis, he determined that the effective tranfer area was approximately 5% greater than the actual plate area. This effect is neglected here.

The mass of active gel in the wheels was calculated from measured surface densities and the calculated length of tape. Also shown in Table 4.1 are experimentally determined values for the gel masses. The discrepancies are discussed in section 5.2. The specific heats of the matrices are also discussed there.

The dimensional parameters listed in Table 4.1 may differ from those reported in Schultz (1986) and Bharathan, et al., (1986a,b). It is believed that those reported here are more accurate and are consistent between wheels.

Chapter 5

Analysis of the Experimental Data and Comparison with Models

The experimental data obtained at SERI on the performance of the three desiccant wheels described in the previous chapter are analyzed here. The objective is to verify that the dehumidifier model considered in Chapter 2 (and the assumptions upon which it is based) can accurately predict the behavior of "real" desiccant dehumidifiers.

For any model to accurately predict actual performance, the proper parameters must be supplied. While the use of design information is desirable, it may not always be accurate. In section 5.1, a pressure drop analysis is used to estimate the distributions of passage sizes in the wheels. Results from heat and mass transfer tests at very low rotation speeds are used to check the active amount of silica gel in the wheels in section 5.2. In section 5.3, estimates of the overall heat and mass transfer coefficients are obtained from the results of very high rotation speed experiments. The concepts for the low and high rotation speed analyses were suggested to the author by Maclaine-cross (1985b).

Using the parameters obtained from the above analyses as inputs to the finite difference model MOSHMX, the model predictions are compared against the experimental data for a range of conditions at medium rotation speeds (dehumidification conditions). These results are presented in section 5.4.

5.1 Pressure drop analysis

An analysis of pressure drop can provide information on the flow regime

and allow validation of models useful for predicting the parasitic power requirements of a dehumidifier. The presence of unknown distributions of passage sizes in the wheels tested prevents such confirmation here. However, established theory can be used to estimate the distributions of passage sizes.

5.1.1 General formulation

The pressure drop across each period of the wheel, not including the entrance contraction and exit expansion losses, can be written as

$$\Delta P = \frac{\rho v^2}{2} \frac{4 f_{app} L}{D_{hu}} = \frac{2\mu L}{\rho} \frac{\dot{m}}{A_c D_{hu}^2} (f_{app} Re)_e \tag{5.1}$$

where

$$Re = \frac{\dot{m} D_{hu}}{\mu A_c} \tag{5.2}$$

is the bulk Reynolds number for the period under consideration (the subscript j has been omitted for convenience). This would also be the Reynolds number for a channel if the matrix were uniform. Eq. (5.1) defines the effective dimensionless pressure drop, $(f_{app} Re)_e$. For laminar flow through a uniform matrix, the dimensionless pressure drop can be written as

$$(f_{app} Re)_u = (fRe) + K \frac{Re D_{hu}}{4L} \tag{5.3}$$

The first term represents the pressure loss for fully developed flow in the channels. The second term accounts for the incremental effects of velocity profile development.

The parallel plate channels in the wheels tested are actually narrow rectangles. The nominal (area weighted) aspect ratio is approximately 0.009. The corresponding fully developed friction factor - Reynolds number, (fRe), is 23.7 (Shah and London, 1980). For smooth parallel plates in which the flow becomes fully developed before leaving the channel, Lundgren, et al., (1964) have determined that the entrance coefficient, K, is 0.686. Other results near this value have been obtained (Shah and London, 1978).

5.1.2 Experimental pressure drop results

Values for the effective dimensionless pressure drop have been obtained by Eq. (5.1) from the experimental data for the three wheels and are plotted in Fig 5.1. The results for the original dehumidifier are from heat and mass transfer experiments. Errors in estimating the appropriate average air viscosity may be a partial cause for the spread of the data. No significant difference between the process and regeneration stream can be detected, however.

The pressure drop tests for the rewound and the microbead wheels were done with the wheels in equilibrium with laboratory air conditions; no heat and mass transfer effects are present (Bharathan, et al., 1986a,b). The apparent differences in pressure drop across the two sides of the wheel are suspected to be due to small systematic errors in the pressure measurements. The data reported here are taken from the nondimensional results presented in Bharathan, et al., (1986a,b) and have been adjusted to account for the different values of the parameters used to describe the wheels as noted at the end of Chapter 4.

Also shown in Fig. 5.1 is the dimensionless pressure drop expected for a uniform matrix with smooth passages. The experimental values fall below the

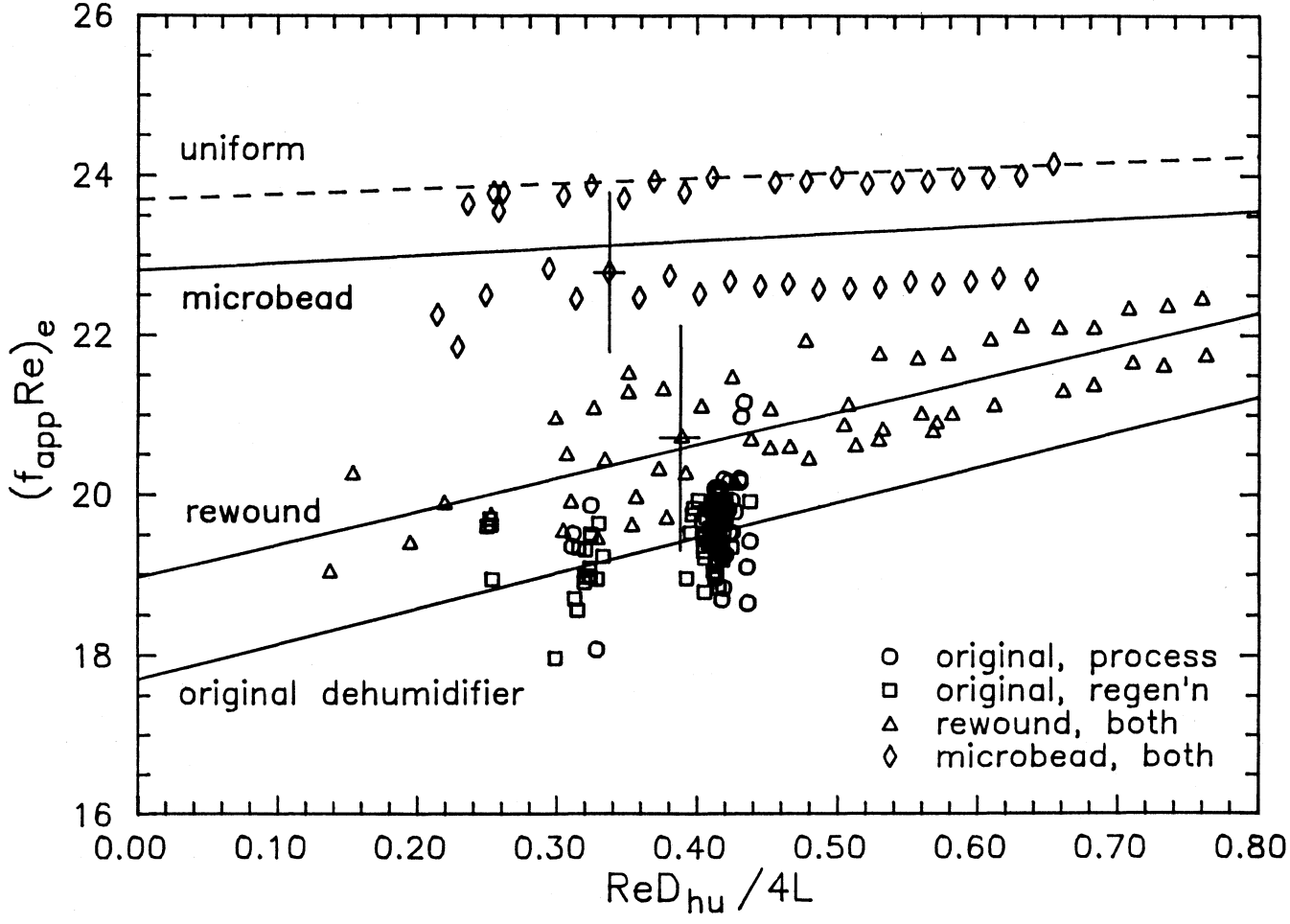

Fig. 5.1 Experimental pressure drop results for the three wheels tested. Estimated uncertainties are shown by the crossed lines (see Appendix D).

uniform result because of the distributions of passage sizes in the wheels which create a maldistribution of flow through the matrices. Shah and London (1980), among others, have suggested a procedure for analyzing this problem. Their procedure will be adapted here to estimate the distribution of passage sizes in the dehumidifiers tested.

5.1.3 Model for distribution of passage sizes

To model this problem, a discrete distribution of passage sizes divided into n bins is considered. Each bin contains a fraction χ_k of the total number of passages. The pressure drop across each passage in a period is the same as the total pressure drop and can be written as

$$\Delta P = \frac{2\mu L}{\rho} \frac{\dot{m}_k}{A_{ck} D_{hk}^2} (f_{app} Re)_k \tag{5.4}$$

where the Reynolds number is for the specific passage being considered,

$$Re_k = \frac{\dot{m}_k D_{hk}}{\mu A_{ck}} \tag{5.5}$$

Equating Eqs. (5.1) and (5.4) results in a relation for the flow rate in each passage, $\dot{m}_k$, relative to the flow rate for a uniform passage, $\dot{m}_u$,

$$\frac{\dot{m}_k}{\dot{m}_u} = \frac{A_{ck}}{A_{cu}} \left(\frac{D_{hk}}{D_{hu}} \right)^2 \frac{(f_{app} Re)_e}{(f_{app} Re)_k} \tag{5.6}$$

For parallel passages, the free flow area for a channel is directly proportional to the hydraulic diameter so that $(A_{ck}/A_{cu}) = (D_{hk}/D_{hu})$. Therefore, the

relative channel flow rate is proportional to the cube of the relative hydraulic diameter. Conservation of mass and of "length" require that

$$\sum_{k=1}^{n} \chi_k \, (\dot{m}_k / \dot{m}_u) \;=\; 1 \qquad\qquad \sum_{k=1}^{n} \chi_k \, (D_{hk} / D_{hu}) \;=\; 1 \tag{5.7}$$

The following relation is obtained for the dimensionless pressure drop by combining Eqs. (5.1), (5.4), and (5.7),

$$\frac{1}{(f_{app}Re)_e} \;=\; \sum_{k=1}^{n} \frac{\chi_k \, (D_{hk}/D_{hu})^3}{(f_{app}Re)_k} \tag{5.8}$$

The denominator in Eq. (5.8) can be written as

$$(f_{app}Re)_k \;=\; (fRe)_k \;+\; K_k \frac{\dot{m}_k}{\dot{m}_u} \frac{D_{hk}}{D_{hu}} \frac{ReD_{hu}}{4L} \tag{5.9}$$

where the Reynolds number for the channel has been written in terms of the bulk Reynolds number. Given a specific distribution, the set of equations Eqs. (5.6), (5.8), and (5.9) can be solved for the dimensionless pressure drop and channel flow rates by a simple iterative procedure.

A 31-bin approximation of a lognormal distribution (Hastings and Peacock, 1975) is used here to represent the rather wide range of spacings in the wheels tested,

$$\chi_k \;=\; \frac{1}{(2\pi)^{1/2}} \, e^{-d_k^2/2} \, \Delta d_k \tag{5.10}$$

where

$$d_k \;=\; ln \, (D_{hk}/D_{hu}) \, / \sigma \qquad\qquad \Delta d_k \;=\; \Delta \, (D_{hk}/D_{hu}) \, / \sigma \, (D_{hk}/D_{hu})$$

The lognormal distribution is a transformation of the normal distribution such that its range extends from zero to infinity. In this way, "negative" channel widths are avoided. With the choice of shape made, the distribution of passage spacings is then represented by a single parameter, σ, the standard deviation.

When the dimensionless pressure drop, $(f_{app}Re)_e$, is plotted against the entrance length parameter, $ReD_{hu}/4L$, for a given standard deviation, a nearly linear relationship results. These curves are well approximated by linear least squares fits over the range of Reynolds numbers considered in the experiments, $0.2 < ReD_{hu}/4L < 0.8$. The y-axis intercept, which represents the effective fully developed friction factor - Reynolds number, $(fRe)_e$, is a function of the standard deviation of the distribution and the entrance coefficient. Fig. 5.2 shows this dependence for the lognormal distribution with $(fRe)_k = 23.7$ and two values of the channel entrance coefficient, K_k, where all channels are assumed to have the same coefficient.

The slopes of the experimental data are greater than Lundren's theoretical value, especially for the original and rewound wheels. The effective slope, K_e, is shown in Fig. 5.3 for various channel entrance coefficients for the lognormal distribution.

5.1.4 Comparison of experiments and model

The distribution of passage spacings for each wheel can be estimated by finding the standard deviation such that the $(fRe)_e$ from Fig. 5.2 matches that obtained from the experimental data shown in Fig. 5.1. The channel entrance coefficient, K_k, can then be found from Fig. 5.3 by matching the effective slope,

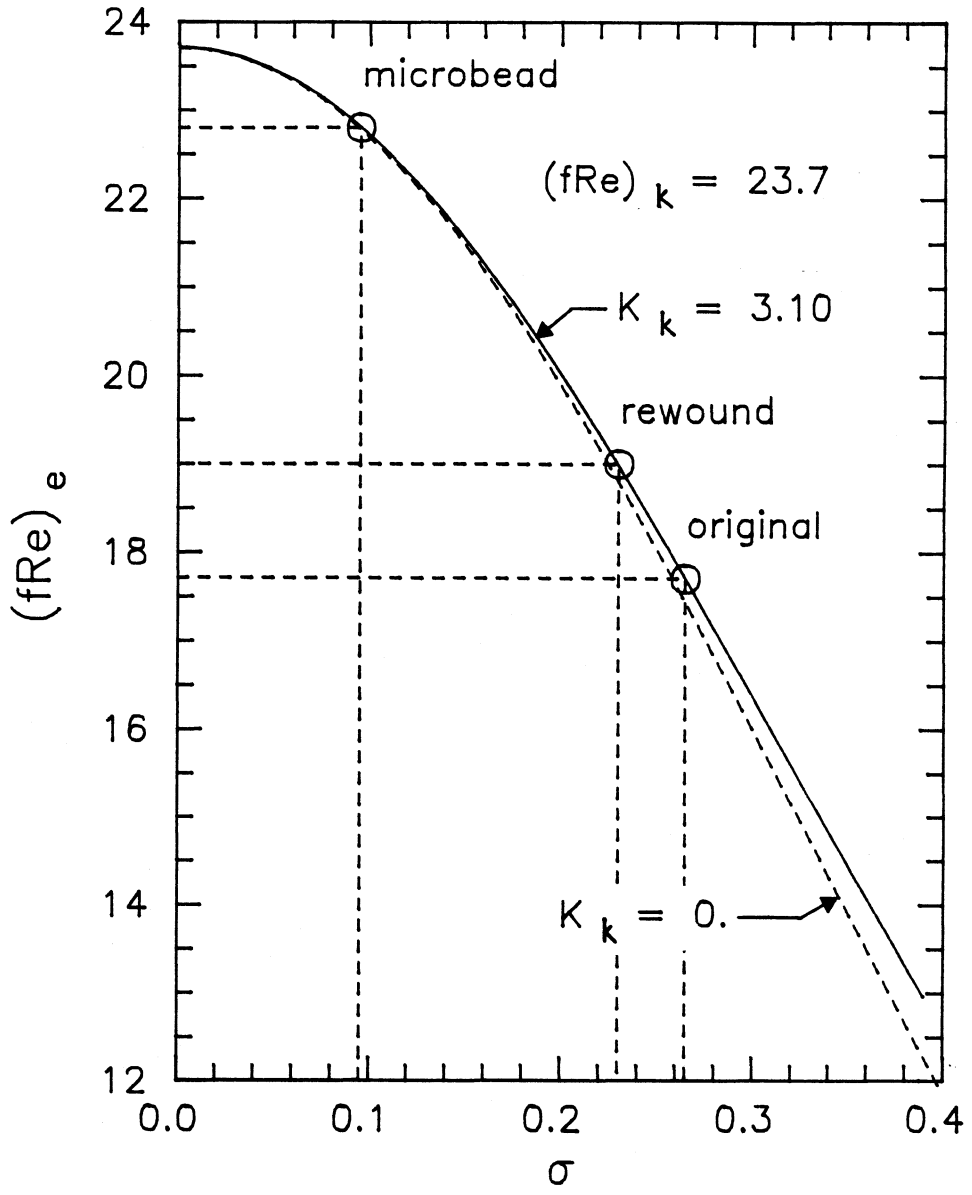

Fig. 5.2 Effective fully developed friction factor - Reynolds number for the lognormal distribution.

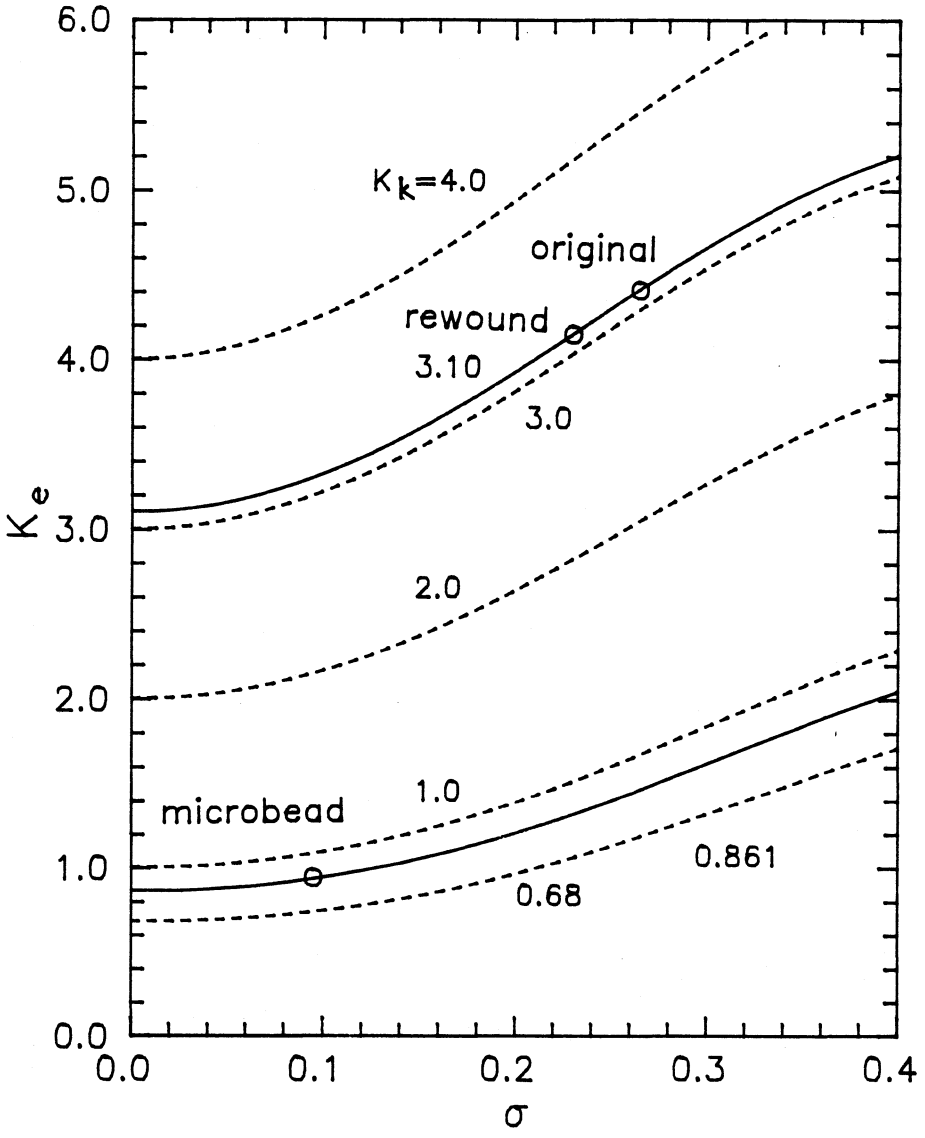

Fig. 5.3 Effective slope of the dimensionless pressure drop versus entrance length relation for the lognormal distribution with channel entrance coefficient as a parameter.

K_e, with the experimental value. The solutions are shown in Figs. 5.2 and 5.3 and are listed in Table 5.1 along with uncertainties based on the spread of the data. The range of experimental data for the original wheel is insufficient to accurately fit a line through. The channel entrance coefficient found for the rewound wheel is assumed to apply to the original wheel as they use the same coated tape and have similar nominal channel spacings. This determines the effective slope of the data (which does in fact agree well with the least squares line through the data, such as it is). The y-intercept is then determined by forcing the line to go through the average $(f_{app}Re)_e$ for the data points near $ReD_{hu}/4L = 0.42$.[1]

Table 5.1 Experimental pressure drop parameters and estimated distributions of passage spacings. $(fRe)_k = 23.7$

wheel	original	rewound	microbead
experimental			
$(fRe)_e$	17.7	19.0	22.8
K_e	4.41	4.15	0.94
estimated			
K_k	3.10	3.10	0.86
σ	.265	.230	.095
uncertainties			
$(fRe)_e$	17.3-18.1	18.6-19.4	22.1-23.5
σ	.254-.276	.219-.242	.041-.128

[1]This procedure actually requires the *simultaneous* solution of the two relations for $(fRe)_e$ and K_e to determine the standard deviation, σ, of the distribution.

The corresponding distributions of passage sizes and individual channel flows are shown in Fig. 5.4. Also pictured is the flow rate weighted by the probability density which shows that a small number of large passages are carrying a significant amount of the flow due to the cubic relationship of channel flow and spacing; hence the reduction in pressure drop. The consequences for heat and mass tranfer are even more severe as will be seen in section 5.3.

The entrance coefficient, K, for the original and rewound wheels is significantly greater than Lundgren's theoretical value for smooth parallel plates. Van den Bulck (1987) found similar results from his experiments with a small single-blow matrix (with very uniform spacing) consisting of the same tape and gel combination. For a hydraulic diameter of 2.06 mm, he obtained a value of $K_k = 4.96$ compared with 3.10 obtained here for similar sized passages. Van den Bulck suggests that these larger values compared with Lundgren's are due to separation in the entrance region of the flow around the particles that protrude into the flow stream. Based on a dimensional analysis, Van den Bulck suggested that K_k depends on the ratio $(D_p/D_{hk})^2$, where D_p is the diameter of the desiccant particles. This would indicate that the entrance coefficients are not the same for each channel as assumed above. The lower value of the K_k found here is then another consequence of the large passage sizes (with smaller K_k's) which carry a significant portion of the flow.

For the microbead wheel, the desiccant particles are smaller, spherical in shape, and more uniform in size than the crushed gel particles used in the other wheels. This makes for much smoother channel walls and is reflected in the lower value of K_k found for the microbead wheel (see Table 4.1).

With the above procedure, estimates of a distribution of passage sizes

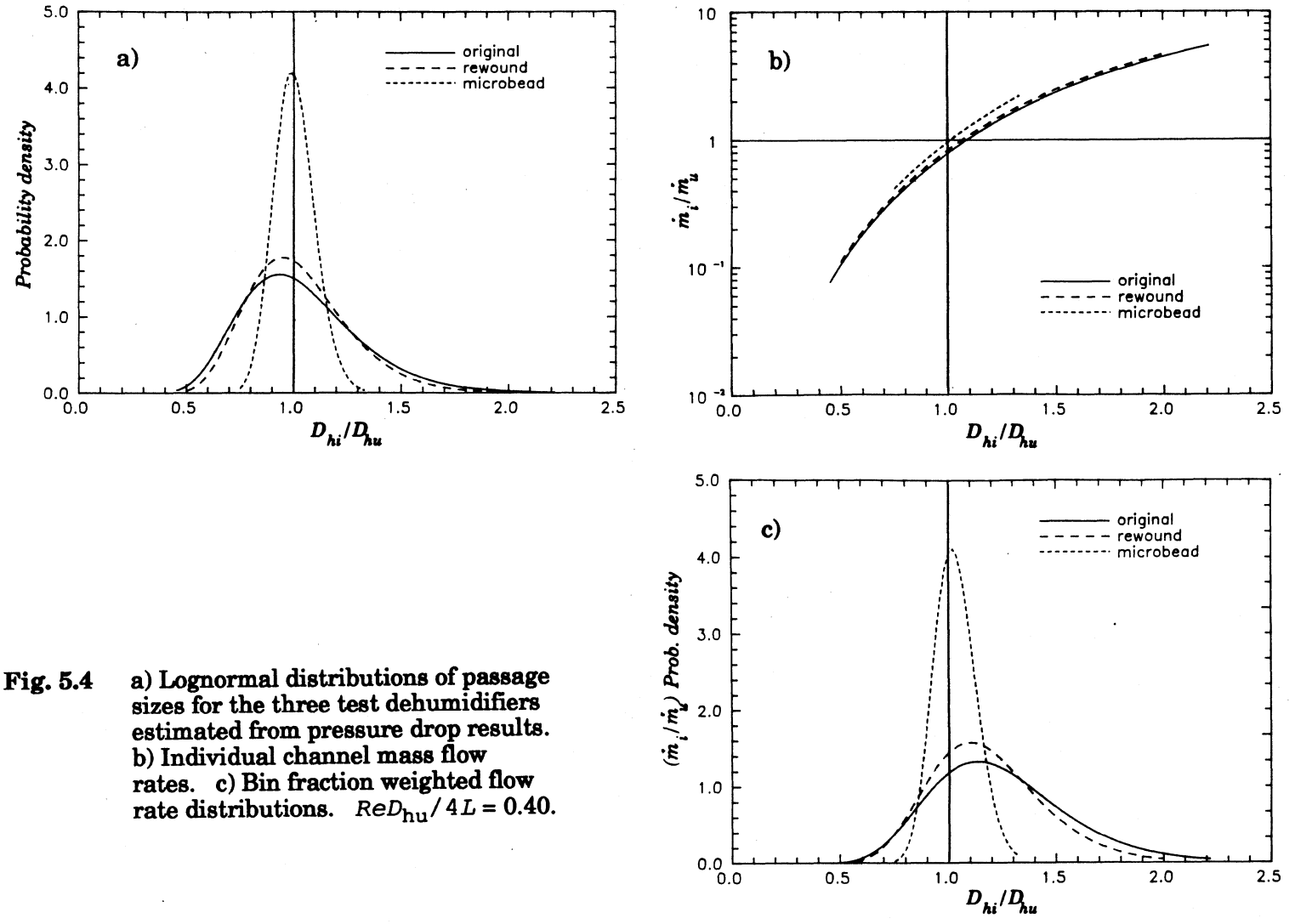

Fig. 5.4 a) Lognormal distributions of passage sizes for the three test dehumidifiers estimated from pressure drop results. b) Individual channel mass flow rates. c) Bin fraction weighted flow rate distributions. $ReD_{hu}/4L = 0.40$.

described by one parameter (e.g., the standard deviation) can be made from the experimental data. The distributions obtained for the wheels in Table 5.1 seem reasonable compared with visual inspection. However, there are many distribution shapes which will produce agreement with the experimental pressure drop results. Each of these will result in a different value for the channel entrance coefficient. *A priori* knowledge of the entrance coefficient (possibly as a function of channel roughness and Reynolds number) would allow the determination of a distribution described by two parameters. However, such an effort may not be useful as matrices with such wide distributions of passage sizes as in the original and rewound wheels are not practical for commercial applications. Narrower distributions may be adequately handled by simple 2 or 3 bin distributions as suggested by Shah and London (1980).

5.2 Low rotation speed analysis

The mass of silica gel in each of the wheels has been calculated from geometrical considerations and measurements of the area density of the coated tape and are given in Table 4.1. These values can be checked against experimental data by a simple procedure described in the following. In addition, the effective specific heat of the matrix can be determined and will be compared with calculated values below.

Schultz (1986) and Bharathan, et al., (1986a,b) have used the analogy method to also estimate the active silica gel available in the wheels. However, the specific heat of the matrix must be specified. The method presented here is more straightforward and allows an independent estimate of the effective specific heat to be made rather than relying on a value calculated from geometrical

considerations. In addition, a more accurate representation of the silica gel equilibrium relation is used.

5.2.1 Mass of silica gel in the wheels

At very low rotation speeds, the dehumidifier comes to equilibrium with the inlet air stream before it rotates into the next period. The matrix essentially undergoes a single-blow process. In terms of the analogy theory described in Appendix C and in section 2.2.2, the slower second transfer zone breaks through the wheel before it rotates to the next period as shown schematically in Fig. 5.5. This condition occurs when the reciprocal of the nondimensional wave speed for the second zone is less than unity,

$$\gamma_{2j}\Gamma_j < 1 \tag{5.11}$$

for both periods. The γ_{ij} (analogous to the ratio of the specific heat of the air to that of the matrix) are functions of the moist air, desiccant equilibrium, and matrix thermal properties. The group $\gamma\Gamma$ is analogous to C_r/C_{min} for rotary sensible heat excahngers.

At these low rotation speeds, a simple mass balance on each period gives the following equation for the desiccant mass,

$$M_{DD} = \dot{m}_{DA,j}\, T \frac{w_{j,i} - w_{j,o}}{W(t_{j,i}, w_{j,i}) - W(t_{3-j,i}, w_{3-j,i})} \tag{5.12}$$

Eq. (5.12) depends directly on the isotherm relation for the desiccant. Van den Bulck (1987) has surveyed a wide range of data available on the equilibrium properties of regular density silica gels such as the type used in the wheels tested

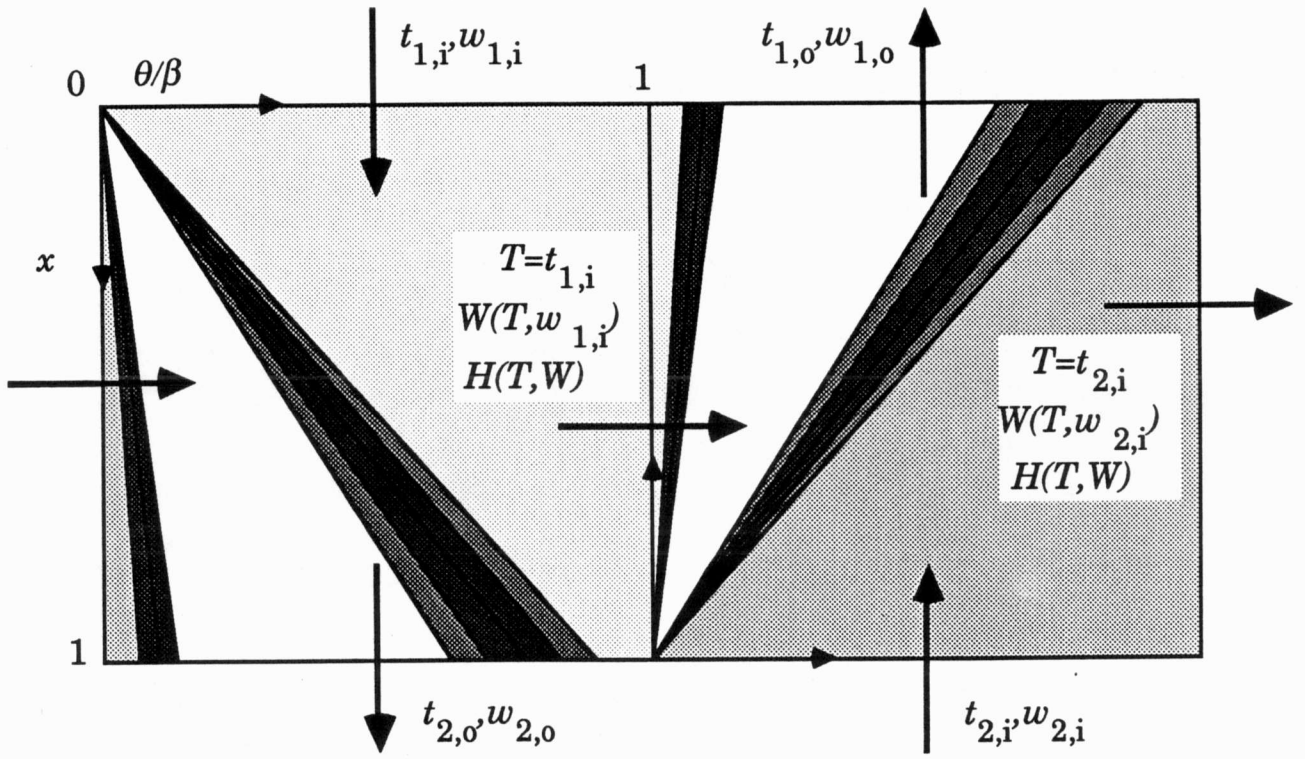

Fig. 5.5 Schematic representation of transfer zone breakthrough at low rotation speeds.

here. He has represented this data using a two term, four parameter model based on the Dubinin-Polanyi adsorption potential theory (Ruthven, 1984). He has also verified this isotherm model through its use in the detailed modeling of heat and mass transfer data from single blow experiments. The silica gel used in those experiments is identical to that used here in the original and rewound wheels. The isotherm relation is presented in Appendix B.

Using Van den Bulck's isotherm, the amount of silica gel in the wheels has been obtained from experimental data using Eq. (5.12). Fig. 5.6 shows the experimentally determined gel mass relative to the calculated value for the three wheels as a function of the reciprocal of the average nondimensional wave speed. The experiments considered are tabulated in Appendix E. The gel mass ratio is essentially constant for all three wheels over the range $0.1 < \overline{\gamma}_{21}\Gamma_1 < 0.4$. Examination of the outlet profile measurements from the original wheel data point labeled as "$\dot{N} = 1.0$ rev/hr" indicates that complete breakthrough of the transfer zones has occurred. Beyond this range, the spread of the transfer zone front due to nonconstant properties and finite transfer coefficients becomes sufficiently large that complete breakthrough does not occur (that is, the transfer zones are much wider than shown in Fig. 5.5). In this case, the denominator of Eq. (5.12) is no longer valid in the mass balance.

The average value of the experimental to calculated gel mass ratio for all three wheels is $0.91 \pm .04$. The expected value is unity. This discrepancy could be the result of errors in the calculation of the gel masses, uncertainties in the equilibrium relationship, or some factor, such as the adhesive, which prevents all of the silica gel present from participating in the sorption process. Van den Bulck's efforts in verifying his isotherm relation suggest that it is reliable. Other

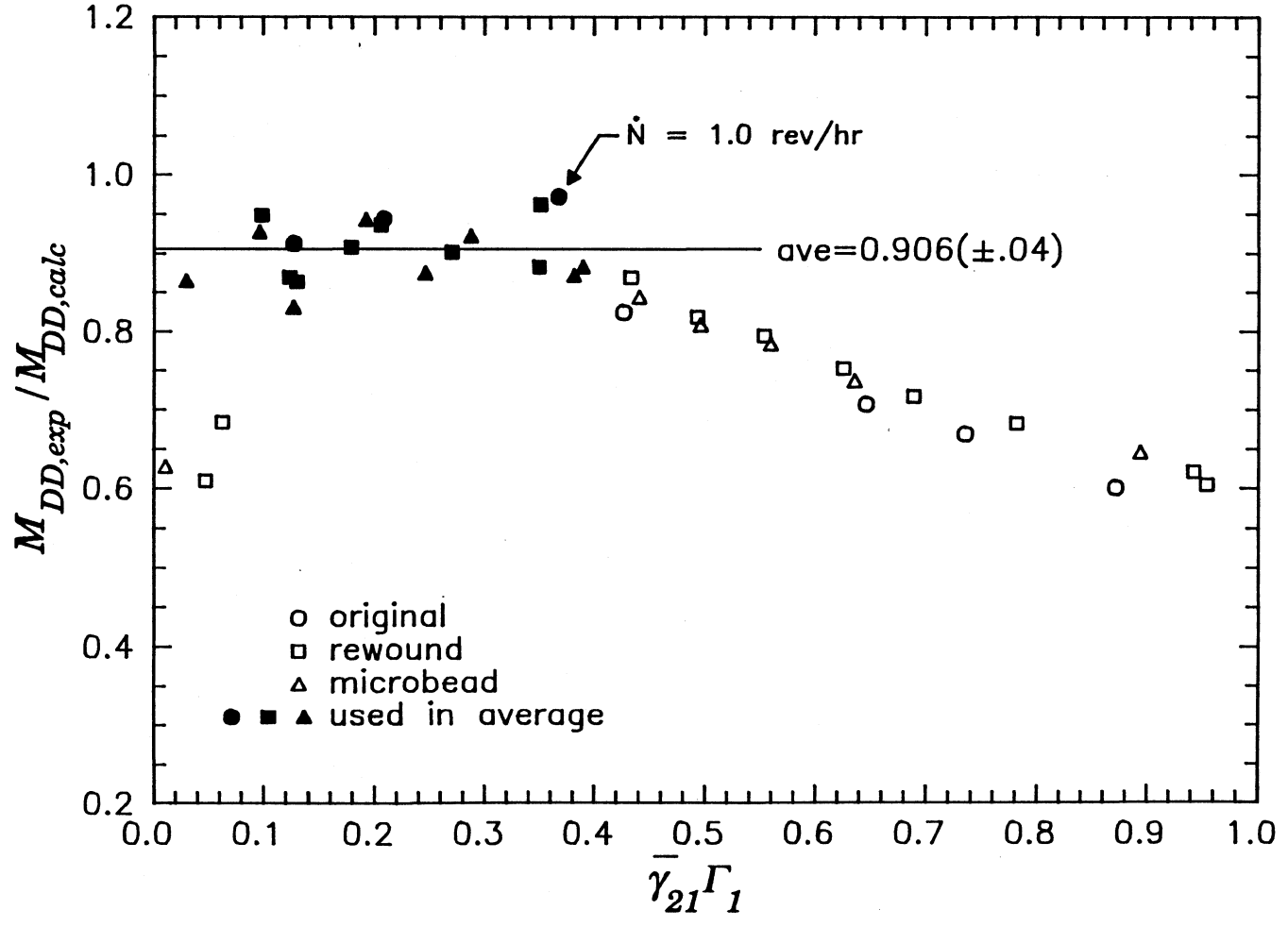

Fig. 5.6 Experimentally determined silica gel masses in the three wheels.

isotherm relations available, such as Brandemuehl's (1982, described in Appendix B) and fits to very limited manufacturers' data result in gel mass ratios down to 0.74. Bharathan, et al., (1986b) estimated the active fraction of gel in the microbead wheel to be only 0.625 using a polynomial fit to manufacturer's data. There is little reason to suspect that such a large fraction of the desiccant is not active. Therefore, the experimentally determined active silica gel masses, listed in Table 4.1, consistent with Van den Bulck's isotherm will be used in the following analyses.[2] The above discussion points out the importance of having accurate equilibrium data available for the desiccant under consideration.

A rather narrow range of inlet states were used in the low rotation speed experiments. A wider range would allow better confirmation of the isotherm relation.

5.2.2 Specific heat of the matrix

The effective specific heat of the matrix can be determined from an energy balance on each period at low rotation speeds. The change in the enthalpy of the matrix from when it enters period j to when it leaves is given by

$$H_j - H_{3-j} = \frac{\dot{m}_{DA,j}}{M_{DD}/T} (h_{j,i} - h_{j,o}) \tag{5.13}$$

where

$$H_j = H(T_j, W_j) \qquad T_j = t_{j,i} \qquad W_j = W(T_j, w_{j,i})$$

$$H(T, W) = (c_{DM} + c_{WL} W)\, T + \Delta H_W$$

---

[2]Manufacturer's data (Bharathan, et al., 1986b) indicates that the microbead gel may have a larger moisture capacity than the crushed gel used in the other wheels for relative humidities greater than 60-70%. These conditions were rarely encountered in the experiments.

and ΔH_W is the integral heat of wetting. If H_0 is defined as the matrix enthalpy excluding the heat capacity of the matrix,

$$H_0 = c_{WL} WT + \Delta H_W \tag{5.14}$$

then the matrix specific heat is given by

$$c_{DM} = \frac{(H_j - H_{3-j}) - (H_{0,j} - H_{0,3-j})}{T_j - T_{3-j}} \tag{5.15}$$

The experimental results are plotted in Fig. 5.7. The scatter in the data is the result of small errors in temperature meaurements that are magnified by the nearly isenthalpic nature of the sorption process. The average value for the points indicated in the figure is 3100 J/kg$_{DD}$-C. This is approximately double the value calculated for the tape and gel combination as shown in Table 4.1. This suggests that the spacers as well as the spokes and other structural components of the wheel are participating in the heat storage process at low rotation speeds. However, even including the thermal mass of the spacers, the calculated values for the original and rewound wheels are at least 35% less than the experimental value. Only the microbead wheel results agree.

The time constant of the spacers in the original wheel is estimated to be approximately 50 seconds. At the very low rotation speeds considered here (< 1.5 rev/hr), a spacer is exposed to an air stream for over 25 time constants and therefore participates strongly in the heat storage process. However, at rotation speeds for optimum dehumidification (10-15 rev/hr), the exposure time is only 2-4 time constants and the spacers may not participate as fully in the heat

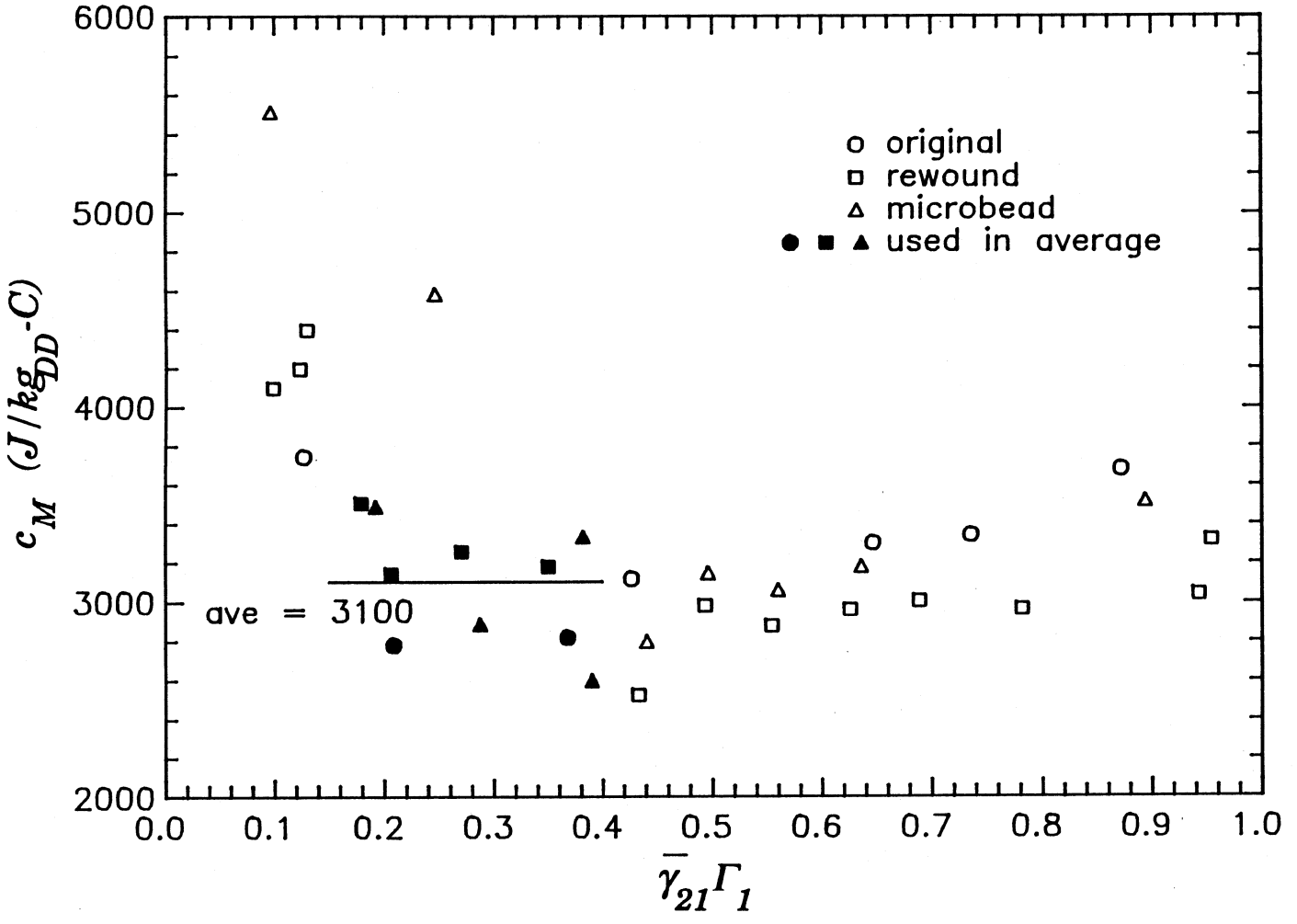

Fig. 5.7 **Matrix specific heats determined from experimental data at low rotation speeds.**

storage process. The effective matrix specific heat will be assumed to be bounded by the experimentally determined value at low rotation speeds and that of the tape and gel combination alone at very high rotation speeds where the spacers participate little in the exchange processes. The modeling of nonhomogeneous matrices is discussed further in section 5.4.

5.3 High rotation speed analysis

For models such as MOSHMX to be useful, the describing parameters should be obtainable from established heat and mass transfer theory. The essentially unknown distributions of passage spacings in the wheels tested make it questionable that this can be done here. However, effective overall heat and mass transfer coefficients can be determined from experimental results at very high rotation speeds as described below. The coefficients obtained are then related to established theory.

5.3.1 High rotation speed model

At very high rotation speeds, the desiccant wheel acts as a total heat or enthalpy exchanger. In the limit of infinite rotation speed, examination of the conservation equations, Eqs. (2.10b,d), indicates that T and W become constant with time and all dependent variables become functions only of the distance through the wheel. The transfer rate equations, Eqs. (2.10a,c), become uncoupled and independent of the thermal properties of the matrix. Each is reducible to a form analogous to that for a direct counterflow heat exchanger.[3]

---

[3]This continues to neglect carryover of the air in the matrix from one period to the other.

This is consistent with the fact that the counterflow rotary heat exchanger effectiveness for high rotation speeds (for $C_r/C_{min} > 5$) approaches that for a direct counterflow heat exchanger (Kays and London, 1984). Therefore, it is possible to obtain the effective overall heat and mass transfer coefficients for the MOSHMX model from the experimentally determined effectivenesses using the direct counterflow ε-Ntu relationship.

For laminar flow and equal face areas per period, the group $(hA_s)_j$ is the same for both periods. The overall number of transfer units for mass transfer, $Ntu_{w,o}$, and heat transfer, $Ntu_{t,o}$, are related to the number of transfer units for the period with the minimum capacity rate by

$$Ntu_o = Ntu_{min}/2 \tag{5.16}$$

where the analogous capacity rates are given by

$$C_{w,j} = \dot{m}_{DA,j} \qquad C_{t,j} = \dot{m}_{DA,j}c_A \tag{5.17}$$

The corresponding humidity ratio and temperature effectivenesses are

$$\varepsilon_w = \frac{w_{j,o} - w_{j,i}}{w_{3-j,i} - w_{j,i}} \tag{a}$$

(5.18)

$$\varepsilon_t = \frac{t_{j,o} - t_{j,i}}{t_{3-j,i} - t_{j,i}} \tag{b}$$

These effectivenesses can be calculated directly from the experimental data. As is convention (Kays and London, 1984), the effectivenesses used here are for the period with the minimum capacity rate as determined by Eqs. (5.17).

Fig. 5.8 shows the humidity ratio and temperature effectivenesses

predicted by MOSHMX for a range of inlet states and rotation speeds for various combinations of heat and mass transfer Ntu's. Van den Bulck's isotherm relation is used with c_{DM} = 1420 J/kg$_{DD}$-C corresponding to that for the tape and gel combination. The results have been plotted against the reciprocal of the average velocity of the faster first transfer wave (see Appendix C). $\bar{\gamma}_1$ is evaluated at the average of the two inlet states as suggested by Maclaine-cross and Banks (1972). The dashed lines show the rotary counterflow relation for $C_{min}/C_{max} = 1$.

5.3.2 Correction of experimental effectivenesses to "infinite" rotation speed

Fig. 5.8 shows that the humidity ratio effectiveness in the MOSHMX model is independent of the heat transfer coefficient; similarly for the temperature effectiveness. In addition, the effectivenesses become independent of rotation speed for $\bar{\gamma}_1\Gamma_1 > 5$.[4] Due to mechanical limitations, the required "high" rotation speeds could not be obtained in the experiments. The values of $\bar{\gamma}_1\Gamma_1$ for the three wheels tested ranged from 1.2 to 9 (see Appendix E). For this range, Fig. 5.8 indicates that only small corrections are needed to convert the experimentally determined effectivenesses at finite rotation speeds to those expected at "infinite" rotation speed. The overall heat and mass Ntu's can then be found from the corrected effectivenesses using the direct counterflow heat exchanger relations.

---

[4]The temperature effectiveness shows less dependence on $\bar{\gamma}_1\Gamma_1$ because the outlet temperature lies between the two inlet temperatures for the inlet states considered. The temperature effectiveness is therefore always $0 \le \varepsilon_t \le 1$. However, the humidity ratio effectiveness can be greater than unity or less than zero. For example, the outlet humidity ratio of the process period at medium rotation speeds is less than either inlet humidity ratio so the effectiveness is greater than unity.

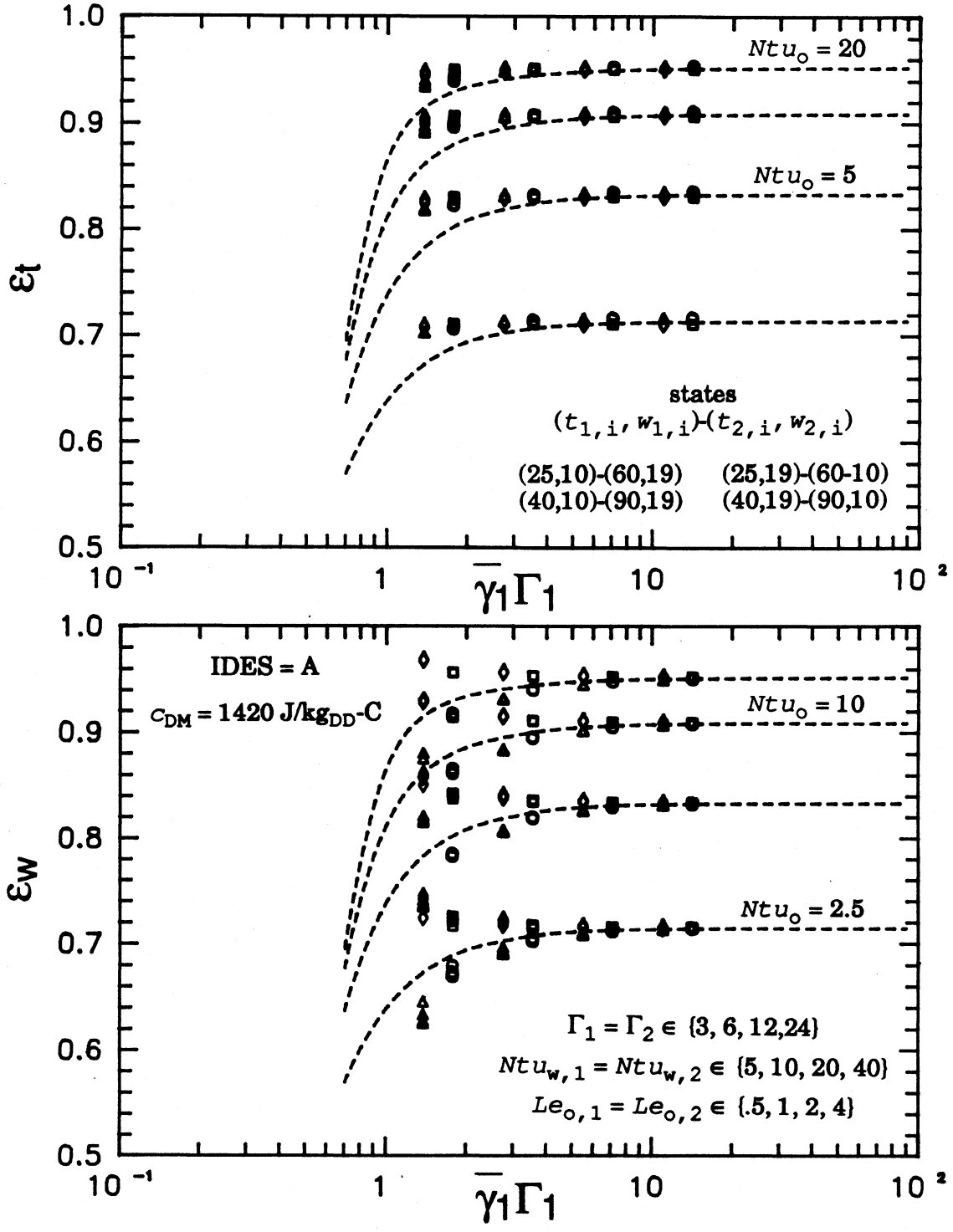

Fig. 5.8 Temperature (upper) and humidity ratio (lower) effectivenesses predicted by MOSHMX at high rotation speeds.

Maclaine-cross (Bharathan, et al., 1986a) has suggested a correction procedure based on the analogy method. Dividing Eq. (C.7) for the outlet state predicted by the analogy method by the difference in inlet humidity ratios, the humidity ratio effectiveness for period 1 can be written as

$$\varepsilon_{w,1} = \frac{w_{2,i} - w_{IP}}{w_{2,i} - w_{1,i}} \eta_{11} + \frac{w_{IP} - w_{1,i}}{w_{2,i} - w_{1,i}} \eta_{21} \tag{5.19}$$

where the η's are given by the rotary exchanger effectiveness relation with $\bar{\gamma}_{ij}\Gamma_j$ as the parameter analogous to C_r/C_{min} for sensible heat exchangers. w_{IP} is the intersection point defined in Appendix C; it is the intermediate state between the two transfer zones. A similar relation can be written for the effectiveness at "infinite" rotation speed. The correction is then given by

$$\begin{aligned} \varepsilon_{w,1}^{\infty} - \varepsilon_{w,1} = & \frac{w_{2,i} - w_{IP}}{w_{2,i} - w_{1,i}} (\eta_{11}^{\infty} - \eta_{11}) \\ & + \frac{w_{IP} - w_{1,i}}{w_{2,i} - w_{1,i}} (\eta_{21}^{\infty} - \eta_{21}) \end{aligned} \tag{5.20}$$

where "∞" indicates the value for infinite rotation speed. Maclaine-cross (Bharathan, et al., 1986a) suggests that this correction can be correlated solely as a function of the parameter analogous to C_r/C_{min}. Fig. 5.9 shows the author's correlation of the rotary heat exchanger effectiveness correction as a function of C_r/C_{min} for a range of Ntu_o and C_{min}/C_{max}. The corrections are less than .01 for $C_r/C_{min} > 1.5$. Application of this correction to the MOSHMX predictions in Fig. 5.8 is shown in Fig. 5.10 and indicates that the procedure works well.

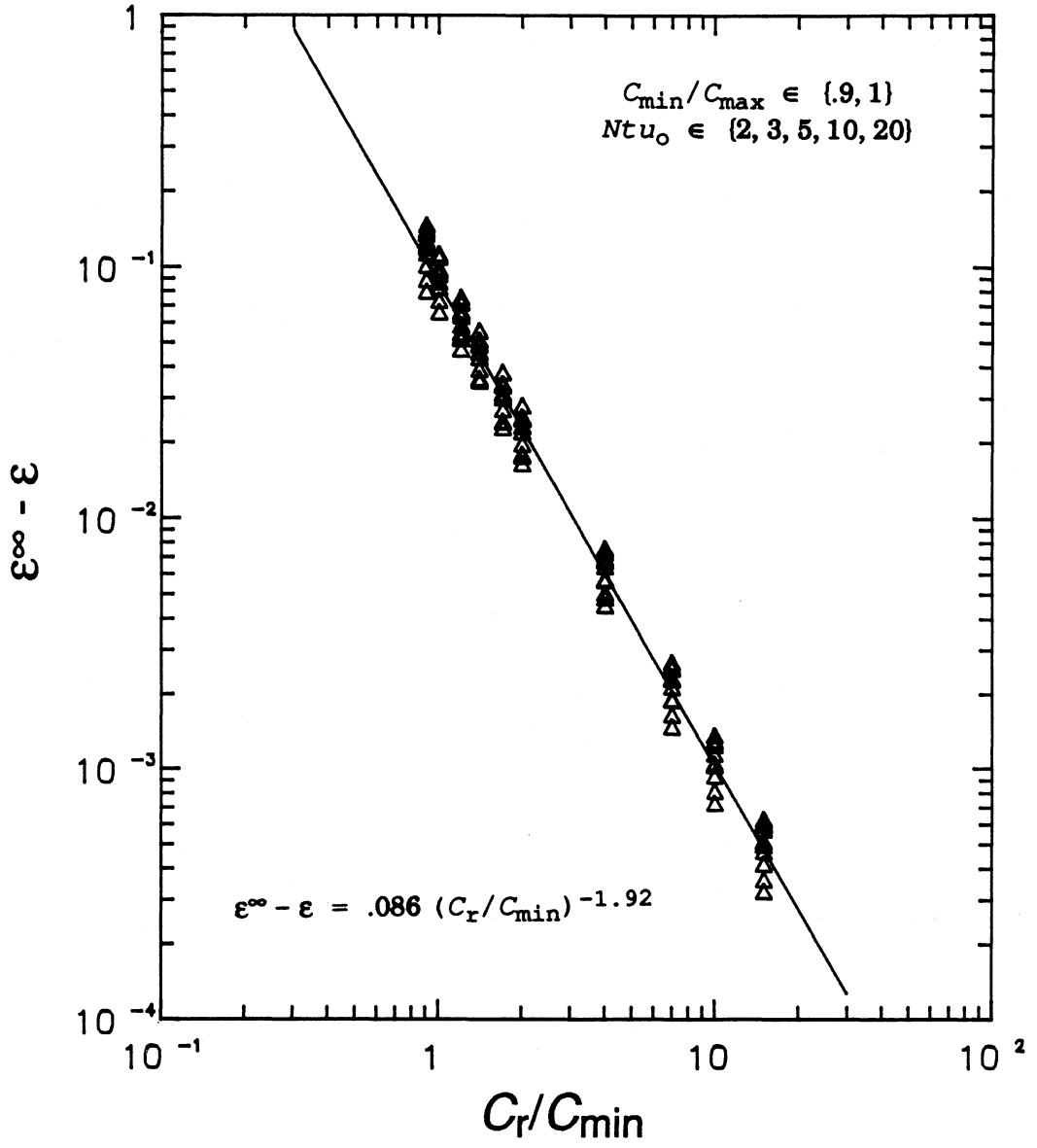

Fig. 5.9 Correlation of rotary heat exchanger effectiveness correction to "infinite" rotation speed.

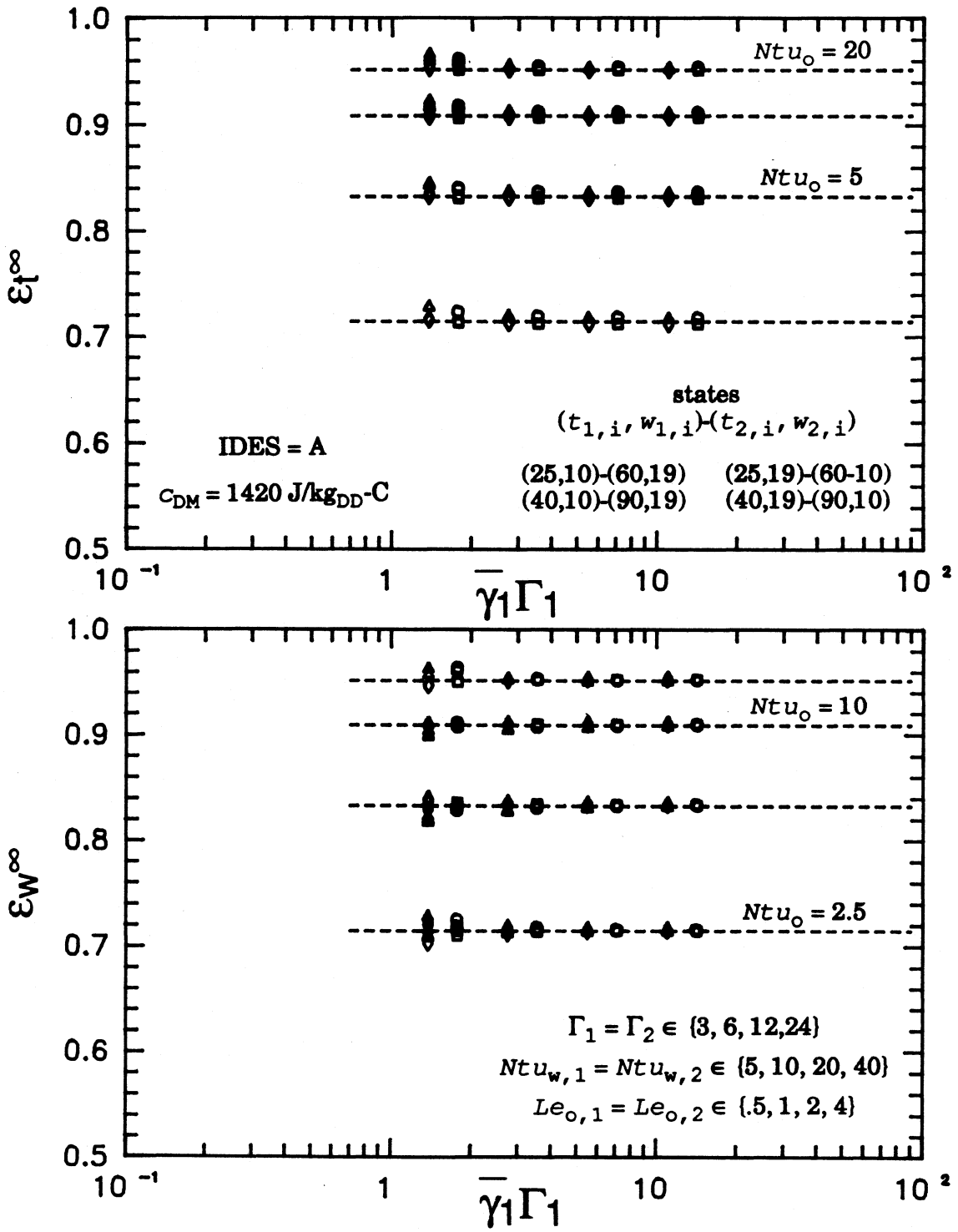

Fig. 5.10 Temperature (upper) and humidity ratio (lower) effectivenesses predicted by MOSHMX corrected to "infinite" rotation speed.

5.3.3 Experimental overall heat and mass transfer coefficients

The effective overall heat and mass transfer Ntu's can now be found from the corrected high rotation speed experimental data for the three wheels tested using the direct counterflow heat exchanger relation. The results are listed in Appendix E. The $Ntu_{\min}$'s for the minimum capacity rate period are then calculated from Eq. (5.16). From these values, the effective overall transfer coefficients in the form of the Nusselt number for heat transfer and Sherwood number for mass transfer are determined as

$$Nu_e = \frac{ReD_{hu}}{4L} Pr\, Ntu_{t,\min} \tag{5.21}$$

$$Sh_e = \frac{ReD_{hu}}{4L} Sc\, Ntu_{w,\min} \tag{5.22}$$

The nominal uniform hydraulic diameter is used in the definitions of the Nusselt and Sherwood numbers. The overall Lewis number is given by

$$Le_o = \frac{Ntu_{t,o}}{Ntu_{w,o}} = \frac{Nu_e}{Sh_e} Le \tag{5.23}$$

where Le is the Lewis number for air and is taken to be 0.851.

The high rotation speed experimental results for Nu_e are shown in Fig. 5.11. Also shown are the expected values for a uniform matrix assuming a constant heat flux boundary condition and for distributions of passage sizes corresponding to those found from the pressure drop analysis. These are discussed further below.

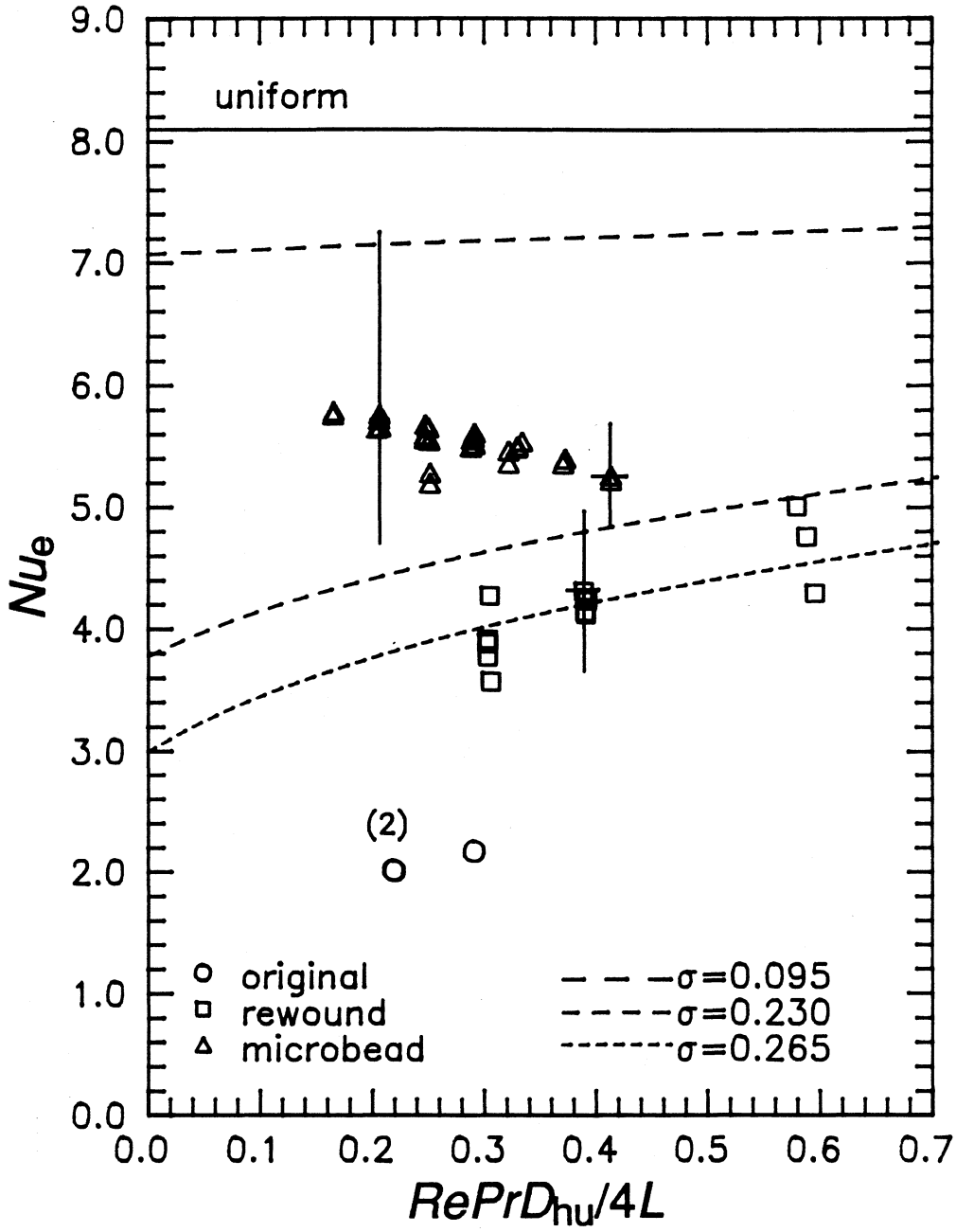

Fig. 5.11 Effective Nusselt numbers determined from high rotation speed experimental data.

The negative slope of the Nu_e data in Fig. 5.11 for the microbead wheel has proven difficult to explain. The low Reynolds number results are from experiments where the temperature effectiveness is near 0.95. $Ntu_{t,o}$ is very sensitive to effectiveness at these high values as indicated by the large uncertainty bar. A small systematic error in either the temperature measurements or in the leakage rate corrections would strongly affect the Nu_e obtained. Doubts about the leakage correction procedure used for the microbead wheel were expressed in section 3.5.1. Estimates of the possible effects of carryover of air from one period to the next using the analysis of Banks (1984) indicate that carryover affects the Nu_e by only 2-4%.

Fig. 5.12 shows the experimental results for Sh_e along with the expected value for a uniform matrix assuming that the solid-side moisture transfer resistance is negligble. Again, the negative slope of the microbead data remains unexplained. The overall Lewis numbers, Le_o, are shown in Fig. 5.13. The average value for the rewound wheel is 1.16 (±.08). The two points available for the original wheel which uses the same silica gel are just slightly above this. The average value for the microbead wheel is 1.07 for the range $.28 < RePrD_{hu}/4L < .42$. The decrease in Le_o for lower Re's has not been investigated. The generally lower value of the Lewis number for the microbead wheel is suspected to be due to the smaller particle sizes used.

In his analysis of single-blow heat and mass transfer in a desiccant matrix, Van den Bulck (1987) found the overall Lewis number to be in the range of 3-7 for the same desiccant as used in the rewound wheel. This is significantly higher than obtained here from the periodic steady-state experiments. The author speculates that this difference may be due to the shorter exposure time to

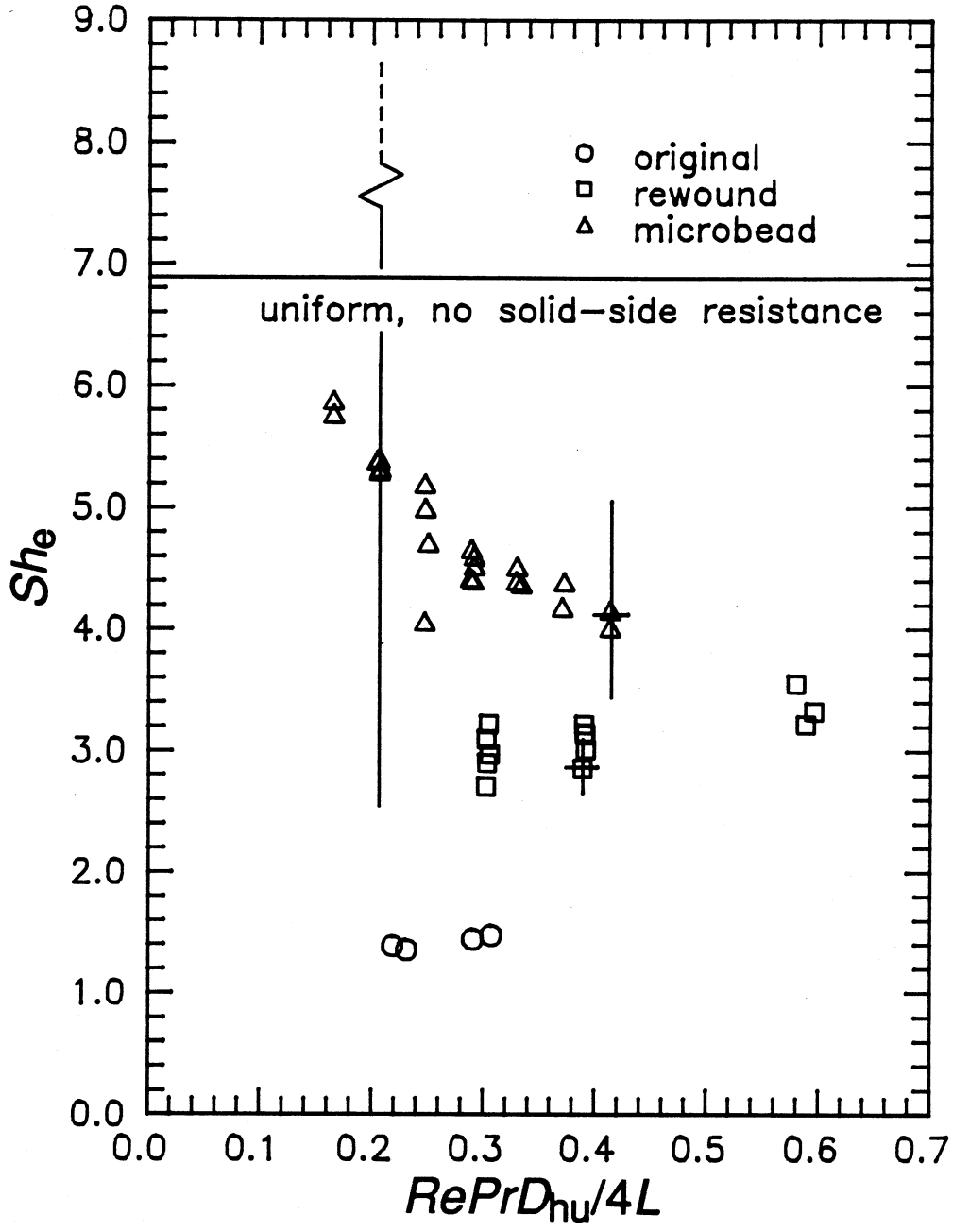

Fig. 5.12 Effective Sherwood numbers determined from high rotation speed experimental data.

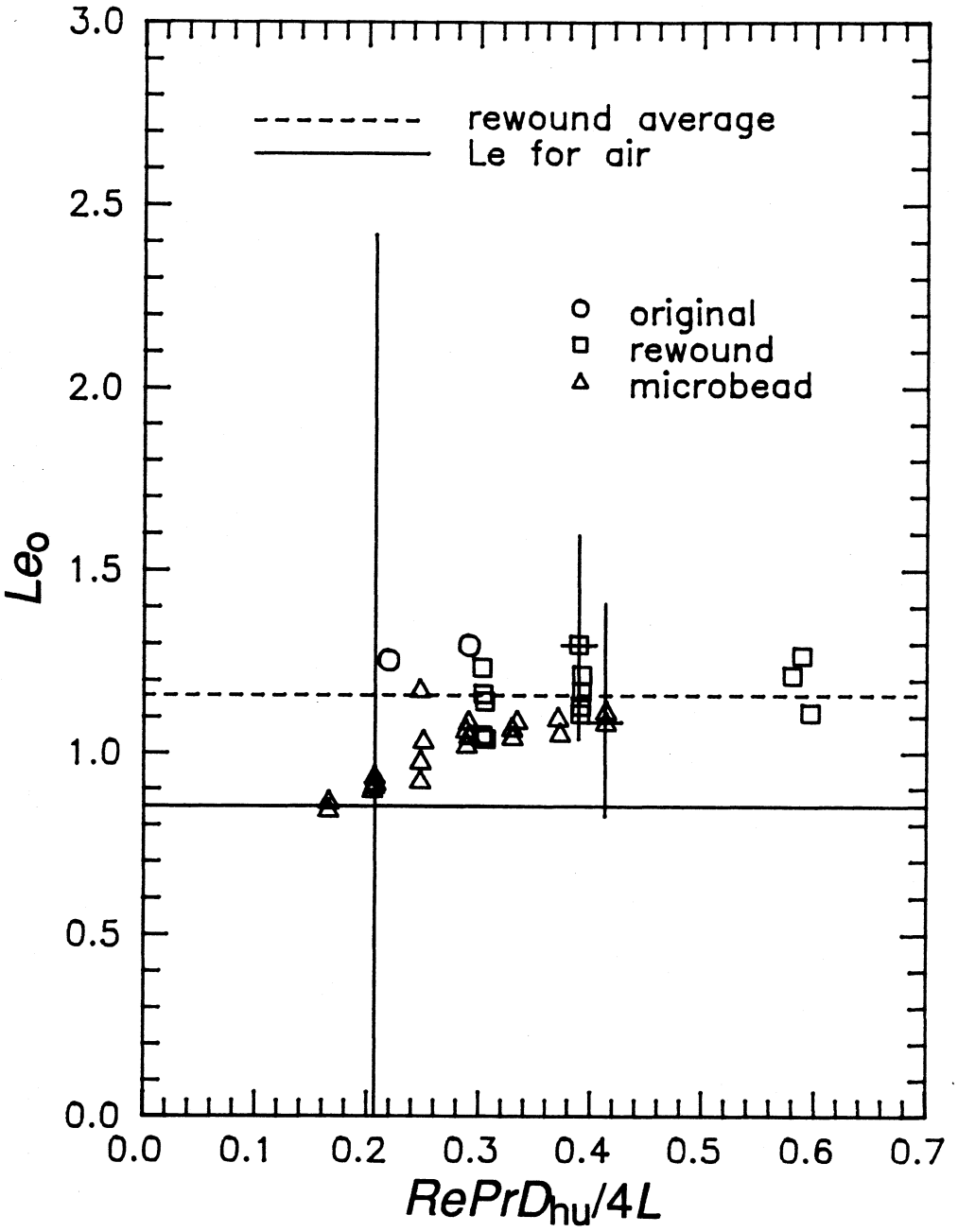

Fig. 5.13 Overall Lewis numbers determined from high rotation speed experimental data.

an air stream experienced by the desiccant particles in the rotary experiments, that is, the time history of the particles are much different in the two cases. Lack of time has prevented further investigation leaving this matter unresolved for the present.

Linear least squares fits to the experimentally determined Nu_e and Le_o are listed in Table 5.2. Using these relations to calculate the input parameters, the predictions by MOSHMX of the process stream outlet states are compared with the experimental values for the rewound and microbead wheels as shown in Fig. 5.14. Agreement is generally within the experimental uncertainty. The larger discrepancies are for experimental results at somewhat lower rotation speeds and suggests that the proper value of the matrix specific heat has not been input to the model. These results indicate that the MOSHMX model, using constant overall transfer coefficients, can accurately predict the performance of enthalpy exchangers. In this case, the appropriate coefficients were determined

Table 5.2 Linear least squares fits to experimentally determined Nu_e and Le_o.

original wheel		
	$Nu_e = 1.536 + 2.185\, RePrD_{hu}/4L$	
	$Le_o \approx 1.3$	
rewound wheel		
	$Nu_e = 3.085 + 2.761\, RePrD_{hu}/4L$	
	$Le_o = 1.16\,(\pm.08)$	
microbead wheel		
	$Nu_e = 6.113 - 2.014\, RePrD_{hu}/4L$	(*x-axis range*)
	$Le_o = 0.584 + 1.621\, RePrD_{hu}/4L$	(.15 - .28)
	$Le_o = 0.954 + 0.350\, RePrD_{hu}/4L$	(.28 - .42)

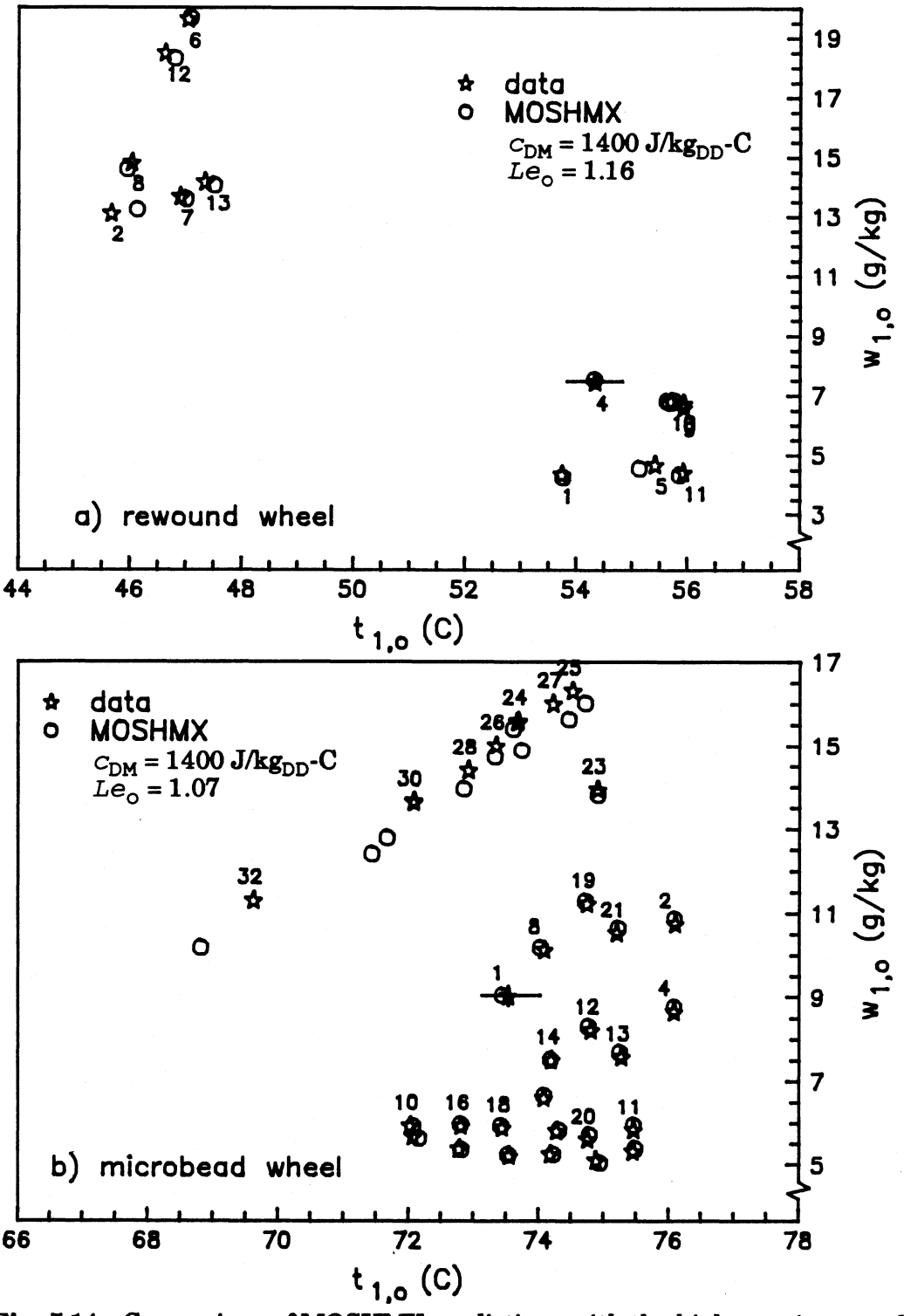

Fig. 5.14 Comparison of MOSHMX predictions with the high rotation speed experimental data. a) rewound wheel. b) microbead wheel. The numbers labeling the data points refer to the experiment numbers in Appendix E.

by a model that is strongly related to the MOSHMX model and so good agreement is to be expected. In the next section, the experimentally determined overall heat and mass transfer coefficients are related to fundamental theory.

5.3.4 Effect of distribution of passage sizes on effective transfer coefficients

The experimental Nu_e's shown in Fig. 5.11 lie much below the value expected for a uniform matrix. This is caused by the distribution of passage spacings in the wheels. To handle this problem, Shah and London (1980) assume that each channel is independent of its neighbors in the matrix. The wheel is then modeled as a set of exchangers operating in parallel as shown schematically in Fig. 5.15. For a discrete distribution of passage sizes, each bin is represented by an independent wheel.

Given a distribution of passage sizes, the flow rates through the individual channels can be determined as described in section 5.1.3. The heat transfer Ntu's for an individual channel in the k^{th} bin are then given by

$$Ntu_{t,k} = \frac{Nu_k}{Pr \frac{\dot{m}_k}{\dot{m}_u} \frac{D_{hk}}{D_{hu}} ReD_{hu}/4L} \tag{5.24}$$

which is analogous to Eq. (5.21). As in the pressure drop analysis, the Reynolds number for the channel has been written in terms of the bulk Reynolds number. At high rotation speeds, the effectiveness of the k^{th} "wheel" is given by the direct counterflow exchanger relation. For the case of equal capacity rates ($C_{min}/C_{max} = 1$), the wheel effectiveness is given by

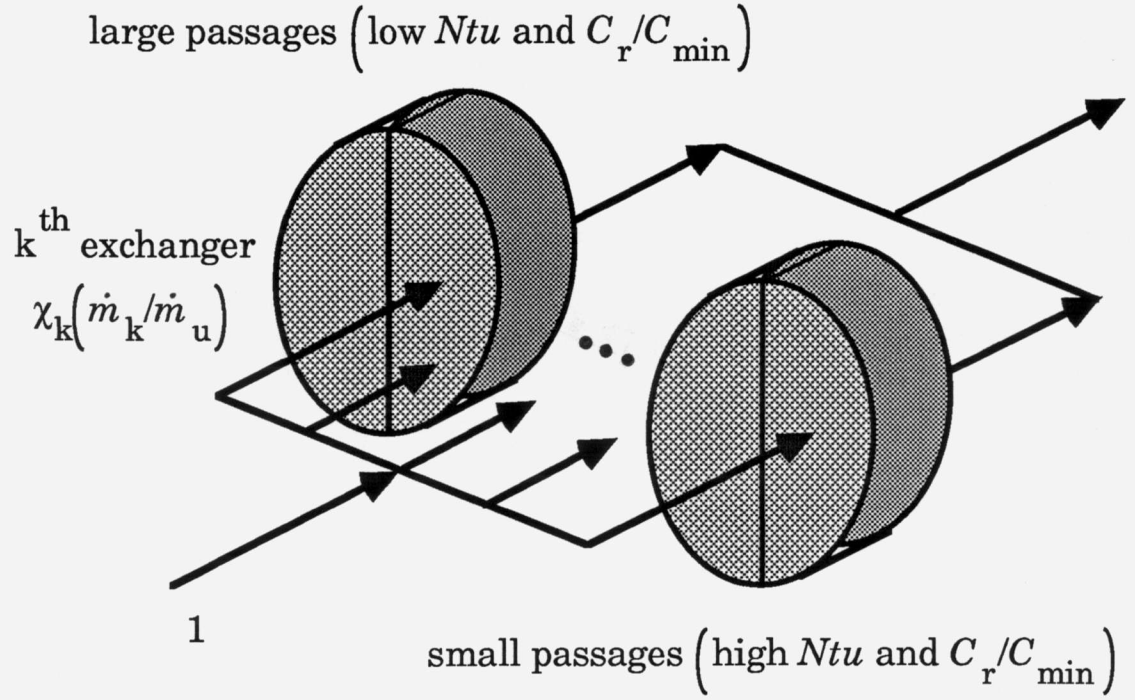

Fig. 5.15 Representation of a wheel with a distribution of passage sizes as a set of parallel exchangers.

$$\varepsilon_k = Ntu_{to,k} / (1 + Ntu_{to,k}) \tag{5.25}$$

Weighting each of the bin effectivenesses by the fraction of the total mass flow through the bin, the overall effectiveness of the wheel becomes

$$\varepsilon_e = \sum_{k=1}^{n} \chi_k (\dot{m}_k / \dot{m}_u) \varepsilon_k \tag{5.26}$$

This comes from an energy balance assuming constant properties. The overall effective heat transfer Ntu's are obtained from

$$Ntu_{t,o} = \varepsilon_e / (1 - \varepsilon_e) \tag{5.27}$$

A similar procedure can be employed for capacity rate ratios other than unity. The effective Nusselt number is then obtained from Eq. (5.21). In the limit as the Reynolds number goes to zero, Eq. (5.24) becomes undefined. It can be shown, however, that the effective Nusselt number for parallel plates is given by (Maclaine-cross, 1969)

$$Nu_e = Nu_k \frac{[\sum \chi_k (D_{hk}/D_{hu})^3]^2}{\sum \chi_k (D_{hk}/D_{hu})^7} \tag{5.28}$$

For the average aspect ratio of .009 for the three wheels, the channel Nusselt number is 8.10 for a constant heat flux boundary condition (Shah and London, 1980). The choice of the constant flux boundary condition has recently been justified by Van den Bulck (1987) through his analysis of experimental results from a single-blow desiccant matrix.

Fig. 5.16 shows the effective Nusselt number as a function of the standard deviation of a lognormal distribution of passage sizes. The pressure drop

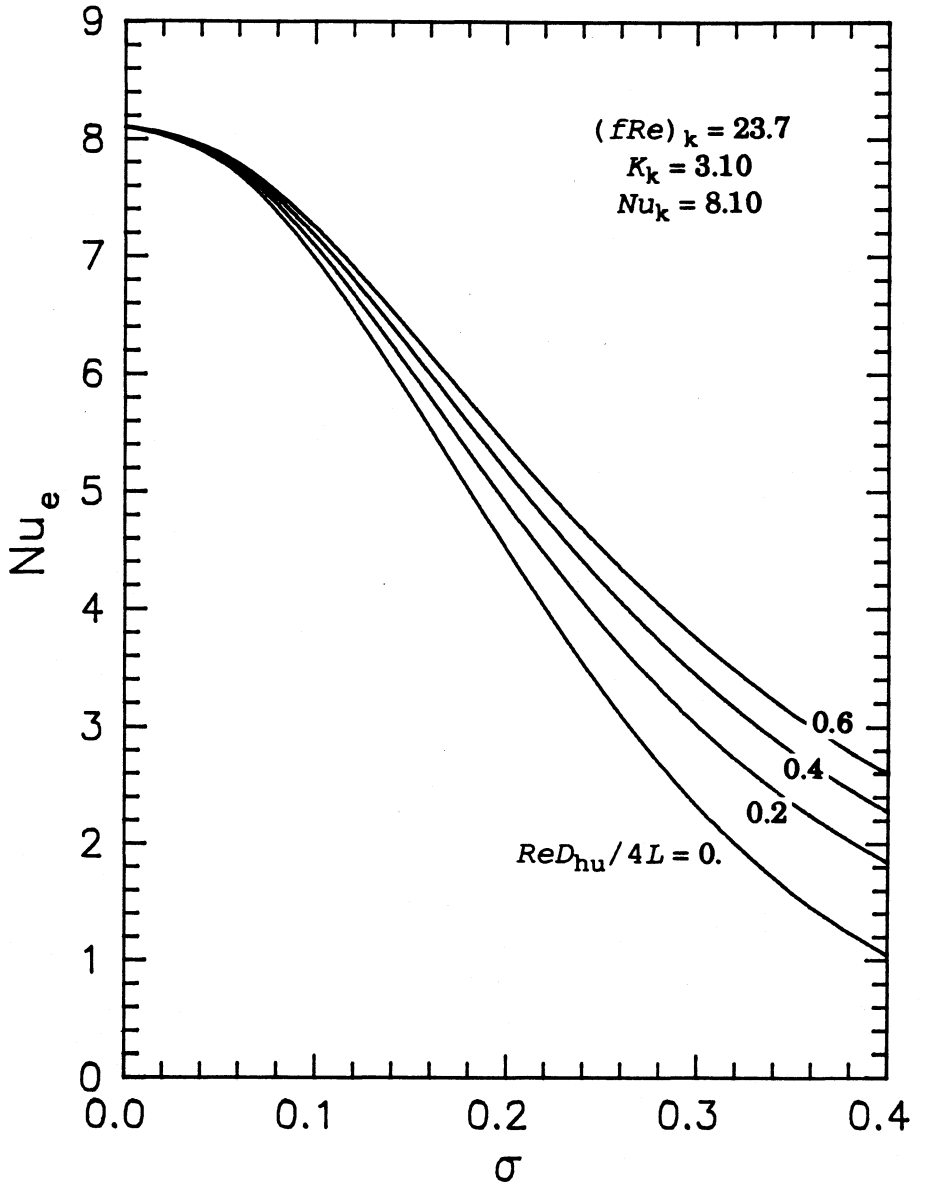

Fig. 5.16 Effective Nusselt number for a lognormal distribution.

parameters which determine the flow distribution are consistent with those used above to model the test wheels. The Nusselt number falls off very rapidly as the width of the distribution increases. This is a consequence of the fact that the channel Ntu's for parallel plates are inversely proportional to the fourth power of the channel spacing. This can be seen from Eqs. (5.24) and (5.6). The variation with entrance length parameter is due to the entrance pressure drop effects which tend to produce a more uniform flow through the matrix.

Using the above equations, the Nu_e variation with $ReD_{hu}/4L$ is plotted in Fig. 5.11 for the standard deviations determined from the pressure drop analysis. It is apparent that those distributions do not accurately represent the actual wheels. Comparison of the pressure drop and heat transfer results indicate that the true distributions are lower in the peak near the nominal spacing and have wider bases than those determined from the pressure drop results.

From Fig. 5.11, (fortuitously) the lognormal distribution of passage spacings with a standard deviation of 0.265 accurately predicts the Nu_e results for the rewound wheel. The experimental data show a somewhat greater slope which may be due to entrance effects which have been ignored in the above model. Accounting for the combined hydrodynamic and thermal entrance effects, the Nusselt number for a nominal channel may be about 1% greater than assumed above (Kays and Crawford, 1980); larger passages would be more affected. In addition, separation of flow around the particles in the entrance region that is suspected of creating the increased entrance pressure drop coefficient may also act to increase the transfer coefficient.

A similar procedure can be used to model the effective mass transfer coefficient. The experimental value for the overall Lewis number indicates that

there is a significant solid-side resistance to mass transfer. This resistance is a strong function of the state of the desiccant, shape of the particle, and the time dependent history of the air stream (boundary conditions). For simplicity, the solid-side resistance is taken to be a constant here; this has been used satisfactorily to model single-blow mass exchangers (Ruthven, 1984). This resistance model is shown schematically in Fig. 5.17 considering the desiccant to be a sheet lining the wall of a parallel plate passage.

Given this model, the overall mass transfer coefficient for a passage in the k^{th} bin is given by

$$\frac{1}{g_k} = \frac{1}{g_{ak}} + \frac{1}{g_s} \tag{5.29}$$

Assuming all channels have the same air-side Sherwood number, the ratio of the solid- and air-side resistances for a channel can be written in terms of the ratio for the nominal channel as

$$\frac{g_{ak}}{g_s} = \frac{g_{au}/g_s}{D_{hk}/D_{hu}} \tag{5.30}$$

The overall Lewis number for a channel then becomes

$$Le_{o,k} = \left(1 + \frac{g_{au}/g_s}{D_{hk}/D_{hu}} \right) Le \tag{5.31}$$

where the air-side Sherwood number is taken to be equal to the Nusselt number by analogy (Bird, et al., 1960). By following a procedure identical to that above for heat transfer in a high rotation speed exchanger, the effective Sherwood

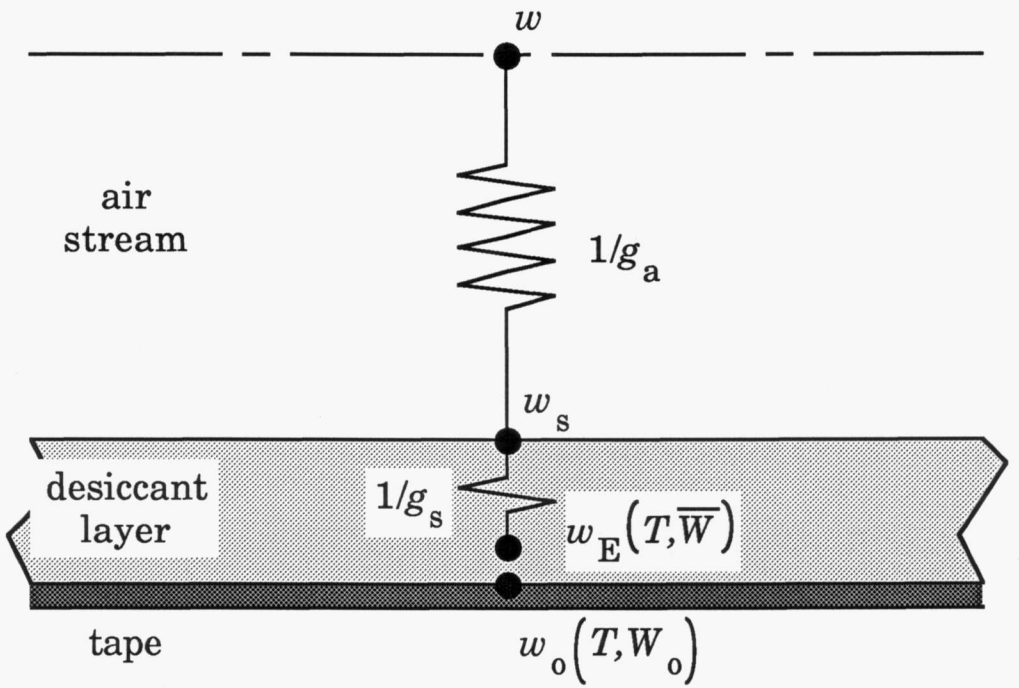

Fig. 5.17 Simple mass transfer resistance model considering the desiccant to be a sheet lining the wall of a parallel plate passage.

number and hence the overall Lewis number for the wheel can be determined for a given distribution of passage sizes.

In Fig. 5.18, the overall Lewis number for a lognormal distribution consistent with the heat transfer results for the rewound wheel is shown as a function of the ratio of the solid- to air-side mass transfer resistances for the nominal size channel. The overall Lewis number from the rewound wheel data indicates that two-thirds of the overall mass transfer resistance is on the air-side and one-third on the solid-side. Fig. 5.19 shows the overall Lewis number as a function of distribution width and indicates that the width of the distribution has very little effect on its value. This eliminates the distribution of passage spacings as an explanation of the differences in overall Lewis numbers obtained here and by Van den Bulck.

The assumption of independent channels made above may be satisfactory if large temperature differences between neighbors do not exist. This may not be true for the original and rewound wheels with their large distributions of passage sizes. In this case, the experimentally determined transfer coefficients will contain the effects of heat transfer between channels and the distribution width determined above may not be appropriate.

5.4 Comparison of MOSHMX predictions with experimental results

In this section, predictions by the MOSHMX model are compared with experimental data from the three test wheels operated at medium rotation speeds, that is, near optimum dehumidifying conditions. The parameters determined from the above analyses of the low and high rotation speed data are used as inputs to MOSHMX.

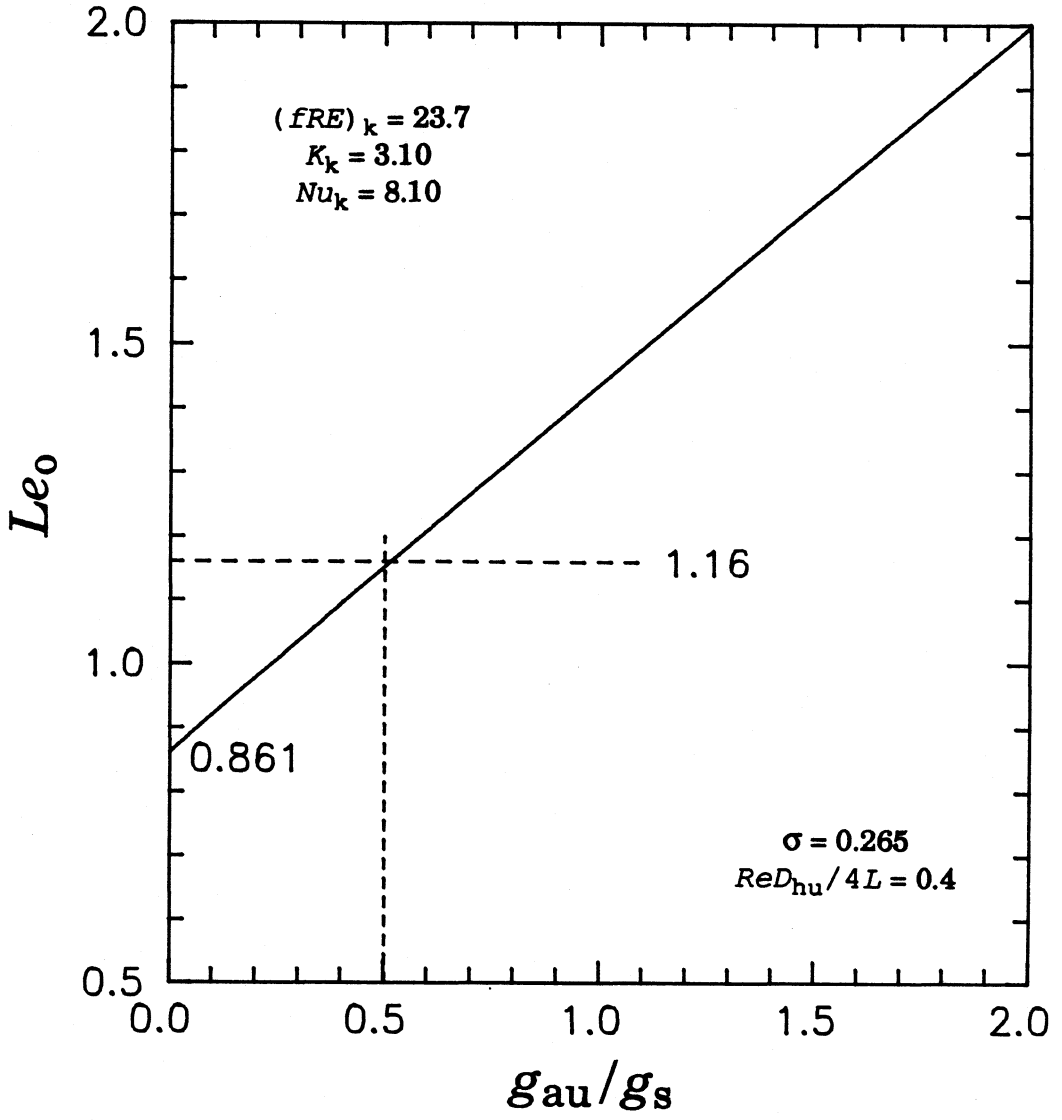

Fig. 5.18 Overall Lewis number for a lognormal distribution as a function of the ratio of the solid- to air-side mass transfer resistances.

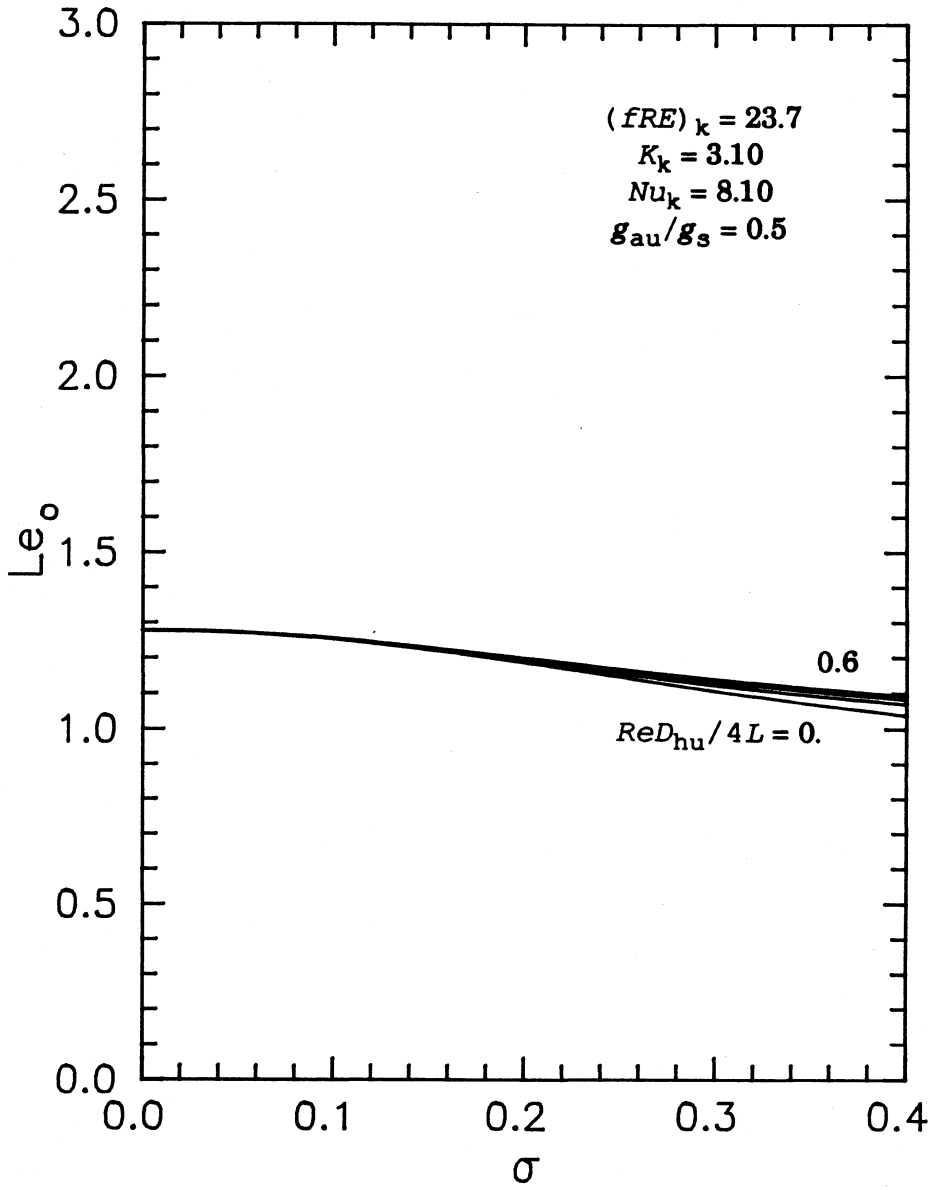

Fig. 5.19 Overall Lewis number as a function of the width of the lognormal distribution.

Schultz (1986) and Bharathan, et al., (1986a,b) have used the efficiency parameters defined in the analogy method to represent the experimental data in earlier reports. The resulting description is compact, however, the physical interpretation is not direct. Here, direct comparisons of the process outlet temperature and humidity ratio from the model and data are made on psychrometric charts. The figures can become a little cluttered, however, the author feels that temperatures and humidity ratios are much easier to interpret.

5.4.1 Uniformly spaced passages and homogeneous matrix properties

In Fig. 5.20, MOSHMX predictions of the process stream outlet state are compared with experimental data from the original wheel. The inlet states are nearly identical in each experiment; only the rotation speed varies (the experimental data are listed in Appendix E). For the model, the passages are assumed to be uniformly spaced, however, Nu_e is obtained from Table 5.2 and $Le_o = 1.16$ as determined from the high rotation speed analysis. The matrix properties are also assumed to be homogeneous and a range of matrix specific heats from that of the tape and gel combination alone to that obtained from the low rotation speed analysis are considered.

The agreement is not particularly good, especially for points at the lower rotation speeds. Uncertainties in the mass flow rates and rotation speeds used to calculate the parameters for MOSHMX are too small to explain the discrepancies. Bharathan, et al., (1986a,b), using the analogy method, were not successful in accurately predicting the experimental results from the rewound and microbead wheels, either. This was due in part to using a polynomial fit to manufacturer's data for the isotherm relation. In addition, they constrained the matrix specific

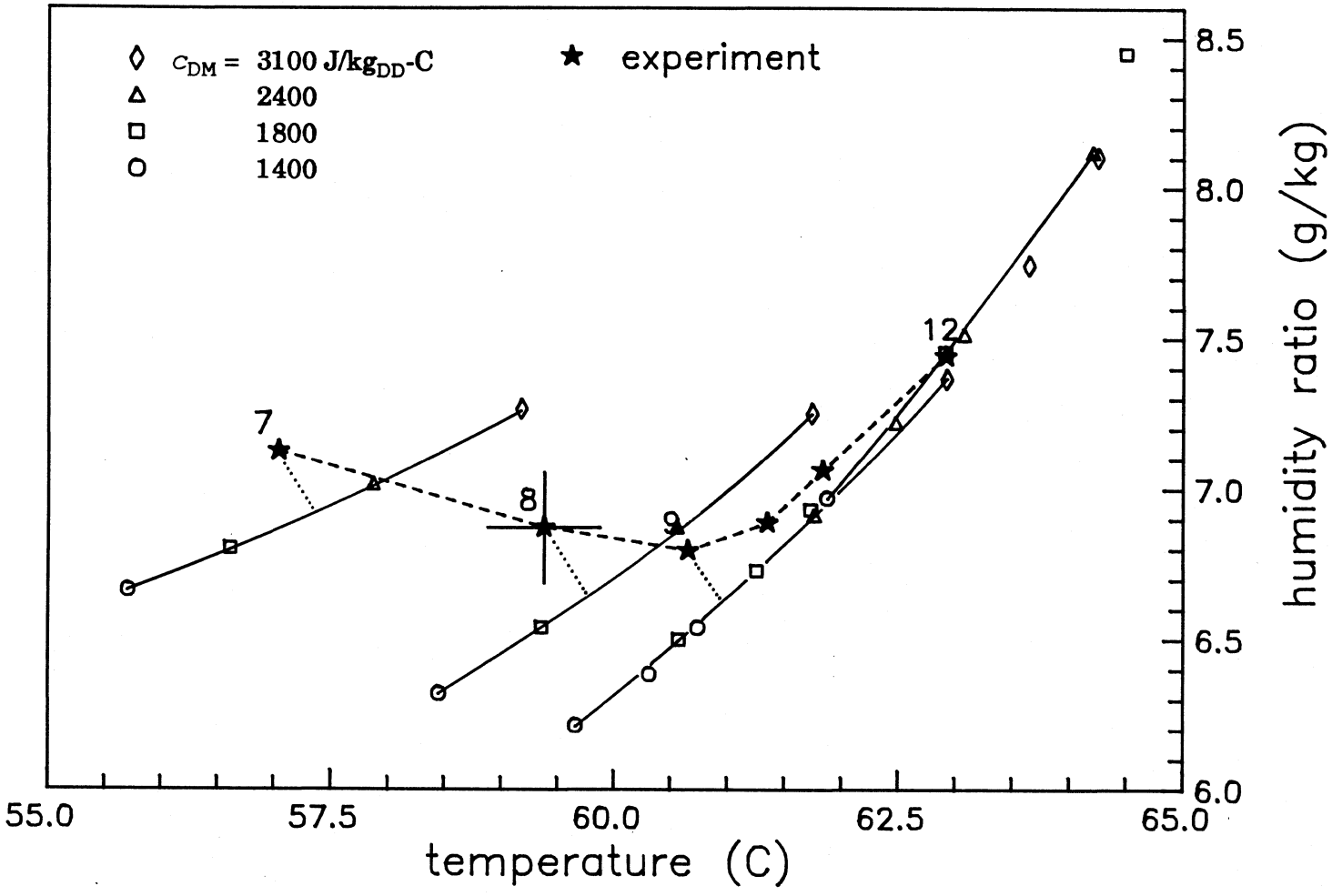

Fig. 5.20 Comparison of the process outlet states predicted by MOSHMX (uniform and homogeneous model) with experimental data from the original wheel. Experiment numbers refer to Appendix E.

heat to a value estimated from design information and did not include the spacers, although they did account for a linear variation with temperature.

The model essentially determines two variables, the process outlet temperature and the humidity ratio, based on several input parameters. With the proper choice of these parameters, it would appear possible for MOSHMX to accurately predict the correct outlet states. For example, numerical experimentation has shown that with the proper variation of the matrix specific heat and the overall Lewis number as functions of rotation speed, MOSHMX can accurately predict the experimental data shown in Fig. 5.20. The required variations of specific heat can be explained qualitatively in terms of the time constant of the spacers (see section 5.2.2). Similar arguments involving the time constant associated with the moisture diffusion process in the desiccant particles can be made for the Lewis number. These ideas were not pursued further in lieu of the simpler[5] model presented below.

5.4.2 Uniform passage spacings and *non*homogeneous matrix properties

The localized nature of the additional heat capacity contained in the spokes and spacers suggests that the dehumidifier may be modeled as two parallel exchangers as shown in Fig. 5.21. A fraction, ξ, of the inlet air flow is assumed to be affected by the presence of the spacers in the "b" exchanger. The remaining fraction of the air flow through the "a" exchanger sees only the desiccant-coated tape. Each exchanger is assumed to have uniform passage

---

[5]Simpler in terms of relating the parameters needed by MOSHMX to basic heat and mass transfer theory. The "simpler" model requires more computational effort.

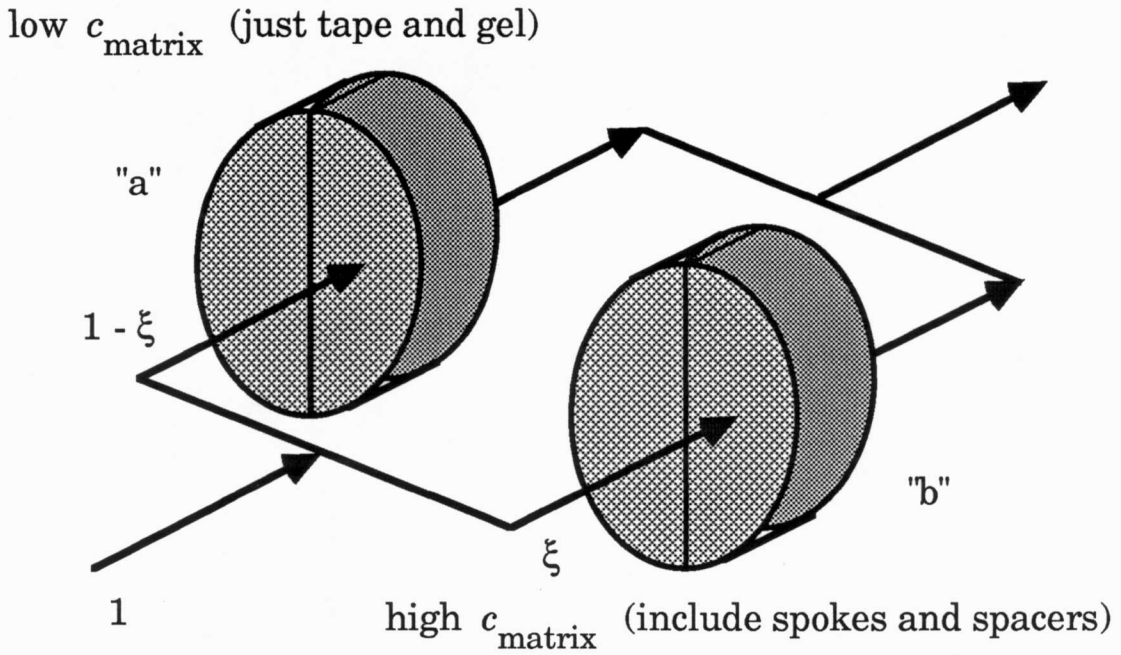

Fig. 5.21 Representation of a wheel with nonhomogeneous matrix properties as two parallel exchangers.

spacings with overall heat and mass transfer coefficients determined from Table 5.2.

For the analysis here, the specific heat of the "a" matrix is taken as

$$c_{DMa} = 1400 \quad [J/kg_{DD}\text{-}C] \tag{5.32}$$

which is approximately that calculated for the desiccant-coated tape used in the wheels tested. The specific heat of the "b" matrix per unit mass of dry desiccant is given by

$$c_{DMb} = 1400 + 1700/\xi \quad [J/kg_{DD}\text{-}C] \tag{5.33}$$

where $\xi = 1$ results in a value of 3100 which corresponds to that found from the low rotation speed data. The outlet states from the exchangers are weighted by the fraction of the air flow through each to obtain the average outlet state of the wheel,

$$\begin{aligned} w_{1,o} &= (1-\xi)\, w_{1,oa} + \xi w_{1,ob} \\ h_{1,o} &= (1-\xi)\, h_{1,oa} + \xi h_{1,ob} \\ t_{1,o} &= t(h_{1,o}, w_{1,o}) \end{aligned} \tag{5.34}$$

Fig. 5.22 shows a comparison of this model with the homogeneous model for conditions corresponding to data point "9" in Fig. 5.20; Fig. 5.23 shows the comparison with the full set of experiments.[6] Excellent agreement between the nonhomogeneous model and the experimental results is seen for points "7" through "11" given the proper choice of flow fraction. At higher rotation speeds,

---

[6]A comparison with a wider range of rotation speeds from very low to high is shown in Appendix E.

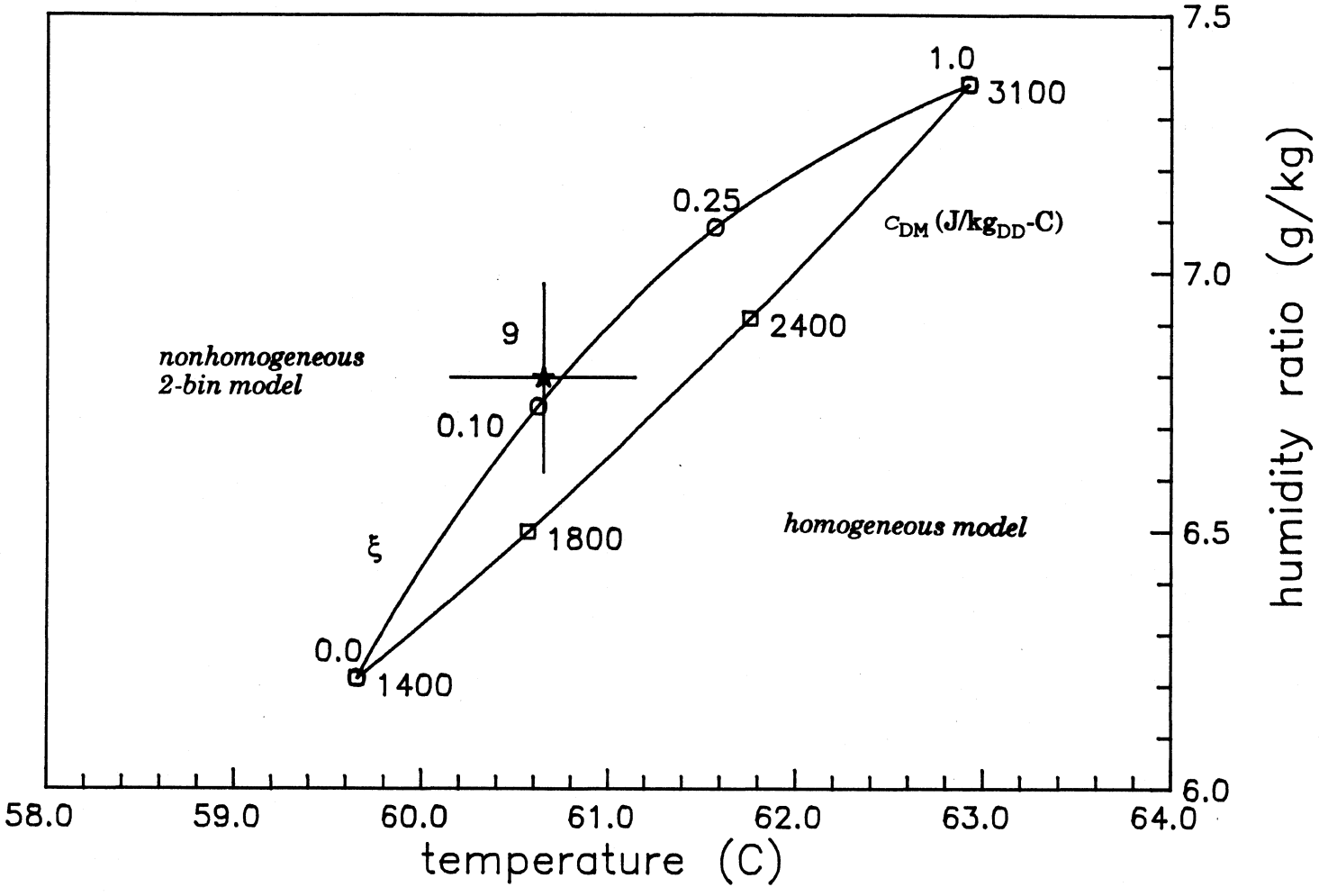

Fig. 5.22 Comparison of the homogeneous and nonhomogeneous models corresponding to point "9" in Fig. 5.20 (original wheel).

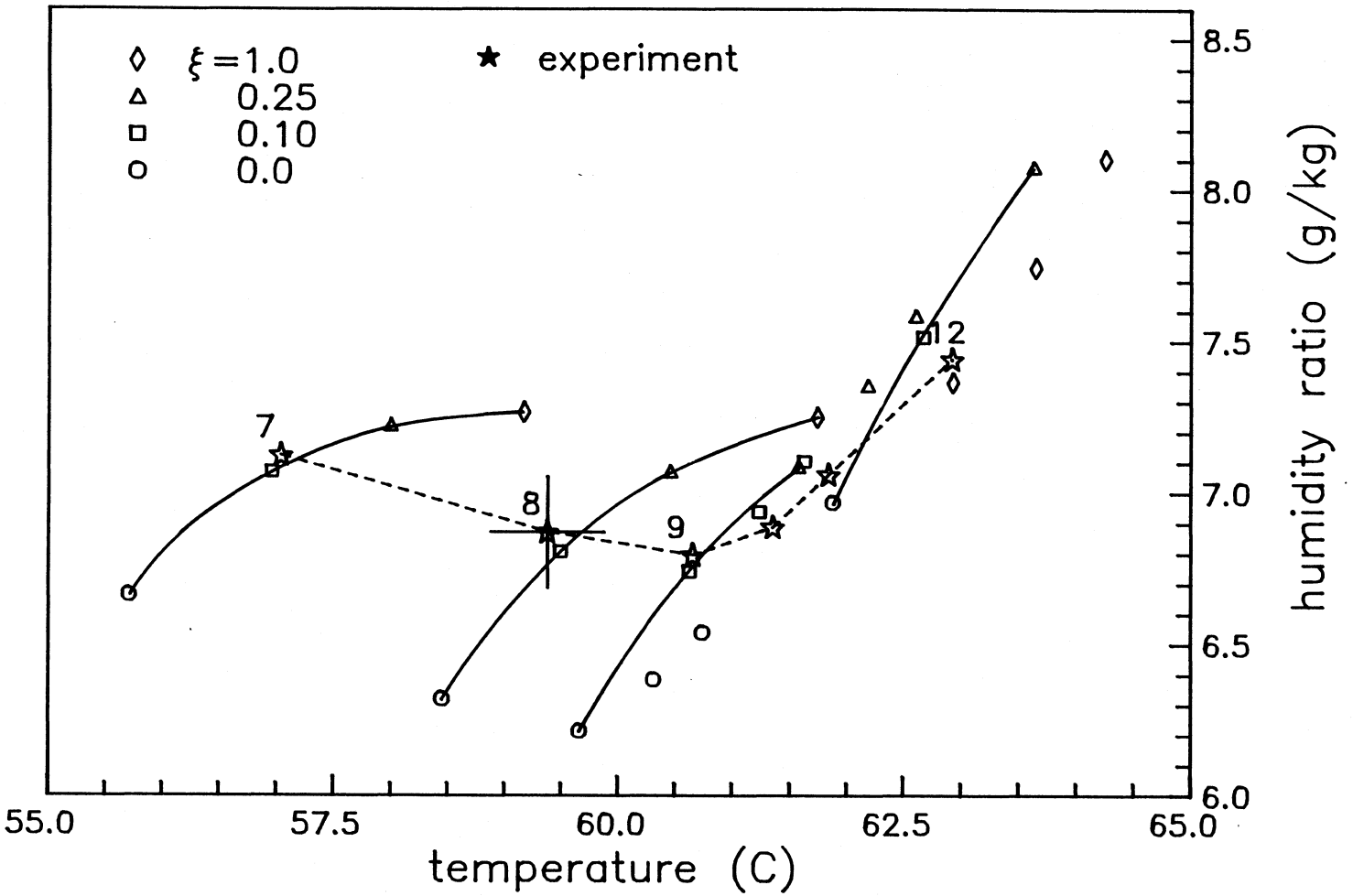

Fig. 5.23 Comparison of the process outlet states predicted by MOSHMX (uniform and *non*homogeneous model) with experimental data from the original wheel.

the homogeneous model appears to provide better agreement. This is explained in the following paragraph.

The wheel rotation speed at the point of maximum dehumidification (minimum $w_{1,o}$, point "9"), is 10 rev/hr. Based on the time constant for the spacers of approximately 50 sec estimated in section 5.2.2, the spacers are exposed to an air stream for approximately 3 time constants, sufficient to strongly participate in the transfer processes. At higher rotation speeds (point "12" is at 20 rev/hr), the spacers can not fully participate. Therefore, the coefficient "1700" in Eq. (5.33) is no longer appropriate. Reducing this coefficient has the effect of reducing the curvature of the locus of outlet states as a function of flow fraction ξ. This would improve the agreement of the model with the data for these higher rotation speeds and is consistent with the results in section 5.3.3 where the homogeneous model accurately predicted the very high rotation speed experimental data. No attempt is made here to account for the time constant of the spacers as the rotation speeds involved are intermediate between those for optimum dehumidification and enthalpy exchange and so would not be encountered in practice. However, the effect could be important in dehumidifier wheels in which the time constant of the spacers (or other localized structural components) is shorter than in the wheels tested here.

The results indicate that approximately 10% of the flow and matrix are affected by the presence of the spacers in the region near optimum dehumidification. Assuming the desiccant-coated tape to act as a simple fin, a rough estimate indicates that approximately 3-5% of the matrix is affected by the presence of the spacers. The thermal conductivity and conduction area of the desiccant-coated tape are difficult to estimate, making this calculation very

uncertain. However, it will be important to be able to estimate the impact of the spacers if MOSHMX (or a similar model) is to be used in the design process.

MOSHMX predictions for a range of regeneration inlet states are compared with experimental data from the original wheel in Fig. 5.24. Again, good agreement is noted at a flow fraction of approximately 10%. The relative humidities of the regeneration inlet states range from 2-10%, the process inlet state is 50%. The results suggest that Van den Bulck's isotherm relation accurately represents the desiccant properties under these conditions.

Fig. 5.25 shows a comparison of the MOSHMX predictions with experimental data from the original wheel for a range of process inlet states and a constant regeneration state. The experimental results for point "4" are suspect because the mass and energy balance closures are not very good. Points "2" and "3" are for rather low humidity ratios (8 g/kg); the discrepancies between the model and experiments may be due to the isotherm relation.

Fig. 5.26 shows a comparison with data from the rewound wheel for a range of inlet humidity ratios which are approximately the same for both streams. Point "4" is at very humid conditions ($w_{j,i} \approx 21.5$ g/kg). The effect of flow rate is shown in Fig. 5.27. The results indicate that the effective transfer coefficients determined experimentally from the high rotation speed data allow MOSHMX to accurately predict the performance of an exchanger operating at rotation speeds for optimum dehumidification. It appears that a slightly smaller fraction of the air flow and matrix are affected by the spacers than in the original wheel.

MOSHMX predictions are compared with data from the microbead wheel for a range of inlet humidity ratios in Fig. 5.28. Again, very good agreement is

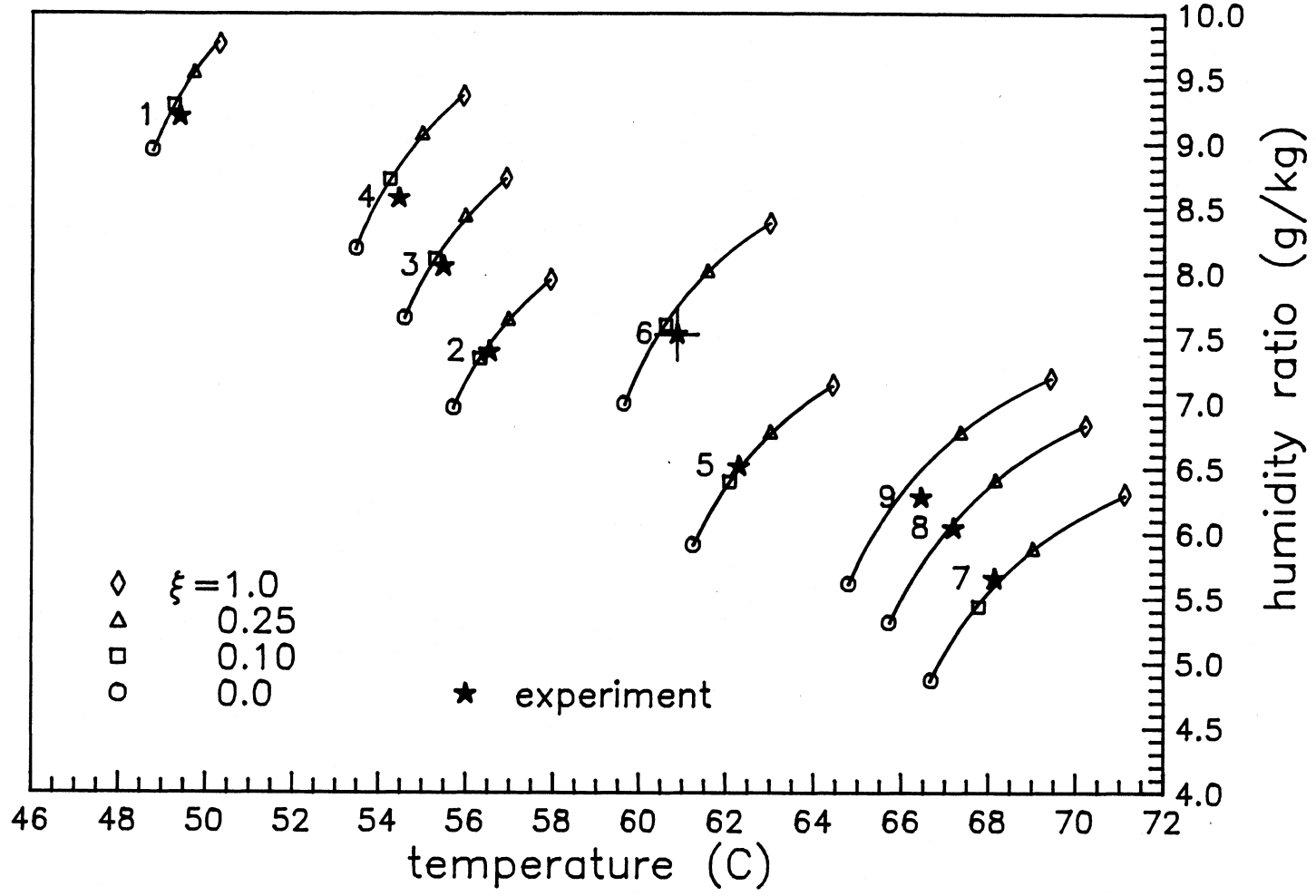

Fig 5.24 Comparison of process outlet states predicted by MOSHMX with experimental data from the original wheel for a range of regeneration inlet states. Experiment numbers refer to Appendix E.

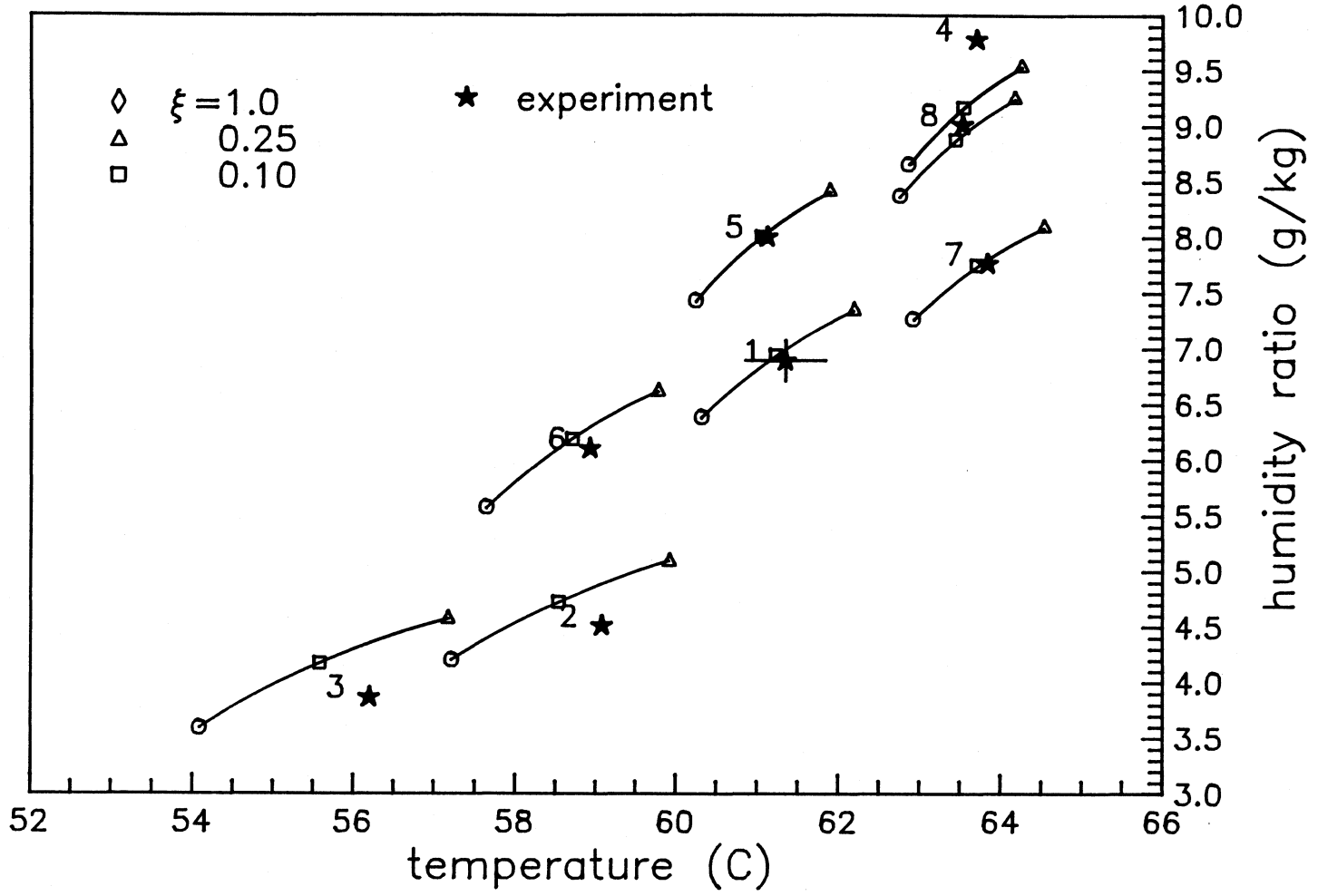

Fig 5.25 Comparison of process outlet states predicted by MOSHMX with experimental data from the original wheel for a range of process inlet states.

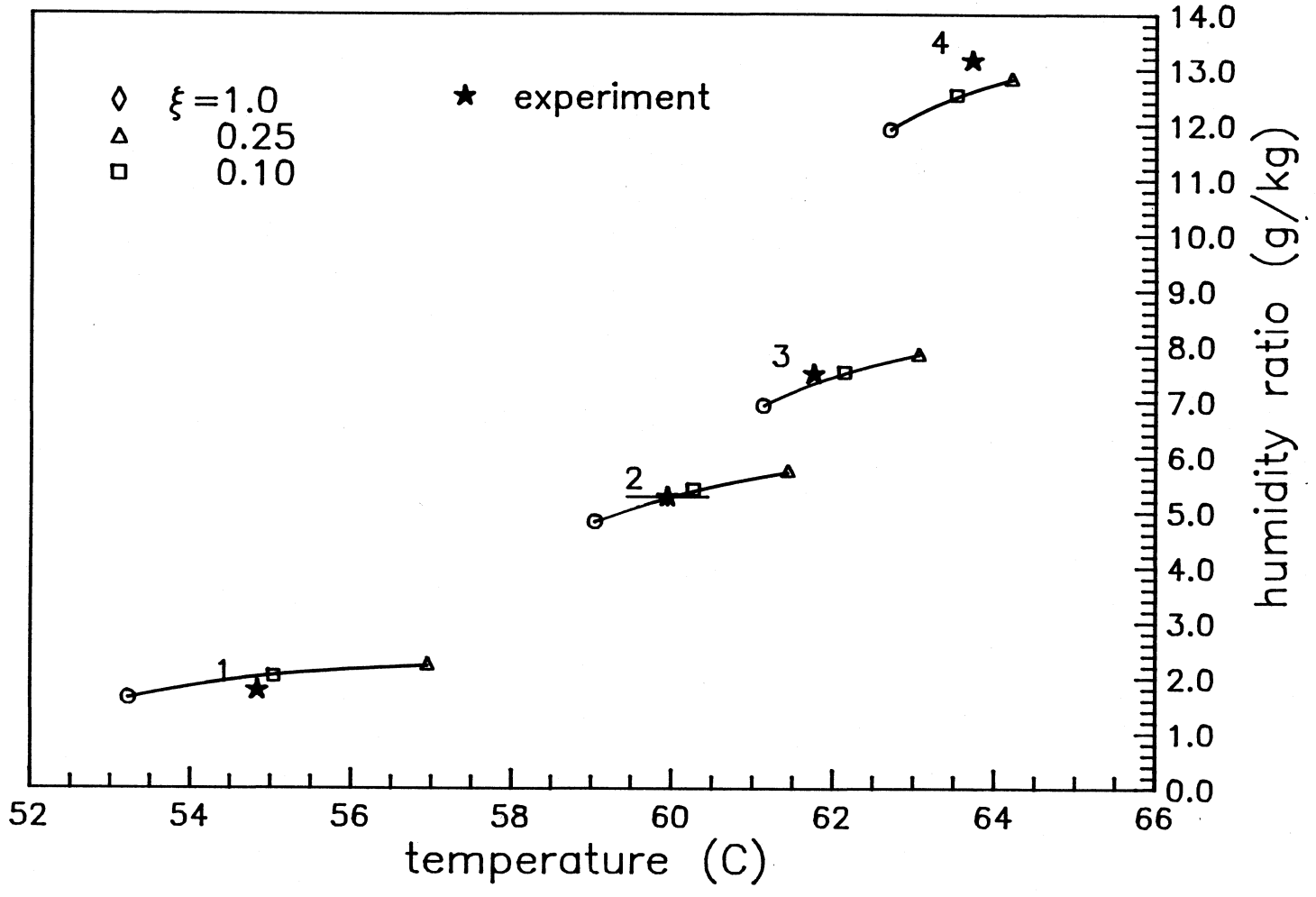

Fig 5.26 Comparison of process outlet states predicted by MOSHMX with experimental data from the rewound wheel for a range of inlet humidity ratios.

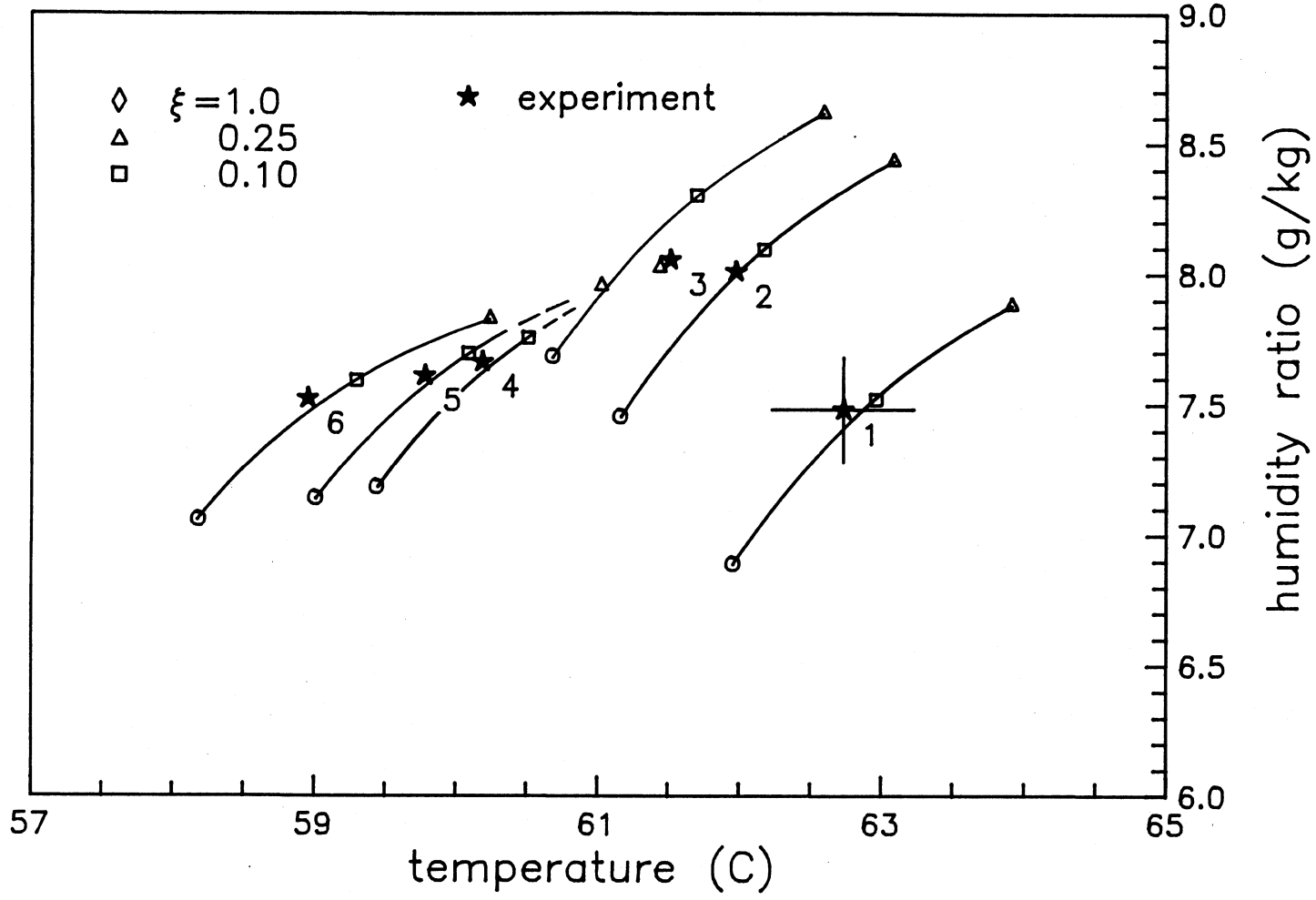

Fig 5.27 Comparison of process outlet states predicted by MOSHMX with experimental data from the rewound wheel for a range of flow rates.

obtained. The process inlet state for point "1" is approximately 70% relative humidity. This is near the region where the manufacturer's data indicates that the sorption properties of the microbead gel may diverge from those of the crushed gel used in the other wheels. Fig. 5.29 shows the impact of flow rate. Larger discrepancies occur at the lower flow rates where the model overpredicts the performance of the wheel. This supports the contention that the transfer coefficients derived from the high rotation speed experiments (especially those at lower flow rates) may be subject to unaccounted for errors as discussed in section 5.3.3.

The variation of the outlet states as a function of rotation angle were measured during several of the experiments on the original wheel. A representative example is shown in Fig. 5.30. A flow fraction of $\xi = 0.1$ is used in MOSHMX. The outlet profile temperature measurements are averaged over approximately 10-15 minutes of operation and so contain the effects of the spokes and spacers passing by. The outlet humidity ratios are averaged over a shorter period (one at a time per period), however, these averages include several passes by the spokes and spacers.

In general, MOSHMX reproduces the profiles very well, especially for the process period. MOSHMX appears to predict a sharper and faster moving transfer zone for $0.1 < \theta/\beta < 0.2$ in the regeneration period. This result has been observed by Schlepp and Barlow (1984) and Pesaran and Mills (1984) in comparisons of their models with single-blow experiments. This could be due to uncertainties in the property relations or in the mass transfer coefficient for the regeneration period used in the model. This problem requires further

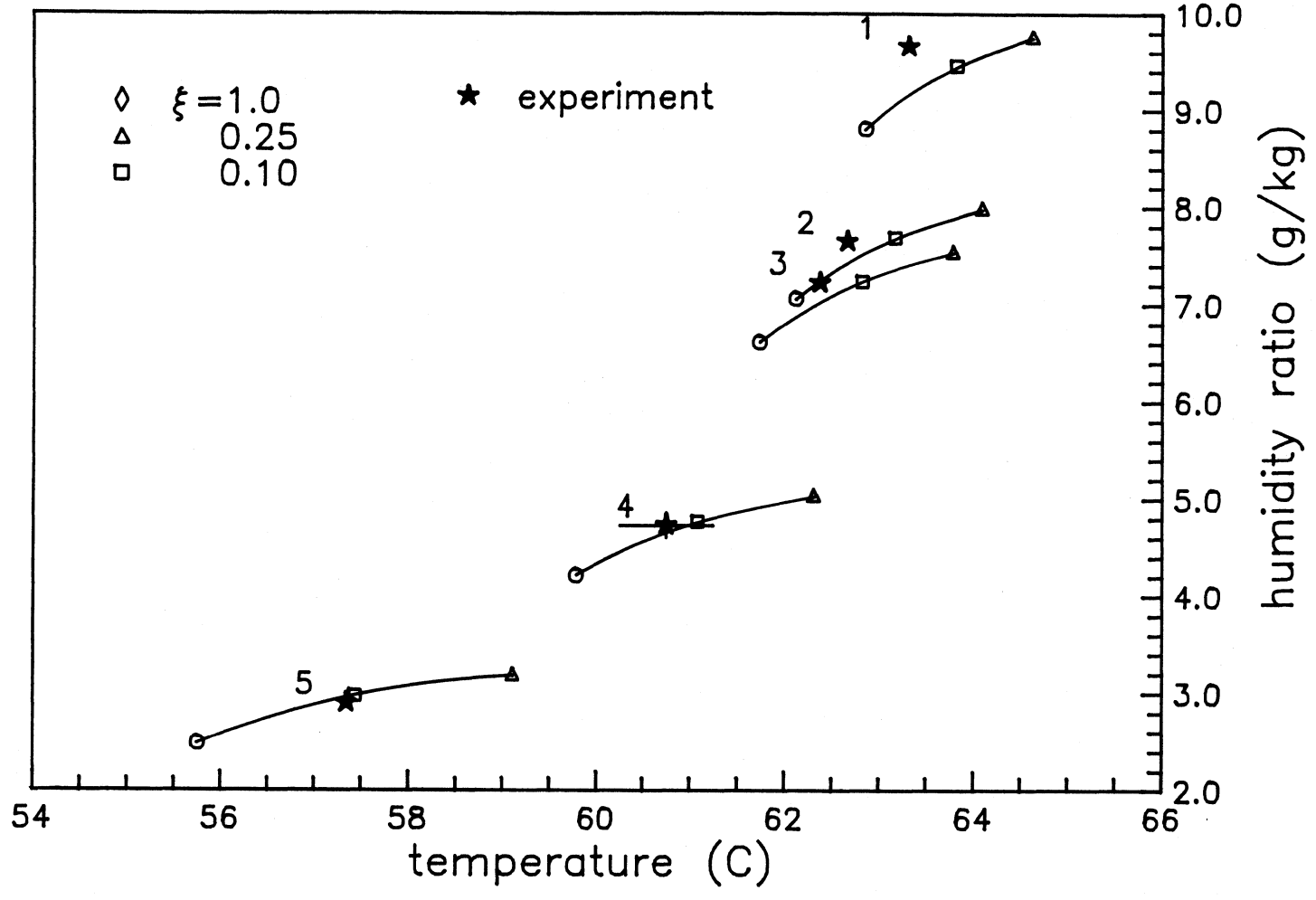

Fig 5.28 Comparison of process outlet states predicted by MOSHMX with experimental data from the microbead wheel for a range of inlet humidity ratios.

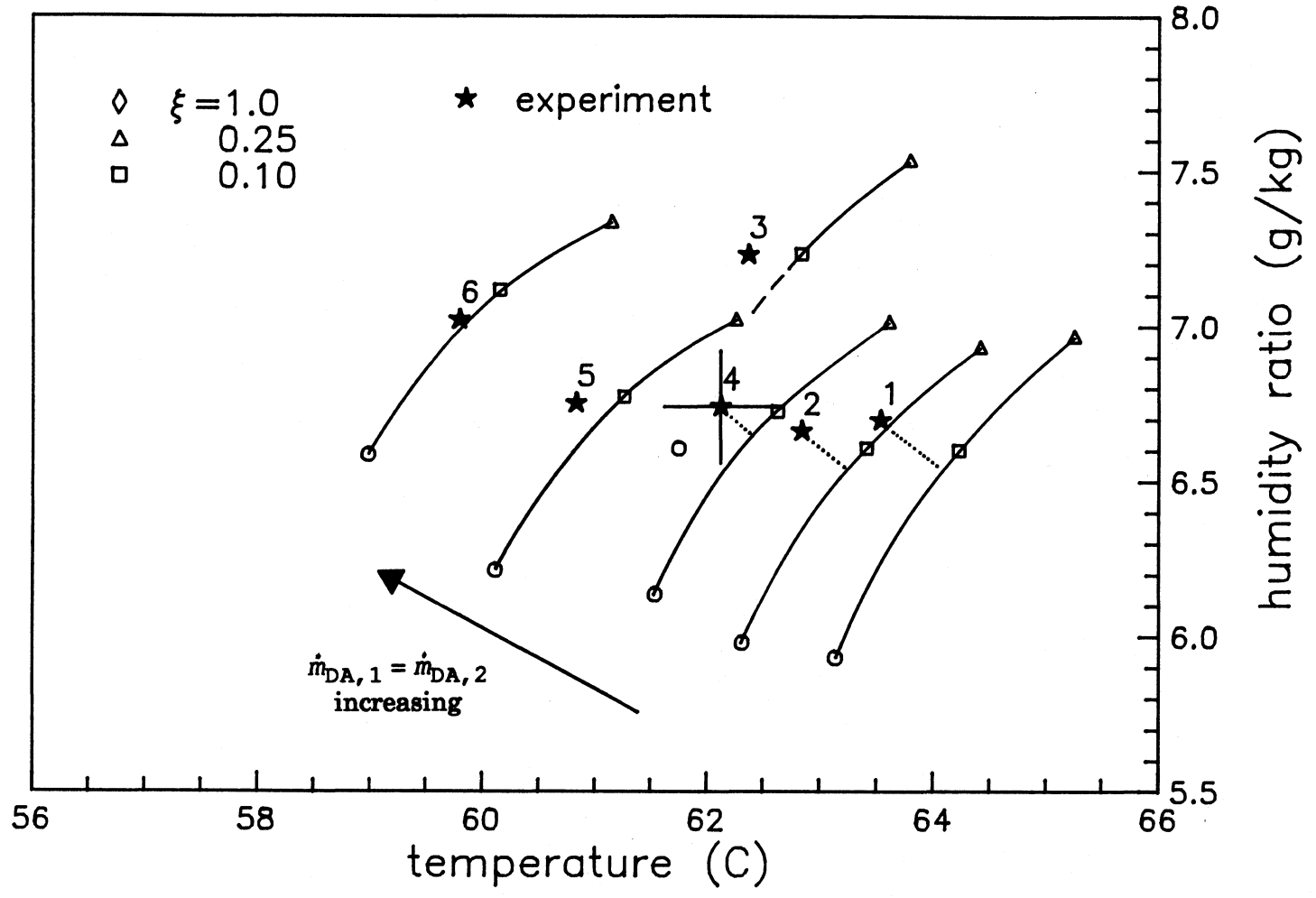

Fig 5.29 Comparison of process outlet states predicted by MOSHMX with experimental data from the microbead wheel for a range of flow rates.

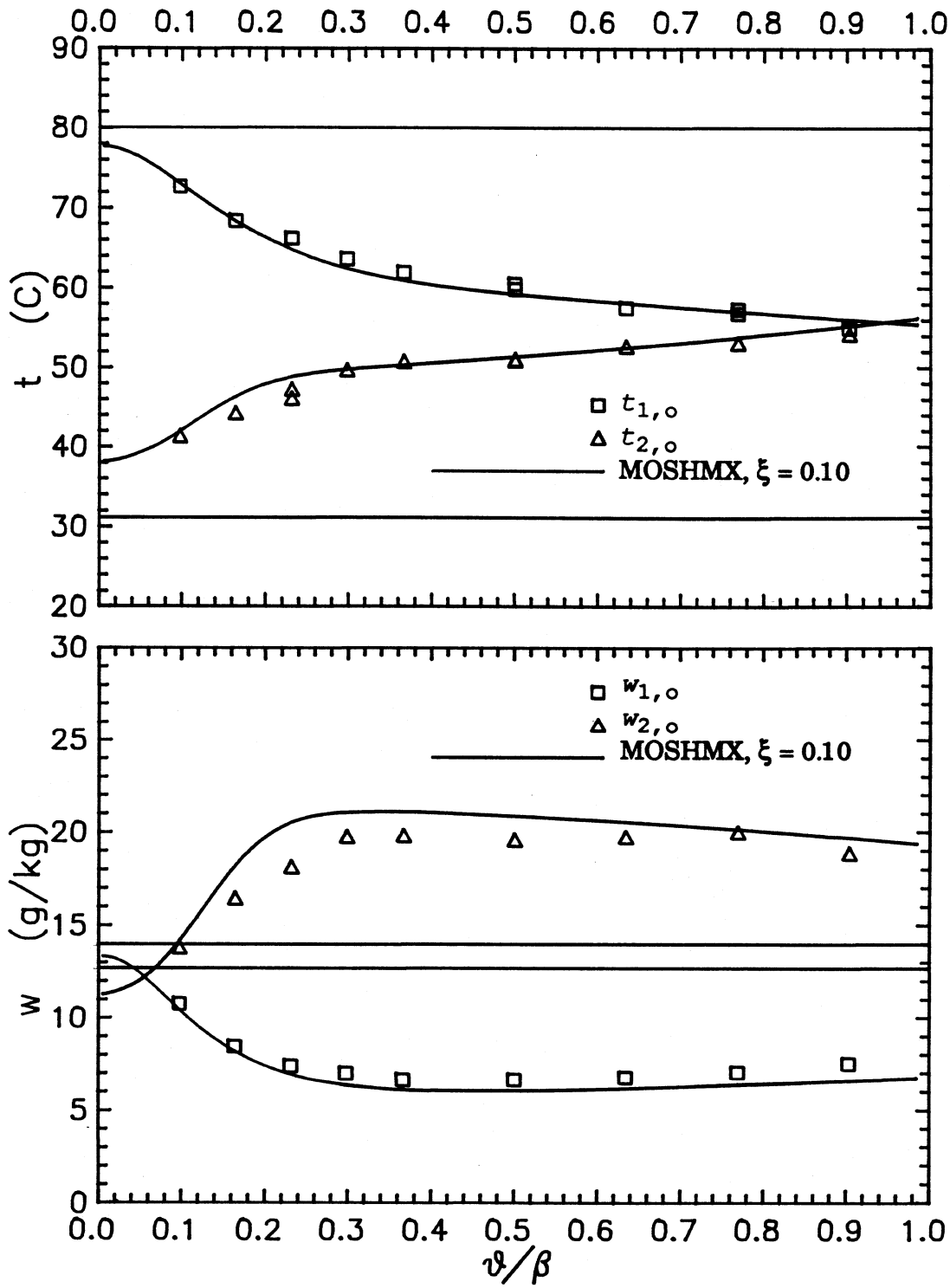

Fig. 5.30 Profiles of outlet states as a function of rotation angle for experiment 05-06-86 2A (original wheel, also point "11" in Fig. 5.23).

consideration to fully understand the heat and mass tranfer processes in the wheel.

There appear to be discrepancies between the integrated average humidity ratios from the measured profiles and the bulk measurements made in the experiments. The reason for this has not been determined. It is not likely to be the sensors as the same sensor was used to measure the bulk outlet and the profile humidity ratios in each period (see section 3.2).

Other sets of data are presented in Appendix E along with a comparison with MOSHMX predictions. Agreement between the model and experiments are similar to those presented above.

5.4.3 Modeling of a distribution of passage sizes explicitly with MOSHMX

In the previous section, the distribution of passage sizes present in the dehumidifiers tested was accounted for by experimentally determined effective overall heat and mass transfer coefficients. Here, the distribution of passage sizes will be modeled explicitly.

As in section 5.3.4, each channel is assumed to be independent and the wheel to act as a set of parallel exchangers as in Fig. 5.15. The individual channel Ntu's for bin k, $Ntu_{t,k}$ and $Ntu_{w,k}$, are calculated as in section 5.3.4. In addition, the mass capacity rate ratio for each channel is given by

$$\Gamma_{j,k} = \Gamma_j / (\dot{m}_{j,k}/\dot{m}_{j,u}) \tag{5.35}$$

Each of the n parallel exchangers which represent a particular channel width can be split again into two wheels to represent nonhomogeneous matrix properties as in Fig. 5.21. In Fig. 5.31, a 22-bin model representing an 11-bin

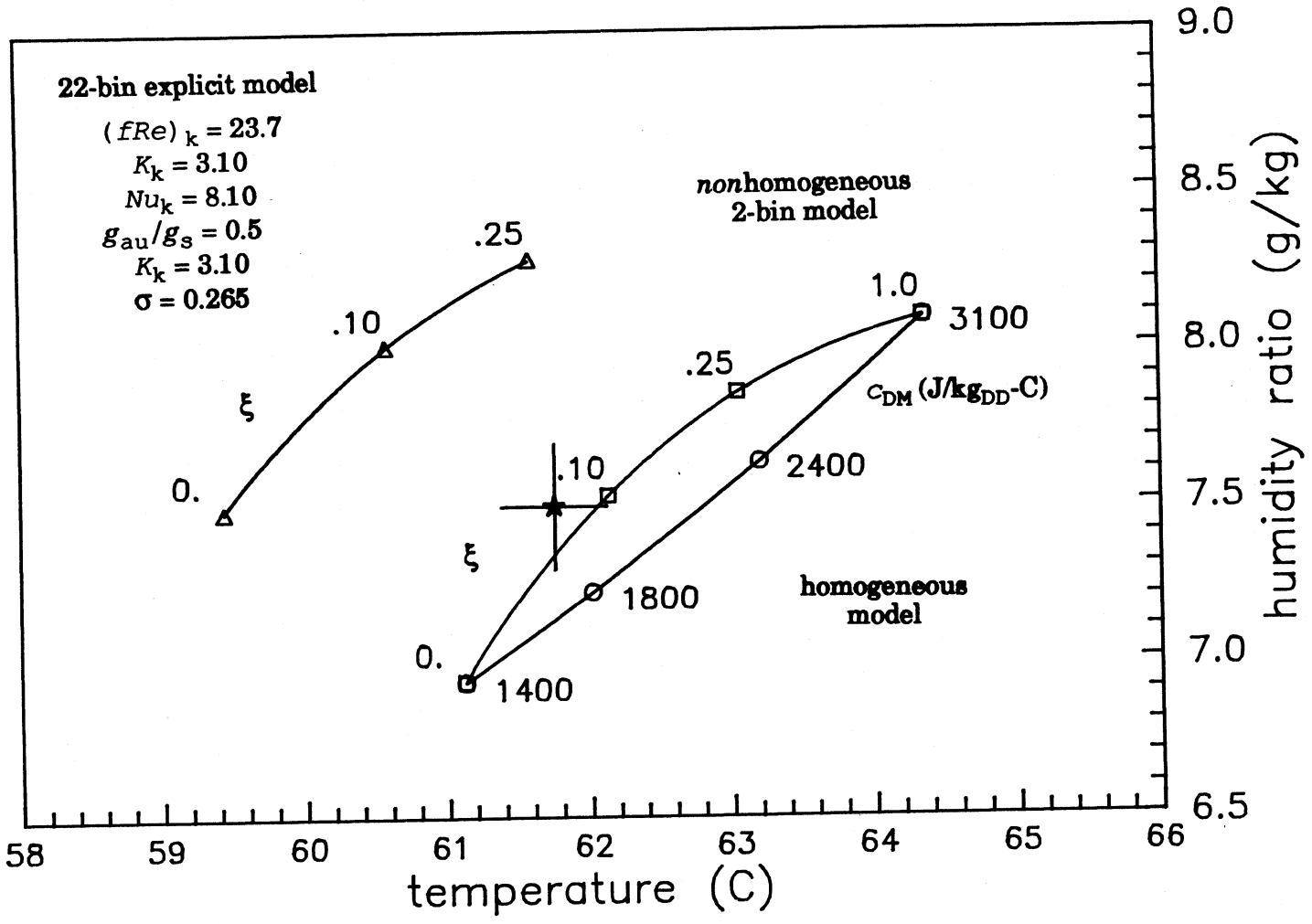

Fig 5.31 Comparison of explicit model for distribution of passage sizes with other models and experiment 11-18-85 2A (rewound wheel).

distribution of passage sizes each with 2 bins representing different specific heats is compared with the "1-bin" homogeneous model and a 2-bin nonhomogeneous model. A range of specific heats is considered in the homogeneous model. A range of flow fractions, ξ, are used in the two nonhomogeneous models. The effective transfer coefficients for the homogeneous and 2-bin models are obtained from Table 5.2 using the operating conditions for experiment "11-18-85 2A" on the rewound wheel (also shown in Fig. 5.31). The 22-bin model uses the channel parameters $(fRe)_k = 23.7$, $K_k = 3.10$, $Nu_k = 8.10$, $g_{au}/g_s = 0.5$, and a lognormal standard deviation of 0.265. When these parameters are introduced into the procedure in section 5.3.4, they result in the Nu_e and Le_o used in the homogeneous and 2-bin models.

The comparison shows that the explicit model does not work very well, at least for this wide distribution of passage spacings. The reason for this is that the channels are not independent of each other. Fig. 5.32 shows the outlet temperature profiles for several different passage sizes. There exist large temperature differences between neighboring channels. The consequent heat transfer affects the mass transfer. This leads to the conclusion then that the effective transfer coefficients determined from the high rotation speed experiments account for these interactions as well as for the effects of the distribution of passage spacings. It is somewhat surprising that the transfer coefficients derived from the high rotation speed results allow MOSHMX to accurately predict medium rotation speed behavior as the temperature distributions are likely to be very different in the two cases.

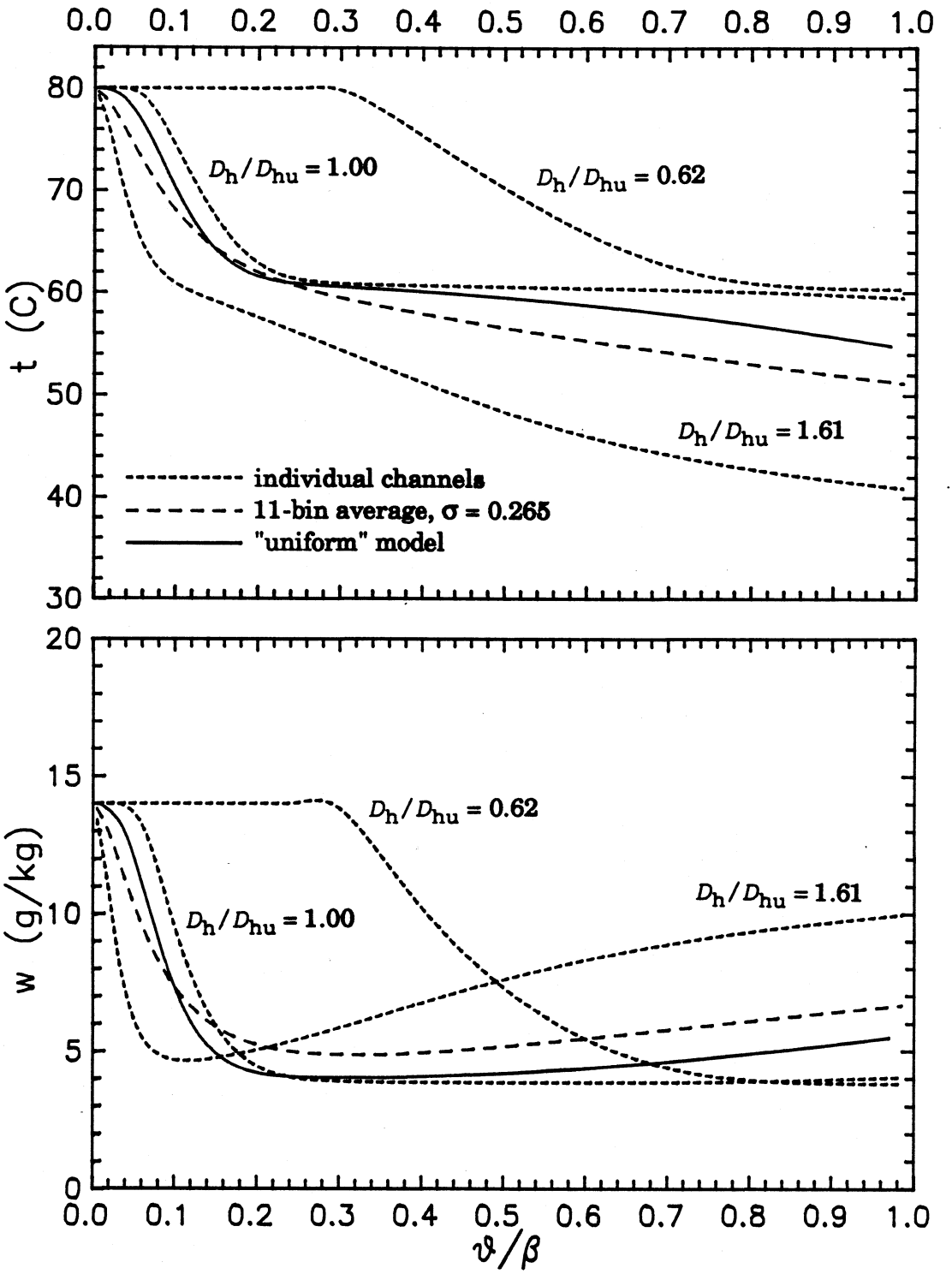

Fig. 5.32 Profiles of the process stream outlet states predicted by MOSHMX for several bins representing a distribution of passage sizes.

5.5 Summary

Verification of the MOSHMX model against the experimental data available is complicated by the presence of distributions of passage sizes and nonhomogeneous matrix properties in the wheels tested. In addition, uncertainties exist in model parameters derived from design information alone.

A pressure drop analysis shows the significant impact of a distribution of passage sizes. However, it provides insufficient information to fully characterize the shape and size of the distribution, at least for the rather wide distributions present in the wheels considered here. The experimental pressure drop data indicate that the very rough passages of the original and rewound wheel result in an increased pressure drop (approximately 8%) due to effects in the entrance region compared with smooth channels. The effects of passage spacing variation and increased entrance losses will need to be included when estimating the parasitic power consumption of dehumidifiers.

The consistency of the active mass of desiccant in a dehumidifier wheel and the isotherm relation used to model that desiccant can be checked by analyzing the results of very low rotation speed experiments. Experimental results from the three wheels tested agree well with the isotherm relation developed by Van den Bulck (1987). In addition, an independent estimate of the effective specific heat of the matrix can also be obtained from these experiments. The experimental results indicate that the spacers and other structural components strongly participate in the transfer processes at low and medium rotation speeds.

By considering results from high rotation speed experiments where the

wheel acts as an enthalpy exchanger, overall heat and mass transfer coefficients can be derived which allow a MOSHMX-type model to accurately predict exchanger performance. These transfer coefficients are shown to be very sensitive to the distribution of passage sizes. For the silica gel-coated tape considered here, an overall Lewis number of 1.2 was found. The variance of this value from the much larger values obtained by Van den Bulck remains unresolved.

Comparisons of the MOSHMX model with medium rotation speed experimental data show that the assumption of homogeneous matrix properties does not work well for the wheels tested here. By modeling the nonhomogeneous matrix properties as two parallel exchangers, good agreement between the model and data was attained. The data indicate that approximately 90% of the flow sees only the desiccant-coated tape, the other 10% is affected by the presence of the spacers. Analytical estimation of the effect of structural components is at present uncertain.

Modeling the distribution of passage spacings explicitly is not successful in predicting the experimental results. This is due to heat transfer between neighboring channels which is not accounted for in the explicit model. The overall transfer coefficients determined from the high rotation speed experiments contain the effects of this coupling. Use of these coefficients then allows MOSHMX to accurately predict the performance of "real" dehumidifiers.

Chapter 6

Conclusions and Recommendations

Air conditioning systems using desiccant dehumidifiers are becoming viable alternatives to conventional vapor compression machines. However, continuing success will require further advances in performance and a better understanding of dehumidifier processes.

The objective of the work presented in this thesis is to verify the accuracy of tools used in the analysis of desiccant dehumidifiers. This has involved the comparison of models against one another and the comparison of predictions by the models against experimental data. The conclusions and recommendations which result from this work are presented below.

6.1 Models of desiccant dehumidifiers

A wide variety of models for desiccant dehumidifiers exist. Computationally simple models are useful for simulating the performance of a desiccant system over long periods of time to ascertain the competitiveness of a concept. More detailed models are useful for studying potential improvements in dehumidifier design and performance.

Two particular detailed models have been used extensively to investigate both dehumidifier and system performance. The program MOSHMX (Maclaine-cross, 1974) is a finite difference solution of a conventional set of partial differential equations which are assumed to represent the processes in rotary dehumidifiers. It makes use of techniques to increase its efficiency and potential accuracy. The program DESSIM is based on a heuristic "pseudo-steady-state"

concept (Barlow, 1984). The program employs dimensional quantities and is conceptually and computationally straightforward.

From a comparison of the "pseudo-steady-state" concept with the finite difference solutions, it is found that the "pseudo-steady-state" concept locally uncouples the mass transfer from the heat transfer. However, the errors that are introduced result in compensating errors during calculations at the next space or time step and the errors decrease as the grid size decreases. *It is therefore concluded that the "pseudo-steady-state" model can accurately predict the behavior of desiccant dehumidifiers relative to a finite difference solution. This validates previous work that has been reported using the DESSIM model.*

The finite difference solution is found to be more computationally efficient with superior mass and energy balance closure and numerical stability. Together with its more fundamental nature, *it is recommended that the finite difference solution, either in MOSHMX or substituted into DESSIM, be used as the preferred tool for the investigations of dehumidifiers.*

Due to its heuristic nature, *it is recommended that modifications of the "pseudo-steady-state" concept not be used to model other types of desiccant dehumidifier devices* (at least for quantitative results) such as the direct solar-regenerated collector/dehumidifier. Rather, a more fundamental development should be employed.

6.2 Experimental facility and test dehumidifiers

The models discussed in this work are based on a set of simplifying assumptions. In particular, overall transfer coefficients which contain both the air- and solid-side transfer resistances are assumed and taken to be constant. In

addition, the matrix is assumed to consist of uniformly sized channels and have homogeneous properties. The usefulness of these models depends upon validation of the assumptions or modifications to account for departures from the assumptions.

6.2.1 Experimental facility

A facility has been designed and constructed at the Solar Energy Research Institute to provide experimental data for the purpose of verifying the validity of the model assumptions. The facility contains the equipment, controls, and instrumentation necessary for the accurate experimental characterization of rotary desiccant dehumidifiers. Data reduction and correction procedures have been developed to compensate for seal leakage rates and energy and mass balance errors.

The facility as been found adequate for obtaining the steady-state performance of state-of-the-art rotary dehumidifiers. However, improvements in measurement accuracy and uncertainty will be needed to characterize devices of advanced design. In addition, improvements in controls will be needed to study the transient response of rotary dehumidifiers.

6.2.2 Test dehumidifiers

Three rotary dehumidifiers were contructed for testing purposes. They consisted of a silica gel-coated tape which was spirally wound into a parallel plate matrix. This design was chosen because of the well established momentum, heat, and mass transfer characteristics of laminar flow in parallel plate passages. However, manufacturing difficulties resulted in nonuniform passage sizes. In

addition, the presence of the spacers and other localized structural components created nonhomogeneous matrix properties. These are not consistent with the assumptions made in the models and introduce additional complexities which must be dealt with. *It is recommended that in future experiments, great effort is taken to ensure that the channel spacings are uniform and the matrix properties homogeneous.*

6.3 Validation of models against experiments

For models to be useful in the design and development process, the parameters required should be obtainable from established theory. The presence of distributions of passage sizes and nonhomogeneous matrix properties make this questionable for the wheels tested here. However, procedures have been presented to account for these effects.

6.3.1 Pressure drop analysis

An analysis of pressure drop can provide an estimate of the width of the distribution of passage sizes present in an exchanger. However, at most a two parameter distribution can be determined. This is not sufficient for the wide distributions present in the wheels tested here. It may be satisfactory for narrower distributions which will be required for high performance devices.

The pressure drop analysis showed that the very rough channels created by the silica gel particles caused a significant increase in the pressure loss associated with the entrance region compared with that expected for smooth plates. The effective entrance coefficient, K, was found to be approximately 3.10 for the rewound wheel. This results in an 8% increase in overall pressure drop

over that expected for smooth channels. *The increased pressure drop associated with very rough channels should be accounted for in any estimate of the parasitic power consumption for a rotary dehumidifier. Further quantification of this phenomena should be undertaken if dehumidifier designs employing such rough-walled channels are considered.*

6.3.2 Desiccant properties

Dehumidifier models must employ accurate representations of the desiccant sorption properties. Limited manufacturer's data may not be satisfactory. A procedure has been presented for testing the consistency of the desiccant properties against the results of experiments at very low rotation speeds. *The silica gel properties determined by Van den Bulck* (1987) *have been found to be accurate for the desiccants used in the test dehumidifiers.*

6.3.3 Effective overall transfer coefficients

Estimation of the coefficients for heat and mass transfer from basic theory is confounded by the distribution of passage sizes present. The overall transfer coefficients can be determined from experimental results at high rotation speeds, however. When supplied to MOSHMX, these coefficients allow the model to reproduce the high rotation speed experimental data as well as to accurately predict dehumidifier performance at medium rotation speeds (dehumidification conditions) over a range of inlet states. *This indicates that the assumption of constant overall transfer coefficients made in MOSHMX is satisfactory for modeling the wheels tested here.* However, estimation of transfer coefficients from established theory remains untested.

The experimentally determined transfer coefficients contain the effects of heat transfer between neighboring channels due to the distribution of passage sizes. Because of this coupling, it is not likely that an accurate estimate of the overall transfer coefficients can be obtained from the passage spacing distribution, at least for wide distributions.

An overall Lewis number of 1.0-1.2 has been obtained from experimental data. This indicates that the average solid-side mass transfer resistance is about one-half the air-side resistance. Van den Bulck (1987) found much larger values (3-7) from his single-blow experiments. The difference is suspected to be due to the different time histories of the desiccant particles in the two configurations. *It is recommended that the issue of solid-side mass transfer resistance be pursued further to resolve this difference and allow accurate prediction of the overall mass transfer coefficient.*

6.3.4 Nonhomogeneous matrix properties

The localized nonhomogeneous properties created by the spacers were found to significantly effect the performance of the dehumidifier. *Accurate modeling the dehumidifier requires that nonhomogeneous properties be accounted for.* By considering the wheel to consist of two parallel exchangers, MOSHMX can accurately predict the results of experiments. However, the fraction of the matrix and flow affected by the spacers has not been determined analytically. *Techniques for estimating the effect of nonhomogeneous properties need to be developed to accurately model desiccant dehumidifiers.*

Appendix A

The Ventilation Cycle Desiccant Air Conditioning System

Current interest in desiccant air conditioning systems began with Pennington's (1955) invention of a regenerative dehumidifier which he incorporated into an evaporative cooling system. This configuration of components, shown in Fig. A.1, is commonly referred to as the ventilation cycle because "fresh" outside air is processed and supplied to the space to be conditioned. Conventional air conditioning systems usually recirculate the room air. The ventilation cycle has received much of the research and development attention given to desiccant cooling systems.

A.1 Cycle description

In the ventilation cycle, outside air (state 1) is dried (state 2) as it passes through the desiccant dehumidifier. The temperature of the air also rises due to the heat of sorption that is released as the water is adsorbed by the desiccant. The air stream is then sensibly cooled in a heat exchanger (state 3) using evaporatively cooled exhaust air (state 6) as the low temperature sink. The process air stream is further evaporatively cooled (state 4) and passed to the space to be conditioned (state 5). The heat exchanger reclaims energy from the process air stream at state 2 and transfers it to the regeneration air stream (state 7). Additional thermal energy is supplied to reach the required regeneration temperature (state 8). The moisture in the desiccant is then removed by the hot air stream (state 9).

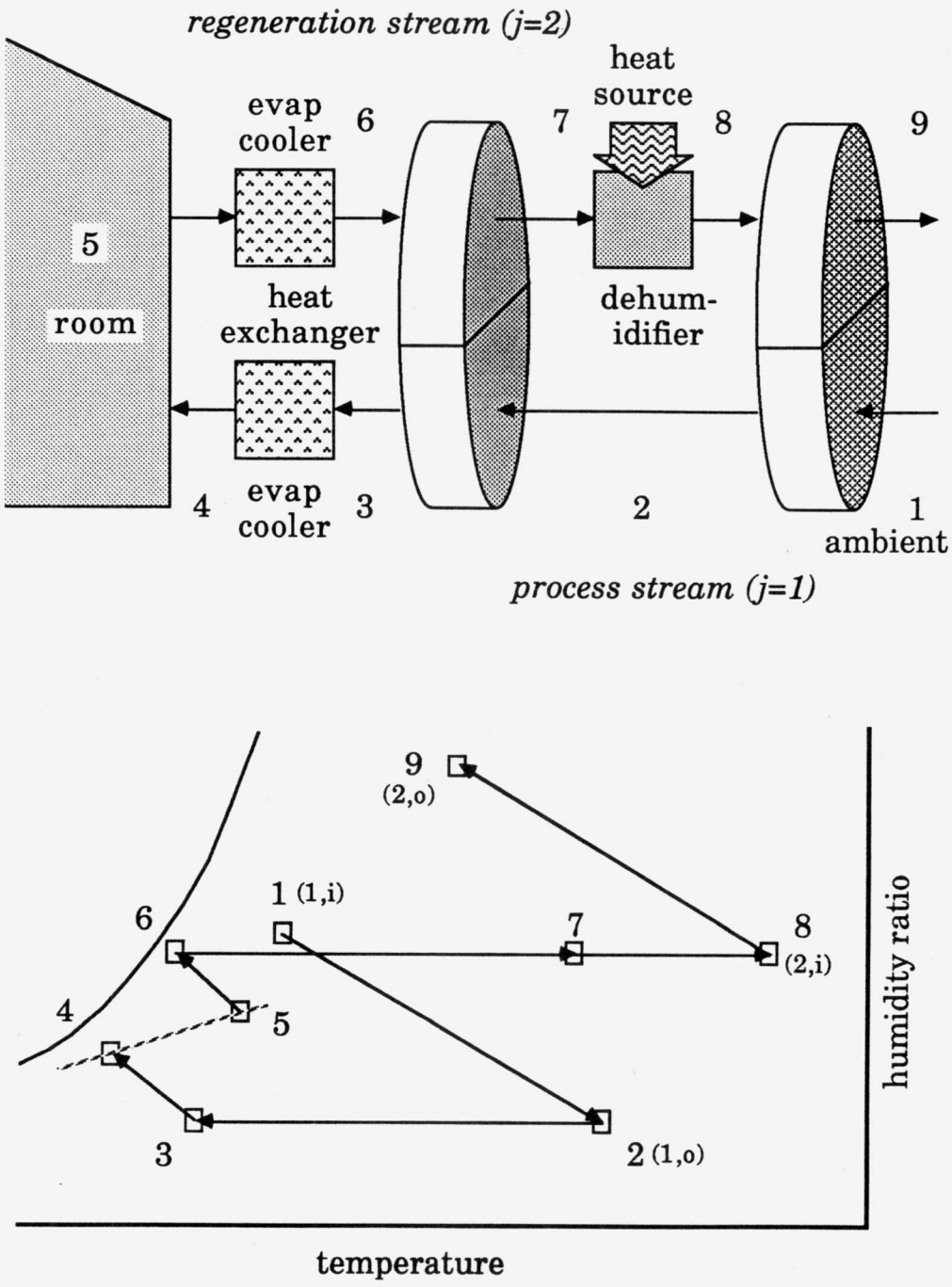

Fig. A.1 Ventilation cycle desiccant air conditioning system.

The cooling capacity of the ventilation cycle is given by the mass flow rate of air times the enthalpy difference between the space and supply air states,

$$Q_{tot} = \dot{m}_{DA,1}(h_5 - h_4) \tag{A.1}$$

The effectiveness of the evaporative cooler determines the fraction of sensible cooling (temperature reduction) and latent cooling (moisture reduction). The thermal coefficient of performance is measured as

$$COP_t = Q_{tot}/Q_{reg} \tag{A.2}$$

where the regeneration energy input is given by

$$Q_{reg} = \dot{m}_{DA,2}(h_8 - h_7) \tag{A.3}$$

In addition, an electrical coefficient of performance is defined by

$$COP_e = Q_{tot}/Q_{elec} \tag{A.4}$$

to account for the parasitic energy consumed by the fans, water pumps, and motors to rotate the wheels.

This system can be easily modified to the recirculation cycle by dehumidifiying the exhaust room air and using outside air for the regeneration stream. This configuration may have an performance advantage under more humid climatic conditions.

A.2 Current state of the art

Table A.1 summarizes the progress that has been made in the development of residential scale desiccant air conditioning systems. Several of the

Table A.1 Summary of desiccant cooling system development

system	cycle	$t_{2,i}$ (C)	ε_{HX}	capacity (kW)	capacity (kJ/kg)	COP_t	COP_e	source
IGT Solar-MEC I[1]	recirc		0.85	8.2	8.0	0.45		field test
IGT Solar-MEC III[1]	recirc	110	0.90	9.5	21.1	0.46	8.0	lab tests
	vent	110	0.90	7.5	16.7	0.51	6.5	lab tests
AiResearch SODAC[2]	recirc	93	0.90	4.6	10.9	0.60	5.8	lab tests
	vent	93	0.90	3.4	7.9	0.48	4.3	lab tests
IIT[3]	cross-cooled	65	0.90	3.3	13.0	0.62		lab tests
IGT HCOP[1]	vent		0.95	8.4	18.7	0.95	6.2	projection
EXXON[4]	vent	77	0.93	2.3	12.9	1.05	5.4	lab tests
	vent	77	0.93		15.1	1.3	8.7	projection
ASK[5]	vent		0.92	≈6.		≈1.0	≈5.	field tests

[1]Macriss and Zawacki (1982)
[2]Rousseau (1982)
[3]Worek and Lavan (1982)
[4]Huskey, et al. (1982)
[5]Venhuizen (1984); Coellner (1986); Lof, et al. (1987)

systems are described briefly in Chapter 4. Various studies have suggested that thermal *COP*'s greater than 1.0-1.2 are needed for desiccant systems to compete successfully with conventional systems (Booz-Allen and Hamilton, 1980, 1981; Scholten and Morehouse, 1983, Jurinak, et al., 1984).

ASK Corp. (formerly American Solar King) has begun to market a ventilation cycle residential desiccant air conditioning system. Originally called the Sunaire™, the regeneration energy was to be supplied by an array of flat plate solar collectors (Venhuizen, 1984). With the disappearance of tax credits for solar energy systems, the unit is now regenerated by heat from a natural gas-fired boiler and is called the Energymaster® (Coellner, 1986a). The dehumidifier wheel consists of corrugated laminar flow matrix impregnated with lithium chloride. Over 200 units are currently in operation, mostly in the southwestern states where the dry climate allows the evaporative cooling elements to enhance the system performance and where the cost of electricity is relatively high compared with natural gas (Coellner, 1986a,b).

Beba, et al. (1986) and Lof, et al., (1987) have recently tested the Energymaster® under actual operating conditions at Colorado State University. They report average thermal COP's of 0.8-1.0 and electric COP's of 5-6. These seem to be somewhat below expectations, especially given the mild, dry conditions in Fort Collins. However, the typical cooling load imposed was only about two-thirds of the machine's full capacity. The Gas Research Institute (GRI) is currently funding the development and testing of a similar system by Tecogen, Inc. (Cohen, 1986).

A.3 Ventilation cycle performance map

Fig. A.2 shows the cooling capacity and thermal *COP* for a ventilation cycle as a function of the dehumidifier outlet state (state 2) for the set of parameters and conditions given in Table A.2. Outlet states predicted for a silica gel dehumidifier at various levels of performance are shown as well as the impact of the measurement uncertainties presented in Chapter 3 and Appendix D.

The figure indicates that the cooling capacity is very sensitive to the outlet humidity ratio. The COP_t improves as the temperature increases and the humidity ratio decreases. The levels of measurement uncertainty indicate that the consequent uncertainty in COP_t is about ±5% near $COP_t = 1$ for errors in temperature and ±5% for errors in humidity ratio. The uncertainty in cooling capacity is about ±3% for errors in humidity ratio.

For desiccant systems to be competitive, very high performance components are required. "Better" desiccant properties and optimization of operation can improve performance further. However, the answer may lie in new configurations of components.

Table A.2 Parameters for system modeled in Fig. A.2.

System (map is independent of dehumidifier)

$t_5 = 26.7$ C $\quad w_5 = 11.1$ g/kg
$t_8 = 80$ C $\quad w_8 = 14$ g/kg
$\varepsilon_{EC} = .95$ $\quad \varepsilon_{HX} = .95$
$\dot{m}_{DA,2}/\dot{m}_{MD,1} = 1.0$

Dehumidifier (for individual points only)

$t_1 = 30$ C $\quad w_1 = 14$ g/kg
$Le_o = 1.0$
IDES = A (see App. B)
$c_{DM} = 1500$ J/kg$_{DD}$-C

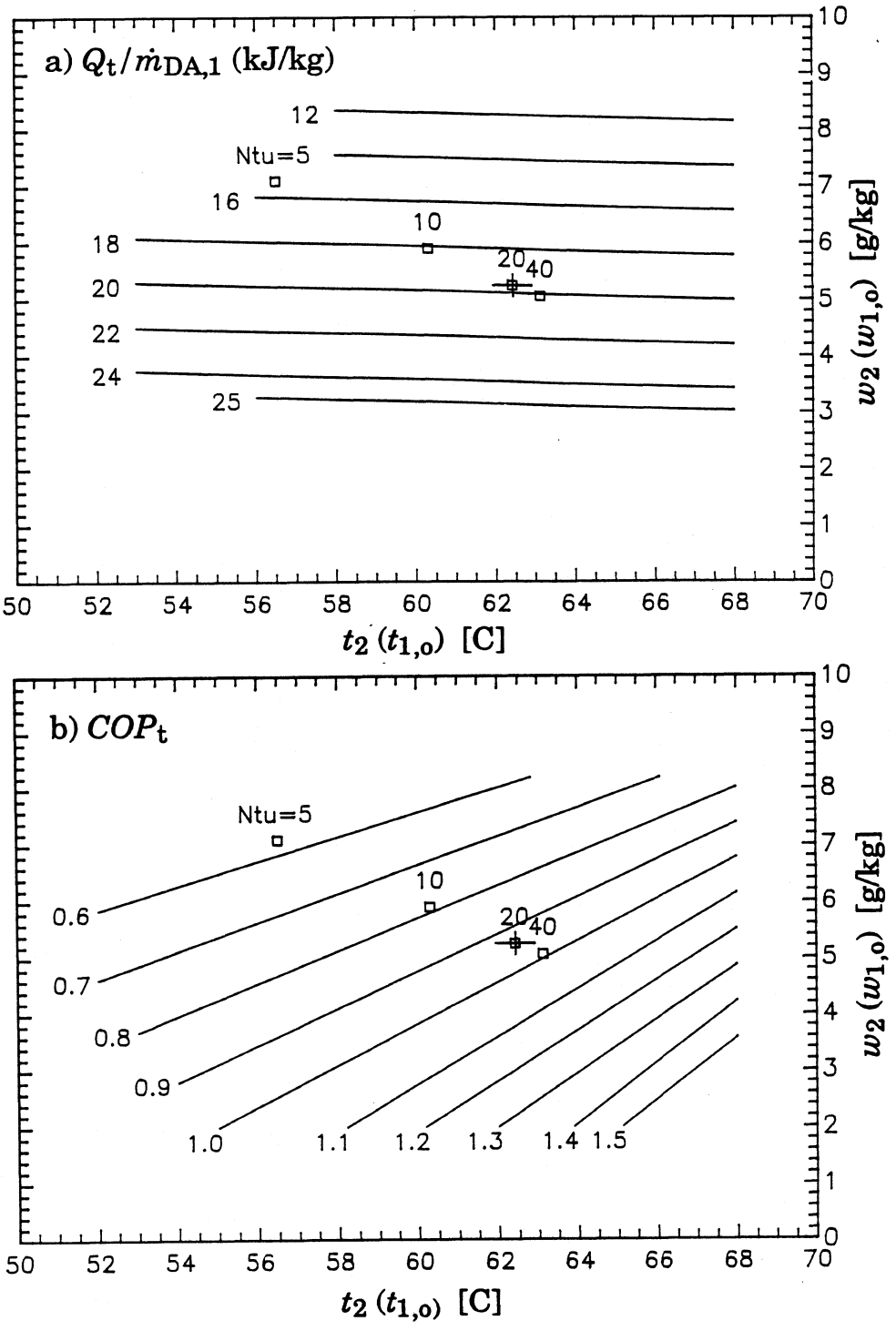

Fig. A.2 Performance of the ventilation cycle as a function of the dehumidifier outlet state for the conditions in Table A.2. a) cooling capacity. b) thermal *COP*.

Appendix B

Property Relations

The property relations used in this work for water, air, and silica gel are presented in this appendix. All equations are written for conventional SI units. The following equation is used to relate the Kelvin and Celsius temperature scales,

$$T[\mathrm{K}] = 273.15 + t[\mathrm{C}] \tag{B.1}$$

where the upper and lower case symbols are used in this appendix to distinguish between the two temperature scales.

B.1 Water and water vapor

The specific enthalpy of water vapor and the heat of vaporization of water as functions of temperature are represented as linear least squares fits to data presented in ASHRAE (1977) for the range $0 < t < 100$ C,

$$h_{WV} = 2\,502\,500 + 1\,756.6\,t \qquad [\mathrm{J/kg_W}] \tag{B.2}$$

$$h_v = 2\,502\,400 - 2\,430.2\,t \qquad [\mathrm{J/kg_W}] \tag{B.3}$$

The following functions for the specific heats of vapor and liquid and the enthalpy of liquid water are derived from Eqs. (B.2) and (B.3),

$$c_{WV} = 1\,756.6 \qquad [\mathrm{J/kg_W\text{-}C}] \tag{B.4}$$

$$c_{WL} = 4\,186.6 \qquad [\mathrm{J/kg_W\text{-}C}] \tag{B.5}$$

$$h_{WL} = 100 + 4\,186.6\,t \qquad [J/kg_W] \tag{B.6}$$

The vapor pressure of water over ice is required to convert dewpoint temperatures below 0 C to humidity ratios. A least squares fit to data in ASHRAE (1977) for the range -15 < t < 0 C gives

$$P_{sat} = exp(28.917 - 6\,146.61/T) \qquad [Pa] \tag{B.7}$$

Maclaine-cross (1974) has fit the vapor pressure of water over liquid for the range 0 < t < 90 C as

$$P_{sat} = exp(23.281\,99 - 3\,780.82/T - 225\,805/T^2) \tag{B.8}$$

The current version of MOSHMX used by the author incorporates the polynomial expression presented in ASHRAE (1985) which has a larger range of applicability.

B.2 Moist air

Moist air is treated as an ideal gas misture. The universal gas constant $\Re$ is taken to be 8314.4 J/kgmole-K (CRC, 1975). In density calculations, the gas constant R is taken to be 289.6 J/kg-K where the molecular weight of moist air is determined at an average humidity ratio of 15 g/kg. The density of moist air is then

$$\rho = P_{TOT}/RT \tag{B.9}$$

The specific heat of dry air is taken to be

$$c_{DA} = 1\,007.6 \qquad [J/kg_{DA}\text{-}C] \tag{B.10}$$

based on data in Hilsenrath (1960) for the range $0 < t < 100$ C and $.8 < P_{TOT} < 1.0$ atm. The enthalpy of moist air becomes

$$h = c_{DA}t + wh_{WV} \qquad [J/kg_{DA}] \tag{B.11}$$

This expression agrees to with .08% of data for saturated air in ASHRAE (1977). The humidity ratio is determined from the saturation pressure as (ASHRAE, 1977)

$$w = .62198[\phi/(1-\phi)] \qquad [kg_W/kg_{DA}] \tag{B.12}$$

where ϕ is the relative humidity,

$$\phi = P_{sat}/P_{TOT} \tag{B.13}$$

Mason and Monchik (1965) present data for the viscosity of air. For the low humidity ratios considered in this work, the moist content has a negligible impact on the viscosity. A least squares fit for dry air for the range $0 < t < 100$ C is given by

$$\mu = (17.22 + .0457t)\cdot 10^{-6} \qquad [kg/m\text{-}s] \tag{B.14}$$

The Prandtl number varies only about 1% over the range of temperatures encountered in this work. As bulk averages are used in the analysis in Chapter 5, this variation is ignored and the value is taken to be (Holman, 1976)

$$Pr = .705 \tag{B.15}$$

Similarly, the Schmidt number is taken to be constant (Holman, 1976)

$$Sc = .60 \tag{B.16}$$

The corresponding Lewis number for air is then

$$Le = Sc/Pr = .851 \tag{B.17}$$

B.3 Silica gel properties

B.3.1 "IDES = A" equilibrium properties

Van den Bulck (1987) has recently surveyed the data available on the equilibrium properties of regular density silica gels. He has correlated these data using the Dubinin-Polanyi adsorption potential theory (Ruthven, 1984) in the form

$$W = W_{o,1} e^{-(A/E_{o,1})^2} + W_{o,2} e^{-(A/E_{o,2})^2} \tag{B.18}$$

where A is the adsorption potential,

$$A = -\Re\, T \ln\phi \tag{B.19}$$

and is the difference in free energy between the adsorbed phase and saturated liquid at the same temperature. Van den Bulck discerned two distinct groups of data, each fit by a different set of coefficients in Eq. (B.18). The following set of coefficients is used here based on his analysis of results from experiments on a

single-blow matrix using the same silica gel as used in the original and rewound wheels described in Chapter 3,

$$\begin{aligned} W_{o,1} &= 0.117 \ kg_W/kg_{DD} \\ E_{o,1} &= 7.74 \cdot 10^6 \ J/kgmole \\ W_{o,2} &= 0.237 \ kg_W/kg_{DD} \\ E_{o,2} &= 2.50 \cdot 10^6 \ J/kgmole \end{aligned} \tag{B.20}$$

This isotherm is shown in Fig. B.1 along with manufacturer's data for the silica gels used in the wheels tested (see Table 4.1) and experimental data from Chuah, et al., (1986) which again uses the same gel as in the original and rewound wheels. Chuah's data was not used by Van den Bulck in his determination of the coefficients in Eq. (B.20).

Eq. (B.18) completely specifies the equilibrium properties of the desiccant. The differential heat of sorption is determined from the Clausius-Clapyron relation as

$$\frac{h_s}{h_v} = \left.\frac{\partial ln P_{ve}}{\partial ln P_{sat}}\right)_W = 1 + \frac{T\, ln\phi}{d ln P_{sat}/d(1/T)} \tag{B.21}$$

where P_{ve} is the vapor pressure of water in equilibrium with the moist silica gel and $Tln\phi$ is a function of the desiccant loading through Eqs. (B.19) and (B.18).

B.3.2 "IDES = B" equilibrium properties

Much of the previous work involving the model MOSHMX has used the silica gel isotherm relation obtained by Brandemuehl (1982) which is based on the data of Hubbard (1954). Integration of the Clausius-Clapyron equation, Eq. (B.21), yields

$$lnP_{ve} = (h_s/h_v)\, lnP_{sat} + C \tag{B.22}$$

A regression analysis of the data, assuming the ratio h_s/h_v is independent of temperature resulted in the following relations,

$$h_s/h_v = 1 + .2843\, e^{-10.28\, W} \tag{B.23}$$

$$P_{ve} = 3387.7(2.112\, W P_{sat}/3387.7)^{h_s/h_v} \tag{B.24}$$

where 3387.7 = 101325[Pa]/29.91[in. Hg]. This isotherm relation is also shown in Fig. B.1.

B.3.3 Matrix enthalpy

The enthalpy of the moist silica gel is given by

$$H = (c_{DM} + c_{WL} W)\, t + \Delta H_w \tag{B.25}$$

where ΔH_w is the integral heat of wetting,

$$\Delta H_w = \int_0^W \left(1 - \frac{h_s}{h_v}\right) dW \tag{B.26}$$

The effective specific heat of the matrix is given by the temperature derivative of the enthaply function at constant water content. Note that the temperature derivative of the integral heat of wetting is zero for Van den Bulck's isotherm while it is not zero for Brandemuehl's. For Brandemuehl's isotherm, the temperature dependence of the integral heat of wetting accounts for about 3% of the effective specific heat of the matrix.

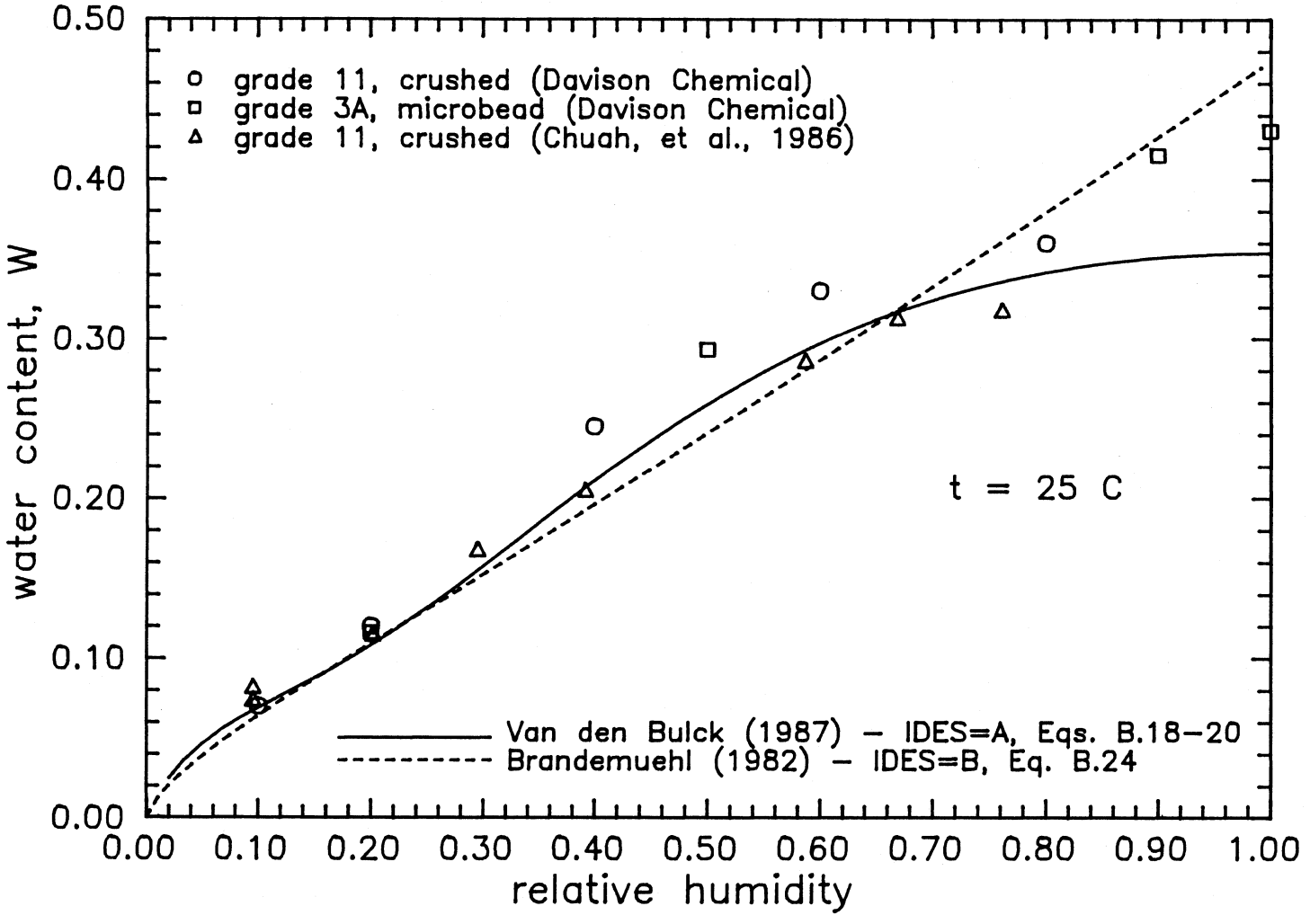

Fig. B.1 Van den Bulck's and Brandemuehl's isotherms for regular density silica gels.

B.4 Miscellaneous properties

The specific heat of dry silica gel is taken to be 921 J/kg_{DD}-C (Bullock and Threlkeld, 1966). The specific heat of the tape and adhesive is assumed to be that of Mylar (Smith and Dole, 1956) and is taken to be 1250 J/kg_{tape}-C evaluated at an average temperature of 45 C. The temperature dependence has been neglected. The specific heat of the tape used in the SERI single-blow tests (polyester film with rubber thermosetting adhesive) was measured to be approximately 1765 J/kg_{tape}-C at 45 C. This may partially explain the difference between the calculated and experimentally determined specific heat of the matrix.

Appendix C

The Analogy Method

This appendix presents a brief outline of the analogy method for describing the performance of rotary adiabatic dehumidifiers. The analogy method is based on a transformation of the governing equations into two sets of equations which are approximately uncoupled and have the same form as those for heat transfer alone. In essence, the dehumidifier is considered as the superposition of two rotary exchangers using the known rotary heat exchanger solution.

C.1 Transformation of the equations

By defining new dependent variables called the combined potentials F_1 and F_2, the partial differential equations describing the dehumidifier, Eqs. (2.1), can be transformed into the following set of equations (Maclaine-cross and Banks, 1972; Jurinak, 1982),

$$\frac{\partial F_{im}}{\partial \theta} + \beta_j \gamma_i \Gamma_j \frac{\partial F_{if}}{\partial x} = 0$$

$$\frac{\partial F_{if}}{\partial x} = Ntu_{i,j}(F_{im} - F_{if}) \qquad i=1,2 \qquad \text{(C.1)}$$

where the subscripts m and f indicate the potential evaluated at the matrix and fluid state, respectively. The transformation requires the assumptions that

$$\frac{\partial F_{im}}{\partial h} = \frac{\partial F_{if}}{\partial h} \qquad \frac{\partial F_{im}}{\partial w} = \frac{\partial F_{if}}{\partial w} \tag{C.2}$$

and

$$Le_o = 1 \tag{C.3}$$

Eqs. (C.2) are true when the matrix and fluid are in equilibrium; they are approximately true for high transfer coefficients. Eq. (C.3) is approximately true for the dehumidifiers considered in this work and is expected to hold for other high performance dehumidifiers. In this case, $Ntu_{i,j} = Ntu_{w,j}$.

The characteristic potentials can not be uniquely determined. However, paths of constant F_i can be obtained by numerically integrating the following property relations (Banks, 1972; Jurinak, 1982),

$$-\frac{1}{\alpha_i} = \left.\frac{\partial w}{\partial t}\right)_{F_i} = \{ B + (-1)^i [B^2 - 4AC]^{1/2} \}/2A \tag{C.4}$$

$$A = \frac{\partial W}{\partial w}\frac{\partial h}{\partial w} - \frac{\partial H}{\partial w}$$

$$B = \frac{\partial H}{\partial t} - \frac{\partial h}{\partial t}\frac{\partial W}{\partial w} - \frac{\partial h}{\partial w}\frac{\partial W}{\partial t}$$

$$C = \frac{\partial h}{\partial t}\frac{\partial W}{\partial t}$$

where partial derivatives with respect to temperature hold humidity ratio constant and *vice versa*. The F_i potentials for a matrix composed of silica gel alone are shown on a psychrometric chart in Fig. C.1. F_1 lines resemble adiabatic saturation lines and F_2 lines are similar to relative humidity curves. The presence of additional heat capacity material, such as the tape and adhesive

used in the wheels tested here, results in F_1 lines that are flatter and F_2 lines that are steeper than those shown in Fig. C.1.

The combined capacitance ratios, γ_i, are functions of the moist air and desiccant properties and are related to Eq. (C.4) by (Jurinak, 1982)

$$\gamma_i = \frac{\partial W}{\partial w} - \frac{\partial W}{\partial t}\alpha_{3-i} \tag{C.5}$$

These capacitance ratios are analogous to the ratio of matrix to air specific heats in sensible heat exchangers.

C.2 Analogy solution

Eqs. (C.1) are generally coupled because the γ_i are functions of both combined potentials, however, there is only a weak dependence on F_{3-i}. The utility of the analogy method comes from ignoring this dependence and treating Eqs. (C.1) as independent for $i=1,2$. With the assumption that the two sets of equations are independent, the dehumidifier outlet state is determined by the superposition of the two F_i exchangers.

The group $\gamma_i\Gamma_j$ is analogous to the parameter C_r/C_{min} for sensible heat exchangers. With this correspondence, Eqs. (C.1) have the same form as those for a rotary sensible heat exchanger. The effectivenesses of the F_i exchangers for period j are defined as

$$\eta_{ij} = \frac{F_{ij,i} - F_{ij,o}}{F_{ij,i} - F_{i(3-j),i}} = fn\left(Ntu_{i,j},\ \overline{\gamma}_{ij}\Gamma_j\right) \tag{C.6}$$

and are obtained from the known rotary sensible heat exchanger solutions (Kays

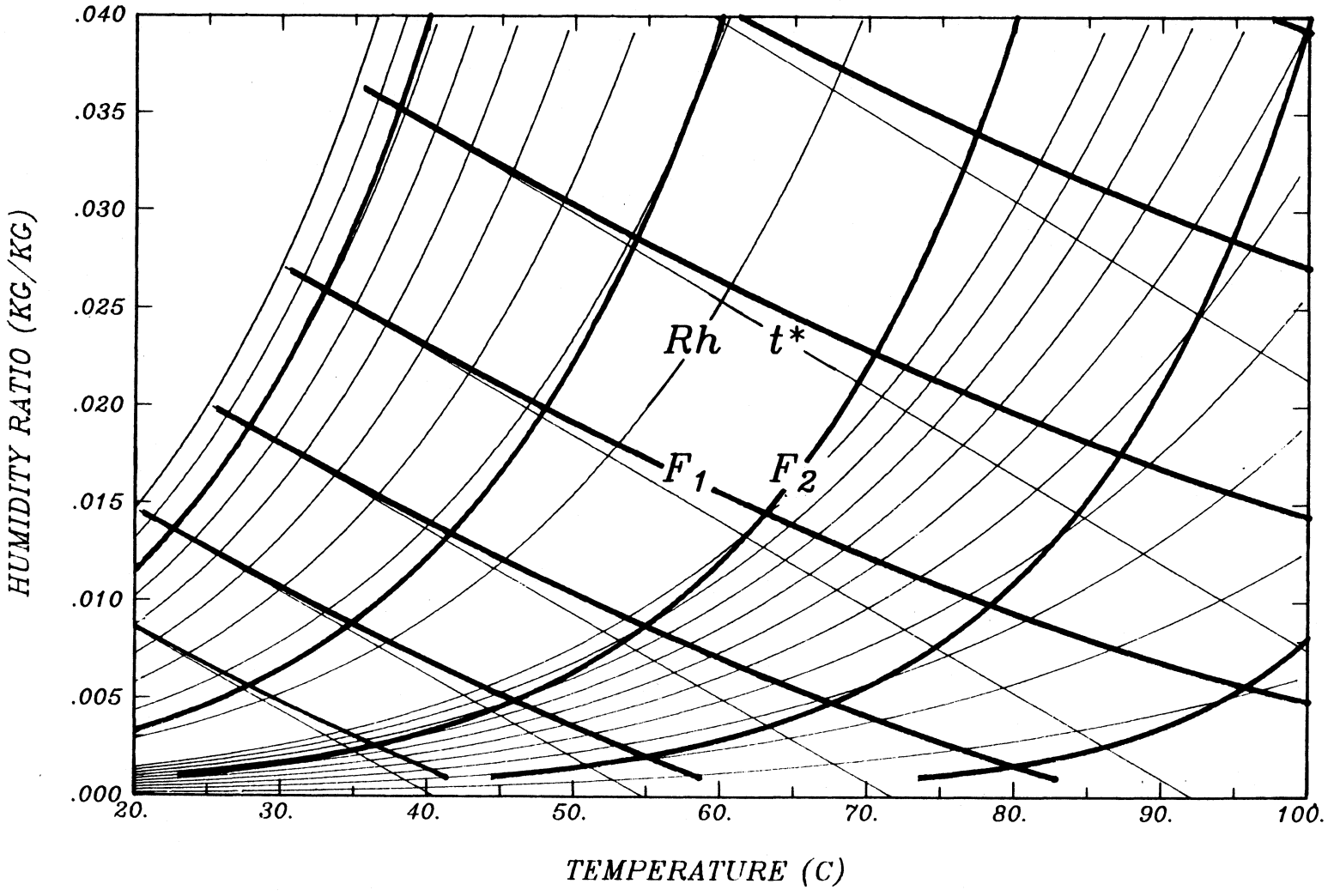

Fig. C.1 Combined potentials for a dehumidifier matrix composed of silica gel alone.

and London, 1984). Maclaine-cross and Banks (1972) discuss methods for determining the proper average capacitance ratios, $\overline{\gamma}_{ij}$. The F_i effectivenesses are shown in Fig. C.2 for the process period (j=1). The point where the F_1 line through the process inlet state crosses the F_2 line through the regeneration inlet state is called the intersection point and is the optimum outlet state from the dehumidifier. It is therefore desirable to have a small F_1 effectiveness and a large F_2 effectiveness.

Eqs. (C.6) are not directly usable because the combined potentials can not be uniquely determined. Jurinak (1982) has developed curvefits for the potentials shown in Fig. C.1 based on an arbitrary datum and scale. Much effort was required and the properties of other desiccants may not be conducive to this process. A simpler approach is to assume that the combined potentials are linear functions of temperature and humidity ratio. The outlet state of the dehumidifier is then given by (Maclaine-cross and Banks, 1972; Jurinak, 1982)

$$s_{j,o} = s_{j,i} + \eta_{1j}(s_{3-j,i} - s_{IP,j}) + \eta_{2j}(s_{IP,j} - s_{j,i}) \qquad (C.7)$$

where s represents either temperature t or humidity ratio w and IP indicates the value at the intersection point. A comparison with the MOSHMX finite difference solution indicates that this approximation is satisfactory for outlet states near the intersection point, that is, "good" dehumidifiers (Jurinak and Banks, 1982).

C.3 Wave analysis

Further insight into the processes occurring in the dehumidifier can be

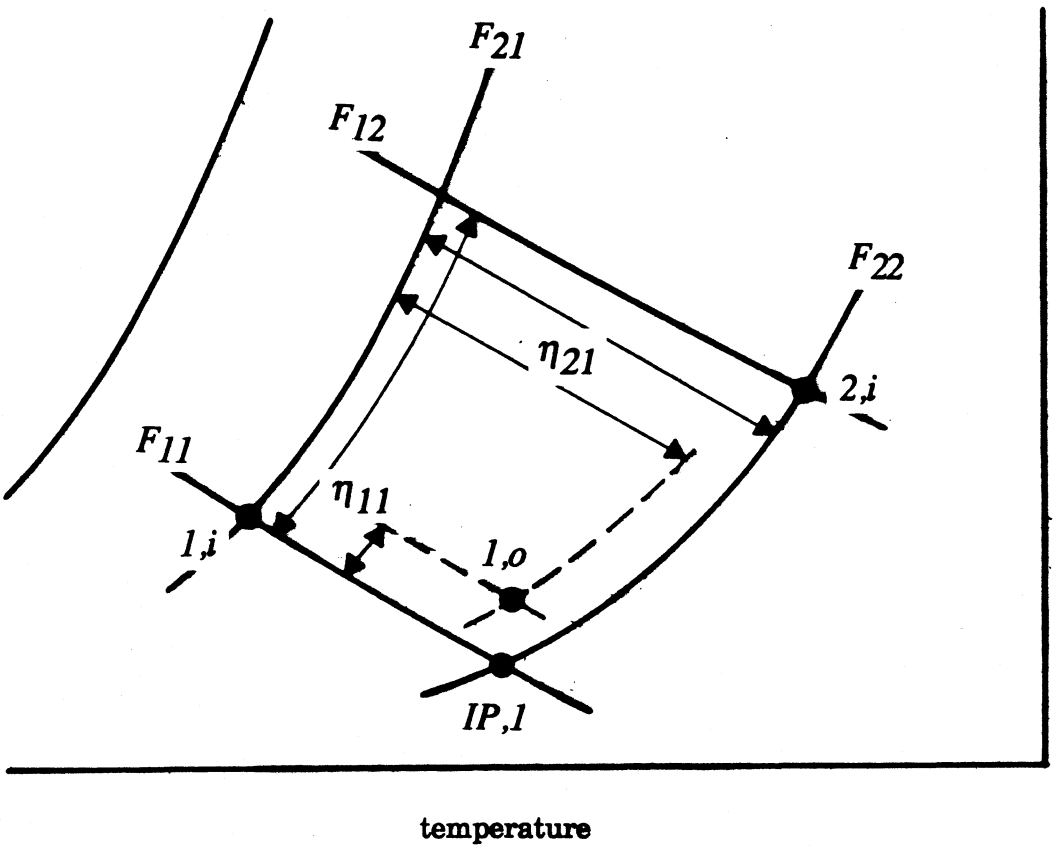

Fig. C.2 Dehumidifier process stream outlet state in terms of F_i effectivenesses.

obtained by considering the case of equilibrium between the desiccant and the air stream, that is, infinite transfer coefficients. Eqs. (C.1) can then be written as

$$\frac{\partial F_i}{\partial(\theta/\beta_j)} + \frac{1}{\gamma_i \Gamma_j}\frac{\partial F_i}{\partial x} = 0 \qquad \text{(C.8)}$$

Eqs. (C.8) represent a pair of hyberbolic partial differential equations. The solutions to these equations describe the propogation of waves or fronts of constant F_i through the matrix with time. The speed at which these waves travel is given by

$$\left.\frac{dx}{d(\theta/\beta_j)}\right)_{F_i} = \frac{1}{\gamma_i \Gamma_j} \qquad \text{(C.9)}$$

The values of γ_1 are much smaller than those for γ_2 and so fronts of constant F_1 propogate much faster than those for F_2. The F_1 wave front corresponds to the fast moving thermal transfer zone and the F_2 wave front corresponds to the slower moving mass transfer zone.

Fig. C.3 is a schematic representation of a dehumidifier showing the F_i wave fronts for a dehumidifier operating near optimum rotation speed. The vertical axis represents the distance along the dehumidifier flow channels. The horizontal axis can be considered as the circumferential coordinate (ϕ) as if a cylindrical section of the wheel had been cut and laid flat or as the history of an angular slice of the wheel in time (θ) as it rotates from one air stream to the other. The right boundary is identical to the left boundary. Fig. C.4 shows the temperature and humidity ratio profiles corresponding to the superposition of the F_i wave fronts in Fig. C.3.

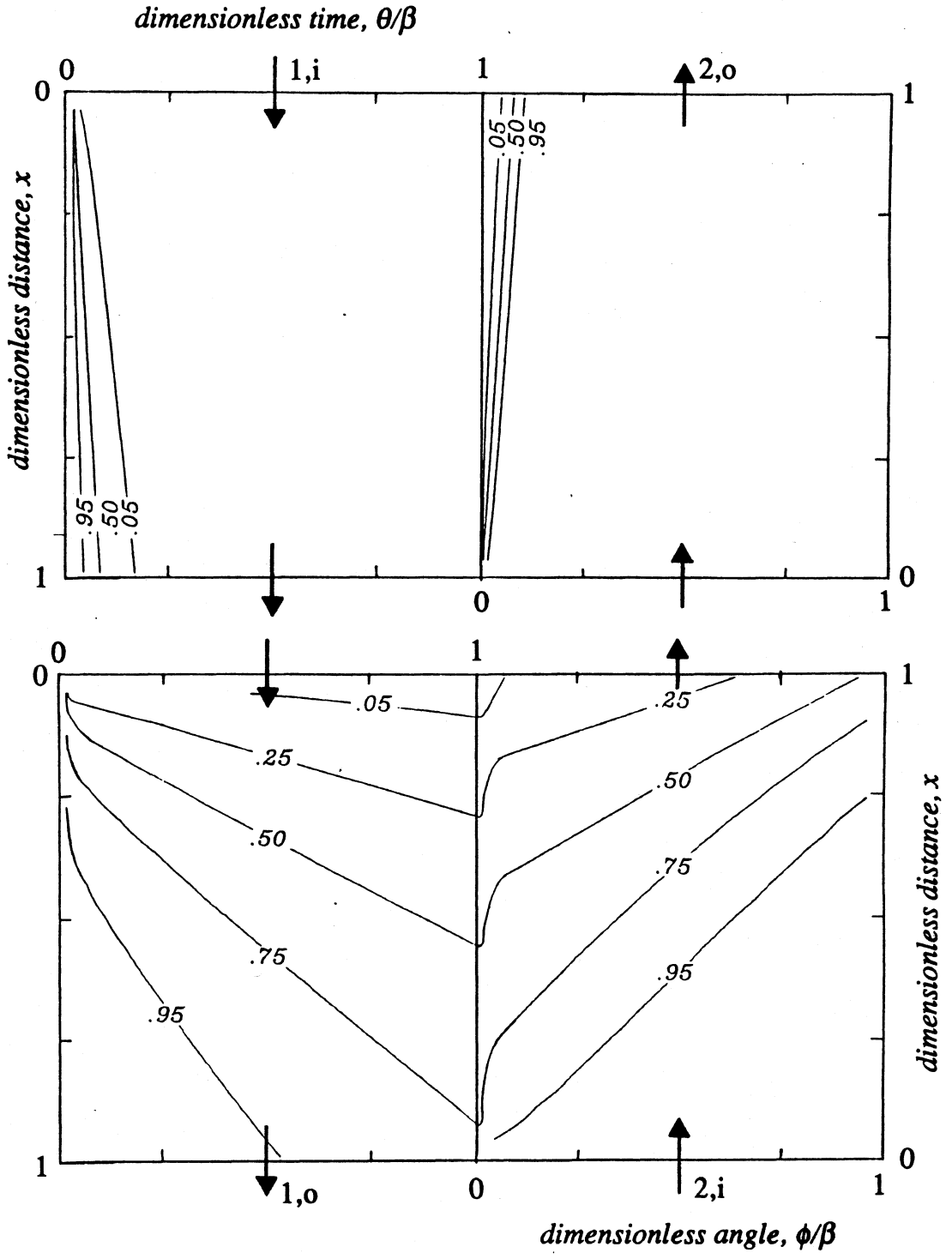

Fig. C.3 Time-distance mapping showing the normalized F_1 (upper) and F_2 (lower) wave fronts within a dehumidifier operating near optimum rotation speed.

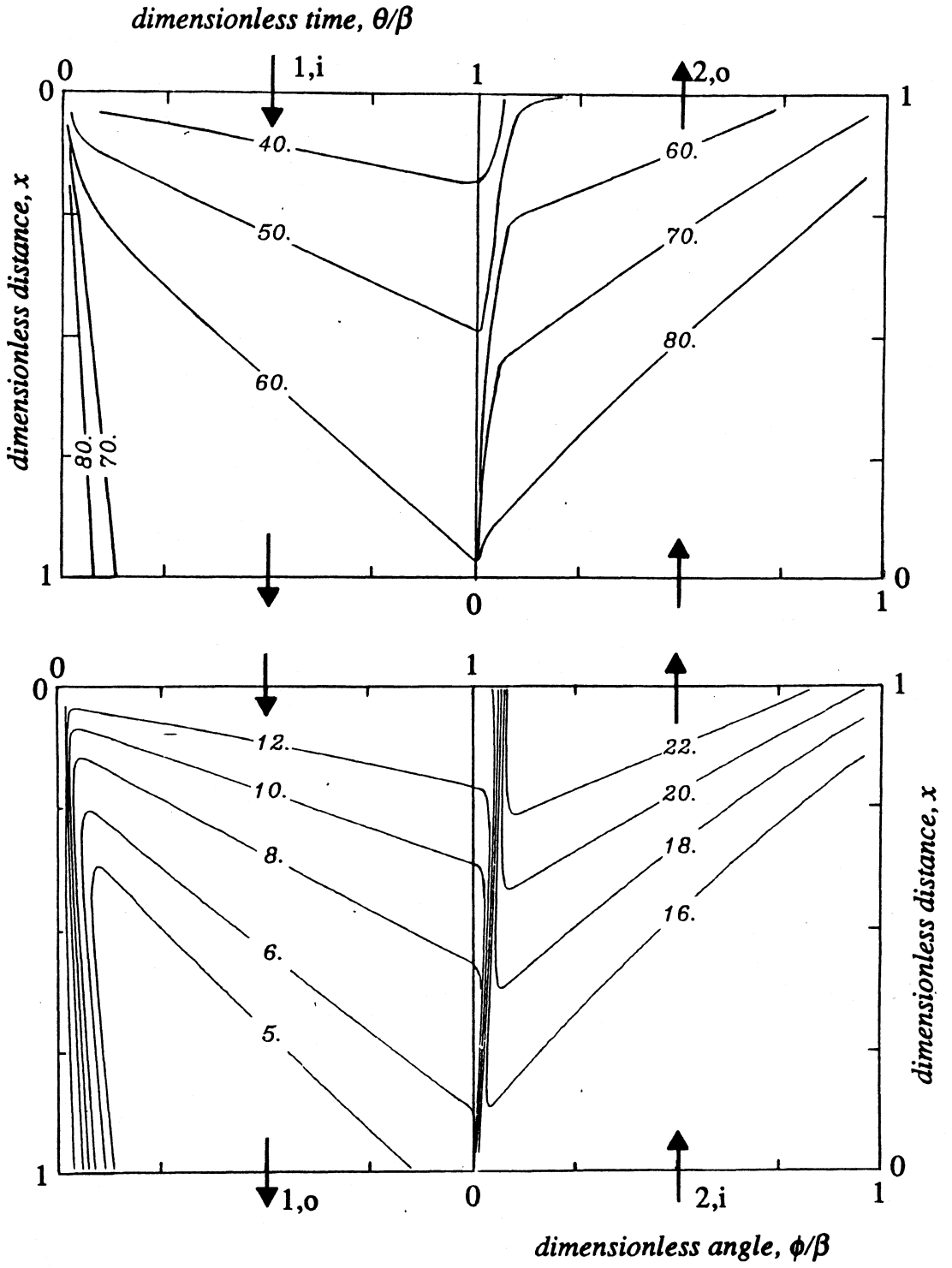

Fig. C.4 Time-distance mapping showing temperature (upper) and humidity ratio (lower) profiles within a dehumidifier corresponding to Fig. C.3.

Appendix D

Uncertainty Analysis

This appendix presents a summary of the estimated uncertainties in the primary measurements and the consequent uncertainties in quantities derived from these measurements.

D.1 Primary measurements

Many of the errors associated with the primary measurements are of the systematic type. If errors from multiple sources are present, the individual errors are assumed to be independent and are combined as the sum-of-squared-errors based on a Taylor series expansion (Bevington, 1969)

$$\delta F(x, y, \ldots)^2 = \left(\frac{\partial F}{\partial x}\delta x\right)^2 + \left(\frac{\partial F}{\partial y}\delta y\right)^2 + \ldots \qquad \text{(D.1)}$$

D.1.1 Temperature

Uncertainties in the primary temperature measurements result from uncertainties in the calibration of the thermocouple wire, calibration of the electronic reference junction in the data acquisition unit, and environmental effects. Samples of the special limits of error thermocouple wire used were calibrated by the SERI Instrument Services branch. The wire was found to give readings from 0-.31 C higher than the standard National Bureau of Standards tables (this is within the factory specification of ±.5 C). The average uncertainty due to wire calibration is assumed to be ±.25 C. This is a sytematic type error.

The manufacturer's specification for the uncertainty in the electronic

reference junction in the data acquisition unit is ±.20 C. This is again a systematic type error. This uncertainty applies only to "absolute" temperature measurements; it does not affect differences between temperatures.

Conduction errors are estimated to be negligible. Radiation errors are expected to be less than .1 C. Heat losses from the ducts between the face of the wheel and the measurement location are estimated to be less than .15 C. These again are systematic type errors.

It is likely that the condition of the wheels, the presence of spokes, etc. create a variety of random errors. These should be removed by the averaging process done by the data acquisition program for the steady-state results. The above systematic errors are assumed to combine in a random fashion according to Eq. (D.1). The resulting uncertainties in primary temperatures reported by the data acquisition system are ±.37 C.

D.1.2 Pressure

The electronic differential pressure sensors were calibrated against a Hook gage manometer with a resolution of .05 Pa. These tests indicated a differential pressure sensor uncertainty of ±1%. The uncertainties in the absolute pressure measurements are assumed to also be ±1%.

D.1.3 Flow rates

Air flow rate measurements are affected by uncertainties in temperature, pressure (differential and absolute), and in the discharge coefficient of the nozzle. The uncertainty in mass flow rate is then given by

$$\left(\frac{\delta \dot{m}}{\dot{m}}\right)^2 = \left(\frac{\delta C}{C}\right)^2 + \frac{1}{4}\left[\left(\frac{\delta P_{TOT}}{P_{TOT}}\right)^2 + \left(\frac{\delta P_{noz}}{P_{noz}}\right)^2 + \left(\frac{\delta T}{T}\right)^2\right] \qquad (D.2)$$

where C is the discharge coefficient. Bean (1971) gives the uncertainty in discharge coefficient as ±2%. The resulting uncertainty in the measured air mass flow rate is ±2.1%. Since the uncertainty in the discharge coefficient is so dominant, the uncertainty in flow rate is essentially systematic in nature and of similar magnitude for all experiments. The uncertainty in the ratio of flow rates is therefore expected to be small.

D.1.4 Humidity ratio

Uncertainties in humidity ratio arise from uncertainties in the calibration of the dewpoint hygrometers and total pressure measurements. Uncertainties in the correlations used for saturation pressure are small and have been neglected. The uncertainty in humidity ratio is then given by

$$\left(\frac{\delta w}{w}\right)^2 = \frac{1}{1 - P_{sat}/P_{TOT}}\left[\left(\frac{1}{\delta P_{sat}}\frac{\delta P_{sat}}{\delta T}\right)^2 \delta T_{DP}^2 + \left(\frac{\delta P_{TOT}}{P_{TOT}}\right)^2\right] \qquad (D.3)$$

The accuracy of the dewpoint sensor calibration is specified by the manufacturer to be ±.2 C. Observation of the four sensors while monitoring the same air sample showed that, on average, the sensors were within ±.1-.2 C of the average. This consistency suggests adequate agreement with the manufacturer's specifications. Combining these two uncertainties, the uncertainty in dewpoint measurement is taken to be ±.25 C. The uncertainty in the measured humidity ratio is then approximately ±2.3% over the range the range encountered in the experiments.

D.1.5 Wheel rotation speed

The uncertainty in wheel rotation speed results from uncertainties in the calibration procedure and drift in the output signal from the controller with time. The combined uncertainties are estimated to be ±1%.

D.2 Corrected measurements

D.2.1 Corrections for seal leakage rates

The above primary measurements must be corrected for seal leakage rates in order to characterize the performance of the dehumidifiers. The quantities affected are the flow rates through the dehumidifier core and the outlet temperatures and humidity ratios; the inlet states are not affected.

By applying Eq. (D.1) to the mass balance used to calculate the mass flow rate of air through the dehumidifier core from the measured flow rate and the leakage rates, the following relation is obtained,

$$\frac{\delta \dot{m}}{\dot{m}} = \left(\frac{\dot{m}_m}{\dot{m}}\right) \left\{ \left(\frac{\delta \dot{m}_m}{\dot{m}_m}\right)^2 + \left(\frac{\delta l}{l}\right)^2 \left[\left(\frac{\delta l_o}{\dot{m}_m}\right)^2 + \left(\frac{\delta l_c}{\dot{m}_m}\right)^2 + \left(\frac{\delta l_r}{\dot{m}_m}\right)^2 \right] \right\}^{1/2} \quad \text{(D.4)}$$

The uncertainty in the core mass flow rate is estimated to be ±2.6%. The uncertainty in the leakage rates is taken to be ±20% (typical leakage rates are shown in Table 3.1). Similarly, the uncertainty of the corrected outlet humidity ratio is estimated to be ±2.7% and the uncertainty in the corrected outlet temperature is ±.50 C. These results are summarized in Table 3.2.

D.2.2 Mass and energy balance closure

The imposition of water and energy balance closure on the dehumidifier outlet states described in section 3.5.2 results in corrections to the humidity ratios and temperatures that are generally the same magnitude as the estimated uncertainties. This indicates that the estimated measurement uncertainties and the correction procedures are reasonable.

D.3 Uncertainties in the wheel parameters

The estimated uncertainties in the parameters that describe the geometry of the dehumidifier wheels and are used in the calculation of other parameters are listed in Table 4.1. In addition to those listed, the uncertainty in the average center-to-center spacing of the passages is ±.7% for the original and rewound wheels and ±.3% for the microbead wheel. The uncertainty in the net face area of the wheel is taken to be ±1.5%. These uncertainties were obtained by applying Eq. (D.1) to physical measurements made on the wheels. The hydraulic diameter depends on the center-to-center spacing and the effective thickness of the desiccant coated sheet. The uncertainty in the effective sheet thickness was obtained from Van den Bulck (1987).

D.4 Nondimensional groups

D.4.1 Reynolds number

Using the most basic set of parameters, the Reynolds number Re depends on the air mass flow rate, the center-to-center spacing, and the net face area of the wheel. The consequent uncertainty in Re becomes ±3.1% by applying

Eq. (D.1). The uncertainty of the entrance length parameter $ReD_h/4L$ is then ±3.7% for the original and rewound wheels and ±3.3% for the microbead wheel.

D.4.2 Apparent friction factor - Reynolds number

The nondimensional pressure drop ($f_{app}Re$) is determined from the experimental data through Eq. (5.1) and is a function of the pressure drop, mass flow rate, cube of the hydraulic diameter, the center-to-center passage spacing, and the net face area of the wheel. The consequent uncertainty in ($f_{app}Re$) is ±6.8% for the original and rewound wheels and ±4.4% for the microbead wheel, much of this due to the uncertainty in hydraulic diameter. These uncertainties are shown in Fig. 5.1.

D.4.3 Effective Nusselt and Sherwood numbers and overall Lewis number

The experimental effectivenesses upon which the effective Nusselt and Sherwood numbers are calculated from Eqs. (5.18). The uncertainty in these effectivenesses is determined by applying Eq. (D.1). Because of the highly nonlinear nature of the dependence of the number-of-transfer-units (Ntu's) on the effectiveness, the range of Ntu is obtained by substituting the upper and lower bounds of the effectiveness into

$$Ntu = \varepsilon/(1-\varepsilon) \tag{D.5}$$

The range of uncertainty in Nu_e and Sh_e are then obtained by applying Eq. (D.1) to Eqs. (5.21) and (5.22), using the upper and lower bounds on the Ntu's to determine the upper and lower bounds on Nu_e and Sh_e. The results of these calculations are shown for several data points in Figs. 5.11 and 5.12.

The upper bound of uncertainty in the overall Lewis number Le_o is obtained by taking the ratio of the upper bound on the heat transfer Ntu and the lower bound on the mass transfer Ntu; and *vice versa* for the lower bound. The results are shown for several points in Fig. 5.13.

D.5 Uncertainties in MOSHMX predictions

The predictions of any model are subject to the uncertainties of the parameters input to the model. The MOSHMX model depends on the inlet states, the equilibrium relation and the matrix properties, the heat and mass tranfer Ntu_j's, and the mass capacity rate ratio Γ_j (Eq. 2.4). The effect of uncertainties in the inlet states can be estimated using the analogy method discussed in Appendix C. The uncertainty in the predicted outlet states are generally the same order of magnitude as the the uncertainty in the inlet states.

The predictions of MOSHMX are somewhat sensitive to the values of the transfer coefficients for the original and rewound wheels tested here. Predictions for the microbead wheel are less sensitive to Ntu's because of the higher effectivenesses achieved. This should be the case for other high performance dehumidifiers also.

The uncertainty in Γ_j is approximately ±2.7% based on the uncertainties in mass flow rate and rotation speed. This assumes that the experimentally determined gel mass is consistent with the equilibrium properties used. This uncertainty has only a small effect on the predicted outlet states. The uncertainties in the effective matrix specific heat and fraction of the flow affected by the spacers and spokes overshadows the other uncertainties discussed above.

Appendix E

Tabulation of Experimental Data

This appendix contains a tabulation of the experimental data from the three dehumidifier wheels tested at the Solar Energy Research Institute. The tabulation of data for the *original* wheel in Table E.1 is taken from this author's data records and have not been published elsewhere. The experimental data for the *rewound* and *microbead* wheels were obtained from Bharathan, et al., (1986a,b) and Tables E.2 and E.3 have been produced from these reports. The data listed in these tables is described below by heading.

run no. Each experiment is identified by its run number which indicates the date the experiment was performed and the experiment number for that day.

period The period indicates the flow stream for which the data in the next five columns is given; process: $j = 1$, regen'n: $j = 2$.

$\dot{m}_{DA,j}$ The mass flow rate of dry air through the wheel for period j. The values listed include the corrections for seal leakage rates.

$t_{j,i}$ The inlet temperature as measured.

$w_{j,i}$ The inlet humidity ratio as measured.

$t_{j,o}$ The outlet temperature corrected for the effects of seal leakage rates and mass and energy unbalances (using Eqs. (3.3)).

$w_{j,o}$ The outlet humidity ratio corrected for the effects of seal leakage rates and mass unbalances (using Eqs. (3.3)).

$\dot{N}$, P_{TOT} The upper value (N) is the wheel rotation speed as measured. The lower value (P_{TOT}) is the average total pressure in the dehumidifier.

E_{wr}, E_{hr} The relative water (upper) and energy (lower) unbalances for the dehumidifier calculated from Eqs. (3.4) using the outlet states corrected only for seal leakage rates.

Table E.1 Experimental data from *original* wheel corrected for leakage rates and unbalances.

run no.	period	$\dot{m}_{DA,j}$ (kg_{DA}/s)	$t_{j,i}$ (C)	$w_{j,i}$ (g/kg)	$t_{j,o}$ (C)	$w_{j,o}$ (g/kg)	$\dot{N}$ (rev/hr) P_{TOT} (Pa)	E_{wr} (%) E_{hr} (%)
04-11-85 0A	process	.208	31.00	14.07	31.29	14.01	.000	200.0
	regen'n	.213	80.00	12.72	79.71	12.77	82107	200.0
04-11-85 1A	process	.208	30.99	14.07	35.10	12.92	.335	57.2
	regen'n	.212	79.97	12.54	75.85	13.67	82100	147.5
04-11-85 2A	process	.208	31.00	14.05	37.69	12.05	.567	31.1
	regen'n	.212	79.97	12.49	73.27	14.45	82060	69.7
04-19-85 1A	process	.208	30.98	14.05	43.37	10.46	1.179	5.1
	regen'n	.213	79.97	12.40	67.65	15.92	80841	18.9
04-19-85 2A	process	.208	31.00	13.99	47.24	9.36	1.782	4.9
	regen'n	.213	79.97	12.55	63.91	17.08	80950	26.7
04-19-85 3A	process	.208	30.99	13.96	50.10	8.67	2.399	3.5
	regen'n	.213	79.97	12.60	61.16	17.77	80978	23.1
04-23-85 1A	process	.210	30.99	15.95	31.77	15.99	.000	200.0
	regen'n	.213	79.96	4.43	79.18	4.39	81845	124.0
04-23-85 2A	process	.208	30.99	15.75	69.88	6.97	134.992	-.4
	regen'n	.214	79.97	4.19	41.81	12.74	81877	10.6
04-23-85 3A	process	.209	34.99	15.65	35.53	7.25	134.993	5.2
	regen'n	.213	34.97	4.02	34.44	12.26	81864	1.6
04-23-85 4A	process	.207	31.00	14.17	69.43	12.97	134.994	28.3
	regen'n	.214	79.99	14.00	42.83	15.16	81842	8.8
04-25-85 2A	process	.156	30.99	15.54	71.57	7.78	134.990	-2.2
	regen'n	.161	79.97	5.93	40.33	13.46	80972	9.3
04-25-85 3A	process	.157	35.00	15.65	35.16	8.11	134.992	9.5
	regen'n	.161	34.68	5.81	34.53	13.21	80972	1.0
04-25-85 4A	process	.156	30.99	14.00	71.23	13.18	134.992	5.2
	regen'n	.161	79.94	14.02	40.99	14.82	80970	8.6
04-26-85 1A	process	.208	31.01	13.92	57.05	7.12	4.997	-2.5
	regen'n	.213	79.98	12.64	54.57	19.27	81900	11.8
04-26-85 2A	process	.208	30.99	13.99	60.66	6.79	9.998	-1.9
	regen'n	.213	79.98	12.31	51.16	19.31	82000	7.1
05-04-85 1A	process	.208	31.00	14.01	54.26	7.71	3.498	.5
	regen'n	.213	79.98	12.46	57.22	18.60	81576	16.5
05-04-85 2A	process	.207	31.00	14.06	59.39	6.87	7.497	-.3
	regen'n	.213	79.97	12.57	52.36	19.57	81659	10.0
05-06-85 1A	process	.207	31.00	14.03	61.36	6.89	12.498	-1.7
	regen'n	.213	79.97	12.54	50.51	19.49	82116	7.6
05-06-85 2A	process	.207	30.99	13.95	61.84	7.06	14.998	-.4
	regen'n	.213	79.96	12.65	50.03	19.35	82093	6.7
05-06-85 1B	process	.208	31.00	14.02	62.93	7.44	19.998	-1.0
	regen'n	.214	79.98	12.47	49.02	18.87	81960	7.3

Table E.1 Experimental data from *original* wheel. (cont.)

run no.	period	$\dot{m}_{DA,j}$ (kg_{DA}/s)	$t_{j,i}$ (C)	$w_{j,i}$ (g/kg)	$t_{j,o}$ (C)	$w_{j,o}$ (g/kg)	$\dot{N}$ (rev/hr) P_{TOT} (Pa)	E_{wr} (%) E_{hr} (%)
05-06-85 2B	process	.208	30.99	13.99	64.43	8.24	29.997	1.2
	regen'n	.214	79.97	12.42	47.56	18.00	82080	6.5
05-07-85 1A	process	.207	30.99	13.92	66.83	9.84	52.520	2.5
	regen'n	.214	79.97	12.48	45.26	16.44	82451	6.9
05-07-85 1B	process	.207	31.00	14.06	58.12	7.46	9.998	-.3
	regen'n	.167	79.98	12.60	46.44	20.79	82298	6.7
05-07-85 2B	process	.207	31.00	13.95	52.48	8.07	2.997	-.8
	regen'n	.167	79.97	12.30	53.21	19.61	82245	11.7
05-08-85 1A	process	.207	31.00	13.95	56.46	7.30	5.998	-1.0
	regen'n	.167	79.97	12.60	48.45	20.85	82177	12.7
05-08-85 2A	process	.207	31.00	13.86	43.16	10.25	.998	3.2
	regen'n	.166	79.97	12.32	64.62	16.81	82246	12.9
05-08-85 3A	process	.207	31.00	14.07	59.23	7.76	14.997	-1.0
	regen'n	.167	79.97	12.60	45.11	20.42	82223	5.4
05-08-85 4A	process	.207	31.12	14.02	60.07	8.16	19.998	-.2
	regen'n	.167	79.96	12.59	44.23	19.85	82156	5.4
05-08-85 1B	process	.208	31.81	14.12	60.87	7.53	11.997	-1.3
	regen'n	.213	79.97	15.09	51.86	21.50	82113	8.2
05-08-85 2B	process	.208	31.15	14.04	54.44	8.57	11.998	.0
	regen'n	.213	69.97	15.28	47.40	20.60	82120	6.7
05-09-85 1A	process	.208	31.00	14.02	49.38	9.20	11.998	2.3
	regen'n	.214	59.98	12.48	42.09	17.17	82061	12.1
05-09-85 2A	process	.207	31.00	14.07	67.19	6.04	11.998	-2.3
	regen'n	.213	89.97	12.53	54.88	20.33	82039	6.8
05-09-85 3A	process	.208	31.00	14.11	55.45	8.05	11.997	.6
	regen'n	.213	69.97	12.58	46.21	18.48	81917	7.2
05-09-85 4A	process	.208	31.00	13.96	56.51	7.39	11.998	-.9
	regen'n	.214	69.98	9.94	45.12	16.32	81846	7.8
05-09-85 1B	process	.207	31.00	14.03	68.14	5.65	11.997	-2.2
	regen'n	.213	89.97	10.05	53.86	18.19	81777	6.4
05-09-85 2B	process	.207	31.00	13.94	66.44	6.27	11.998	-2.6
	regen'n	.213	89.96	14.76	55.73	22.20	81791	4.6
05-10-85 1A	process	.208	31.00	14.07	62.29	6.51	11.998	-1.2
	regen'n	.213	79.96	10.16	49.49	17.50	81108	8.0
05-10-85 1B	process	.208	37.00	8.05	59.08	4.50	11.998	-2.5
	regen'n	.213	79.97	12.58	58.63	16.04	80710	6.8
05-10-85 2B	process	.207	30.99	8.03	56.20	3.86	11.998	-2.3
	regen'n	.213	79.99	12.54	55.64	16.59	80579	3.7
05-10-85 3B	process	.208	30.99	17.87	63.71	9.78	11.998	11.3
	regen'n	.213	79.99	12.68	48.08	20.55	80489	26.4

Table E.1 Experimental data from *original* wheel. (end)

run no.	period	$\dot{m}_{DA,j}$ (kg_{DA}/s)	$t_{j,i}$ (C)	$w_{j,i}$ (g/kg)	$t_{j,o}$ (C)	$w_{j,o}$ (g/kg)	$\dot{N}$ (rev/hr) P_{TOT} (Pa)	E_{wr} (%) E_{hr} (%)
05-13-85 1A	process	.208	25.67	17.40	61.13	8.00	11.997	-1.1
	regen'n	.214	79.97	12.47	45.46	21.60	81749	10.1
05-13-85 2A	process	.207	25.64	14.04	58.93	6.10	11.998	-1.1
	regen'n	.213	79.96	12.47	47.67	20.19	81831	6.2
05-13-85 3A	process	.207	37.00	14.02	63.84	7.76	11.998	1.0
	regen'n	.213	79.97	12.55	53.90	18.63	81856	11.8
05-13-85 4A	process	.207	30.99	17.52	63.53	9.01	11.998	1.3
	regen'n	.213	79.98	12.39	48.28	20.67	81823	12.1
05-13-85 1B	process	.207	30.99	14.02	58.61	7.48	11.998	1.7
	regen'n	.167	79.96	12.57	45.81	20.67	81713	8.7
05-13-85 2B	process	.207	31.00	14.01	47.57	9.69	11.998	8.0
	regen'n	.167	59.97	12.59	39.41	17.96	81606	14.7
05-13-85 3B	process	.207	30.99	14.00	64.10	6.55	11.998	-.9
	regen'n	.167	89.96	12.50	49.11	21.72	81710	9.0
05-14-85 1A	process	.207	31.00	14.14	54.14	8.10	11.998	.5
	regen'n	.167	69.97	9.99	41.24	17.47	81584	10.5
05-14-85 2A	process	.207	31.00	14.19	63.55	7.05	11.998	-2.2
	regen'n	.167	89.96	15.11	49.94	23.96	81561	5.8
05-14-85 1B	process	.207	31.00	14.04	48.60	9.02	1.997	3.6
	regen'n	.130	79.96	12.33	51.76	20.34	81650	19.9
05-14-85 2B	process	.206	30.99	13.97	52.56	8.07	3.997	1.8
	regen'n	.130	79.96	12.52	45.62	21.94	81737	10.5
05-14-85 3B	process	.206	31.00	13.94	53.71	7.99	5.998	1.1
	regen'n	.130	79.95	12.67	43.89	22.15	81819	7.4
05-15-85 1A	process	.207	31.00	14.04	54.76	8.26	9.998	2.3
	regen'n	.130	79.95	12.53	42.24	21.72	82243	8.6
05-15-85 2A	process	.209	30.40	13.97	30.99	13.84	.000	200.0
	regen'n	.213	70.38	14.20	69.80	14.33	82331	200.0
05-15-85 3A	process	.209	30.40	14.10	31.04	13.96	.000	200.0
	regen'n	.213	70.37	14.16	69.74	14.29	82389	200.0

Table E.2 Experimental data from *rewound* wheel corrected for leakage rates and unbalances.

run no.	period	$\dot{m}_{DA,j}$ (kg_{DA}/s)	$t_{j,i}$ (C)	$w_{j,i}$ (g/kg)	$t_{j,o}$ (C)	$w_{j,o}$ (g/kg)	$\dot{N}$ (rev/hr) P_{TOT} (Pa)	E_{wr} (%) E_{hr} (%)
10-30-85 2A	process	.220	29.99	15.35	62.82	7.43	15.301	-1.0
	regen'n	.222	79.98	15.14	47.64	22.99	82383	3.3
10-30-85 3A	process	.220	30.00	15.84	64.72	8.57	25.623	-4.8
	regen'n	.222	79.98	15.47	45.78	22.68	82291	2.1
10-30-85 4A	process	.220	29.99	16.77	65.33	9.71	29.958	-2.9
	regen'n	.222	79.97	16.50	45.17	23.50	82211	1.4
10-30-85 5A	process	.220	30.00	18.36	65.00	9.71	19.279	-3.8
	regen'n	.222	79.96	16.61	45.45	25.19	82101	1.0
11-06-85 1E	process	.219	29.99	16.40	59.33	8.15	6.350	-6.0
	regen'n	.221	79.97	16.72	51.03	24.89	82212	-1.2
11-06-85 2E	process	.219	29.99	16.18	61.23	7.90	9.116	-3.1
	regen'n	.222	79.95	16.40	49.31	24.56	82235	4.6
11-06-85 3E	process	.219	29.99	16.15	62.26	7.94	12.234	-3.9
	regen'n	.222	79.94	16.40	48.31	24.50	82280	3.5
11-06-85 4E	process	.219	29.99	15.77	63.26	8.01	16.923	-3.7
	regen'n	.222	79.96	16.00	47.36	23.66	82291	5.3
11-06-85 5E	process	.219	29.99	15.61	63.93	8.44	22.817	-.7
	regen'n	.222	79.96	15.85	46.70	22.93	82304	5.2
11-07-85 2A	process	.219	30.00	17.49	66.20	10.48	35.086	-3.9
	regen'n	.222	79.98	16.42	44.46	23.33	82036	2.8
11-07-85 4A	process	.219	30.00	17.45	68.04	12.34	55.146	4.2
	regen'n	.222	79.97	16.45	42.59	21.49	81975	5.9
11-07-85 5A	process	.219	30.00	17.44	68.87	13.10	65.590	4.9
	regen'n	.222	79.98	16.43	41.76	20.71	81953	5.4
11-13-85 4B	process	.220	30.00	14.50	64.02	7.95	26.665	-.3
	regen'n	.222	79.96	14.93	46.47	21.42	82047	1.8
11-14-85 1A	process	.219	30.00	14.68	67.01	9.76	47.730	1.3
	regen'n	.222	79.99	14.46	43.66	19.31	82581	5.1
11-12-85 1A	process	.171	30.01	16.19	64.73	8.47	16.382	-.6
	regen'n	.173	79.96	15.97	45.87	23.61	81872	11.6
11-12-85 1B	process	.171	30.01	17.43	62.78	8.62	8.448	-4.5
	regen'n	.173	79.97	17.74	47.82	26.45	81757	1.0
11-12-85 2B	process	.171	30.00	16.36	63.51	7.81	10.092	-2.5
	regen'n	.173	79.98	15.64	47.06	24.09	81646	7.4
11-08-85 1A	process	.217	30.00	6.78	54.83	1.77	9.703	-.5
	regen'n	.219	79.96	6.85	55.35	11.82	80860	6.6
11-18-85 1A	process	.219	30.00	12.43	59.94	5.27	11.123	-3.6
	regen'n	.221	79.97	12.88	50.44	19.97	81614	11.4
11-18-85 2A	process	.220	30.00	15.79	61.76	7.49	10.502	-.5
	regen'n	.222	79.98	14.85	48.64	23.08	81622	4.5

Table E.2 Experimental data from *rewound* wheel. (cont.)

run no.	period	$\dot{m}_{DA,j}$ (kg_{DA}/s)	$t_{j,i}$ (C)	$w_{j,i}$ (g/kg)	$t_{j,o}$ (C)	$w_{j,o}$ (g/kg)	$\dot{N}$ (rev/hr) P_{TOT} (Pa)	E_{wr} (%) E_{hr} (%)
11-18-85 3A	process	.221	30.00	22.06	63.71	13.16	9.608	-1.4
	regen'n	.223	79.97	21.19	46.76	30.01	81474	2.6
11-12-85 3B	process	.190	29.99	15.84	62.74	7.48	10.291	-1.6
	regen'n	.192	79.97	15.17	47.74	23.44	81649	8.1
11-12-85 4B	process	.210	30.00	16.25	61.97	8.01	10.626	-1.2
	regen'n	.212	79.97	16.62	48.50	24.78	81630	7.2
11-12-85 5B	process	.229	30.00	16.46	61.51	8.05	10.653	-4.7
	regen'n	.232	79.98	16.84	49.07	25.14	81569	-.5
11-12-85 1C	process	.249	29.99	15.65	60.19	7.66	10.036	-2.9
	regen'n	.251	79.97	16.03	50.17	23.95	81562	9.0
11-12-85 2C	process	.268	29.99	15.50	59.78	7.61	10.369	-2.8
	regen'n	.271	79.97	15.76	50.65	23.56	81569	5.2
11-12-85 3C	process	.288	30.00	15.21	58.95	7.52	10.294	-2.8
	regen'n	.290	79.96	15.58	51.32	23.21	81692	4.5
10-29-85 2A	process	.191	33.00	19.95	65.46	11.02	10.998	1.0
	regen'n	.194	79.97	18.72	48.20	27.52	83110	15.8
10-29-85 4A	process	.191	29.99	20.02	64.57	10.45	10.894	-2.9
	regen'n	.194	79.96	18.44	46.12	27.86	83044	-1.0
11-13-85 1A	process	.191	27.15	18.70	62.36	9.38	11.205	-3.4
	regen'n	.193	79.96	19.06	45.40	28.28	81812	3.7
11-13-85 2A	process	.191	33.00	18.72	64.52	10.40	10.752	-3.9
	regen'n	.193	79.96	19.28	49.02	27.52	81832	9.5
11-13-85 3A	process	.191	36.00	18.60	65.68	10.94	11.404	-3.7
	regen'n	.193	79.95	19.13	50.80	26.71	81934	8.7
11-13-85 4A	process	.191	29.99	18.62	63.32	9.89	11.367	-2.7
	regen'n	.193	79.96	19.27	47.25	27.91	81819	1.8
11-05-85 1B	process	.220	29.99	15.20	42.19	11.67	9.851	11.7
	regen'n	.221	49.97	15.74	37.86	19.26	81539	-14.7
11-13-85 1B	process	.220	30.00	14.76	42.37	11.19	10.071	-.9
	regen'n	.222	49.98	15.21	37.75	18.74	81966	-4.9
11-13-85 2B	process	.220	29.99	14.56	54.96	7.98	10.593	-4.4
	regen'n	.222	69.97	15.16	45.36	21.68	81958	8.0
11-13-85 3B	process	.220	29.99	14.36	66.38	5.67	10.499	-3.8
	regen'n	.222	89.97	15.05	54.13	23.67	81880	6.7
11-04-85 1B	process	.220	30.00	14.59	33.44	13.63	.279	-8.2
	regen'n	.222	79.97	14.91	76.50	15.86	82318	-19.4
11-05-85 1A	process	.220	29.99	14.72	40.76	11.23	1.000	-9.9
	regen'n	.221	79.98	14.82	69.09	18.30	81521	-39.5
11-14-85 1B	process	.220	29.99	14.71	50.48	8.70	2.698	-5.4
	regen'n	.222	79.97	14.19	59.55	20.15	82553	8.7

Table E.2 Experimental data from *rewound* wheel. (cont.)

run no.	period	$\dot{m}_{DA,j}$ (kg_{DA}/s)	$t_{j,i}$ (C)	$w_{j,i}$ (g/kg)	$t_{j,o}$ (C)	$w_{j,o}$ (g/kg)	$\dot{N}$ (rev/hr) P_{TOT} (Pa)	E_{wr} (%) E_{hr} (%)
11-14-85 2B	process	.220	30.00	15.00	52.84	8.33	3.419	-3.0
	regen'n	.222	79.97	14.43	57.26	21.04	82440	-2.5
11-14-85 3B	process	.220	29.99	14.98	56.03	7.57	4.660	-4.6
	regen'n	.222	79.96	14.36	54.15	21.70	82291	-2.4
11-21-85 1A	process	.220	30.00	15.33	31.64	15.03	.130	2.9
	regen'n	.221	79.97	16.05	78.31	16.34	81095	-27.7
11-22-85 1A	process	.220	30.00	14.25	34.01	13.15	.358	1.4
	regen'n	.221	79.97	13.61	75.90	14.71	81548	8.9
11-22-85 2A	process	.220	30.00	14.47	35.82	12.79	.517	-4.0
	regen'n	.221	79.98	13.85	74.07	15.53	81416	19.0
11-22-85 3A	process	.220	30.00	14.54	36.72	12.55	.593	.6
	regen'n	.221	79.97	14.20	73.16	16.19	81364	28.5
11-22-85 4A	process	.220	30.00	14.59	34.26	13.43	.374	-.5
	regen'n	.221	79.97	14.31	75.65	15.47	81283	16.2
11-22-85 5A	process	.220	30.00	14.58	32.11	14.13	.181	1.8
	regen'n	.221	79.97	14.22	77.83	14.66	81393	-23.5
11-22-85 1B	process	.220	29.99	13.69	38.30	11.29	.787	5.8
	regen'n	.221	79.97	13.99	71.57	16.38	81516	43.8
11-25-85 1A	process	.220	30.00	14.94	42.77	10.97	1.246	5.9
	regen'n	.221	79.97	14.36	67.08	18.32	80850	63.9
11-25-85 1B	process	.220	30.01	14.74	45.25	10.14	1.601	-.5
	regen'n	.221	79.97	14.15	64.63	18.73	80758	28.9
11-25-85 2B	process	.220	30.02	14.72	44.09	10.51	1.427	.7
	regen'n	.221	79.97	14.20	65.80	18.40	80752	28.9
11-25-85 3B	process	.220	30.00	14.62	40.87	11.41	1.013	2.4
	regen'n	.221	79.97	14.10	68.99	17.30	80789	26.8
11-25-85 4B	process	.220	30.00	14.61	46.33	9.72	1.810	-2.7
	regen'n	.221	79.97	14.13	63.56	18.99	80788	11.3
11-25-85 5B	process	.220	30.00	15.25	47.47	9.98	1.967	-2.5
	regen'n	.221	79.97	14.69	62.43	19.93	80823	8.2
11-25-85 1C	process	.220	29.99	14.45	48.32	8.99	2.257	-3.2
	regen'n	.221	79.97	14.45	61.60	19.88	80862	8.0
11-25-85 2C	process	.220	29.99	14.53	50.24	8.53	2.714	-4.1
	regen'n	.222	79.97	14.50	59.80	20.45	80902	2.3
11-25-85 3C	process	.220	29.99	14.64	51.20	8.38	2.983	-3.8
	regen'n	.222	79.97	14.63	58.87	20.83	81017	-1.9
11-26-85 1A	process	.220	30.00	14.77	55.53	7.51	4.469	-4.2
	regen'n	.222	79.97	14.30	54.66	21.50	81731	9.3
11-26-85 2A	process	.220	30.01	14.81	53.78	7.93	3.774	-3.2
	regen'n	.222	79.97	14.33	56.37	21.15	81694	-2.7

Table E.2 Experimental data from *rewound* wheel. (end)

run no.	period	$\dot{m}_{DA,j}$ (kg_{DA}/s)	$t_{j,i}$ (C)	$w_{j,i}$ (g/kg)	$t_{j,o}$ (C)	$w_{j,o}$ (g/kg)	$\dot{N}$ (rev/hr) P_{TOT} (Pa)	E_{wr} (%) E_{hr} (%)
10-31-85 2A	process	.218	29.99	5.90	46.04	14.81	121.192	1.8
	regen'n	.226	49.99	17.48	34.65	8.89	81358	3.8
10-31-85 3A	process	.170	29.99	8.25	46.63	18.48	122.049	3.8
	regen'n	.176	49.96	20.84	34.02	10.96	81228	1.6
11-01-85 1B	process	.218	30.00	7.15	47.04	19.61	598.800	-1.2
	regen'n	.226	49.97	22.26	33.68	10.24	82059	.1
11-01-85 1D	process	.331	37.76	14.12	55.94	6.74	601.900	-2.0
	regen'n	.336	59.99	4.72	41.97	11.99	82147	200.0
11-01-85 2D	process	.223	26.51	18.47	54.34	7.47	598.400	3.6
	regen'n	.220	59.98	4.99	31.55	16.14	81989	-51.5
11-01-85 3D	process	.174	29.98	16.06	55.92	6.61	598.400	-2.3
	regen'n	.172	59.96	5.00	33.58	14.56	81853	44.6
11-15-85 1A	process	.169	29.99	3.75	47.35	14.16	638.800	.8
	regen'n	.173	49.96	15.81	33.10	5.64	81929	2.4
11-18-85 2A	process	.218	30.01	4.95	46.90	13.66	638.900	2.5
	regen'n	.222	49.98	15.43	33.49	6.88	80899	3.5
11-18-85 3A	process	.333	30.00	5.07	45.66	13.11	638.200	2.9
	regen'n	.339	49.98	15.59	34.72	7.70	81097	2.6
11-18-85 1C	process	.172	29.97	17.23	55.69	6.82	645.600	2.8
	regen'n	.171	59.95	4.90	33.92	15.38	81181	200.0
11-19-85 1A	process	.171	30.00	15.51	55.92	4.43	594.600	-.9
	regen'n	.171	59.95	2.30	33.86	13.38	82121	19.9
11-19-85 2A	process	.220	30.02	16.26	55.42	4.68	606.700	-2.7
	regen'n	.220	59.98	1.97	34.38	13.55	82311	-7.6
11-20-85 1A	process	.337	30.00	11.34	53.74	4.36	605.500	-3.8
	regen'n	.334	59.98	2.12	35.86	9.17	82324	-7.7

Table E.3 Experimental data from *microbead* wheel corrected for leakage rates and unbalances.

run no.	period	$\dot{m}_{DA,j}$ (kg_{DA}/s)	$t_{j,i}$ (C)	$w_{j,i}$ (g/kg)	$t_{j,o}$ (C)	$w_{j,o}$ (g/kg)	$\dot{N}$ (rev/hr) P_{TOT} (Pa)	E_{wr} (%) E_{hr} (%)
03-03-86 1A	process	.178	29.96	14.22	74.76	5.61	925.752	2.8
	regen'n	.173	79.70	4.80	33.49	13.66	81324	-.1
03-03-86 2A	process	.208	29.97	15.01	74.28	5.81	932.447	4.7
	regen'n	.204	79.75	4.73	34.41	14.11	81239	1.1
03-04-86 1A	process	.208	29.97	15.87	74.09	6.60	944.956	4.6
	regen'n	.202	79.74	5.50	34.16	15.04	81029	.8
03-04-86 2A	process	.238	29.98	14.41	73.44	5.89	928.332	3.8
	regen'n	.231	79.79	4.73	34.85	13.51	81174	-.7
03-04-86 3A	process	.268	29.99	14.55	72.81	5.94	931.969	3.7
	regen'n	.261	79.82	4.62	35.66	13.46	81318	-.6
03-04-86 1B	process	.148	29.96	15.14	75.46	5.84	935.848	4.6
	regen'n	.144	79.65	5.10	32.78	14.66	81129	1.9
03-04-86 2B	process	.298	29.98	13.16	72.03	5.94	936.811	4.2
	regen'n	.290	79.83	4.70	36.45	12.12	81363	-.7
03-05-86 1A	process	.149	29.95	20.12	75.21	10.53	921.618	4.1
	regen'n	.144	79.64	9.73	32.70	19.65	80694	1.0
03-05-86 1B	process	.179	29.96	19.97	74.75	11.23	926.284	4.6
	regen'n	.174	79.71	10.36	33.51	19.35	81056	1.2
03-06-86 1A	process	.209	29.97	18.70	74.09	10.13	943.456	3.7
	regen'n	.203	79.74	9.13	34.17	17.95	81079	.4
03-06-86 2A	process	.239	29.98	16.92	73.53	9.02	960.276	4.7
	regen'n	.233	79.79	7.97	34.97	16.07	81351	.7
03-06-86 5A	process	.178	29.96	16.90	74.81	8.22	935.514	4.8
	regen'n	.173	79.71	7.38	33.45	16.31	81099	1.3
03-06-86 1B	process	.149	29.95	17.23	75.28	7.58	934.778	6.0
	regen'n	.144	79.64	6.76	32.62	16.75	81071	2.6
03-07-86 1A	process	.118	29.94	16.41	76.08	8.65	949.481	5.0
	regen'n	.115	79.54	8.19	32.13	16.15	80559	4.0
03-07-86 2A	process	.118	29.95	19.45	76.10	10.75	959.437	5.5
	regen'n	.115	79.56	10.22	32.13	19.15	80349	4.5
03-10-86 1A	process	.208	29.97	16.46	74.20	7.51	933.651	4.9
	regen'n	.203	79.74	6.42	34.27	15.59	80040	2.1
03-10-86 2A	process	.297	29.99	13.00	72.07	5.69	945.854	4.3
	regen'n	.290	79.82	4.39	36.54	11.88	80191	-.1
03-10-86 3A	process	.267	29.97	12.63	72.78	5.38	950.167	4.4
	regen'n	.260	79.80	4.24	35.68	11.68	80082	-.1
03-10-86 4A	process	.237	29.98	12.49	73.55	5.22	948.695	4.2
	regen'n	.231	79.78	4.24	34.94	11.70	79988	.2

Table E.3 Experimental data from *microbead* wheel. (cont.)

run no.	period	$\dot{m}_{DA,j}$ (kg_{DA}/s)	$t_{j,i}$ (C)	$w_{j,i}$ (g/kg)	$t_{j,o}$ (C)	$w_{j,o}$ (g/kg)	$\dot{N}$ (rev/hr) P_{TOT} (Pa)	E_{wr} (%) E_{hr} (%)
03-11-86 1A	process	.207	29.97	12.09	74.18	5.25	917.201	3.5
	regen'n	.202	79.74	4.44	34.32	11.45	79345	.3
03-11-86 2A	process	.177	29.95	12.10	74.89	5.11	929.852	.4
	regen'n	.173	79.70	4.32	33.62	11.48	79271	-1.1
03-11-86 3A	process	.147	29.95	11.47	75.46	5.32	936.820	4.5
	regen'n	.143	79.64	4.85	32.79	11.17	79305	1.2
03-14-86 1A	process	.229	29.98	15.33	30.85	15.26	.108	-200.0
	regen'n	.223	79.78	15.63	78.88	15.70	79654	38.4
03-14-86 2A	process	.229	29.96	15.31	31.38	15.04	.309	-59.4
	regen'n	.223	79.76	15.04	78.28	15.32	79751	17.0
03-17-86 1A	process	.229	29.97	15.01	33.60	14.08	1.016	-16.5
	regen'n	.223	79.77	15.32	75.97	16.27	79352	16.7
03-17-86 2A	process	.229	29.97	15.06	36.45	13.18	2.026	-7.8
	regen'n	.223	79.77	15.40	73.00	17.33	79314	-35.9
03-17-86 4A	process	.228	29.97	15.00	39.07	12.25	3.022	-5.3
	regen'n	.223	79.77	15.27	70.33	18.09	79405	-44.1
03-17-86 5A	process	.228	29.98	15.25	41.64	11.64	4.083	-3.0
	regen'n	.223	79.78	15.49	67.70	19.18	79341	-45.8
03-20-86 1A	process	.229	29.97	14.96	42.68	11.07	4.550	.4
	regen'n	.223	79.77	14.67	66.55	18.67	81821	-32.6
03-20-86 2A	process	.178	30.00	14.39	45.00	9.94	4.543	3.8
	regen'n	.174	79.74	14.43	64.25	18.99	81764	-12.5
03-20-86 3A	process	.178	30.02	15.36	44.26	11.07	3.965	2.5
	regen'n	.174	79.74	14.67	65.00	19.05	81997	-18.3
03-25-86 1A	process	.178	29.97	15.83	42.08	12.21	3.064	4.5
	regen'n	.174	79.71	15.23	67.15	18.93	80511	10.5
03-25-86 3A	process	.178	29.97	15.86	38.45	13.52	1.974	9.0
	regen'n	.174	79.71	15.29	70.90	17.69	80564	12.7
03-25-86 4A	process	.178	29.96	15.97	34.81	14.82	1.012	11.7
	regen'n	.174	79.71	15.20	74.66	16.38	80731	35.8
03-26-86 1A	process	.178	29.98	15.96	51.25	9.68	7.073	4.5
	regen'n	.174	79.71	15.55	57.86	21.97	81461	7.1
03-26-86 2A	process	.178	29.96	16.03	56.03	8.51	10.340	2.8
	regen'n	.174	79.72	15.62	53.08	23.32	81572	9.7
03-27-86 1A	process	.178	29.98	14.53	59.42	6.48	15.564	1.2
	regen'n	.174	79.72	14.29	49.73	22.53	81468	8.6
03-27-86 2A	process	.178	30.36	13.67	61.08	5.63	20.415	.2
	regen'n	.174	79.73	13.49	48.47	21.72	81646	1.9
03-27-86 3A	process	.178	30.44	14.69	62.75	6.31	25.982	-.3
	regen'n	.174	79.72	14.51	46.89	23.09	81692	-.1

Table E.3 Experimental data from *microbead* wheel. (cont.)

run no.	period	$\dot{m}_{DA,j}$ (kg_{DA}/s)	$t_{j,i}$ (C)	$w_{j,i}$ (g/kg)	$t_{j,o}$ (C)	$w_{j,o}$ (g/kg)	$\dot{N}$ (rev/hr) P_{TOT} (Pa)	E_{wr} (%) E_{hr} (%)
03-31-86 1A	process	.178	30.01	16.07	63.66	6.92	31.136	-5.9
	regen'n	.174	79.72	15.72	45.57	25.08	80114	-11.8
03-31-86 2A	process	.178	29.97	15.70	63.80	7.03	35.097	.2
	regen'n	.174	79.72	15.33	45.36	24.20	80052	.6
03-31-86 3A	process	.178	29.97	15.86	64.25	7.28	40.308	.5
	regen'n	.174	79.71	15.53	44.91	24.30	79986	.7
04-01-86 1A	process	.178	30.03	15.57	64.23	7.37	45.475	-.5
	regen'n	.174	79.75	15.84	45.06	24.23	80747	1.7
04-01-86 2A	process	.178	29.96	16.22	65.02	8.11	55.070	-.5
	regen'n	.174	79.70	16.35	44.14	24.65	80512	-.8
04-01-86 3A	process	.178	29.97	16.20	65.54	8.44	66.219	-.9
	regen'n	.174	79.71	16.40	43.63	24.33	80354	-1.1
04-01-86 4A	process	.178	29.97	16.27	66.06	8.83	76.990	-1.7
	regen'n	.174	79.71	16.47	43.10	24.08	80005	-2.3
04-01-86 5A	process	.178	29.99	16.48	66.68	9.37	89.195	-2.7
	regen'n	.174	79.72	16.65	42.49	23.92	79814	-3.3
04-02-86 1A	process	.178	29.96	15.22	67.74	9.19	113.701	-5.2
	regen'n	.175	79.72	15.16	41.56	21.29	78745	-2.4
04-02-86 1B	process	.228	29.97	15.39	46.66	10.43	6.693	7.0
	regen'n	.223	79.77	15.40	62.57	20.47	78735	-.9
04-02-86 2B	process	.228	29.98	16.56	52.05	10.02	9.857	2.4
	regen'n	.223	79.78	16.70	57.16	23.39	79223	-3.6
04-04-86 1A	process	.228	29.96	14.70	56.53	7.17	15.955	1.6
	regen'n	.223	79.76	14.50	52.64	22.20	79596	5.7
04-04-86 2A	process	.228	29.98	14.77	59.06	6.73	20.439	1.0
	regen'n	.223	79.79	14.58	50.17	22.80	80035	2.5
04-04-86 3A	process	.228	30.01	14.77	60.61	6.51	25.429	.7
	regen'n	.223	79.77	14.65	48.64	23.10	80228	1.1
04-04-86 4A	process	.228	29.98	15.07	61.58	6.64	30.100	.9
	regen'n	.223	79.79	14.85	47.68	23.47	80162	1.5
04-04-86 5A	process	.228	30.00	15.04	62.04	6.72	35.100	.1
	regen'n	.224	79.79	15.55	47.41	24.01	80360	.6
04-07-86 7A	process	.228	29.98	14.57	62.65	6.19	40.636	-2.4
	regen'n	.224	79.77	14.09	46.72	22.62	80785	-4.2
04-07-86 3A	process	.228	29.96	14.59	63.33	6.40	50.433	-2.0
	regen'n	.224	79.75	14.09	46.00	22.43	80753	-3.6
04-07-86 4A	process	.228	29.97	14.83	63.97	6.80	60.304	-1.7
	regen'n	.224	79.78	14.35	45.41	22.52	80790	-3.0
04-07-86 5A	process	.228	29.97	15.14	64.52	7.27	70.321	-1.6
	regen'n	.224	79.77	14.64	44.84	22.65	80648	-2.8

Table E.3 Experimental data from *microbead* wheel. (cont.)

run no.	period	$\dot{m}_{DA,j}$ (kg_{DA}/s)	$t_{j,i}$ (C)	$w_{j,i}$ (g/kg)	$t_{j,o}$ (C)	$w_{j,o}$ (g/kg)	$\dot{N}$ (rev/hr) P_{TOT} (Pa)	E_{wr} (%) E_{hr} (%)
04-08-86 1A	process	.228	29.97	15.56	64.79	8.07	80.807	2.3
	regen'n	.224	79.77	15.44	44.58	23.07	80570	2.8
04-08-86 2A	process	.228	29.97	15.50	65.21	8.29	90.949	2.6
	regen'n	.224	79.77	15.40	44.16	22.74	80566	2.1
04-08-86 3A	process	.228	29.97	15.66	65.76	8.72	103.560	2.2
	regen'n	.224	79.76	15.50	43.59	22.57	80546	1.3
04-08-86 4A	process	.228	29.99	15.66	66.36	15.62	119.313	-200.0
	regen'n	.224	79.78	15.46	42.75	15.50	80415	-90.0
04-10-86 1A	process	.178	29.96	15.10	63.53	6.70	35.537	.6
	regen'n	.174	79.71	14.87	45.61	23.47	79794	3.0
04-10-86 2A	process	.208	29.97	15.11	62.84	6.66	35.739	.5
	regen'n	.204	79.75	14.84	46.46	23.45	79857	2.0
04-10-86 3A	process	.238	29.98	15.22	62.12	6.74	35.578	1.0
	regen'n	.233	79.80	14.68	47.16	23.34	80099	1.1
04-11-86 1A	process	.268	29.97	14.95	60.83	6.75	35.048	-.9
	regen'n	.263	79.81	14.96	48.54	23.31	79757	-2.0
04-11-86 2A	process	.298	29.98	15.08	59.79	7.02	34.910	-.4
	regen'n	.292	79.83	15.43	49.56	23.65	79898	-2.9
04-11-86 3A	process	.229	29.97	18.67	63.31	9.66	34.818	5.7
	regen'n	.225	79.77	19.02	46.13	28.19	79906	11.9
04-11-86 4A	process	.228	29.97	16.42	62.66	7.65	35.101	-.2
	regen'n	.224	79.77	16.50	46.74	25.42	79767	.1
04-11-86 5A	process	.227	29.96	12.33	60.75	4.73	34.731	.3
	regen'n	.223	79.75	12.17	48.56	19.90	79882	1.3
04-11-86 1B	process	.227	29.97	8.78	57.34	2.90	34.782	-2.7
	regen'n	.222	79.77	9.86	51.89	15.87	80023	-2.5
04-14-86 2A	process	.229	29.95	15.12	36.17	13.32	35.703	1.6
	regen'n	.223	39.89	15.58	33.51	17.42	80263	-3.6
04-14-86 3A	process	.228	29.97	15.08	42.70	11.41	35.432	-.5
	regen'n	.223	49.87	15.61	36.90	19.36	80244	13.8
04-14-86 4A	process	.228	29.97	14.79	49.18	9.42	35.597	.9
	regen'n	.223	59.83	15.27	40.28	20.76	80400	3.7
04-14-86 5A	process	.228	29.95	14.70	55.59	7.83	35.793	.6
	regen'n	.224	69.80	15.20	43.86	22.19	80533	4.9
04-14-86 1B	process	.228	29.97	15.41	67.96	5.97	35.765	.0
	regen'n	.224	89.74	16.49	51.41	26.10	80651	2.5
04-14-86 2B	process	.228	26.52	15.68	60.61	6.68	35.653	.8
	regen'n	.224	79.77	16.76	45.37	25.93	80506	-.1
04-14-86 3B	process	.228	30.01	15.72	62.37	7.23	35.801	1.2
	regen'n	.224	79.80	16.17	47.11	24.81	80710	4.0

Table E.3 Experimental data from *microbead* wheel. (end)

run no.	period	$\dot{m}_{DA,j}$ (kg_{DA}/s)	$t_{j,i}$ (C)	$w_{j,i}$ (g/kg)	$t_{j,o}$ (C)	$w_{j,o}$ (g/kg)	$\dot{N}$ (rev/hr) P_{TOT} (Pa)	E_{wr} (%) E_{hr} (%)
04-15-86 1A	process	.228	34.94	15.10	64.04	7.55	35.909	-.4
	regen'n	.223	79.76	15.17	50.20	22.88	80479	.1
04-15-86 1C	process	.228	39.94	14.68	65.88	8.11	35.535	.0
	regen'n	.223	79.78	14.51	53.39	21.23	80358	6.3
04-16-86 1A	process	.228	29.97	15.04	69.62	11.31	223.129	-3.3
	regen'n	.224	79.76	14.98	39.59	18.78	79340	-1.6
04-16-86 2A	process	.228	29.97	15.17	72.07	13.64	354.189	-11.8
	regen'n	.224	79.78	15.14	37.02	16.70	79449	-1.8
04-16-86 3A	process	.228	29.96	15.19	72.91	14.41	478.879	-31.2
	regen'n	.224	79.77	15.14	36.09	15.94	79572	-2.1
04-16-86 4A	process	.228	29.97	15.49	73.34	15.01	606.730	-62.3
	regen'n	.224	79.78	15.45	35.67	15.94	79446	-2.4
04-16-86 5A	process	.228	29.96	15.93	73.68	15.60	791.831	-79.1
	regen'n	.224	79.77	15.83	35.29	16.17	79383	-2.3
04-16-86 1B	process	.178	29.96	14.82	74.91	13.95	796.605	-27.9
	regen'n	.175	79.70	13.94	33.98	14.83	79217	-1.5
04-29-86 1A	process	.178	29.96	15.80	72.07	13.66	232.371	-14.6
	regen'n	.175	79.71	16.25	37.04	18.42	79353	-2.0
04-29-86 2A	process	.178	29.97	16.03	73.66	15.57	355.216	-65.2
	regen'n	.175	79.71	16.46	35.33	16.93	79496	-2.2
04-29-86 3A	process	.178	29.97	15.96	74.22	16.01	482.082	-200.0
	regen'n	.175	79.71	16.41	34.73	16.36	79594	-1.9
04-29-86 4A	process	.178	29.96	16.08	74.52	16.31	607.040	-131.4
	regen'n	.175	79.71	16.52	34.40	16.29	79567	-2.0

The following set of tables lists the experiments considered in the various analyses performed in Chapter 5. Each of the figures in Chapter 5 and the corresponding table of data are listed below in Table E.4.

Table E.4 List of figures with corresponding table of data.

Figure	Table	Figure	Table
5.6	E.4	5.23	E.8
5.7	E.4	5.24	E.9
5.11	E.6	5.25	E.10
5.12	E.6	5.26	E.11
5.13	E.6	5.27	E.12
5.14	E.7	5.28	E.13
5.20	E.8	5.29	E.14

Table E.5 Low rotation speed experiments considered in section 5.2. "*" indicates that the value was used in the average.

run no.	$\bar{\gamma}_{21}\Gamma_1$	$\frac{M_{DD,exp}}{M_{DD,calc}}$	c_{DM} (J/kg$_{DD}$-C)	$\dot{N}$ (rev/hr)
		original wheel		
04-11-85 1A	0.127	0.9122 *	3744	0.335
04-11-85 2A	0.208	0.9433 *	2780 *	0.567
05-08-85 2A	0.368	0.9717 *	2820 *	0.998
04-19-85 1A	0.427	0.8242	3118	1.18
04-19-85 2A	0.646	0.7066	3300	1.78
05-14-85 1B	0.735	0.6683	3342	2.00
04-19-85 3A	0.872	0.6001	3683	2.40
05-07-85 2B	1.109	0.5219	3890	3.00
05-04-85 1A	1.280	0.4835	4025	3.50

Table E.5 Low rotation speed experiments. (cont.)

run no.	$\bar{\gamma}_{21}\Gamma_1$	$\frac{M_{DD,exp}}{M_{DD,calc}}$	c_{DM} (J/kg$_{DD}$-C)	$\dot{N}$ (rev/hr)
		rewound wheel		
11-21-85 1A	0.048	0.6095	12855	0.130
11-22-85 5A	0.063	0.6836	8911	0.181
11-04-85 1B	0.099	0.9483 *	4099	0.279
11-22-85 1A	0.124	0.8693 *	4196	0.358
11-22-85 4A	0.130	0.8635 *	4398	0.374
11-22-85 2A	0.179	0.9077 *	3505 *	0.517
11-22-85 3A	0.206	0.9359 *	3141 *	0.593
11-22-85 1B	0.271	0.9016 *	3255 *	0.787
11-25-85 3B	0.350	0.8825 *	3179 *	1.013
11-05-85 1A	0.352	0.9618 *	1958	1.000
11-25-85 1A	0.434	0.8689	2525	1.25
11-25-85 2B	0.494	0.8182	2983	1.43
11-25-85 1B	0.554	0.7940	2878	1.60
11-25-85 4B	0.626	0.7521	2961	1.81
11-25-85 5B	0.689	0.7163	3006	1.97
11-25-85 1C	0.782	0.6823	2966	2.26
11-25-85 2C	0.942	0.6204	3040	2.71
11-14-85 1B	0.954	0.6038	3316	2.70
11-25-85 3C	1.040	0.5836	3128	2.98
		microbead wheel		
03-14-86 1A	0.011	0.6272	43937	0.108
03-14-86 2A	0.029	0.8646 *	11519	0.309
03-17-86 1A	0.096	0.9271 *	5512	1.016
03-25-86 4A	0.127	0.8304 *	7374	1.012
03-17-86 2A	0.192	0.9429 *	3486 *	2.03
03-25-86 3A	0.246	0.8746 *	4582	1.97
03-17-86 4A	0.287	0.9219 *	2885 *	3.02
03-25-86 1A	0.382	0.8717 *	3330 *	3.06
03-17-86 5A	0.390	0.8828 *	2597 *	4.08
03-20-86 1A	0.440	0.8435	2796	4.55
03-20-86 3A	0.496	0.8076	3143	3.96
03-20-86 2A	0.559	0.7834	3058	4.54
04-02-86 1B	0.635	0.7360	3179	6.69
03-26-86 1A	0.894	0.6449	3517	7.07

Table E.6 High rotation speed experiments considered in section 5.3.3 and Figs. 5.11, 5.12, and 5.13.

run no.	j_{min}	$\frac{m_{DA,min}}{m_{DA,max}}$	$\bar{\gamma}_1\Gamma_{min}$	$\frac{RePrD_{hu}}{4L}$	ε_t^∞	Nu_e	ε_w^∞	Sh_e	Le_o
			original wheel						
04-23-85 3A	1	.982	1.71	.307			.742	1.474	
04-23-85 2A	1	.972	1.40	.290	.798	2.170	.751	1.442	1.294
04-25-85 4A	1	.969	1.55	.219	.832	2.011			
04-25-85 3A	1	.981	2.21	.231			.779	1.354	
04-25-85 2A	1	.971	1.79	.218	.832	2.016	.795	1.384	1.253
			rewound wheel						
11-20-85 1A	2	.991	4.69	.589	.805	4.762	.764	3.221	1.267
11-18-85 3A	1	.982	4.33	.596	.788	4.297	.770	3.327	1.111
11-01-85 1D	1	.985	3.93	.580	.817	5.013	.786	3.554	1.212
11-01-85 2D	2	.987	5.63	.391	.849	4.249	.828	3.133	1.168
11-19-85 2A	1	1.000	6.23	.389	.847	4.311	.811	2.856	1.297
11-01-85 1B	1	.965	5.50	.392	.856	4.236	.828	3.016	1.213
11-18-85 2A	1	.982	6.66	.390	.848	4.142	.834	3.216	1.107
10-31-85 2A	1	.965	1.20	.391	.853	4.122	.836	3.147	1.128
11-01-85 3D	2	.989	7.37	.304	.880	4.272	.864	3.221	1.141
11-18-85 1C	2	.994	7.81	.303	.868	3.913	.850	2.900	1.161
11-19-85 1A	1	1.000	7.94	.302	.865	3.882	.839	2.703	1.233
10-31-85 3A	1	.966	1.44	.306	.866	3.573	.861	2.973	1.038
11-15-85 1A	1	.977	8.75	.302	.870	3.776	.865	3.095	1.048

Table E.6 High rotation speed experiments. (cont.)

run no.	j_{min}	$\frac{m_{DA,min}}{m_{DA,max}}$	$\bar{\gamma}_l\Gamma_{min}$	$\frac{RePrD_{hu}}{4L}$	ε_t^∞	Nu_e	ε_w^∞	Sh_e	Le_o
			microbead wheel						
03-06-86 2A	2	.975	2.08	.333	.902	5.537	.894	4.372	1.091
03-07-86 2A	2	.975	3.82	.165	.957	5.787	.964	5.763	.867
03-10-86 3A	2	.974	2.26	.370	.888	5.354	.878	4.180	1.099
03-07-86 1A	2	.975	4.19	.164	.957	5.758	.965	5.875	.844
03-10-86 4A	2	.975	2.55	.329	.903	5.484	.896	4.396	1.070
03-10-86 2A	2	.976	1.99	.413	.872	5.221	.858	4.011	1.117
03-04-86 1A	2	.971	2.57	.288	.917	5.551	.915	4.661	1.024
03-06-86 1A	2	.971	2.21	.291	.917	5.606	.913	4.601	1.051
03-11-86 3A	2	.973	4.11	.204	.944	5.646	.950	5.385	.900
03-04-86 2B	2	.973	1.95	.413	.874	5.255	.864	4.154	1.086
03-04-86 1B	2	.973	3.67	.205	.944	5.718	.950	5.399	.910
03-06-86 5A	2	.972	2.77	.247	.931	5.678	.933	4.993	.979
03-06-86 1B	2	.966	3.35	.206	.947	5.761	.951	5.296	.937
03-10-86 1A	2	.976	2.43	.290	.915	5.567	.908	4.400	1.089
03-03-86 2A	2	.981	2.61	.291	.912	5.512	.908	4.522	1.048
03-04-86 3A	2	.974	2.07	.372	.889	5.394	.883	4.389	1.056
03-11-86 2A	2	.977	3.36	.246	.928	5.558	.915	4.055	1.176
03-04-86 2A	2	.971	2.34	.329	.904	5.497	.900	4.516	1.046
03-05-86 1B	2	.972	2.42	.249	.930	5.652	.927	4.711	1.036
03-03-86 1A	2	.972	3.12	.247	.930	5.589	.936	5.195	.924
03-05-86 1A	2	.966	2.93	.206	.946	5.657	.951	5.319	.919
03-11-86 1A	2	.976	2.83	.288	.915	5.489	.909	4.417	1.066
04-16-86 1B	2	.983	2.11	.251	.924	5.548			
04-16-86 5A	2	.982	1.56	.321	.902	5.462			
04-29-86 4A	2	.983	1.51	.251	.920	5.280			
04-16-86 4A	2	.982	1.21	.321	.900	5.358			
04-29-86 3A	2	.983	1.20	.251	.919	5.194			

Table E.7 High rotation speed experiments considered in Fig. 5.14.

exp. no.	run no.	$t_{1,o}$ (C)	$w_{1,o}$ (g/kg)	$\dot{N}$ (rev/hr)	Γ_1	$Ntu_{t,1}$
			rewound wheel			
1	11-20-85 1A	53.74	4.36	606	6.39	7.9
2	11-18-85 3A	45.66	13.11	638	6.81	7.9
3	11-01-85 1D	55.93	6.75	602	6.47	8.0
4	11-01-85 2D	54.34	7.47	598	9.54	10.5
5	11-19-85 2A	55.42	4.69	607	9.81	10.6
6	11-01-85 1B	47.04	19.62	599	9.77	10.6
7	11-18-85 2A	46.90	13.66	639	10.42	10.6
8	10-31-85 2A	46.03	14.81	121	1.98	10.6
9	11-01-85 3D	55.93	6.61	598	12.23	12.7
10	11-18-85 1C	55.70	6.82	646	13.35	12.8
11	11-19-85 1A	55.92	4.43	595	12.36	12.9
12	10-31-85 3A	46.63	18.48	122	2.55	12.8
13	11-15-85 1A	47.34	14.16	639	13.44	12.9
			microbead wheel			
1	03-06-86 2A	73.53	9.03	960	4.05	15.8
2	03-07-86 2A	76.10	10.75	959	8.20	34.0
3	03-10-86 3A	72.78	5.38	950	3.59	13.9
4	03-07-86 1A	76.08	8.66	949	8.12	34.1
5	03-10-86 4A	73.54	5.22	949	4.04	16.0
6	03-10-86 2A	72.06	5.69	946	3.21	12.3
7	03-04-86 1A	74.08	6.61	945	4.58	18.4
8	03-06-86 1A	74.08	10.13	943	4.55	18.3
9	03-11-86 3A	75.45	5.32	937	6.43	27.1
10	03-04-86 2B	72.02	5.95	937	3.17	12.3
11	03-04-86 1B	75.46	5.84	936	6.38	26.8
12	03-06-86 5A	74.80	8.22	936	5.30	21.9
13	03-06-86 1B	75.27	7.58	935	6.33	26.6
14	03-10-86 1A	74.19	7.51	934	4.53	18.4
15	03-03-86 2A	74.28	5.81	932	4.52	18.5
16	03-04-86 3A	72.80	5.94	932	3.51	13.9
17	03-11-86 2A	74.89	5.11	930	5.30	22.1
18	03-04-86 2A	73.44	5.89	928	3.94	15.9
19	03-05-86 1B	74.75	11.24	926	5.22	21.7
20	03-03-86 1A	74.75	5.61	926	5.25	21.9
21	03-05-86 1A	75.20	10.53	922	6.24	26.5
22	03-11-86 1A	74.18	5.25	917	4.47	18.6
23	04-16-86 1B	74.91	13.95	797	4.52	21.8
24	04-16-86 5A	73.68	15.60	792	3.50	16.6

Table E.7 High rotation speed experiments in Fig. 5.14. (cont.)

exp. no.	run no.	$t_{1,o}$ (C)	$w_{1,o}$ (g/kg)	$\dot{N}$ (rev/hr)	Γ_1	$Ntu_{t,1}$
25	04-29-86 4A	74.52	16.31	607	3.44	21.8
26	04-16-86 4A	73.34	15.01	607	2.68	16.6
27	04-29-86 3A	74.22	16.01	482	2.73	21.8
28	04-16-86 3A	72.91	14.41	479	2.12	16.6
29	04-29-86 2A	73.66	15.57	355	2.01	21.8
30	04-16-86 2A	72.07	13.64	354	1.57	16.5
31	04-29-86 1A	72.07	13.66	232	1.32	21.7
32	04-16-86 1A	69.62	11.31	223	0.99	16.5

Table E.8 Experimental data from *original* wheel for variation in rotation speed (associated with Figs. 5.20 and 5.23).

$t_{1,i} \approx 31.0$ C $\quad t_{2,i} \approx 80.0$ C $\quad \dot{m}_{DA,j} \approx 0.21$ kg_{DA}/s

$w_{1,i} \approx 14.0$ g/kg $\quad w_{2,i} \approx 12.5$ g/kg $\quad Re_j \approx 170$

exp. no.	run no.	$t_{1,o}$ (C)	$w_{1,o}$ (g/kg)	Γ_1	$\dot{N}$ (rev/hr)
1	04-11-85 1A	35.10	12.92	0.006	0.335
2	04-11-85 2A	37.69	12.04	0.010	0.567
3	04-19-85 1A	43.36	10.46	0.022	1.179
4	04-19-85 2A	47.24	9.36	0.033	1.78
5	04-19-85 3A	50.10	8.67	0.044	2.40
6	05-04-85 1A	54.25	7.71	0.064	3.50
7	04-26-85 1A	57.04	7.12	0.092	5.00
8	05-04-85 2A	59.38	6.87	0.138	7.50
9	04-26-85 2A	60.65	6.80	0.183	10.00
10	05-06-85 1A	61.35	6.89	0.229	12.50
11	05-06-85 2A	61.84	7.06	0.275	15.0
12	05-06-85 1B	62.92	7.44	0.366	20.0
13	05-06-85 2B	64.42	8.24	0.550	30.0
14	05-07-85 1A	66.82	9.84	0.964	52.5

Table E.9 Experimental data from *original* wheel for variation in regeneration inlet state (associated with Fig. 5.24).

	$t_{1,i} \approx 31.0$ C	$\dot{N} \approx 12$ rev/hr	$\dot{m}_{DA,j} \approx 0.21$ kg_{DA}/s			
	$w_{1,i} \approx 14.0$ g/kg	$Ntu_{t,j} \approx 7.3$	$Re_j \approx 170$			
exp. no.	run no.	$t_{2,i}$ (C)	$w_{2,i}$ (g/kg)	$t_{1,o}$ (C)	$w_{1,o}$ (g/kg)
1	05-09-85 1A	59.98	12.48	49.37	9.20
2	05-09-85 4A	69.98	9.94	56.51	7.39
3	05-09-85 3A	69.97	12.58	55.45	8.05
4	05-08-85 2B	69.97	15.28	54.44	8.57
5	05-10-85 1A	79.96	10.16	62.28	6.51
6	05-08-85 1B	79.97	15.09	60.86	7.53
7	05-09-85 1B	89.97	10.05	68.13	5.65
8	05-09-85 2A	89.97	12.53	67.18	6.04
9	05-09-85 2B	89.96	14.76	66.44	6.28

Table E.10 Experimental data from *original* wheel for variation in process inlet state (associated with Fig. 5.25).

	$t_{2,i} \approx 80.0$ C	$\dot{N} \approx 12$ rev/hr	$\dot{m}_{DA,j} \approx 0.21$ kg_{DA}/s			
	$w_{2,i} \approx 12.5$ g/kg		$Re_j \approx 170$			
exp. no.	run no.	$t_{1,i}$ (C)	$w_{1,i}$ (g/kg)	$t_{1,o}$ (C)	$w_{1,o}$ (g/kg)
1	05-06-85 1A	31.00	14.03	61.35	6.89
2	05-10-85 1B	37.00	8.05	59.07	4.50
3	05-10-85 2B	30.99	8.03	56.20	3.86
4	05-10-85 3B	30.99	17.87	63.70	9.78
5	05-13-85 1A	25.67	17.40	61.12	8.00
6	05-13-85 2A	25.64	14.04	58.92	6.10
7	05-13-85 3A	37.00	14.02	63.83	7.76
8	05-13-85 4A	30.99	17.52	63.52	9.01

Table E.11 Experimental data from *rewound* wheel for variation in inlet humidity ratio (associated with Fig. 5.26).

	$t_{1,i} \approx 30.0$ C	$\dot{N} \approx 10$ rev/hr	$\dot{m}_{DA,j} \approx 0.22$ kg_{DA}/s
	$t_{2,i} \approx 80.0$ C	$Ntu_{t,j} \approx 10.7$	$Re_j \approx 195$

exp. no.	run no.	$w_{1,i}$ (g/kg)	$w_{2,i}$ (g/kg)	$t_{1,o}$ (C)	$w_{1,o}$ (g/kg)
1	11-08-85 1A	6.78	6.85	54.83	1.77
2	11-18-85 1A	12.43	12.88	59.94	5.27
3	11-18-85 2A	15.79	14.85	61.75	7.49
4	11-18-85 3A	22.06	21.19	63.71	13.16

Table E.12 Experimental data from *rewound* wheel for variation in flow rates (associated with Fig. 5.27).

	$t_{1,i} \approx 30.0$ C	$t_{2,i} \approx 80.0$ C	$\dot{N} \approx 10$ rev/hr
	$w_{1,i} \approx 15.8$ g/kg	$w_{2,i} \approx 16.0$ g/kg	

exp. no.	run no.	$\dot{m}_{DA,1}$ (kg_{DA}/s)	$\dot{m}_{DA,2}$ (kg_{DA}/s)	$t_{1,o}$ (C)	$w_{1,o}$ (g/kg)
1	11-12-85 3B	0.190	0.192	62.73	7.48
2	11-12-85 4B	0.210	0.212	61.97	8.01
3	11-12-85 5B	0.229	0.232	61.51	8.06
4	11-12-85 1C	0.249	0.251	60.18	7.66
5	11-12-85 2C	0.268	0.271	59.77	7.61
6	11-12-85 3C	0.288	0.290	58.95	7.52

Table E.14 Experimental data from *microbead* wheel for variation in inlet humidity ratio (associated with Fig. 5.28).

	$t_{1,i} \approx 30.0$ C	$\dot{N} \approx 35$ rev/hr	$\dot{m}_{DA,j} \approx 0.22$ kg_{DA}/s		
	$t_{2,i} \approx 80.0$ C	$Ntu_{t,j} \approx 16.3$	$Re_j \approx 120$		
exp. no.	run no.	$w_{1,i}$ (g/kg)	$w_{2,i}$ (g/kg)	$t_{1,o}$ (C)	$w_{1,o}$ (g/kg)
1	04-11-86 3A	18.67	19.02	63.31	9.66
2	04-11-86 4A	16.42	16.50	62.66	7.65
3	04-14-86 3B	15.72	16.17	62.37	7.23
4	04-11-86 5A	12.33	12.17	60.75	4.73
5	04-11-86 1B	8.78	9.86	57.34	2.90

Table E.15 Experimental data from *microbead* wheel for variation in flow rates (associated with Fig. 5.29).

	$t_{1,i} \approx 30.0$ C	$t_{2,i} \approx 80.0$ C	$\dot{N} \approx 35$ rev/hr		
	$w_{1,i} \approx 15.2$ g/kg	$w_{2,i} \approx 15.2$ g/kg			
exp. no.	run no.	$\dot{m}_{DA,1}$ (kg_{DA}/s)	$\dot{m}_{DA,2}$ (kg_{DA}/s)	$t_{1,o}$ (C)	$w_{1,o}$ (g/kg)
1	04-10-86 1A	0.178	0.174	63.53	6.70
2	04-10-86 2A	0.208	0.204	62.84	6.66
3	04-14-86 3B	0.228	0.224	62.37	7.23
4	04-10-86 3A	0.238	0.233	62.12	6.74
5	04-11-86 1A	0.268	0.263	60.83	6.75
6	04-11-86 2A	0.298	0.292	59.79	7.02

References

ASHRAE, 1977,1985, *Handbook of Fundamentals*, American Society of Heating, Refrigertion, and Air Conditioning Engineers, New York.

Banks, P.J., 1972, "Coupled Equilibrium Heat and Single Adsorbate Transfer in Fluid Flow Through a Porous Medium: 1. Characteristic Potentials and Specific Capacity Ratios," *Chemical Engineering Science*, vol. 27, pp. 1143-1155.

Banks, P.J., 1984, "The Representation of Regenerator Fluid Carryover by Bypass Flows," *J. Heat Transfer*, Trans. ASME, vol. 106, pp. 216-220.

Banks, P.J., 1985, "Prediction of Heat and Mass Regenerator Performance Using Nonlinear Analogy Method," parts 1 and 2, *J. Heat Transfer*, Trans. ASME, vol. 107, pp. 222-238.

Barker, J.M., and Kettleborough, C.F., 1980a, "The Adiabatic Adsorption-Desorption Characteristics of Silica Gel Beds - Part 1: Theory," 80-WA/Sol-30, ASME Winter Annual Meeting, Chicago.

Barker, J.M., and Kettleborough, C.F., 1980b, "The Adiabatic Adsorption-Desorption Characteristics of Silica Gel Beds - Part 2: Curve Fits," 80-WA/Sol-30, ASME Winter Annual Meeting, Chicago.

Barlow, R., and Collier, K., 1981, "Optimizing the Performance of Desiccant Beds for Solar Regenerated Cooling," *AS/ISES 1981*, Proc. 1981 Annual Meeting of AS/ISES, American Solar Energy Society, Inc., Boulder, CO.

Barlow, R.S., 1982, "Analysis of the Adsorption Process and of Desiccant Cooling Systems - A Pseudo-Steady-State Model for Coupled Heat and Mass Transfer," SERI/TR-631-1330, Solar Energy Research Institute, Golden, CO.

Barlow, R.S., 1983, "An Assessment of Dehumidifier Geometries for Desiccant Cooling Systems," SERI/TR-252-1529, Solar Energy Research Institute, Golden, CO.

Bean, H.S., ed., 1971, *Fluid Meters, Their Theory and Application*, Report of ASME Research Committee on Fluid Meters, 6th edition, American Society of Mechanical Engineers, New York.

Beba, S., Cler, G., and Lof, G.O.G., 1986, "Performance of a Solar Desiccant Cooling System," *ASES '86*, Proceedings of the 1986 Annual Meeting of the American Solar Energy Society, American Solar Energy Society, Inc., Boulder, CO, pp. 228-231.

Bevington, P.R., 1969, *Data Reduction and Error Analysis for the Physical Sciences*, McGraw-Hill, New York.

Bharathan, D., Parsons, J.M., and Maclaine-cross, I., 1986a, "Experimental Studies of Heat and Mass Exchange in Parallel-Passage Rotary Desiccant Dehumidifiers for Solar Cooling Applications," SERI/TR-252-2897(draft), Solar Energy Research Institute, Golden, CO.

Bharathan, D., Parsons, J.M., and Maclaine-cross, I., 1986b, "Experimental Study of an Advanced Silica-Gel Dehumidifier," SERI/TR-252-2983(draft), Solar Energy Research Institute, Golden, CO.

Bird, R.B., Stewart, W.E., and Lightfoot, E.N., 1960, *Transport Phenomena*, Wiley, New York.

Biswas, P., Kim, S., and Mills, A.F., 1984, "A Compact Low Pressure Drop Desiccant Bed for Solar Air Conditioning Applications: 1. Analysis and Design," *J. Solar Energy Engineering*, Trans. ASME, vol. 106, no. 2, pp. 153-158.

Booz-Allen and Hamilton, Inc., 1980, "Evaluation of Residential and Commercial Solar/Gas Heating and Cooling Technologies," GRI-79/0105, Gas Research Institute, Chicago, IL.

Booz-Allen and Hamilton, Inc., 1981, "Competitive Assesment of Desiccant Solar/Gas Systems for Single Family Residences," GRI-??/????(draft), Gas Research Institute, Chicago, IL.

Bowlen, K.L., 1986, "A Desiccant/Refrigeration Hybrid System for Air Conditioning Buildings," Proceedings of the Desiccant Cooling and Dehumidification Opportunities for Buildings Workshop, June 10-11, 1986, Chattanooga, Tennessee Valley Authority, Chattanooga, TN.

Brandemuehl, M.J., 1982, "Analysis of Heat and Mass Transfer Regenerators with Time Varying or Spatially Nonuniform Inlet Conditions," Ph.D. thesis, Dept. of Mechanical Engineering, University of Wisconsin - Madison.

Bullock, C.E., and Threlkeld, J.L., 1966, "Dehumdification of Moist Air by Adiabatic Adsorption," *ASHRAE Transactions*, vol. 72, pt. 1, pp. 301-313.

Burns, P.R., Mitchell, J.W., and Beckman, W.A., 1985a, "Hybrid Desiccant Cooling Systems in Supermarket Applications," *ASHRAE Transactions*, vol. 91, pt. 1.

Burns, P.R., Mitchell, J.W., and Beckman, W.A., 1985b, "Solar Hybrid Desiccant Cooling Systems in Supermarket Applications," *INTERSOL 85*, Proc. Ninth Biennial Congress of the International Solar Energy Society, Pergamon Press, New York, pp. 700-706.

Carnahan, B., Luther, H.A., and Wilkes, J.O., 1969, *Applied Numerical Methods*, John Wiley and Sons, New York, p. 78.

Chinery, G.T., 1986, "Electrical Utility Perspective on Desiccant Cooling and Dehumidification," Proceedings of the Desiccant Cooling and Dehumidification Opportunities for Buildings Workshop, June 10-11, 1986, Chattanooga, Tennessee Valley Authority, Chattanooga, TN.

Chinery, G.T., and Penney, T., 1987, *Desiccant Newsletter*, Issue no. 1, Tennessee Valley Authority, Chattanoogo, TN.

Chuah, Y.K., Norton, P., and Kreith, F., 1986, "Transient Mass Transfer in Parallel Passage Dehumidifiers With and Without Solid Side Resistance," SERI/TR-250-????(draft), Solar Energy Research Institute, Golden, CO.

Coellner, J.A., 1986, "Energymaster® - Desiccant Cooling in the Marketplace," Proceedings of the Desiccant Cooling and Dehumidification Opportunities for Buildings Workshop, June 10-11, 1986, Chattanooga, Tennessee Valley Authority, Chattanooga, TN.

Cohen, B.M., et al., 1984, "Field Development of a Desiccant-Based Space-Conditioning System for Supermarket Applications," Thermo Electron Corp., GRI-84/0111, Gas Research Institute, Chicago, IL.

Cohen, B.M., et al., 1986, "Field Development of a Desiccant-Based Space-Conditioning System for Supermarket Applications," Proceedings of the Desiccant Cooling and Dehumidification Opportunities for Buildings Workshop, June 10-11, 1986, Chattanooga, Tennessee Valley Authority, Chattanooga, TN.

Collier, R.K., Cale, T.S., and Lavan, Z., 1986, "Advanced Desiccant Materials Assessment," GRI-86/0191, Gas Research Institute, Chicago, IL.

CRC, 1975, *Handbook of Chemistry and Physics*, 56th edition, CRC Press, Cleveland, OH.

Crum, D.R., Mitchell, J.W., and Beckman, W.A., 1987, "Advanced Desiccant Cycles," *Solar Engineering - 1987*, Proc. ASME-JSME-JSES Solar Energy Conf., Honolulu, ASME, New York, pp. 841-847.

Davison Chemical Divison, W.R. Grace and Co., "Silica Gel Grade Chart and Application Guide," Technical Bulletin ADS-16-373, Baltimore, MD.

Dunkle, R.V., Banks, P.J., and Maclaine-cross, I.L., 1980, "Wound Parallel Plate Exchangers for Air-Conditiong Applications," *Compact Heat Exchangers--History, Technological Advancement and Mechanical Design Problems*, HTD-Vol. 10, pp. 65-71, American Society of Mechanical Engineers, New York.

Duffie, J.A., and Beckman, W.A., 1980, *Solar Engineering of Thermal Processes*, John Wiley and Sons, New York.

Edwards, D.K., Denny, V.E., and Mills, A.F., 1973, *Transfer Processes*, Holt, Rinehart, and Winston, New York.

Epstein, M., Grolmes, M., Davidson, K., and Kosar, D., 1985, "Desiccant Cooling System Performance: A Simple Approach," *J. Solar Energy Engineering*, Trans. ASME, vol. 107, pp. 21-28.

Grolmes, M.A., and Epstein, M., 1985, "Property and Composition Effects on the Cyclic Performance of Fixed Bed Desiccant Air Dehumidification," 85-HT-69, ASME 23rd National Heat Transfer Conf., Denver, CO.

Hilsenrath, J., et al., 1960, *Tables of Thermodynamic and Transport Properties* ...," Pergamon Press, Oxford.

Holman, J.P., 1976, *Heat Transfer*, McGraw-Hill, New York.

Holmberg, R.B., 1979, "Combined Heat and Mass Transfer in Regenerators with Hygroscopic Material," *J. Heat Transfer*, Trans. ASME, vol. 101, pp. 205-210.

Howe, R.R., Beckman, W.A., and Mitchell, J.W., 1983, "Commercial Applications for Solar Hybrid Desiccant Systems," *Progress in Solar Energy, Volume 6*, Proceedings of the Annual Meeting of the American Solar Energy Society, Minneapolis, American Solar Energy Society, Boulder, CO.

Hubbard, S.S., 1954, *Ind. Engng. Chem.*, vol. 46, p. 356.

Huskey, B., et al., 1982, "Advanced Solar/Gas Desiccant Cooling System," GRI-81/10064, Gas Research Institute, Chicago, IL.

Jurinak, J.J., 1982, "Open Cycle Desiccant Cooling -- Component Models and System Simulations," Ph.D. thesis, Dept. of Mech. Engr., University of Wisconsin - Madison.

Jurinak, J.J, and Banks, P.J., 1982, "A Numerical Evaluation of Two Analogy Solutions for a Rotary Silica Gel Dehumidifier, *Heat Transfer in Porous Media*, HTD-Vol. 22, J.V. Beck and L.-S. Yao, eds., ASME, New York.

Jurinak, J.J., and Mitchell, J.W., 1984a, "Recirculation of Purged Flow in an Adiabatic Counterflow Rotary Dehumidifier," *J. Heat Transfer*, Trans. ASME, vol. 106, pp. 369-375.

Jurinak, J.J., and Mitchell, J.W., 1984b, "Effect of Matrix Properties on the Performance of a Counterflow Rotary Dehumidifier," *J. Heat Transfer*, Trans. ASME, vol. 106, pp. 638-645.

Jurinak, J.J., Mitchell, J.W., and Beckman, W.A., 1984, "Open-Cycle Desiccant Air Conditioning as an Alternative to Vapor Compression Cooling in

Residential Applications," *J. Solar Energy Engineering*, Trans. ASME, vol. 106, pp. 252-260.

Kays, W.M., and Crawford, M.E., 1980, *Convective Heat and Mass Transfer*, McGraw-Hill, New York.

Kays, W.M., and London, A.L., 1984, *Compact Heat Exchangers*, McGraw-Hill, New York.

Kim, S., Biswas, P., and Mills, A.F., 1985, "A Compact Low Pressure Drop Desiccant Bed for Solar Air Conditioning Applications: 2. Bench Scale Tests," *J. Solar Energy Engineering*, Trans. ASME, vol. 107, no. 2, pp. 120-127.

Kosar, D.R., 1986, "Gas Research Institute Desiccant Cooling Program," Proceedings of the Desiccant Cooling and Dehumidification Opportunities for Buildings Workshop, June 10-11, 1986, Chattanooga, Tennessee Valley Authority, Chattanooga, TN.

Lambertson, T.J., 1958, "Performance Factors of a Periodic Flow Heat Exchanger," *Trans. ASME*, vol. 80, pp. 586-592.

Lof, G.O.G., Cler, G., and Brisbane, T., 1987, "Performance of a Solar Desiccant Cooling System," *Solar Engineering - 1987*, Proc. ASME-JSME-JSES Solar Energy Conf., Honolulu, ASME, New York, pp. 828-834.

Lundgren, T.S., Sparrow, E.M., and Starr, J.B., 1964, "Pressure Drop Due to the Entrance Region in Ducts of Arbitrary Cross Section," *J. Basic Engineering*, Trans. ASME, vol. 86, pp. 620-626.

Maclaine-cross, I.L., and Banks, P.J., 1972, "Coupled Heat and Mass Transfer in Regenerators - Prediction Using an Analogy wiht Heat Transfer," *Int. J. Heat Mass Transfer*, vol. 15, pp. 1225-1242.

Maclaine-cross, I.L., 1974, "A Theory of Combined Heat and Mass Transfer in Regenerators," Ph.D. thesis, Dept. of Mechanical Engineering, Monash University, Australia.

Maclaine-cross, I.L., 1969, "An Approximate Method for Calculating Heat Transfer and Pressure Drop in Ducts With Laminar Flow," *J. Heat Transfer*, Trans. ASME, Feb., pp. 171-173.

Maclaine-cross, I.L., 1985a, "High Performance Adiabatic Desiccant Open Cooling Cycles," *J. Solar Energy Engineering*, Trans. ASME, vol. 107, pp. 102-103.

Maclaine-cross, I.L., 1985b, personal communication, February.

Macriss, R.A., and Zawacki, T.S., 1984, "High COP Rotating Wheel Solid Desiccant System," 9th Energy Technology Conference, Washington, D.C.

Majumdar, P., Worek, W.M., and Lavan, Z., 1985, "Heat and Mass Transfer in a Composite Desiccant Material," 85-HT-73, ASME 23rd National Heat Transfer Conf., Denver.

Mason, E.A., and Monchick, L., 1965, "Survey of the Equation of State and Transport Properties of Moist Gases," *Humidity and Moisture*, vol. 3, A. Wexler, ed., Reinholt, New York.

Meckler, G., 1987, "Solar Dehumidification System Applications," *Solar Engineering - 1987*, Proceedings of the ASME-JSME-JSES Solar Energy Conf., Honolulu, ASME, New York.

Mitchell, John W., 1986, "State of the Art of Active Solar Cooling," *ASES '86*, Proceedings of the 1986 Annual Meeting of the American Solar Energy Society, American Solar Energy Society, Inc., Boulder, CO, pp. 59-71.

Ohigashi, T., et al., 1983, "Dehumidifying Capacity of Fibrous Activated Carbon Mat Regenerated by Direct Solar Radiation," *Progress in Solar Energy, Volume 6*, Proceedings of the Annual Meeting of the American Solar Energy Society, Minneapolis, American Solar Energy Society, Boulder, CO., pp. 187-191.

Penney, T.R., and Maclaine-cross, I., 1986, "Advances in Open-Cycle Solid Desiccant Cooling," Proceedings of the Desiccant Cooling and Dehumidification Opportunities for Buildings Workshop, June 10-11, 1986, Chattanooga, Tennessee Valley Authority, Chattanooga, TN.

Pennington, N.A., 1955, "Humidity Changer for Air Conditioning," U.S. patent 2,700,537.

Pesaran, A.A., 1983, "Moisture Transport in Silica Gel Particle Beds," Ph.D. thesis, School of Engineering and Applied Science, University of California at Los Angeles.

Pesaran, A.A., and Mills, A.F., 1984, "Modelling of Solid-Side Mass Transfer in Desiccant Particle Beds," *Solar Engineering - 1984*, Proceedings of the ASME Solar Division Sixth Annual Conf., Las Vegas, ASME, New York, pp. 177-185.

Pla-Barby, F.E., Vliet, G.C., and Panton, R.L., 1978, "Performance of Rotary Bed Silica Gel Solid Desiccant Dryers," 78-HT-36, AIAA-ASME Thermophysical and Heat Transfer Conf., Palo Alto.

Rousseau, J., 1982, "Development of a Solar Desiccant Dehumidifier - Final Summary Report," 82-18944, Garrett AiResearch Manufacturing Co., Torrence, CA.

Ruthven, D.M., 1984, *Principles of Adsorption and Adsorption Processes*, John Wiley and Sons, New York.

Saito, Y., 1987, "Regeneration Characteristics of Adsorbent in the Integrated Desiccant/Collector", *Solar Engineering - 1987*, Proc. ASME-JSME-JSES Solar Energy Conf., Honolulu, ASME, New York, pp. 861-866.

Schlepp, D., and Barlow, R., 1984, "Performance of the SERI Parallel-Passage Dehumidifier," SERI/TR-252-1951, Solar Energy Research Institute, Golden, CO.

Schlepp, D.R., and Schultz, K.J., 1984, "High Performance Solar Desiccant Cooling Systems," SERI/TR/252-2497, Solar Energy Research Institute, Golden, CO.

Schlepp, D., Schultz, K., and Zangrando, F., 1984, "Facility Design for Cyclic Testing of Advanced Solid Desiccant Dehumidifiers," SERI/TR-252-2464, Solar Energy Research Institute, Golden, CO.

Scholten, W.B., and Morehouse, J.H., 1983, "Active Program Research Requirements: Final Report," Science Applications, Inc., McLean, VA.

Schultz, K., and Schlepp, D., 1984, "Experimental Test Plan for Cyclic Testing of Parallel Passage Rotary Desiccant Dehumidifiers," (draft report) Solar Energy Research Institute, Golden, CO.

Schultz, K.J., 1986, "SERI Desiccant Cooling Test Facility: Status Report," SERI/TR-252-2718, Solar Energy Research Institute, Golden, CO.

Schultz, K., Barlow, R., Pesaran, A., and Kreith, F., 1987, "An Analysis of a Direct Radiation Solar Dehumidification System," *J. Solar Energy Engineering*, Trans. ASME, vol. 109, pp. 15-21.

Shah, R.K., and London, A.L., 1978, *Laminar Flow Forced Convection in Ducts*, Supplement 1 to *Advances in Heat Transfer*, T.F. Irving and J.P. Hartnett, eds., Academic Press, New York.

Shah, R.K., and London, A.L., 1980, "Effects of Nonuniform Passages on Compact Heat Exchanger Performance," *J. Engineering for Power*, Trans. ASME, vol. 102, pp. 653-659.

Sheridan, J.C., and Mitchell, J.W., 1985, "A Hybrid Solar Desiccant Cooling System," *Solar Energy*, vol. 34, no. 2, pp. 187-193.

Smith, C.W., and Dole, M., 1956, "Specific Heat of Synthetic High Polymers VII: Polyethylene Terephthalate," *J. Polymer Science*, vol. 20, pp. 37-56.

Turner, R.H., Kleiser, J.D., and R.-F. Chen, 1987, "Design Factors in Desiccant Cooling Systems," *Solar Engineering - 1987*, Proceedings of the ASME-JSME-JSES Solar Energy Conf., Honolulu, ASME, New York.

Van den Bulck, E., Mitchell, J.W., and Klein, S.A., 1985a, "Design Theory for Rotary Heat and Mass Exchangers - I. Wave Analysis of Rotary Heat and Mass Exchangers with Infinite Transfer Coefficients," *Int. J. Heat Mass Transfer*, vol. 28, pp. 1575-1586.

Van den Bulck, E., Mitchell, J.W., and Klein, S.A., 1985b, "Design Theory for Rotary Heat and Mass Exchangers - II. Effectiveness-Number-of-Transfer-Units Method for Rotary Heat and Mass Exchangers," *Int. J. Heat Mass Transfer*, vol. 28, pp. 1587-1595.

Van den Bulck, E., Mitchell, J.W., and Klein, S.A., 1986, "The Use of Dehumidifiers in Desiccant Cooling and Dehumidification Systems," *J. Heat Transfer*, Trans. ASME, vol. 108, pp. 684-692.

Van den Bulck, E., 1987, "Convective Heat and Mass Transfer in Compact Regenerative Dehumidifiers," Ph.D. thesis, Dept. of Mechanical Engineering, University of Wisconsin - Madison.

van Leersum, J.G., and Close, D.J., 1982, "Experimental Verification of Open Cycle Cooling System Component Models," report to Solar Energy Laboratory, University of Wisconsin - Madison.

Venhuizen, D., 1984, "Solar King's Cooling Gambit," *Solar Age*, vol. 9, no. 10, pp. 25-27.

Worek, W.M., and Lavan, Z., 1982, "Performance of a Cross-Cooled Desiccant Dehumidifier Prototype," *J. Solar Energy Engineering*, Trans. ASME, vol. 104, pp. 187-196.

Worek, W.M., and Moon, C.-J., 1986, "Off-Design Performance of a Hybrid Vapor-Compression Solid Desiccant Cooling System," 86-WA/Sol-10, ASME Winter Annual Meeting, Anaheim.